506
C215p
no.625

CONTRIBUTIONS TO EMBRYOLOGY

Volume XXXVIII
Nos. 259 to 263

CARNEGIE INSTITUTION OF WASHINGTON PUBLICATION 625
WASHINGTON, D. C.
1966

CONNECTICUT
STATE LIBRARY
DEC 23 1966
HARTFORD,
CONNECTICUT

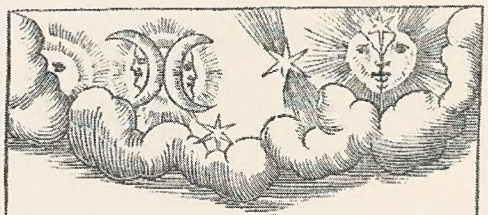

The Beckwith-Browning-Peterson
Teratology Collection

Smithsonian Libraries
2017

CONTRIBUTIONS TO EMBRYOLOGY

Volume XXXVIII

Nos. [illegible] to [illegible]

CARNEGIE INSTITUTION OF WASHINGTON PUBLICATION [illegible]
Washington, D. C.
[illegible]

CONTRIBUTIONS TO EMBRYOLOGY

Volume XXXVIII

Nos. 259 to 263

1902

CARNEGIE INSTITUTION OF WASHINGTON PUBLICATION 625
WASHINGTON, D. C.
1966

This book issued October 1966

Library of Congress Catalog Card Numbers
Contribution 259: 66-24192
260: 66-24191
261: 66-24193
262: 66-24195
263: 66-24194

GARAMOND/PRIDEMARK PRESS, BALTIMORE, MARYLAND

QM
601
.C46
1915
v.38
SCDIRB

CONTENTS

PAGES

259. THE EARLY DEVELOPMENT OF THE EYE IN STAGED HUMAN EMBRYOS, *Ronan O'Rahilly* 1–42

260. THE MORPHOLOGY OF HUMAN UTEROPLACENTAL VASCULATURE, *John W. S. Harris and Elizabeth M. Ramsey* 43–58

261. COMPARISON OF UTEROPLACENTAL VASCULATURE AND CIRCULATION IN THE RHESUS MONKEY AND MAN, *Elizabeth M. Ramsey and John W. S. Harris* 59–70

262. A RADIOAUTOGRAPHIC STUDY OF LABELED GRAFTS IN THE CHICK BLASTODERM: DEVELOPMENT FROM PRIMITIVE-STREAK STAGES TO STAGE 12, *Glenn C. Rosenquist* 71–110

263. MIGRATION OF PRECARDIAC CELLS IN THE CHICK EMBRYO: A RADIOAUTOGRAPHIC STUDY, *Glenn C. Rosenquist and Robert L. DeHaan* 111–121

INDEX OF AUTHORS, VOLUMES I–XXXVIII, 1915–1966 . . . 122–129

CONTRIBUTIONS TO EMBRYOLOGY, NO. 259

THE EARLY DEVELOPMENT OF THE EYE IN STAGED HUMAN EMBRYOS

RONAN O'RAHILLY

Department of Anatomy, Saint Louis University, Saint Louis, Missouri, and
Department of Embryology, Carnegie Institution of Washington,
Baltimore, Maryland

(With 9 plates and 12 figures)

CONTENTS

PAGE

MATERIAL 5

HORIZON x, 4 TO 12 SOMITES 10
  Specimen 4216, 7 Somites 10
  Specimen 391, 8 Somites 10
  Specimen 1201, 8 Somites (Plate 1, Fig. 13) 11
  Specimen 5074, 10 Somites (Plate 1, Fig. 14) 11
  Specimen 3707, 12 Somites (Plate 1, Fig. 15) 11
  Comment on Horizon x (Fig. 2) 11

HORIZON xi, 13 TO 20 SOMITES 12
  Specimen 6344, 13 Somites (Plate 1, Fig. 16) 12
  Specimen 4529, 14 Somites 13
  Specimen 7611, 15 to 16 Somites (Plate 1, Fig. 17) 13
  Specimen 470, 16 to 17 Somites 13
  Specimen 5072, 17 Somites 13
  Specimen 8116, 17 Somites 13
  Specimen 4315, 17 Somites 13
  Specimen 7665, 19 Somites 13
  Specimen 2053, 19 Somites 13
  Comment on Horizon xi (Fig. 3) 13

HORIZON xii, 21 TO 29 SOMITES 15
  Specimen 8943, 22 to 23 Somites (Plate 1, Fig. 18) 15
  Specimens 8505*b*, 23 Somites; 8505*a*, 24 Somites 15
  Specimen 9154, 24 Somites 15
  Specimen 8942, 25 Somites 15
  Specimen 7852, 25 Somites 15
  Specimen 7999, 25 to 26 Somites 15
  Specimen 8941, 28 Somites (Plate 1, Fig. 19) 16
  Specimen 7724, About 29 Somites 16
  Comment on Horizon xii (Fig. 4) 16

HORIZON xiii, 30 OR MORE SOMITES; ABOUT 4 TO 6 MILLIMETERS . . 16
  Specimen 836, 30 Somites, 4 Millimeters (Plate 2, Fig. 20) . . . 16
  Specimen 8066, 32 to 33 Somites, 5.3 Millimeters 16
  Specimen 8581, 4.8 Millimeters 17
  Specimen 7889, 32 Somites, 4.2 Millimeters (Plate 2, Fig. 21) . . 17
  Specimen 8119, 38 Somites, 5.3 Millimeters 17
  Specimen 9296, 4.5 Millimeters 17
  Specimen 8372, 5.6 Millimeters (Plate 2, Fig. 22) 17
  Specimen 9297, 4.5 Millimeters 17
  Comment on Horizon xiii (Fig. 6) 17

PAGE

Horizon xiv, About 5 to 8 Millimeters 20
- Specimen 2841, 5.3 Millimeters 20
- Specimen 8552, 6.5 Millimeters (Plate 3, Fig. 23) 20
- Specimen 8999, 6 Millimeters 21
- Specimen 8308, 5.85 Millimeters 21
- Specimen 8314, 8 Millimeters 21
- Comment on Horizon xiv 21

Horizon xv, About 7 to 9 Millimeters 23
- Specimen 8966, 7.1 Millimeters 23
- Specimen 6505, 7.5 Millimeters 23
- Specimen 8997, 9 Millimeters (Plate 3, Figs. 27, 28, and 29) . . . 23
- Specimen 9140, 7 Millimeters 24
- Specimen 8929, 6.35 Millimeters 24
- Specimen 8968, 8.8 Millimeters 24
- Comment on Horizon xv 24

Horizon xvi, About 7 to 13 Millimeters 25
- Specimen 8773, 11 Millimeters (Plate 4, Fig. 30) 25
- Specimen 9055, 10 Millimeters 25
- Specimen 8436, 10.9 Millimeters 25
- Specimen 617, 7 Millimeters 25
- Specimens 6507, 9 Millimeters; 6509, 8.1 Millimeters; 6510, 10.1 Millimeters 26
- Specimen 6511, 8.1 Millimeters 26
- Specimen 8971, 10 Millimeters 26
- Comment on Horizon xvi 26

Horizon xvii, About 11 to 14 Millimeters 26
- Specimen 8998, 11 Millimeters (Plate 4, Fig. 31) 26
- Specimen 8789, 11.7 Millimeters (Plate 4, Fig. 32) 27
- Specimen 9100, 12 Millimeters 27
- Specimen 6520, 14.2 Millimeters 27
- Specimen 8118, 12.6 Millimeters 28
- Specimen 9282, 12 Millimeters 28
- Specimen 559, 8.6 Millimeters 28
- Comment on Horizon xvii 28

Horizon xviii, About 12 to 17 Millimeters 28
- Specimen 8355, 15 Millimeters 28
- Specimen 9247, 15 Millimeters (Plate 6, Fig. 40) 29
- Specimen 6528, 13.4 Millimeters 29
- Specimens 8812, 12.9 Millimeters; 6524, 11.7 Millimeters; 6527, 14.4 Millimeters 29
- Comment on Horizon xviii 29

PAGE

HORIZON xix, ABOUT 16 TO 19 MILLIMETERS 31
Specimen 9325, 17 Millimeters (Plate 6, Fig. 43) 31
Specimen 9097, 21 Millimeters 31
Specimen 9113, 18.5 Millimeters 31
Specimen 8965, 19.1 Millimeters 31
Specimen 5609, 18 Millimeters 31
Specimens 4501, 18 Millimeters; 8092, 16.3 Millimeters 31
Comment on Horizon xix 32

HORIZON xx, ABOUT 18 TO 23 MILLIMETERS 32
Specimen 8226, 18 Millimeters 32
Specimen 5537, 22 Millimeters 32
Specimen 4148, 21 Millimeters 33
Specimen 4059, 21.6 Millimeters 33
Specimens 460, 21 Millimeters; 462, 20 Millimeters; 966, 23 Millimeters: 5537, 22 Millimeters; 6202, 21 Millimeters; 7274, 18.5 Millimeters; 7906, 19.5 Millimeters; 8157, 20.8 Millimeters . . 33
Comment on Horizon xx 33

HORIZON xxi, ABOUT 22 TO 24 MILLIMETERS 33
Specimen 9614, 22.5 Millimeters 33
Specimens 8553, 22 Millimeters; 1358*F*, 23 Millimeters; 2937, 24.2 Millimeters 34
Specimens 7254, 22.5 Millimeters; 7392, 22.7 Millimeters; 7864, 24 Millimeters 34
Comment on Horizon xxi 34

HORIZON xxii, ABOUT 23 TO 28 MILLIMETERS 34
Specimen 4339, 24.5 Millimeters 34
Specimen 8394, 25.3 Millimeters 34
Specimen 8120, 23.4 Millimeters (Plate 7, Fig. 50) 34
Specimens 1458, 27.5 Millimeters; 4638, 23.4 Millimeters; 6832, 25.8 Millimeters 35
Comment on Horizon xxii 35

HORIZON xxiii, ABOUT 27 TO 31 MILLIMETERS 35
Specimen 4570, 30.7 Millimeters 35
Specimen 7425, 27 Millimeters 36
Specimen 4289, 32.2 Millimeters 36
Specimen 9226, 31 Millimeters 36
Comment on Horizon xxiii 37

DISCUSSION 37

SUMMARY 38

ACKNOWLEDGMENTS 38

LITERATURE CITED 40

THE EARLY DEVELOPMENT OF THE EYE IN STAGED HUMAN EMBRYOS

. . . a knowledge of the minute details of structure at each developmental stage is required both for an understanding of the adult organ and for the diagnosis of the developmental nature of certain deviations from the usual form.

—IDA MANN, *The Development of the Human Eye*

Numerous reports of studies on the development of the eye have appeared since the period between 1817, when Pander showed that the optic vesicles of the chick embryo are outgrowths from the neural tube and 1831, when Huschke showed that the lens arises from the "skin"—*Einstülpung des äusseren Hautsystems.*

Despite the many investigations of the early development of the human eye, a comprehensive documented account of the first few developmental weeks of the visual organ is not available. Vignettes of the initial appearances can be gleaned from the superb papers of Bartelmez and his co-workers on the early embryo, but monographs devoted to the development of the eye as a whole ignore embryonic staging and are based on an inadequate and incomplete series of specimens. The most important work is that of Mann (1964) and of Dejean, Hervouët, and Leplat (1958). The present account is concerned with the detailed development of the human visual organ during the first two months of prenatal life.

MATERIAL

This Contribution is based on an examination of more than 100 early, sectioned embryos, together with relevant models, in the collection of the Department of Embryology, Carnegie Institution of Washington.

The material is classified according to the "developmental horizons" devised by Streeter, who borrowed the term "horizon" from geology and archaeology. The horizons, which are based on both external form and internal structure, are simply "stages" as the term is now used for similar systems devised for various vertebrate embryos (Table 1). It should be noted that, whereas in most species the staging is purely external, in the human both external and internal criteria have been used. However, the human staging, so far, covers only the first two months of prenatal life. In the opinion of the present writer, the term "stage" should not be used unless such a special system has been employed, and particularly not where mere times or measurements of length such as the crown-rump (CR) have been used. Expressions such as "the 39-day stage" or "the 18-mm stage" are thus to be deprecated. Moreover, in very young embryos, the "extent of the flexures and the amount of shrinkage are so variable . . . that simple statements of length are practically meaningless" (Bartelmez and Blount, 1954).

In the present investigation, the embryos ranged from 1½ to 32 mm in length and from three to eight weeks in age. The 100 embryos studied in detail are listed in Tables 2 and 3. Generally, at least six embryos at each stage were examined. Included are not only the best preserved and best stained embryos in the collection but also some specimens of lesser quality. The inferior specimens are included because they have been studied with particular reference to the eye by previous workers and because carefully constructed models of the developing brain were available. Although the designations under the column heading "Quality" in Table 2 were based initially on the views of previous authors, a number of downgrading changes had to be made during the course of this study. With regard to the age of the embryos, the recent revision by Olivier and Pineau (1962) is probably the most reliable. The relevant data are summarized in Table 4.

The paired-somite count is a convenient guide to the developmental level attained during the fourth week of embryonic life, although it should be kept in mind that variations do occur in the degree of development among embryos having similar somite counts. Thus, the rostral neuropore has been recorded as being open in specimens of 17, 18, 19, and 20 somites, and closed in other specimens of 17, 18, and 19–20 somites.

In the first three horizons (x–xii), where the embryos can be arranged conveniently according to somite count, it has been considered best to discuss serially the relevant specimens, whether of Carnegie Collection origin or not, thereby facilitating direct comparisons between closely similar embryos. The terminology used, based mostly on Froriep (1906), is shown in Fig. 1. The term "primary optic vesicle" is replaced by "optic vesicle," "secondary optic vesicle" by "optic cup"; the

TABLE 1. EXAMPLES OF EMBRYONIC STAGING

Species	Number of Stages	Authors	Year
Pisces			
Ictalurus nebulosus	53	Armstrong	1962
Amphibia			
Ambystoma maculatum	46	Harrison	1918*
Rana sylvatica	23	Pollister and Moore	1937
Rana pipiens	23	Miller	1939
	28	Shumway	1940
	25	Taylor and Kollros	1946
Rana fusca	30	Kopsch	1952
Xenopus laevis	66	Nieuwkoop and Faber	1956
Pleurodeles waltlii	56	Gallien and Durocher	1957
Triturus helveticus	56	Gallien and Bidaud	1959
Reptilia			
Lacerta vivipara	40	Dufaure and Hubert	1961
Aves			
Gallus domesticus	46	Hamburger and Hamilton	1951
Anas domestica	46	Koecke	1958
Coturnix c. japonica	33	Zacchei	1961
Mammalia			
Rattus norvegicus	40	Nicholas	1935*
	35	Witschi	1957*
Homo sapiens	23	Streeter	1942–1951
		Heuser and Corner	1957

* Unpublished or privately circulated material.

TABLE 2. HUMAN EMBRYOS IN THE CARNEGIE COLLECTION, USED IN THE PRESENT STUDY OF THE DEVELOPMENT OF THE EYE

Specimen	Somites or Length, mm	Plane	Stain	Quality
	Somites			
		Horizon x		
1201	8	Transverse	H.-Or. G	Good
5074	10	Transverse	Al. coch.	Excellent
3707	12	Oblique	Iron H.	Good
		Horizon xi		
6344	13	Transverse	Al. coch.	Excellent
4529	14	Transverse	Al. coch. Or. G	Excellent
7611	15–16	Transverse	H.-E.	Excellent
470	16–17	Transverse	Al. coch.	Good
5072	17	Transverse	H.-E.	Good
8116	17	Sagittal	Azan	Excellent
4315	17	Transverse	Iron H.	Good
7665	19	Transverse	H.-E. azur	Excellent
2053	19	Transverse	Al. coch.	Excellent

DSI

TABLE 2. Human Embryos in the Carnegie Collection, Used in the Present Study of the Development of the Eye *(Continued)*

Specimen	Somites or Length, mm	Plane	Stain	Quality
Horizon xii				
8943	22–23	Transverse	H.-E.	Excellent
8505*b*	23	Sagittal	Azan	Excellent
8505*a*	24	Transverse	H. phlox.	Excellent
9154	24	Transverse	Iron H. phlox.	Excellent
8942	25	Coronal	Iron H.	Excellent
7852	25	Transverse	H.-E.	Excellent
7999	25–26	Transverse	H.-E.	Excellent
8941	28	Transverse	Iron H.	Excellent
7724	*ca.* 29	Sagittal	H.-E.	Good
	Mm			
Horizon xiii				
836	4.0	Transverse	Al. coch. Azan	Excellent
8066	5.3	Transverse	H.-E.	Excellent
8581	4.8	Sagittal	Azan	Fair
7889	4.2	Coronal	H.-E.	Excellent
8119	5.3	Transverse	H.-E.	Excellent
9296	4.5	Coronal	Azan	Excellent
8372	5.6	Transverse	Azan	Excellent
9297	4.5	Sagittal	Azan	Excellent
Horizon xiv				
2841	5.3	Transverse	H.-E. Or. G	Good
8552	6.5	Transverse	Azan	Excellent
8999	6.0	Sagittal	Azan	Excellent
8308	5.85	Sagittal	Azan	Excellent
8357	6.5	Sagittal	Azan	Good
8314	8.0	Transverse	Azan	Excellent
Horizon xv				
8966	7.1	Sagittal	H.-E.	Excellent
6506	7.5	Coronal	Al. coch.	Excellent
8997	9.0	Coronal	Azan	Excellent
9140	7.0	Coronal	Azan	Distorted
8929	6.35	Transverse	Azan	Fair
8968	8.8	Transverse	H.-E.	Excellent
Horizon xvi				
8773	11.0	Coronal	Azan	Excellent
9055	10.0	Transverse	Azan	Excellent
8436	10.9	Coronal	Azan	Fair
617	7.0	Transverse	Al. coch.	Fair
6507	9.0	Coronal	Al. coch.	Excellent
6509	8.1	Coronal	Al. coch.	Excellent
6510	10.1	Coronal	Al. coch.	Excellent
6511	8.1	Sagittal	Iron H.	Good
Horizon xvii				
8998	11.0	Coronal	Azan	Excellent
8789	11.7	Sagittal	Azan	Excellent
9100	12.0	Sagittal	Azan	Excellent
6520	14.2	Transverse	Al. coch.	Excellent
8118	12.6	Coronal	H.-E.	Excellent
9282	12.0	Transverse	Silver	Fair
Horizon xviii				
8355	15.0	Coronal	Azan	Excellent
9247	15.0	Sagittal	Azan	Excellent
6528	13.4	Coronal	Al. coch.	Excellent
8812	12.9	Transverse	H.-E.	Excellent
6524	11.7	Transverse	Al. coch.	Excellent
6527	14.4	Transverse	Al. coch.	Excellent

TABLE 2. Human Embryos in the Carnegie Collection, Used in the Present Study of the Development of the Eye (*Continued*)

Specimen	Somites or Length, mm	Plane	Stain	Quality
Horizon xix				
9325	17.0	Transverse	Azan	Excellent
9097	21.0	Coronal	Azan	Good
9113	18.5	Transverse	Azan	Fair
8965	19.1	Transverse	H. Or. G	Good
5609	18.0	Coronal	Al. coch.	Good
4501	18.0	Transverse	Coch. Or. G	Good
8092	16.3	Transverse	H.-E. phloxine	Fair
Horizon xx				
8226	18.0	Sagittal	Azan	Good
5537	22.0	Transverse	Al. coch.	Good
6426	21.5	Transverse	H.-E.	Fair
4148	21.0	Coronal	Al. coch. Mallory	Fair
4059	21.6	Coronal	Al. coch. Mallory	Fair
460	21.0	Transverse	H.-E. coch.	Poor
462	20.0	Transverse	Al. coch.	Poor
966	23.0	Coronal	Al. coch.	Poor
5537	22.0	Transverse	Al. coch.	Poor
6202	21.0	Sagittal	H.-E.	Poor
7274	18.5	Transverse	H.-E. phloxine	Poor
7906	19.5	Coronal	H.-E.	Poor
8157	20.8	Coronal	H.-E.	Poor
Horizon xxi				
9614	22.5	Coronal	Azan	Good
8553	22.0	Transverse	H.-E.	Good
1358*F*	23.0	Sagittal	Al. coch.	Fair
2937	24.2	Transverse	H.-E. aur. Or. G	Fair
7254	22.5	Transverse	H.-E.	Poor
7392	22.7	Transverse	H.-E.	Poor
7864	24.0	Coronal	H.-E.	Poor
Horizon xxii				
4339	24.5	Transverse	Al. coch. Mallory	Fair
8394	25.3	Transverse	H.-E. Masson	Good
8120	23.4	Sagittal	H.-E.	Fair
1458	27.5	Sagittal	H.-E. aur. Or. G	Poor
4638	23.4	Transverse	Al. coch. Or. G	Poor
6832	25.8	Coronal	H.-E.	Poor
Horizon xxiii				
4570	30.7	Transverse	H.-E. phloxine	Good
7425	27.0	Coronal	H.-E.	Good
5725	23.0	Coronal	H.-E. aur. Or. G	Fair
4289	32.2	Transverse	Al. coch. Mallory	Fair
4525	30.0	Sagittal	H.-E.	Fair
9226	31.0	Transverse	Azan	Excellent

H.-Or. G = hematoxylin-orange G; H.-E. = H.-eosin; H.E. aur. = H.-E. auramine; Al. coch = alum cochineal; H.-phlox. = H. phloxine.

TABLE 3. Embryos in the Carnegie Collection, Which Have Been Used in Studying the Development of the Eye and for Which Relevant Illustrations Have Been Published

Specimen	Somites	Published Illustrations of Reconstructions and/or Photomicrographs: Authors	Fig. No.
		Horizon x (4–12 somites)	
1201	8	Bartelmez and Evans (1926)	12, 18, 19, 20*a*, 24, 45
		Bartelmez and Dekaban (1962)	68, 71
5074	10	Corner (1929)	1, 2, 13, 15, 16, 17
		Bartelmez and Dekaban (1962)	67, 69
3707	12	Bartelmez and Evans (1926)	15, 40, 41
		Horizon xi (13–20 somites)	
4783	13	Bartelmez and Evans (1926)	7, 16, 20*c*, 37, 38, 39
6344	13	Bartelmez and Blount (1954)	2, 18
4529	14	Heuser (1930)	4, 9, 10, 11, 12, 13
7611	15–16	Streeter (1942)	7, xi
		Bartelmez and Blount (1954)	3, 20, 21
8005	16–17	Bartelmez and Blount (1954)	4
6784	17	Bartelmez and Blount (1954)	19
470	17	Bartelmez and Evans (1926)	17, 20*f*, 34
		Wen (1928)	7
5072	17	Atwell (1930)	1, 8, 9
4315	17	Wen (1928)	4, 5, 7
7665	19	Bartelmez and Blount (1954)	5, 15, 22, 23
		Bartelmez and Dekaban (1962)	64, 66
2053	19	Davis (1923)	21, 22, 23, 24
		Horizon xii (21–29 somites)	
8693	22	Wen (1928)	6, 7
8943	22–23	Bartelmez and Blount (1954)	6, 16, 17
		Bartelmez and Dekaban (1962)	60, 62, 65
8942	25	Bartelmez and Blount (1954)	8, 28
7852	25	Bartelmez and Blount (1954)	9
7999	25–26	Bartelmez and Blount (1954)	7, 24, 26
8941	28	Bartelmez and Blount (1954)	10, 29
7724	*ca.* 29	Gilbert (1957)	11, 12, 30, 31
		Horizon xiii (30 or more somites)	
836	30	Bartelmez and Blount (1954)	11, 12, 30
		Bartelmez and Dekaban (1962)	53, 55
8066	32–33	Bartelmez and Blount (1954)	13
7889	32	Streeter (1945)	8, xiii
		Bartelmez and Blount (1954)	14

so-called choroid[1] fissure is referred to as the retinal fissure; and the term "cerebral stratum of the retina," following the new usage of the *Nomina anatomica* of 1955 and 1960, is extended to include layers 2–10, instead of merely 5–10, of Greeff's enumeration.[2] For detailed bibliographies, the work of Mann (1964) and of Dejean, Hervouët, and Leplat (1958) should be consulted, as well as the recent volume by Duke-Elder and Cook (1963).

TABLE 4. Probable Embryonic Age in Postovulatory Days*

Horizon	No. of Days
x	22
xi	24
xii	26
xiii	28
xiv	32
xv	33
xvi	37
xvii	41
xviii	44
xix	47½
xx	50½
xxi	52
xxii	54
xxiii	56½

* Based on data of Olivier and Pineau (1962).

---

[1] In the anglicized forms of such Latin terms as *chorioidea, plexus chorioideus, glandula thyreoidea,* etc., the first *i* or *e* is omitted: choroid, choroid plexus, thyroid gland. The *i* is retained, however, in *tela chorioidea* because this term is not anglicized. In the current *Nomina anatomica* the above letters have been omitted even in the Latin forms.

[2] Because the layers of the retina are, by convention, numbered from external to internal, and because counting is usually performed either from above downward or from left to right, it is suggested that both photomicrographs and diagrams of the retina should be published with an orientation that places the pigmented stratum uppermost when the layers are shown horizontally, and the pigmented stratum toward the left when the layers are shown vertically.

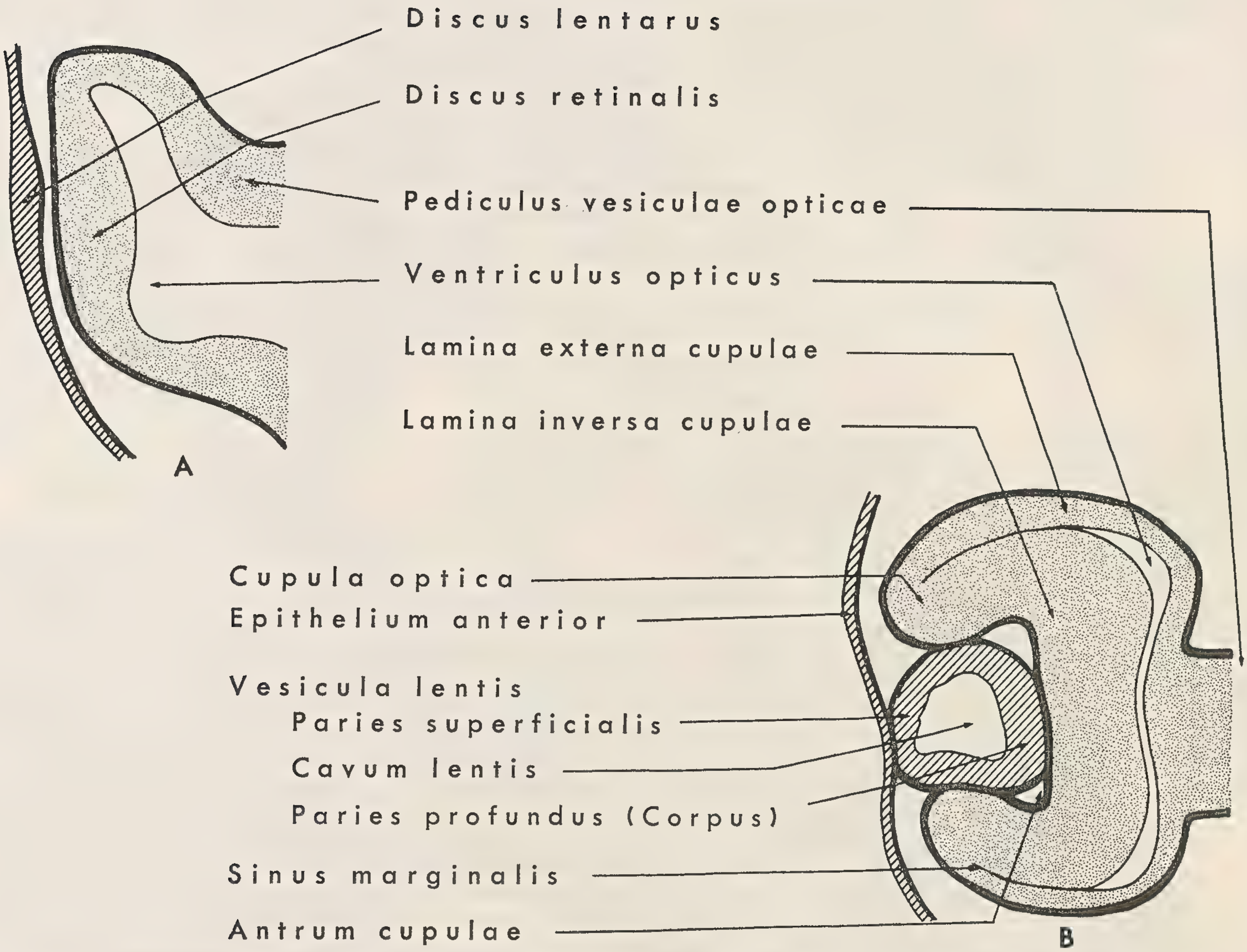

Fig. 1. Terminology proposed here for early development of the eye in vertebrates. It is suggested that these Latin terms be considered for international acceptance; their English equivalents are used in this paper. Two developmental phases are illustrated: *A,* the optic vesicle *(vesicula optica)* at horizon xiii, and *B,* the embryonic eye *(oculus embryonalis)* at horizon xv. In *A,* the optic vesicle includes the stalk *(pediculus)* and the retinal disc *(discus retinalis),* and encloses the optic ventricle *(ventriculus opticus).* The surface ectoderm shows the lens disc *(discus lentarus).* In *B,* the optic cup *(cupula optica)* has formed, and an external layer *(lamina externa)* and an inverted layer *(lamina inversa)* are apparent. The optic ventricle is reduced to a slit, and its extremity at the rim of the cup is the marginal sinus *(sinus marginalis).* The hollow of the cup *(antrum cupulae)* is largely occupied by the lens vesicle *(vesicula lentis),* which has a superficial wall *(paries superficialis),* a lens cavity *(cavum lentis),* and a deep wall *(paries profundus)* or body *(corpus).* The retinal fissure *(fissura retinae)* is not evident in this section.

HORIZON X, 4 TO 12 SOMITES

SPECIMEN 4216, 7 SOMITES

Although, according to Payne (1925), "a careful study of the model and sections shows clearly that an optic sulcus has just begun to make its appearance," Bartelmez and Blount (1954) have pointed out that "no evidence of a thickening that would indicate the differentiation of the primordium" has been presented for this embryo. Politzer (1930) also described two shallow optic sulci in a 7-somite embryo and remarked that they were located near the median plane. Streiter (1951), on the other hand, did not find optic grooves in the 7-somite embryo that he examined.

SPECIMEN 391, 8 SOMITES

Dandy (1910) detected "no suggestion of anlage of the lens, optic or otic vesicles," but Bartelmez and Evans (1926) found "several localized thickenings of the forebrain folds. . . ." In another 8-somite embryo, West (1930) found no sulcus, but observed that the floor of the neural groove on each side was "a little bit thicker" in the future optic area and was characterized there by "a slight inward bulging." Bartelmez, however, thought that this distorted embryo may actually have had only 5 or 6 somites (Heuser and Corner, 1957).

SPECIMEN 1201, 8 SOMITES (PLATE 1, FIG. 13)

According to Bartelmez and Blount (1954), this specimen is "the earliest stage for which the optic primordium has been plotted." The two primordia meet in the median plane at the *torus opticus,* or primitive chiasma ridge. Each primordium is 55 μ at its maximum thickness. A shallow caudally placed sulcus on the future ventricular surface of the optic primordium marks the beginning of the optic evagination. The deep surface of the primordium is in contact with the underlying mesenchyme.

SPECIMEN 5074, 10 SOMITES (PLATE 1, FIG. 14)

The optic primordium, together with its optic sulcus, is present on each side (Corner, 1929). At the rostral limit of the neural tube, a small terminal notch is present where the neural folds project beyond the *torus opticus.* The lateral edge of each primordium has come into contact with the surface ectoderm. Neural crest cells are found underlying the primordium and are apparently derived from the mesencephalic neural crest (Bartelmez and Blount, 1954).

SPECIMEN 3707, 12 SOMITES (PLATE 1, FIG. 15)

This embryo is believed to show early cranioschisis (Bartelmez and Blount, 1954), although the optic region may well be normal. The optic sulcus is deeper and is in closer relation with the ectoderm, but a "very narrow strip of epithelium can still be recognized between the primordium and the ectoderm" (Bartelmez and Evans, 1926).

COMMENT ON HORIZON X (FIG. 2)

At this stage, the embryo is approximately 1½–3 mm in length and three postovulatory weeks in age. A cranial flexure, overlying the mesencephalic flexure, is present, although the dorsum of the embryo may be either convex or concave. The neural folds begin to fuse during horizon x, the rostral neuropore closes during horizon xi, and the caudal neuropore closes during horizon xii.

The term "optic primordium" is used for a thickened area of each neural fold, a portion of whose neuroepithelium subsequently becomes incorporated into an optic cup. It is believed that the definitive optic vesicle arises as a part of the central nervous system rather than from an intermediate zone between the central nervous system and the somatic ectoderm (Bartelmez and Evans, 1926). Thus, the optic primordium is not a placode of the general surface ectoderm.

Groth (1939), however, from his studies of the rabbit, maintained that the otic, retinal, and olfactory plates all arise from "similar parts of the brain anlage," namely, the *Seitenwulst,* or lateral ridge, at the border of the medullary plate. According to the scheme in his Fig. 28, an initially similar origin is envisioned, after which both the otic and the olfactory epithelium remain outside the developing neural tube, whereas the retinal epithelium, before its invagination, becomes incorporated in the wall of the neural tube. According to Bartelmez and Dekaban (1962), in the human, as far as the histological evidence goes, it seems that "the primordia of the optic vesicles arise laterally throughout the length of the forebrain as far as the pros-mesencephalic sulcus and meet at its rostral extremity in the mid-line. This would mean that the forebrain contributes the optic vesicles and their stalks, that is, the retinae and the substrates for the optic nerve fibers."

According to the interpretation of Schulte and Tilney (1915), however, based on their studies of the cat, the optic vesicle and "at least as much of the brain wall as lies ectal to the optic sulcus . . . must be considered of ganglionic equivalency," i.e., comparable to neural crest.

The two optic primordia meet in the median plane at the *torus opticus.* The torus is originally the terminal, rostral end of the neural axis in the median plane during neural fold stages. It occupies the rostral end of the ditelencephalic junction and subsequently constitutes the basis of the optic chiasma.

The caudal end of the primordium differentiates first and leads in development. Apart from the torus, which forms the chiasma, the remainder of each optic primordium gives rise to the thalamic part of the diencephalic wall (Bartelmez and Evans, 1926; Wen, 1928), and to the optic stalk, the optic cup, and the optic neural crest (Bartelmez and Blount, 1954). From their studies of the cat, Schulte and Tilney (1915) concluded that the optic vesicles "give rise to an ectoptic zone which includes the anlages of the thalamencephalon, telencephalon and the infundibular region." In other words, "there has thus been formed from the periphery of the vesicle a series of derivatives which constitute an ectoptic arcade and in each case the process has been the same, a remodeling of the primitive optic vesicle, so that its central region ultimately constitutes the definitive vesicle, while its periphery becomes allotted to . . . other elements of the prosencephalon. . . .”

The optic sulcus is a shallow groove that appears on the caudal portion of the future ventricular surface of the primordium while the neural folds are still open in the forebrain. The sulcus is the beginning of the evagination that will soon constitute the optic vesicle.

The optic primordium and sulcus probably appear first at 8 somites (Bartelmez and Blount, 1954) rather than at 7 (Bartelmez and Evans, 1926). On the other hand, Professor Orts Llorca (personal communication, 1962) thinks it possible in some cases to detect the optic anlage as early as 3 somites. Photomicrographs, kindly lent to the present writer, of such a specimen (Gv), however, seem to suggest that the embryo should have had several more than three pairs of somites.

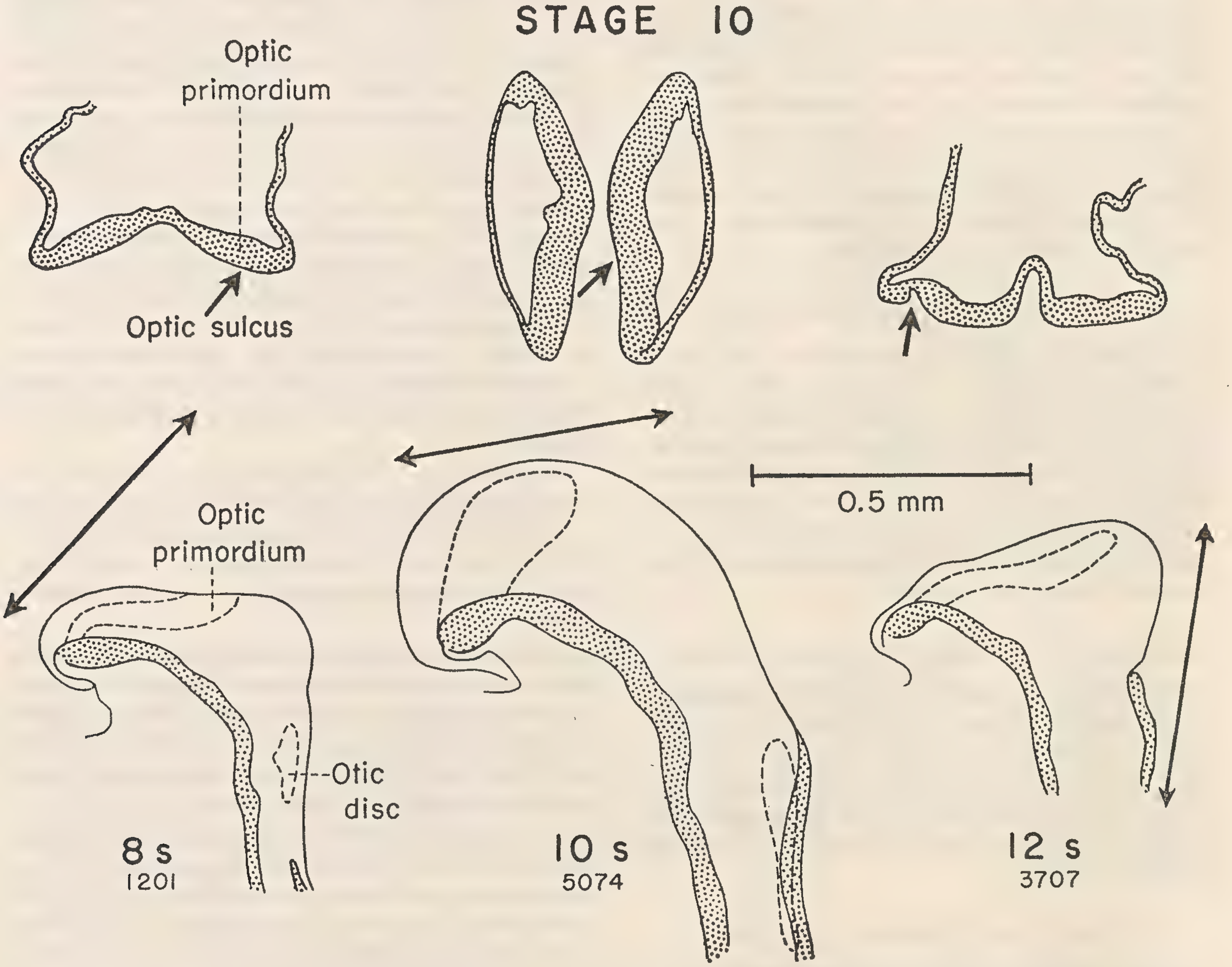

Fig. 2. Projected outlines of the optic primordium at horizon x. The optic sulcus is indicated by an arrow in each of the upper three diagrams. The lower three diagrams represent reconstructions of the right half of the neural plate. The planes of section of the upper drawings are indicated by arrow-tipped lines. (s = somites.)

HORIZON XI, 13 TO 20 SOMITES

Specimen 6344, 13 Somites
(Plate 1, Fig. 16)

The lateral half—that nearest the neuropore—of the optic evagination has made contact with the surface ectoderm, whereas the medial half—that nearest the midbrain—is related to mesencephalic, or rostral, neural crest. In the latter area, the crest forms the beginning of the mesenchymal sheath of the optic vesicle (Bartelmez and Blount, 1954). The terminal notch has become obliterated by fusion of the neural folds beyond the torus, thereby forming the *lamina terminalis*.

Of a 13- to 14-somite specimen that had been treated to show the localization of alkaline phosphatase (Mori, 1959), it was stated that the neural crest attached to the caudal wall of the left optic evagination is "apparently in direct connection with the neural epithelium without interposition" of the basement membrane of the neural epithelium. Thus, Mori wrote, "the impression was gained of an emigration of the neuroblasts from the optic anlage." This is presumably the initial contribution of the optic primordium itself to its own mesenchymal sheath, an event recognized by Bartelmez and Blount (1954) from 16 somites onward.

"Pfannenstiel III," an embryo of 14 somites, which shows a small but definite optic evagination, was illustrated by Keibel and Elze (1908) in their *Normentafel,* and is the earliest specimen figured by Keibel (1912) in the *Embryology;* by Bach and Seefelder (1914) in their *Atlas;* and by Mann (1964) in her well-known monograph.

SPECIMEN 4529, 14 SOMITES

The optic evaginations appear to be flattened rostrocaudally, and they form the optic eminence, a conspicuous feature of the embryo externally. The optic ventricle, as the cavity of the evagination may be called, has the form of a slit. The future thalamic region is distinguishable. It was pointed out by Heuser (1930) that the neural crest cells along the wall of the optic vesicle are probably concerned with "the development of mesoderm in this region."

SPECIMEN 7611, 15 TO 16 SOMITES
(PLATE 1, FIG. 17)

There is evidence of early contributions from the caudal (former medial) half of the optic primordium to its sheath. The "neuroporal" (former lateral) half, i.e., the half that is adjacent to the site of future neuroporal closure, together with the lateral aspect, is in contact with the surface ectoderm.

SPECIMEN 470, 16 TO 17 SOMITES

The preoptic forebrain has grown large enough for the telencephalon medium to be recognized (Bartelmez and Blount, 1954). In this embryo, as in practically all those of horizon xi, the laterally directed optic evagination is marked off from the lateral surface of the brain by a caudal limiting sulcus.

SPECIMEN 5072, 17 SOMITES

The optic evaginations, the most conspicuous external feature of this part of the embryo, bulge laterally from the forebrain. The optic vesicles, as the evaginations may now be termed, are flattened rostrocaudally and are marked off from the wall of the forebrain externally by the caudal limiting sulcus. Dorsally, a short groove separates each vesicle from the diencephalon. Ventrally, the two vesicles appear to spring from a common region of the floor of the forebrain. Internally, each optic ventricle communicates with the cavity of the forebrain by means of a crescentic slit.

SPECIMEN 8116, 17 SOMITES

In sagittal sections, the optic ventricle is seen as a slit, the long axis of which is parallel with the rostral neuropore and with the buccopharyngeal membrane.

SPECIMEN 4315, 17 SOMITES

In addition to the caudal limiting sulcus, a shallow rostral limiting sulcus was distinguished by Wen (1928). Internally, the opening of the optic ventricle is bounded by caudal and rostral ridges, which correspond to the limiting sulci externally.

SPECIMEN 7665, 19 SOMITES

The rostral neuropore is still open. The optic vesicles are ridgelike in appearance. Caudally and laterally, each vesicle is separated from the surface ectoderm by its sheath. Politzer (1928) has described an 18-somite embryo in which the ridgelike vesicles closely resemble those of the Carnegie Collection specimen 7665.

SPECIMEN 2053, 19 SOMITES

The rostral neuropore has just closed. The optic eminence is evident on each side. The optic vesicles are large outpocketings, directed laterally from the rostral end of the forebrain, and are flattened rostrocaudally. Externally, they appear to spring from a common origin in the region of the ventricular floor. Each vesicle is separated from the forebrain by a groove, the caudal limiting sulcus. Internally, the vesicles appear to fuse across the ventricular floor; elsewhere, each vesicle is limited from the cavity of the forebrain by a semilunar opening, the rounded caudal margin of which corresponds to the caudal limiting sulcus externally. Davis (1923) was unable to distinguish diencephalon from telencephalon.

The earliest (4-mm) specimen provided by Leplat in the French monograph (Dejean *et al.,* 1958, their Fig. 7) appears to be at late horizon xi or early horizon xii, but the number of somites is not given.

COMMENT ON HORIZON XI (FIG. 3)

In the earlier specimens of this stage, the rostral neuropore is still wide open, whereas in the latest it

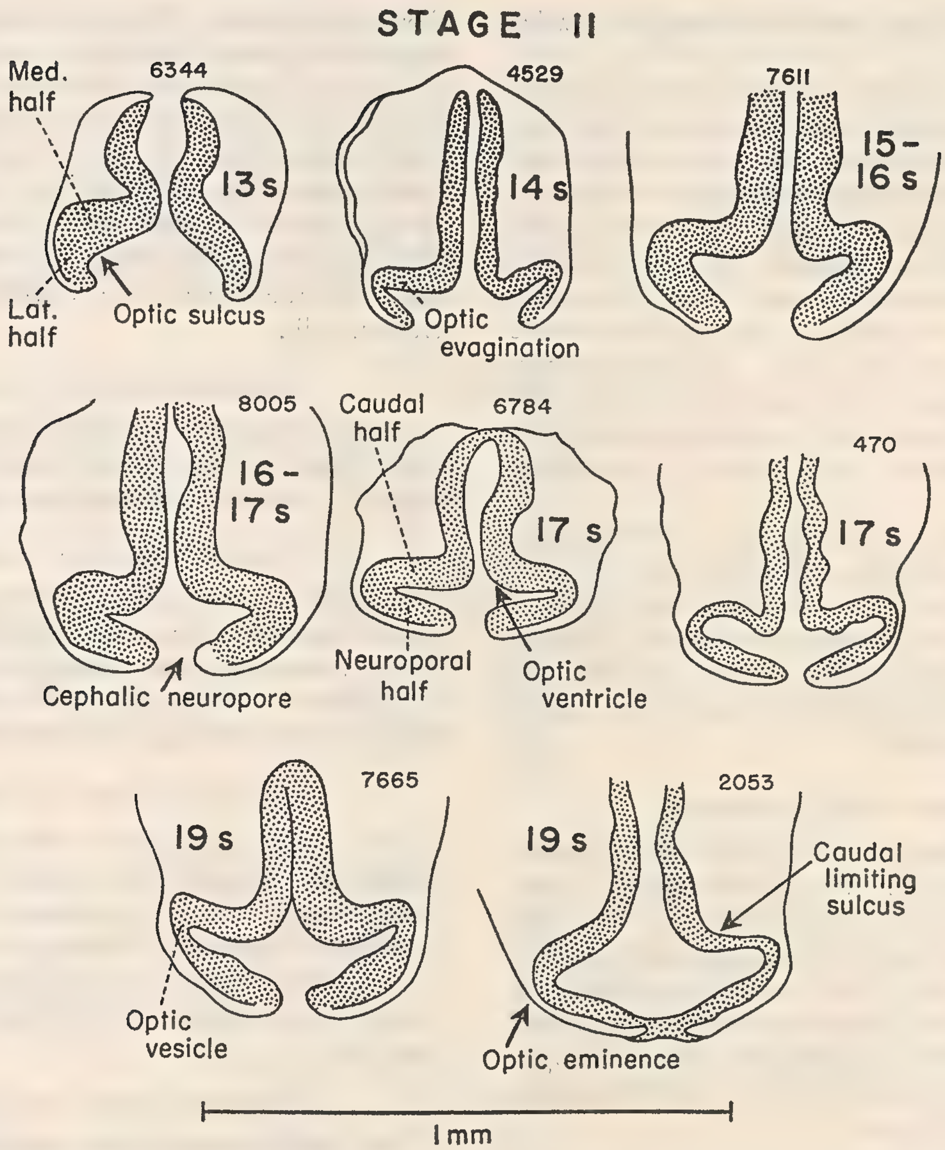

Fig. 3. Projected outlines of the optic evaginations at horizon xi. The closure of the rostral, or cephalic, neuropore can be followed successively in the diagrams. The lateral wall of the forebrain evaginates at the optic sulcus to form the optic evagination, which is converted into the optic vesicle. Its cavity, the optic ventricle, is in wide communication with that of the forebrain. The vesicle produces the optic eminence on the surface of the body.

is closed. The fusion of the neural folds that is proceeding dorsally from the torus meets the fusion that is extending rostrally from the midbrain. As a result of variations in the relative extent of these two fusions, the site of final closure of the neuropore varies.

Most of the lateral wall of the forebrain evaginates at the optic sulcus to form the optic evagination. The evagination will soon constitute the optic vesicle. Its cavity, the optic ventricle, is in wide communication with that of the forebrain. The vesicle makes contact laterally with the surface ectoderm. The wall of the optic vesicle contributes neural crest to its own mesenchymal sheath. The mesenchyme that "crowds against the caudal surface of the optic vesicle" is a portion of what has been termed the "maxillomandibular mesoderm" (Gilbert, 1957). The optic evagination becomes marked off from the lateral surface of the brain by a caudal limiting sulcus. In this context, rostral and caudal, and dorsal and ventral refer to the forebrain and not to the embryo as a whole (Fig. 5). This convention is made necessary by the varying degrees of flexure exhibited by the developing brain. The appearance and development of limiting sulci at the junction between the optic evaginations and the brain result from differential growth between these structures (Wen, 1928). It has been maintained that the optic evagination does not grow laterally across the intervening mesenchyme to reach the surface ectoderm, but rather that the edges of the neural plate grow rostrad ('Espinasse, 1962).

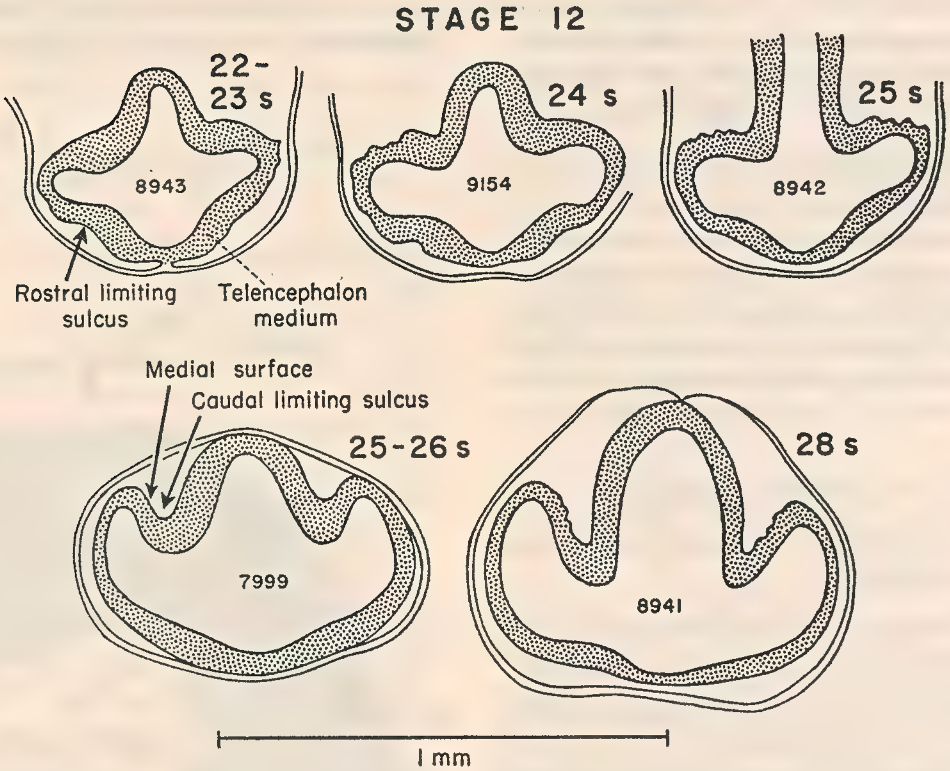

Fig. 4. Projected outlines of the optic vesicles at horizon xii. The caudal growth of the vesicle accentuates the caudal limiting sulcus, and the vesicle develops a medial surface. A rostral limiting sulcus can be made out in some embryos.

HORIZON XII, 21 TO 29 SOMITES

Specimen 8943, 22 to 23 Somites (Plate 1, Fig. 18)

A reconstruction of the brain is illustrated by Bartelmez and Blount (1954), who aptly described the olive-shaped optic vesicle as resembling "a frightened hedgehog" (their Figs. 16 and 17). Its bristling surface is the result of the migration of groups of crest cells from all surfaces of the optic primordium to its mesenchymal sheath. The entire vesicle is separated from the surface ectoderm by the sheath. This embryo shows the maximum development of the optic neural crest. The caudal tip of the vesicle has grown independently, the walls of the vesicle have thickened, and the optic ventricle has become enlarged. Rostrally, the vesicle merges with the wall of the telencephalon medium, but a rostral limiting sulcus can be detected. The *lamina terminalis* can be identified in front of the primordium of the optic chiasma.

Specimens 8505*b*, 23 Somites; 8505*a*, 24 Somites

These twin embryos, which are sectioned in different planes, resemble No. 8943.

Specimen 9154, 24 Somites

Rosenbauer (1955) has described, with particular reference to the blood vessels, a 24-somite embryo in which the optic vesicles closely resemble those of the Carnegie Collection specimen 9154 in appearance.

Specimen 8942, 25 Somites

The almost spherical optic vesicles and most of the telencephalon medium (except near the neuroporal suture) are covered by mesenchyme. The formation of the sheath, however, is not keeping pace with the growth of the optic vesicle. Both the vesicle and the future optic stalk are characterized by bristling surfaces, in contrast with the sharp borders of the telencephalon medium. Sex chromatin is present in the wall of the optic vesicle, in the surrounding mesenchyme, and in the overlying surface epithelium.

Specimen 7852, 25 Somites

The sheath of the optic vesicle is degenerating laterally.

Specimen 7999, 25 to 26 Somites

"On the inferior surface. where emigration [of crest cells] originally began, it has now almost ceased. [Moreover] a few connective-tissue fibrils have already appeared on this surface, marking the beginning of a continuous basement membrane, such as has already developed on the surface of the midbrain"

(Bartelmez and Blount, 1954). A deepening of the caudal limiting sulcus has resulted in the formation of a medial wall for the optic vesicle, and this new surface is giving rise to further neural crest.

Specimen 8941, 28 Somites (Plate 1, Fig. 19)

The optic vesicles appear to be larger and seem to be approaching the surface ectoderm again. The caudal limiting sulcus is deeper and contains well-vascularized mesenchyme. The sheath, which has not kept pace with the vesicle, is thinner and is degenerating laterally. The surfaces of the vesicle are smooth, with the exception of the medial, where neural crest is still being formed.

Specimen 7724, About 29 Somites

In this sagittal series, blood vessels can be seen entering the dorsal limiting sulcus.

Comment on Horizon xii (Fig. 4)

At this stage, the optic vesicle grows caudally (Fig. 5), thereby accentuating the caudal limiting sulcus and gradually developing a medial surface of its own. A shallow rostral limiting sulcus can be detected, at least in some embryos. The maximum extent of optic neural crest formation is reached during this stage, and the optic vesicle becomes covered by a complete sheath. Sex chromatin is present in the optic vesicles of presumed female embryos.

In addition to the crest cells derived from the optic vesicle, which may be designated "optic neural crest" (Bartelmez and Blount, 1954), two other subdivisions should be mentioned: neural crest tissue developed from the wall of the otic pit and vesicle, designated "vestibulocochlear neural crest" (O'Rahilly, 1963), and that developed, later, from the wall of the nasal pit and vomeronasal groove, designated "terminal-vomeronasal neural crest" (O'Rahilly, 1965).

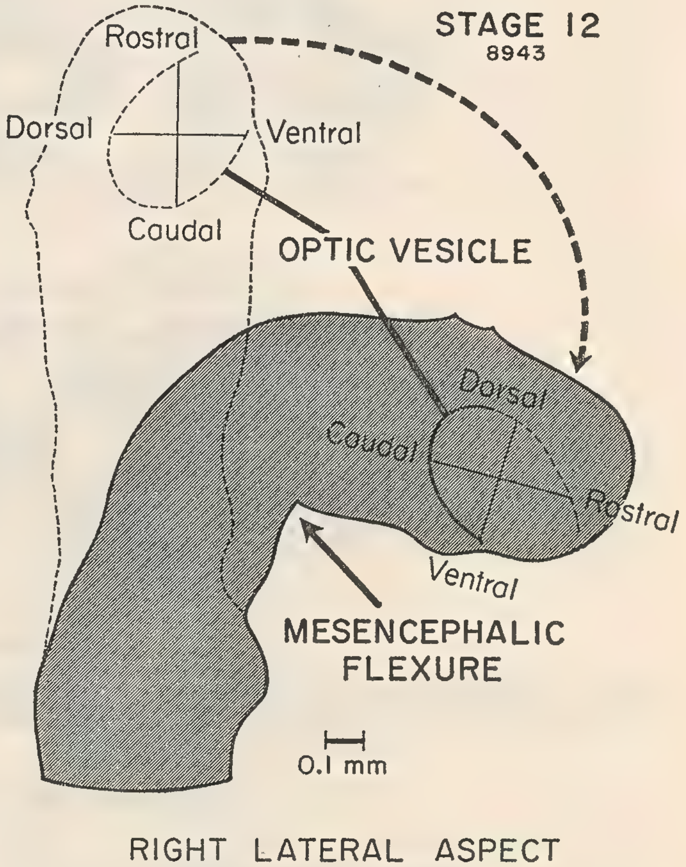

Fig. 5. Terminology used to describe the developing forebrain. An interrupted outline indicates the neural tube (right lateral aspect) as if it were straight. A continuous line represents the natural condition (shaded), i.e., a varying degree of flexure at the midbrain. In this context, rostral and caudal, and dorsal and ventral are retained for the optic vesicle, and are used with reference to a hypothetically straight forebrain.

HORIZON XIII, 30 OR MORE SOMITES; ABOUT 4 TO 6 MILLIMETERS

Specimen 836, 30 Somites, 4 Millimeters (Plate 2, Fig. 20)

The optic vesicles are considerably larger than those in the previous stage of No. 8941. A marked caudal limiting sulcus is evident on a model of the brain. This caudal, or dorsal, sulcus is seen, on section, to be filled with closely packed cells apparently of crest origin. Elsewhere, considerable degeneration of sheath cells is taking place. The optic vesicle is surrounded by a basement membrane, stained with aniline blue, that is continuous with the basement membrane around the forebrain. Mitotic figures can be seen in that part of the wall of both brain and optic vesicles immediately adjacent to the ventricular cavities. The wall of the optic vesicle is thickened ventrolaterally and thereby forms the retinal disc, which contains five to six rows of nuclei. The ectoderm, overlying the retinal disc, is thickened and thereby forms the lens disc, which contains two rows of nuclei. The lens disc is lined by a basement membrane, stained with aniline blue. The space between the retinal and lens discs may well be due to shrinkage.

Specimen 8066, 32 to 33 Somites, 5.3 Millimeters

This specimen shows retinal and lens discs, the oval nuclei of which are oriented perpendicularly to the long axes of the discs. In the optic vesicle and the brain, the mitotic figures, which are well stained in this embryo, are found characteristically adjacent to the ventricular cavities.

SPECIMEN 8581, 4.8 MILLIMETERS

The plane for section of the brain is not strictly sagittal, and the histological appearance leaves much to be desired.

SPECIMEN 7889, 32 SOMITES, 4.2 MILLIMETERS (PLATE 2, FIG. 21)

Capillaries can be detected near the external surface of the optic stalk and the adjacent retina, indicating the beginning of what may be termed the "uveocapillary" lamina (*cf.* choriocapillary lamina). The optic vesicle is surrounded by a basement membrane continuous with that around the forebrain. The retinal disc contains about seven to eight rows of mostly oval nuclei, and its lateralmost portion is almost free of nuclei, constituting the beginning of the nucleus-free marginal zone of the retina. The cavities of the optic vesicle and forebrain are lined by a terminal bar net. The lens disc is lined by a prominent basement membrane and contains about three rows of mostly oval nuclei. The nuclei of both retinal and lens discs are oriented perpendicularly to the long axes of the discs. The periphery of the lens disc is a simple columnar epithelium. The retinal and lens discs are separated only by occasional degenerating cells of the sheath of the optic vesicle. Elsewhere, the two discs make contact by their basement membranes.

SPECIMEN 8119, 38 SOMITES, 5.3 MILLIMETERS

Definite retinal and lens discs are present in this specimen.

SPECIMEN 9296, 4.5 MILLIMETERS

This embryo shows a sharply delimited lens disc. Considerable necrosis is present in both retinal discs of this specimen, far more than is usually seen: for example, the "morphogenetic degeneration" in a photomicrograph of Mann (1964, her Fig. 61*B*).

SPECIMEN 8372, 5.6 MILLIMETERS (PLATE 2, FIG. 22)

Because of a slight indentation of both retinal and lens discs, this specimen may be regarded as transitional between horizons xiii and xiv. Mrs. Dorcas H. Padget (personal communication, 1964) has called the attention of the writer to certain abnormal features in the neural tube of this embryo, including a peculiar constriction of the wall of the tube near the optic stalk.

SPECIMEN 9297, 4.5 MILLIMETERS

In this specimen, both retinal and lens discs are indented to the degree that a lens pit (see horizon xiv) may be said to have begun development.

COMMENT ON HORIZON XIII (FIG. 6)

The limb buds appear at this time. The sources of published illustrations of reconstructions or photomicrographs of the eye region in embryos of horizons x–xiii are indicated in Table 3, and a scheme of the eye in horizons x–xv is provided in Fig. 9.

Optic vesicle

The shape of the optic vesicle makes the optic ventricle appear somewhat quadrilateral in coronal sections of an embryo, whereas in transverse sections (approximately through the long axis of the vesicle) it is ovoid or spheroidal (Fig. 7).

The two optic vesicles appear to be symmetrical, and the characteristic asymmetry of the chick eyes (O'Rahilly and Meyer, 1959) at a similar stage, presumably associated with the turning of the chick embryo onto its side, is not observed. The retinal disc is the future inverted layer of the optic cup. In coronal sections, it appears to protrude slightly into the optic ventricle. In the later specimens, the retinal disc presents an external, striated, nucleus-free marginal zone, or "marginal velum" (Plate 2, Fig. 22). The interconnected cone-shaped processes of the retinal and lens discs are artifacts, as clearly seen in specimen 8314, horizon xiv. These processes, reported by various authors, have been described by Mann (1964) as "direct, protoplasmic continuity between lens and retina." That part of the wall of the vesicle adjoining the retinal disc is the future external, later pigmented, layer of the cup, and, merging with this in the region of the limiting sulci, is the future optic stalk.

The characteristic location of mitotic figures, namely, adjacent to the ventricular cavities, applies to the walls of both the neural tube and the optic vesicles. This location results from the movements of the intermitotic nuclei, which migrate from the lumen between divisions and return for division to their luminal position, where the cells are firmly united by terminal bars (Sauer and Chittenden, 1959). A comparison between the developing neural tube and the optic cup is illustrated in Fig. 8.

Lens

The formation of the lens disc is the classic example of second-grade induction; in other words, the future lens region appears in the surface ectoderm at least partly under the influence of the wall of the optic vesicle (second-grade organizer). In the human embryo, the first indication of the retinal and lens discs is seen at horizon xiii and, since the intervening sheath cells are degenerating, the two discs are more or less in contact depending on the quality of preservation. It will be recalled that the optic evagination first makes contact with the surface ectoderm at horizon xi (e.g.,

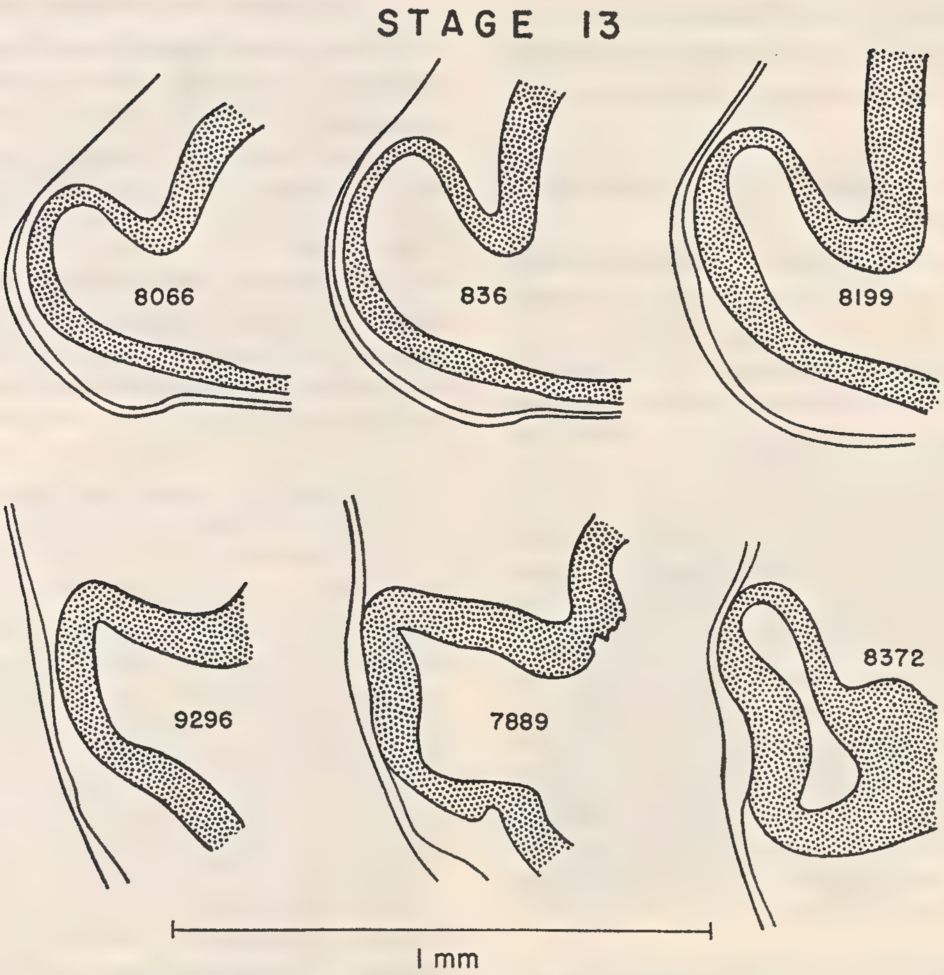

Fig. 6. Projected outlines of the optic vesicle at horizon xiii. The surface ectoderm develops a localized thickening, the lens disc, which is more or less in contact with the retinal disc, or future inverted layer of the optic cup. In the last specimen (8372), a slight indentation of both retinal and lens discs is apparent.

No. 6344), and that the sheath of the optic vesicle during horizons xi (e.g., No. 7665) and xii (e.g., No. 8943) comes to separate the vesicle from the overlying ectoderm. Now, at horizon xiii, the vesicle and the ectoderm again make contact. Observations of the chick embryo made with the electron microscope, however, suggest that the two basement membranes are separated by a minute interepithelial space (Hunt, 1961; Brini, Porte, and Stoeckel, 1962). In addition, the orientation of the nuclei in the lens disc has been studied in detail in the chick embryo (McKeehan, 1951). It is generally believed that the lens disc is a pseudostratified epithelium (Mann, 1964).

A histochemical study (McKay *et al.*, 1955) of a 5-mm embryo of horizon xiii revealed ribonucleoprotein, alkaline glycerophosphatase, and alphanaphthyl alkaline phosphatase in the retina, and glycogen, ribonucleoprotein, and alkaline glycerophosphatase in the lens.

Basement membranes (Fig. 10)

The basement membranes of the eye are initially two: *A,* that covering the optic vesicle, and *B,* that lining the surface ectoderm. This important arrangement has been investigated in a number of species: Laguesse (1923), in chick; Dejean (1923), in rat and sheep; Dejean (1934), in rabbit and sheep; O'Rahilly and Meyer (1960), in chick; Cohen (1961), in mouse; O'Rahilly (1962), in human. The membranes, which have been shown to be periodic acid-Schiff-positive in the chick embryo (O'Rahilly and Meyer, 1960), persist throughout development, and their subsequent behavior will be described in later stages, where they will be distinguished as *A* and *B* (see p. 22).

Mesoderm

The basic precursors of the ocular tissues are now evident: neural ectoderm, optic neural crest, surface ectoderm, and adjacent mesoderm. A uveocapillary lamina

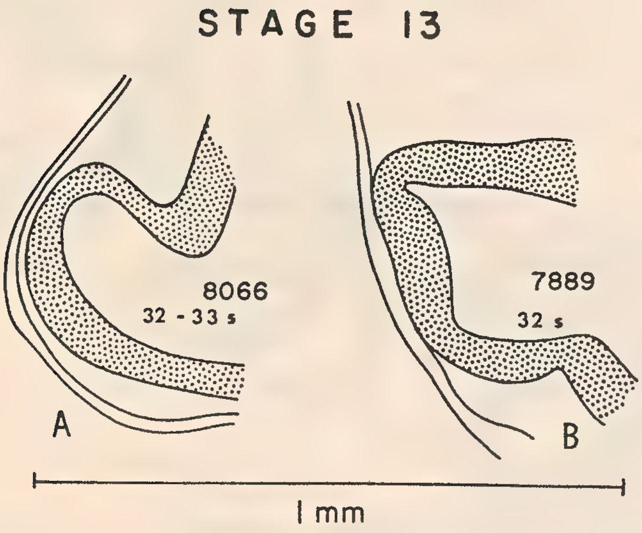

Fig. 7. Optic ventricle at horizon xiii, which appears, *A,* ovoid in transverse section, and *B,* quadrilateral in coronal section.

is present on the external aspect of the optic vesicle. A premandibular condensation, derived from the prechordal mesoderm, is situated dorsal and caudal to the medial surface of each optic vesicle (Gilbert, 1957). Moreover, the primordium of the lateral rectus muscle appears first at horizon xiii, although it does not reach the periphery of the optic cup until three stages later *(ibid.)*.

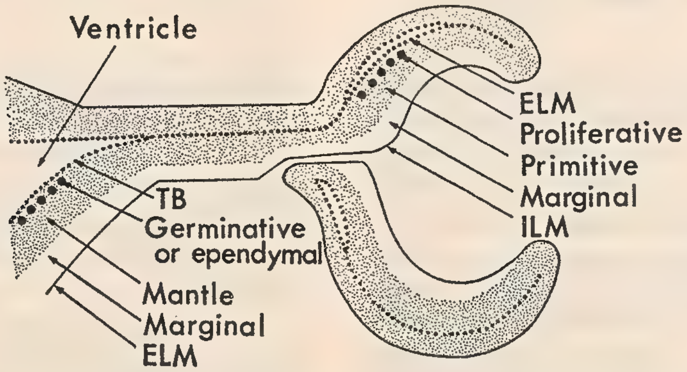

Fig. 8. Comparison of the wall of the developing neural tube and that of the optic cup. The brain wall adjacent to the ventricle is lined by a terminal bar net (TB), as is the retina (its so-called external limiting membrane, ELM), adjacent to the optic ventricle. The underlying germinative, or ependymal, layer of the brain (proliferative layer of the retina) is followed by the mantle layer (primitive layer of the retina), the marginal layer, and a basement membrane (the internal limiting membrane of the retina, ILM). Compare Da Costa (1947, his Fig. 1).

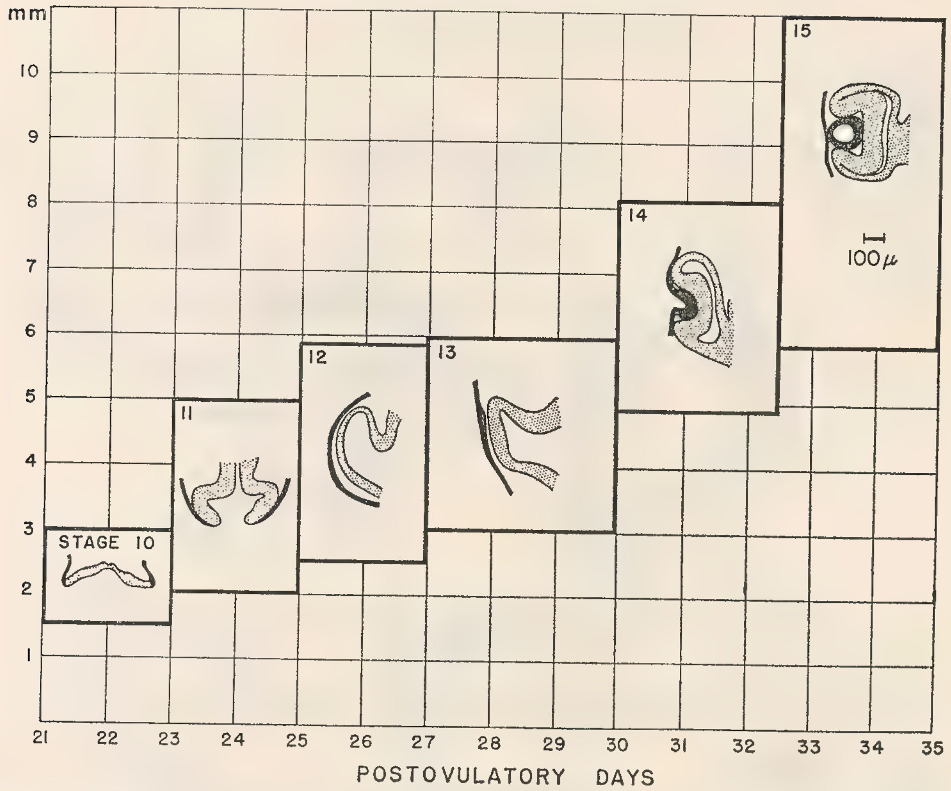

Fig. 9. Summary of development of optic vesicle and optic cup during horizons x–xv. The ordinate shows embryonic length in millimeters, and the abscissa presents embryonic age in postovulatory days. Each rectangle indicates one horizon.

HORIZON XIV, ABOUT 5 TO 8 MILLIMETERS

Specimen 2841, 5.3 Millimeters

Only very slight invagination of the retinal and lens discs is found in this specimen.

Specimen 8552, 6.5 Millimeters
(Plate 3, Fig. 23)

This has been selected as the best preserved and best Azan-stained embryo for a detailed description.

Optic cup

The optic cup measures 238 μ in anteroposterior diameter × 463 μ in equatorial diameter. Its cavity communicates widely with that of the forebrain through a short optic stalk. The caudal limiting sulcus is well marked. On its ventral aspect, the rim of the optic cup is incomplete, and the resulting groove is the retinal fissure. The capillary layer and the basement membrane *A* of the forebrain both continue onto the external layer of the optic cup. Here the capillary layer constitutes the uveocapillaris, and the basement membrane constitutes the basal lamina of the uvea. By means of the retinal fissure, capillaries enter the ventral portion of the lentiretinal space. The basal lamina of the uvea continues around the rim of the optic cup and, on the concave surface of the inverted layer, constitutes a thin internal limiting membrane of the retina. Mitotic figures are present in the optic stalk and in both layers, as well as in the rim, of the optic cup. In all these situations, the figures are close to the cavity of the stalk or the cup.

The external layer of the cup, which does not yet show pigment, contains about three rows of nuclei. It is bounded externally by the basal lamina and internally, next to the cavity, by a terminal bar net. The inverted layer of the cup, about three times as thick as the external layer, contains approximately five to six rows of oval nuclei in its external zone (Plate 3, Fig. 26). The internal zone is almost free of nuclei and presents striations at right angles to the surface that are presumably produced by cell boundaries, although some radial fibers of Müller may also be present. The inverted layer is bounded externally, next to the cavity, by a terminal bar net (the future external limiting membrane) and internally by the delicate internal limiting membrane.

Lens (Plate 3, Fig. 24)

The surface ectoderm, which is in general a simple cuboidal epithelium with a basement membrane, is

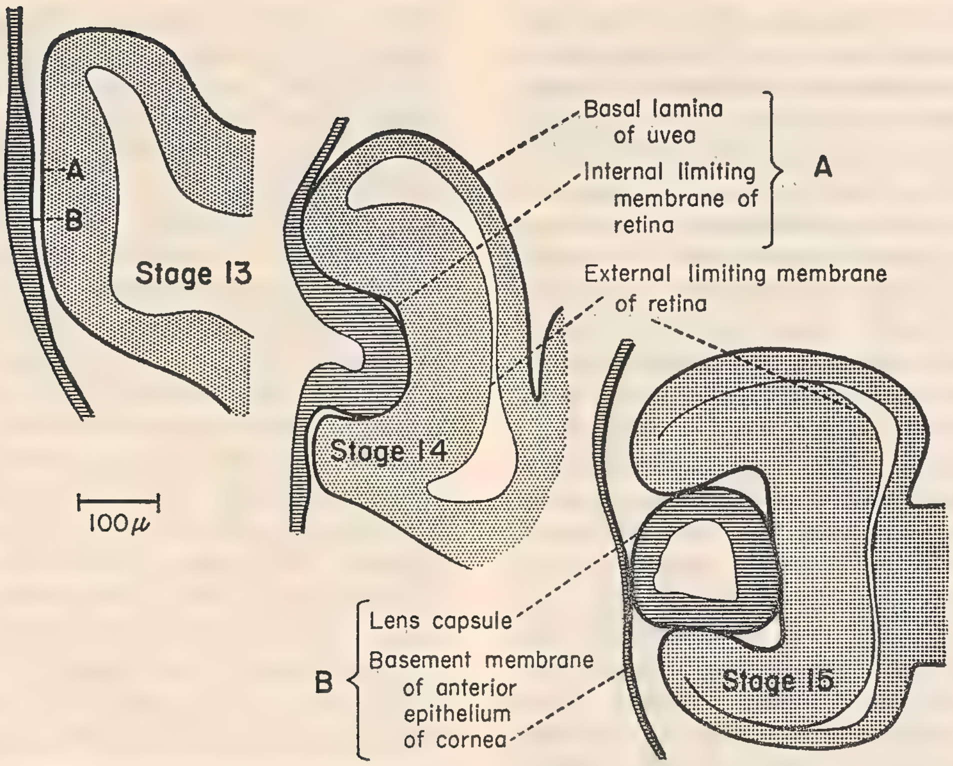
A
B
Stage 13
100μ
Stage 14
Basal lamina of uvea
Internal limiting membrane of retina
A
External limiting membrane of retina
Lens capsule
Basement membrane of anterior epithelium of cornea
B
Stage 15

Fig. 10. Basement membranes of the eye during horizons xiii–xv. At horizon xiii, a basement membrane, *A*, covers the optic vesicle, and another, *B*, lines the surface ectoderm. At horizon xiv, a portion of *A* becomes invaginated into the developing optic cup, and *B* covers the lens pit. By horizon xv, it can be seen that *A* becomes the basal lamina of the uvea and the internal limiting membrane of the retina, whereas *B* forms the lens capsule and the basement membrane of the anterior epithelium of the future cornea. By contrast, the external limiting membrane of the retina is a terminal bar net.

thickened in the region of the optic cup to form the indented lens disc. The lens pit, which is widely open to the surface, contains nuclei and cell remnants, and appears to be lined by a terminal bar net. The rim of the pit presents a sharper margin ventrally than dorsally. The lens disc contains four to five rows of nuclei, mostly oval but frequently round near the retinal aspect, and mitotic figures are present near the pit. The lens disc is lined by a basement membrane that is continuous with that of the surface ectoderm *B*.

Primary vitreous body

The lentiretinal space, narrow throughout, is occupied by a very fine feltwork of fibrils, which stain with aniline blue. Occasional mesenchymal cells are found, and, solely near the retinal fissure, capillaries are present. In extensive areas, the lens and the retina are virtually in contact, being separated only by a deep blue fibrillar band.

SPECIMEN 8999, 6 MILLIMETERS

The sagittal planes in which this embryo has been sectioned are particularly suited to an examination of the retinal fissure, which is seen to be pointing toward the heart. The fissure is confined to the optic cup and does not extend onto the stalk. The optic stalk is lined by a terminal bar net and is covered by a basement membrane that is continuous with the basal lamina of the uvea. The lens is illustrated in Plate 3, Fig. 25.

SPECIMEN 8308, 5.85 MILLIMETERS

In this sagitally sectioned embryo, it can readily be seen that the retinal fissure does not extend onto the optic stalk. This is also true of No. 8357, 6.5 mm, which is not as good a specimen.

SPECIMEN 8314, 8 MILLIMETERS

In this specimen, cone-shaped processes of the retinal and lens epithelia may be seen. They are an artifact, however, and are not found in better preserved embryos, such as No. 8552.

COMMENT ON HORIZON XIV

The cerebral vesicles appear laterally at this time and the pontine flexure begins.

Optic cup

A characteristic feature of this stage is the invagination of the retinal disc. This parallels the indentation of the lens disc, so that the optic cup is formed at the same time as the incipient lens vesicle. The optic cup comprises a thicker inverted layer (the former retinal disc) and a thinner external layer. The external layer is the future pigmented stratum of the retina and is believed to be a pseudostratified epithelium. It is characterized by the absence of a marginal zone, such as is found elsewhere in the superficial part of the wall of the neural tube. The inverted layer is the future cerebral stratum (see p. 9 for definition of this term) of the retina. Apart from the rounding of a few nuclei, little indication of cellular differentiation is apparent, although it is possible that cells of the radial fibers of Müller are present at this stage (Kornzweig, 1942). The inverted layer of the optic cup (Fig. 8), or the cerebral stratum of the retina, like the wall of the neural tube, now presents (1) a proliferative zone comparable to the germinal or ependymal zone of the neural tube, bounded externally by a terminal bar net, which is the future external limiting membrane of the retina, and presenting numerous mitotic figures; (2) a primitive zone, the mantle zone of the neural tube, containing numerous nuclei; and (3) a marginal zone, almost free of nuclei and bounded internally by the internal limiting membrane, which is the basement membrane of the neural tube. As mentioned in the discussion of the previous stage, the so-called proliferative zone is now believed to be merely the location of the mitotic phase of the underlying retinal cells.

The rim of the optic cup is incomplete ventrally and the resulting gap constitutes the retinal or optic cup fissure. This groove is generally known by the undesirable term, "choroid fissure" (see p. 9 for definition of terms), and is sometimes unsatisfactorily termed "fetal fissure," although it is found during the embryonic period. The retinal fissure is seen clearly at horizon xiv, although it is possible that an indication of it may be detected in some earlier specimens. Waterston (1914) believed he had found it in a 27-somite, therefore horizon xii, embryo, but it has been claimed that the specimen in question probably had at least 29 pairs of somites (Streeter, 1942).

Immediately in front of the optic chiasma, the neural wall presents a thin transverse strip, an "optic groove," that extends from the floor of one optic cup to that of the other. Streeter (1945) presumed that it was "associated with the formation of the choroid fissure. It is always sharply demarcated in this age group."

Lens

The lens disc shows various degrees of indentation (Streeter, 1945, his Fig. 5, xiv), forming, in the later specimens of this stage, a distinct lens pit that communicates with the exterior by means of a lens pore. As long as a lens pore is definitely open to the surface on at least one side of the body, the embryo is included in horizon xiv. During its formation, the lens pit is found to contain clumps of disintegrating cell remnants, which Streeter (1945) described as nuclear extrusions from "unwanted cells" of the lens ectoderm. Mann (1964), however, pointed out that "in man the lens pit and the commencing differentiation of the [surface] ectoderm [into epitrichial and germinative layers] appear together." She maintained that epitrichial cells are "formed on the floor of the lens pit," where they become enclosed in the cavity of the lens vesicle, whereas the lens is a derivative of the deep or so-called nervous layer of the surface ectoderm. Moreover, it has been claimed that, in Amphibia, the lens-forming cells are derived from the optic projection of the medullary plate (Chanturishvili, 1958) and hence are neurectodermal. Finally, it has been suggested that the cytolyzing cells in the cavity of the lens vesicle are important in the ontogenesis of the mammalian lens (Chanturishvili, 1958), being necessary for the attainment of adequate optical density (Stewart, 1960).

A histochemical study (McKay *et al.,* 1956) of one 6-mm and two 7-mm embryos of horizon xiv revealed ribonucleoprotein, alpha-naphthyl alkaline phosphatase, and acid phosphatase in the retina, and glycogen, glycoprotein, ribonucleoprotein, and acid phosphatase in the lens. The histochemical reactions of the retina and the lens were similar to those found at the previous stage, "except for the appearance of a hyaline material (primitive vitreous humor) between them which gives the reaction for glycoprotein" (McKay *et al.,* 1956).

Basement membranes (Fig. 10)

As mentioned on p. 18, the optic cup is covered by a basement membrane *A,* which extends around the margin of the cup and lines the inverted layer. This arrangement essentially persists in the adult, as ably described by Arey (1932), who pointed out that the internal lamella of the basal lamina (Bruch's membrane of the choroid) is "the basement membrane of the pigmented epithelium [of the retina, and that] like the internal limiting membrane it bounds the basal surface of the primary epithelium of the optic vesicle and cup, and the two are continuous around the iris margin."

In contrast, the ventricular cavity of the optic cup is lined by a terminal bar net, which is still being incorrectly described as a basement membrane, for example, by Duke-Elder and Cook (1963). As Arey correctly emphasized, in the adult the reticular or fenestrated membrane of the pigmented stratum, generally known as Verhoeff's membrane, is a "terminal bar network," as is also the external limiting membrane of the retina, which is associated with the visual cells. These findings have been confirmed in the adult human eye by means of electron microscopy (Fine, 1961).

Primary vitreous body

The slight interval (antrum of optic cup, lentiretinal space, or future vitreous cavity) between the inverted layer of the retina and the beginning lens vesicle contains a few controversial cells. These may be derived from one or both of the following sources: (1) mesenchymal cells, which may enter at the rim of the cup or may accompany the blood vessels in the retinal fissure; (2) the sheath of the optic vesicle. The first origin is favored by Bartelmez and Blount (1954), who, although they found crest cells in the dorsal limiting sulcus as late as horizon xiv, claim that, in the lentiretinal region, all crest cells degenerate and that there is "no reason to believe that any of the cells of the lateral sheath survive." According to the same authors, most of the sheath on the medial aspect of the optic cup has arisen directly from the wall of the optic vesicle and, because extensive degeneration is not found there in later stages (up to xxiii), they suggest that, "unless the crest cells of the sheath all wander away, some at least remain to enter into the formation of the uveal tunic."

Cone-shaped processes of the retinal and lens epithelia, interconnected by fine strands, have been described by various authors, such as Mann (1964), but these processes are merely a shrinkage artifact, absent in the best specimens. The lentiretinal space, however, as it becomes larger, comes to be occupied by a feltwork of fine fibrils, which are of controversial origin. The cells, fibrils, and matrix together comprise the primary vitreous body. The fibrils "could be formed from the lens [or its basement membrane] initially, the retina [or its basement membrane] all the time, and (problematically) elements of the mesoderm either derived from invaginating cells or from the hyaloid system" (Duke-Elder and Cook, 1963). Studies of the chick embryo made with the electron microscope, however, supply "no argument in favor of a secretion of the vitreous by the lens cells or by the retinal cells. The vitreous appears in the form of a granular and fibrillar material, without relationship to the nearby cells. What is involved is a phenomenon of precipitation analogous to that which takes place during the formation of collagen, of which the vitreous is merely a special form" (Brini, Porte, and Stoeckel, 1962); see also Porte, Brini, and Stoeckel (1962).

Mesoderm

The perioptic blood vessels of No. 3960 have been illustrated by Padget (1948, her Fig. 3).

The primordia of the superior rectus and superior oblique muscles appear first in embryos of horizon xiv, although the characteristic flexure of the superior oblique is not found until three stages later (Gilbert, 1957). Also in embryos of horizon xiv, four peripheral condensations appear in the mesoderm around the optic vesicle. "Toward these peripheral condensations the four rectus muscles grow, and eventually become inserted into them. It is believed that the peripheral condensations contribute to the formation [of the sclera] (Gilbert, 1957).

HORIZON XV, ABOUT 7 TO 9 MILLIMETERS

SPECIMEN 8966, 7.1 MILLIMETERS

In this sagitally sectioned specimen, a slight indication of the retinal fissure can be traced onto the distal portion of the optic stalk. The retinal fissure is directed toward the heart. The lens cavity seems to be barely closed from the surface, and the embryo apparently is early in the horizon. The external surface of the lens vesicle is studded with artifactual cones. Retinal pigment is not yet evident.

SPECIMEN 6505, 7.5 MILLIMETERS

The eye closely resembles in appearance that of No. 8997, about to be described. Under oil immersion, a few pigment granules can be detected in the external layer of the optic cup.

SPECIMEN 8997, 9 MILLIMETERS (PLATE 3, FIGS. 27, 28, AND 29)

This has been selected as the best preserved and best Azan-stained embryo for a detailed description.

Optic cup

The optic cup measures 338 μ in anteroposterior diameter × 463μ in equatorial diameter. The cup is covered by a distinct uveocapillaris in contact with the basal lamina of the uvea. The external layer of the cup shows about three rows of nuclei, and mitotic figures are found near the optic ventricle, where the layer is limited by a terminal bar net. With a high-power, dry or oil-immersion objective, it is possible to see minute circular brown pigment granules in the equatorial and lental portions of the external layer (Plate 3, Fig. 29). In this area also, the external and inverted layers are more or less in contact, thereby obliterating the optic ventricle in that region. The inverted layer of the cup has the same retinal layers as those mentioned for the previous stage. The marginal zone (Plate 3, Fig. 28), which is almost as wide as the nuclear zones, shows an occasional nucleus, which, according to Mann (1964), "may be looked on as the earliest of the ganglion cells." Most of the nuclei of the inverted layer are distinctly oval, with their long axes at right angles to the limiting membranes of the retina. Some of the nuclei stain darkly and, of those near the marginal zone, Mann (1964) considers that "from a study of the subsequent stages [apparently similar cells] can be identified as the first recognizable appearance of the fibres of Müller."

Lens (Plate 3, Fig. 28)

The lens measures 175 μ in diameter. The lens pit is closed, the wall of the lens vesicle being separate from, although making contact with, the surface ectoderm. The cavity of the vesicle contains cell remnants, and in places "unwanted" nuclei can be found apparently leaving the internal surface of the wall of the vesicle. The lens vesicle is surrounded by a capsule, stained with aniline blue, that has been derived ultimately from the basement membrane of the surface ectoderm *B.* Mitotic figures in the lens are situated generally near the internal surface of the vesicle, and this surface seems to be lined by a terminal bar net. The deep, or proximal, wall of the lens is thickened to form a lens body, in which an appreciable nucleus-free zone is present internally, that is, near the cavity of the vesicle. The elongated cells of the lens body constitute early lens fibers. The oval nuclei of the lens, about three rows throughout, are oriented radially.

Vitreous body (Plate 3, Fig. 28)

The lens and the inverted layer of the cup are practically in contact behind (*accolement polaire* of the French authors) and also at the rim of the cup. They are separated only by their apparently united basement membranes, the lens capsule and internal limiting membrane, which produce a striking blue band. Elsewhere, the thicker capsule and the delicate internal limiting membrane are separated by the lentiretinal or vitreous cavity, which contains a blue-staining matrix and fine blue fibrils. Vessels from the uveocapillaris enter through the retinal fissure, as the hyaloid artery, and independently at the rim of the optic cup, where they form an annular vessel. These two sources give rise to a prominent mass in the lentiretinal space, and this vascular mass is in intimate contact with both the capsule of the lens and the internal limiting membrane of the retina. Occasional mesenchymal cells are found in the lentiretinal cavity, and, at the antefissural rim of the optic cup, they appear to be entering from the mesenchymal sheath of the cup.

Future cornea (Plate 3, Fig. 27)

The surface ectoderm, which contains two to three rows of round nuclei, has been restored where the lens vesicle became separated from it, and the same is true of its basement membrane *B.* These layers constitute the anterior epithelium of the future cornea and its basement membrane, which, throughout development and also in the adult, remains distinct from the future anterior limiting lamina, or Bowman's membrane. At the center of the future cornea, the basement membrane is, in places, in contact with the lens capsule, whereas in other areas, it is separated from it by an occasional mesenchymal cell.

SPECIMEN 9140, 7 MILLIMETERS

Unfortunately, this Azan-stained specimen is distorted. Retinal pigment can be seen with a high (4.6-mm), dry objective.

SPECIMEN 8929, 6.35 MILLIMETERS

This Azan-stained series leaves much to be desired histologically. Under oil immersion, retinal pigment is clearly present.

SPECIMEN 8968, 8.8 MILLIMETERS

This specimen shows some shrinkage, and artifactual cones are present around the lens. Mitotic figures are well stained. Under oil immersion, pigment granules are visible in the external layer of the optic cup. The caudal limiting sulcus is evident.

COMMENT ON HORIZON XV

The *epiphysis cerebri* can be recognized at this time in the specimens of horizon XV.

Optic cup

The optic cup is separated from the brain wall by a definite optic stalk. The first indication of retinal pigmentation is found, in the form of small brown granules in the external layer of the optic cup, near the rim. The initial site of pigmentation has been variously located by different authors. Although Streeter (1948) did not acknowledge the presence of "definitive pigment [until horizon xvi], fine refractive granules that are differentiating into pigment can be seen . . . among the older members [of horizon xv]." It should be pointed out that heavy staining renders it difficult to detect the initial appearance of pigment granules unless oil immersion be employed, and, even in lightly stained specimens such as No. 8997, it is not easy to see the granules at horizon xv with a 4-mm, dry objective, much less so with one of 8 mm. Owing to the position of the retinal fissure, that portion of the inverted layer from which nerve fibers will subsequently emerge can be recognized as the region of the future optic disc, or the so-called primitive epithelial papilla, which is not, in fact, a papilla. The rim of the optic cup extends beyond the equator of the lens. Thus, Mann is incorrect in stating that at 13 mm "the margin of the optic cup does not reach beyond the equator of the lens." Duke-Elder and Cook (1963) have claimed that at first, at 8 mm, the inverted layer of the cup "shows the more rapid growth and everts itself over the edge so that the outer pigmented layer does not reach the margin."

Lens

As soon as the lens pits on both sides of the body have become closed to constitute lens vesicles, the embryo is assigned to horizon xv (Streeter, 1945). The lens vesicle is surrounded by a capsule derived from the basement membrane of the surface ectoderm *B.* The deep wall of the vesicle is thickened to form the lens body, which consists of early lens fibers. The primary lens fibers, observed in this and the succeeding stages, are derived from the deep wall of the lens vesicle. They constitute the embryonic nucleus of the lens.

A histogenetic similarity exists between (1) the formation of the lens plate (horizon xiii), pit (xiv), and vesicle (xv); and (2) the formation of the otic plate (horizon x), pit (xi–xii), and vesicle (xiii). Moreover, the similarity includes the behavior of their basement membranes (O'Rahilly, 1963). The lens has even been considered as a "sensory" structure derived from an "epibranchial placode."

Basement membranes (Fig. 10)

With the closure of the lens pit, the surface ectoderm and its basement membrane *B* are restored. The membrane persists to adulthood and constitutes the basement membrane of the anterior epithelium of the cornea.

Future cornea

The restored surface ectoderm constitutes the anterior epithelium of the future cornea.

HORIZON XVI, ABOUT 7 TO 13 MILLIMETERS

SPECIMEN 8773, 11 MILLIMETERS
(PLATE 4, FIG. 30)

This has been selected as the best preserved and best Azan-stained embryo for a detailed description.

Optic cup

The optic cup measures 425 μ in anteroposterior diameter × 575 μ in equatorial diameter. The uveocapillaris and the basal lamina of the uvea are evident. The external layer of the cup contains about three rows of nuclei, an occasional mitotic figure near the optic ventricle, and a few pigment granules that are difficult to discern except under oil immersion. The inverted layer of the cup resembles that seen in the previous stage, and mitotic figures are common near the optic ventricle. The retinal fissure is located ventral to the lens. For part of its course, the lips of the fissure are in close contact with each other and in some areas are probably fused.

Lens

The lens measures 213 × 215 μ in diameter. The wall of the lens vesicle makes contact with the surface ectoderm. The cavity of the vesicle, which is still quite large, contains cell remnants, some of which seem to be in the process of migrating from the wall. The lens capsule stains with aniline blue. The lens body is considerably thicker than that of No. 8997 of the previous stage. It contains three to four rows of more or less rectangular nuclei, and the nucleus-free zone is more evident.

Vitreous body

The lentiretinal space contains fine blue fibrils, mesenchymal cells, and perilental blood vessels. Mesenchymal cells can be seen entering the space between the lens and the rim of the optic cup.

Future cornea

This region is similar to that seen in No. 8997 of the previous stage.

SPECIMEN 9055, 10 MILLIMETERS

The rostral portion of the cup has grown sufficiently to form an obvious rostral limiting sulcus between it and the optic stalk. The retinal pigmentation is more marked than in No. 8773 and can be detected even with an 18-mm objective. The granules are most numerous between the rim of the cup and the equator and are absent near the optic stalk. The retrolental blood vessels are prominent.

SPECIMEN 8436, 10.9 MILLIMETERS

This Azan-stained specimen is unfortunately not in good histological condition. Retinal pigmentation is evident, however.

SPECIMEN 617, 7 MILLIMETERS

Shrinkage has resulted in artifactual cones around the lens. From a model of the brain it can be seen clearly that the retinal fissure is wide open in this specimen. Retinal pigmentation can be observed. The eye has been illustrated by Rones (1932) in his study of the cornea.

SPECIMENS 6507, 9 MILLIMETERS; 6509, 8.1 MILLIMETERS; 6510, 10.1 MILLIMETERS

These specimens resemble No. 8773 in general. In No. 6510, the outline of the rim of the optic cup can be seen from a model to be polygonal rather than circular or oval. This appearance was illustrated by J. F. Didusch (Streeter, 1951, his Fig. 2). Similarly, a careful examination of a model of No. 792 (also horizon xvi) suggests that the rim is pentagonal, comprising five notches, one of which leads into the retinal fissure.

SPECIMEN 6511, 8.1 MILLIMETERS

In this sagittally sectioned specimen, the retinal fissure can be seen to be present along a considerable distal portion of the optic stalk, where the hyaloid artery enters it. At the optic cup, however, the lips of the fissure are in close contact with each other, perhaps even fused, for a short distance.

SPECIMEN 8971, 10 MILLIMETERS

This specimen presents synophthalmia with two lenses and a common median wall for the two continuous optic cups (Orts Llorca, 1957).

COMMENT ON HORIZON XVI

The first cortical (hippocampal) differentiation appears at this time.

Optic cup

In the later specimens, the lips of the retinal fissure, which are also found along the distal portion of the optic stalk, may be in contact or even fused along part of their course. Retinal pigmentation is generally more marked than in the previous stage. Streeter (1948) employed "the arbitrary rule that if the pigment granules can be seen clearly with an 8-mm objective, then pigment is recorded as present [and this] definitive pigment [provides] a useful character for marking the boundary line between horizons xv and xvi." As has been mentioned earlier, however, pigmentation in the form of brown granules can be detected at the earlier stage, and it is doubtful that Streeter's rule is satisfactory as a criterion for distinguishing horizon xv from horizon xvi.

The rim of the optic cup is pentagonal, an appearance that has been investigated in detail by Lindahl (1912). Proceeding anticlockwise, the five notches in the lateral aspect of the right eye have been given the following letters: *S* for *Spalte*—i.e., the retinal fissure, *a*, *b*, *c*, and *d*. The notches develop gradually from 7.7 mm to 17.1 mm, and later the rim becomes quadrangular and then round. According to Lindahl, the notches are not caused by blood vessels, although they come to be occupied by them (Krause, 1956, his Fig. 4).

Lens

The lens vesicle resembles that seen in the previous stage. It is detached from the surface ectoderm from which it arose. The lens body, consisting of early lens fibers, although first referred to by Streeter (1948) at horizon xvi, actually can be observed at horizon xv. Retrolental or perilental blood vessels are prominent and constitute what is generally, although unsatisfactorily referred to as the vascular "capsule," or *tunica vasculosa lentis* (Dejean, 1934).

Mesoderm

The primordium of the medial rectus muscle and the common primordium of the inferior rectus and the inferior oblique appear first in embryos of this stage (Gilbert, 1957).

HORIZON XVII, ABOUT 11 TO 14 MILLIMETERS

SPECIMEN 8998, 11 MILLIMETERS (PLATE 4, FIG. 31)

This and the following specimen have been selected as the best preserved and best Azan-stained embryos for a detailed description. Although No. 8998 is probably too young to show sexual differentiation histologically in the gonads, sex chromatin is present not only in the gonads but also in various other tissues, including those of the eye—for example, lens, retina, uvea, vitreous body, and anterior epithelium of the cornea.

Optic cup

The optic cup measures 567 μ in anteroposterior diameter × 667 μ in equatorial diameter. The uveocapillaris and the basal lamina of the uvea are distinct. The retinal pigment reaches almost to the edge of the rim of the cup; it extends considerably behind the equator but is virtually absent near the optic stalk. Mitotic figures are seen in both layers of the cup but are more numerous in the inverted layer, which presents the usual zones. A few isolated oval and round nuclei are visible in the marginal zone. The lips of the retinal fissure have fused in the optic cup, so that the hyaloid artery now penetrates the cup to gain the lentiretinal space.

Lens (Plate 4, Fig. 33)

The lens measures 288 × 250 μ in diameter. Compared with the previous stage, the lens cavity is smaller, but the body is larger because of the longer lens fibers. The fibers near the equator of the lens are curved with their concavity facing the equator. The younger fibers become progressively shorter as they are traced toward the cells of the superficial wall of the lens. An appearance of nuclear extrusion from the front or superficial wall of the lens vesicle into the lens cavity can still be observed. The hyaloid vessels are intimately related to the capsule on the back or deep aspect of the lens body.

Future cornea

The anterior epithelium and the lens vesicle are more or less in contact along their basement membranes at the center. The triangular or quadrangular interval between the rim of the optic cup, the lens vesicle, and the surface ectoderm is occupied by mesoderm, continuous with that of the orbit, and by prominent annular blood vessels, continuous with those of the uveocapillaris and with the hyaloid vessels.

SPECIMEN 8789, 11.7 MILLIMETERS
(PLATE 4, FIG. 32)

Another excellent specimen for study is supplied in this example.

Optic cup

The optic cup measures 538 × 625 μ. In this sagittally sectioned series it can be seen clearly that a considerable portion of the retinal fissure is closed. Near the rim of the cup, where the fissure forms a notch (Plate 5, Fig. 34), the lips are separated by merely a few mesenchymal cells and the basement membranes, stained with aniline blue, which constitute here the junction of the basal lamina of the uvea and the internal limiting membrane of the retina (Plate 5, Fig. 35). As the sections are traced toward the optic stalk (Plate 5, Fig. 36), the external layer of the cup unites with the external, the inverted with the inverted, and the slitlike optic ventricle becomes continuous across the junctional area (Plate 5, Fig. 37). The external and inverted layers of the cup are, for the most part, in contact with each other, except near the rim, where the optic ventricle remains as a small marginal sinus. The terminal bar net of the external layer is not as prominent as that of the inverted layer. Near the junction of the optic cup and the optic stalk—toward the back of the eye—the dorsal (away from the lower limbs) portion of the inverted layer presents a distinct migration of cells from the proliferative into the marginal zone of the retina (Plate 5, Fig. 38). The cells possess round or oval nuclei. This new layer, represented in No. 8998 by merely a few isolated nuclei, is referred to by Mann (1964) as "the inner neuroblastic layer."

Optic stalk (Plate 5, Fig. 39)

The distal portion of the optic stalk presents a well-marked fissure that is continuous with the retinal fissure in the optic cup. The hyaloid artery enters the stalk fissure and is thereby conveyed into the globe. Where the fissure is present, the stalk appears crescentic in cross section and comprises an external layer and an inverted layer, which are continuous with the corresponding layers of the cup. The stalk is surrounded by a basement membrane that is continuous proximally with that around the brain and distally with the basal lamina of the uvea. The nuclei of the stalk are mostly oval and are arranged radially. Those of the inverted layer are densely stained, and this layer presents a marginal zone. The ventricle is slitlike and is lined by a terminal bar net. Mitotic figures are seen, adjacent to the ventricle, in both layers of the stalk.

Lens

The lens measures 235 × 270 μ in diameter. An appearance of nuclear extrusion is still present. In cross section, a lens fiber appears polygonal and measures approximately 6 μ in diameter.

SPECIMEN 9100, 12 MILLIMETERS

This sagittal series resembles the previous specimen, except that an internal neuroblastic migration is not evident. The lateral portion of the optic stalk and its cavity appear crescentic because of the presence of the retinal fissure in the stalk at this time.

SPECIMEN 6520, 14.2 MILLIMETERS

This is particularly suitable for the study of mitotic figures. The cup has grown in such a way that the optic stalk is now attached more or less directly in line with the center of the lens. In previous stages, the insertion of the stalk on the globe appeared to be symmetrical in coronal series but not in transverse series. The brown pigment granules are numerous in the internal portion of the external layer of the cup. They are found in clumps along the uveal margin, particularly behind the equator, the middle portion of the layer being occupied mostly by the cell nuclei. In this specimen, pigment is observed as far back as the junction of the retina and the optic stalk. In a localized dorsal (away from the lower limbs) portion of the inverted layer, a definite internal neuroblastic migration is evident. An occasional isolated nucleus is also found in the marginal zone in other areas. A reconstruction shows that the retinal fissure is closed in the optic cup.

Specimen 8118, 12.6 Millimeters

An internal neuroblastic migration is present in the marginal zone, and in this coronal series it can clearly be seen to be dorsal (away from the lower limbs) to the entrance of the hyaloid artery into the globe. Mesenchyme appears to be entering the lentiretinal space between the lens and the rim of the optic cup.

Specimen 9282, 12 Millimeters

The employment of silver in this specimen has rendered the pigment granules black, and a few granules are present in what appears to be the lateral end of the optic stalk. Although the epithelia have shrunk, the lens capsule, numerous fibrils in the vitreous body, and the internal limiting membrane of the retina are all clearly outlined. Nerve fibers are not visible in either the retina or the optic stalk. More and better silver-treated specimens at various stages should be of great benefit.

Specimen 559, 8.6 Millimeters

This presents synophthalmia with two lenses and a common median wall for the two continuous optic cups (Mall, 1917).

Comment on Horizon xvii

The fingers appear at this time. Owing to the enormous growth of the brain, the profile of the head and adjacent part of the neck equals the remainder of the body in area.

Optic cup

Retinal pigment, which is by now quite evident, is formed last near the optic stalk. In an area which may be described as dorsal (meaning on the side away from the lower limbs) of the inverted layer of the optic cup, the marginal zone of the retina presents the internal neuroblastic layer (Fig. 12). The oval nuclei of this layer are believed to belong to the radial fibers of Müller, whereas the round nuclei belong to "primitive ganglion cells" (Mann, 1964). It is difficult to state with certainty when the radial fibers can first be seen; they probably appear in the period from horizon xiv to horizon xvii. The inverted layer of the retina at horizon xiv comprises proliferative, primitive, and marginal zones. In horizon xvii, the proliferative zone is still evident, and most of the primitive zone remains as the external neuroblastic layer. Many cells, however, have migrated from the primitive into the marginal zone to form the internal neuroblastic layer, and the two neuroblastic layers are separated by a temporary part of the marginal zone. Thus, in the most differentiated area of the retina, the inverted layer of No. 6520 includes the following: proliferative zone, containing the mitotic figures; external neuroblastic layer—greater part of primitive zone; transient fiber layer of Chievitz—remains of marginal zone; and internal neuroblastic layer—migration from primitive zone into marginal zone. The lips of the retinal fissure have fused in the optic cup. The external layer unites with the external, and the inverted layer with the inverted. The bridge between the two layers, which results from the fusion of the lips of the fissure, disappears. The statement that fusion "of course must occur before the internal limiting membrane is differentiated along the margins of the cleft" (Mann, 1964) is incorrect.

Lens

The lens body has become wider anteroposteriorly, so that the cavity of the lens vesicle is frequently crescentic. The nuclei of the lens vesicle, which in transverse and coronal series formed a circle in horizons xv and xvi, change from O (No. 8998) to D (No. 8118) during horizon xvii. The straight limb of the D, which occupies the lens body, soon becomes indented (No. 6520) to form a "nuclear bow."

HORIZON XVIII, ABOUT 12 TO 17 MILLIMETERS

Specimen 8355, 15 Millimeters

This and No. 9247, next to be described, both of which are particularly suitable for following the course of blood vessels, are the best specimens available at this stage.

Optic cup

The optic cup measures 500 μ in anteroposterior diameter × 600 μ in equatorial diameter. In front of the equator, the pigment granules are located chiefly internal to the nuclei; behind the equator, although the granules are found both external and internal to the nuclei, an aggregation, or "crust," is evident along the uveal (external) margin. In the inverted layer of the cup, the marginal zone is still approximately the same width as the nuclear zones. The internal neuroblastic migration is still localized.

Lens

The lens measures 213 × 200 μ in diameter. The lens fibers are distinct, and the nuclei of the lens body, comprising about five rows, form a curve, or nuclear bow, that is convex toward the crescentic lens cavity. It appears that cellular remnants are still being extruded from the front wall, the epithelium, of the lens. The hyaloid vessels are closely related to the lens capsule behind.

Future cornea

The surface ectoderm comprises a superficial squamous layer of cells and a deeper cuboidal layer lying on the basement membrane. The underlying mesenchyme extends between the surface ectoderm and the lens, where it forms a double row of flattened cells in the center. Between the rim of the cup and the lens, where the prominent annular vessel is found, a considerable quantity of mesenchyme appears to be entering the lentiretinal space.

SPECIMEN 9247, 15 MILLIMETERS
(PLATE 6, FIG. 40)

This sagittal series shows clearly the transition from the open portion, a notch at the cupolar margin, to the closed portion of the retinal fissure. The external layer fuses with the external, the inverted with the inverted, and the bridge of tissue between the external and inverted layers disappears rapidly. At the point of contact, the basement membranes disintegrate. The distribution of pigment described in the previous specimen is also observed here (Plate 6, Fig. 42). Mitotic figures are still evident in the proliferative zone of the inverted layer. Although not as common, they can be observed also in the external, pigmented, layer. A terminal bar net is distinct only in the inverted layer, that is, at the site of the future external limiting membrane. The internal neuroblastic layer is definite but is still localized; although it is more extensive than that seen in No. 8789 of the previous stage, its position is similar. Cellular remnants are noticeable in the lens cavity, and the lens capsule is well developed (Plate 6, Fig. 41). At least a double row of mesenchymal cells is placed between the lens and the overlying surface ectoderm. Eyelid folds are distinct.

SPECIMEN 6528, 13.4 MILLIMETERS

In this coronal series, the internal neuroblastic layer, which is again located dorsally, extends rostrally also. In addition, a more or less separate mass is present caudally, so that the internal neuroblastic migration is basically U shaped, the open end being ventral. The lens nuclei form the letter D, and the lens cavity is becoming crescentic.

SPECIMENS 8812, 12.9 MILLIMETERS;
6524, 11.7 MILLIMETERS;
6527, 14.4 MILLIMETERS

These specimens are in transverse series. In all three, the internal neuroblastic layer is fundamentally U shaped. The caudal limbs—those along the neuraxis toward the midbrain—are connected by the original dorsal migration to the rostral limbs—those in a straight line toward the spinal cord. The rostral is more massive than the caudal limb of the U. In No. 8812, the U is almost closed. Breaks in the U in Nos. 6524 and 8812 suggest that several waves of migration from the primitive zone into the marginal zone are involved in the formation of the new layer. The lens nuclei of No. 8812 form a D, whereas the vertical limb of the D is bowed in the other two specimens. The cavity of the lens vesicle is virtually closed in No. 6527, although a few cell remnants intervene between the lens epithelium and the lens body. Specimen 8812 was associated with maternal rubella.

COMMENT ON HORIZON XVIII

The embryos of this stage closely resemble the more advanced specimens of the previous stage in their external appearance.

Optic cup

The formation of the optic cup and the retinal fissure is summarized in Fig. 11. At horizon xviii, behind the equator, a crust of pigment granules is found along the uveal margin of the external layer of the cup. In the inverted layer, the internal neuroblastic layer is more extensive, and the original dorsal migration develops rostral and caudal limbs (Fig. 12).

An instance of cyclopia with one continuous retina and no lenses has been described in a 16.5-mm embryo at this stage (Orts Llorca, 1955).

Lens

The nuclei of the lens continue their change from the letter D to a condition in which the vertical limb of the D is bowed. The crescentic cavity of the lens vesicle becomes occupied by the primary lens fibers and is obliterated in the most advanced specimens. The lens cavity is at first circular (horizon xv), and then D shaped (xv–xvii), crescentic (xvii–xviii), slitlike (xviii–xix), and closed (xx–xiii). The lens nuclei at first form a cricle (horizons xv–xvii), then a letter D (xvii–xviii), and finally a nuclear bow (xvii–xxiii). Glycogen granules have been reported in the lens epithelium of a human embryo of 15 mm (Sundberg, 1924).

Future cornea

Mesenchyme has invaded the interval between the lens epithelium and the surface ectoderm. This has been referred to as "the first step in the formation of the cornea" (Streeter, 1951). In a published photomicrograph (Streeter, 1948, his Fig. 31) of No. 6527, the mesenchymal cells nearest the lens appear to be condensing into a mesothelium, although it is possible that this appearance is artifactual.

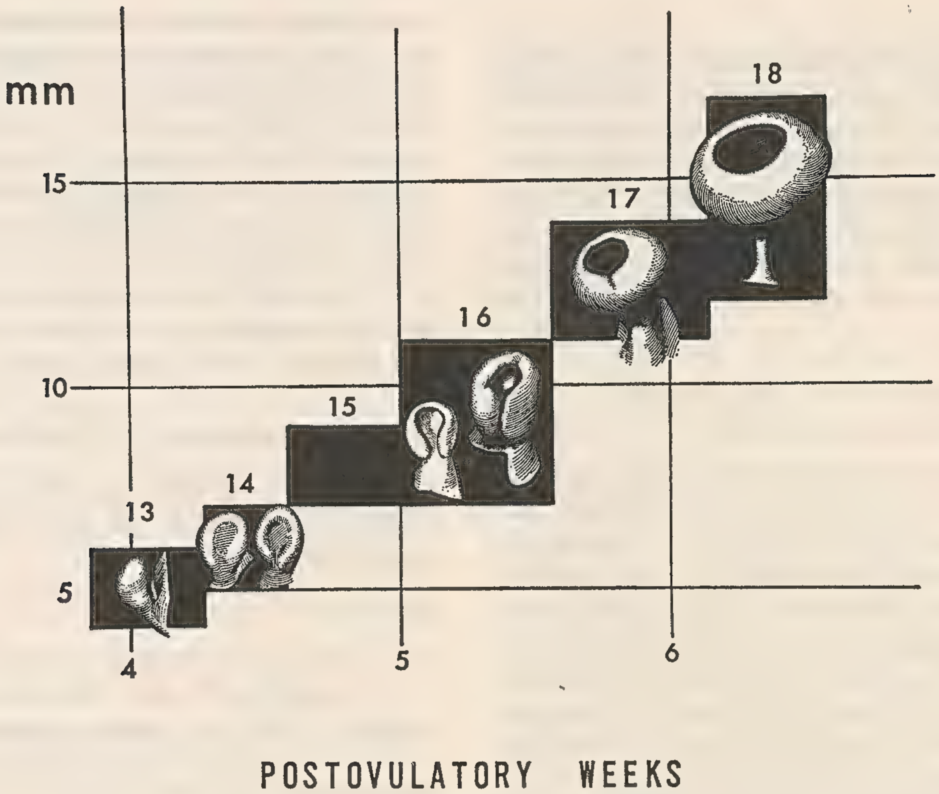

Fig. 11. Summary of development of optic cup and retinal fissure during horizons xiii–xviii. The transformation of the optic vesicle into the optic cup can be followed. The individual drawings were made originally by the late James F. Didusch (see Streeter, 1951, his Fig. 2).

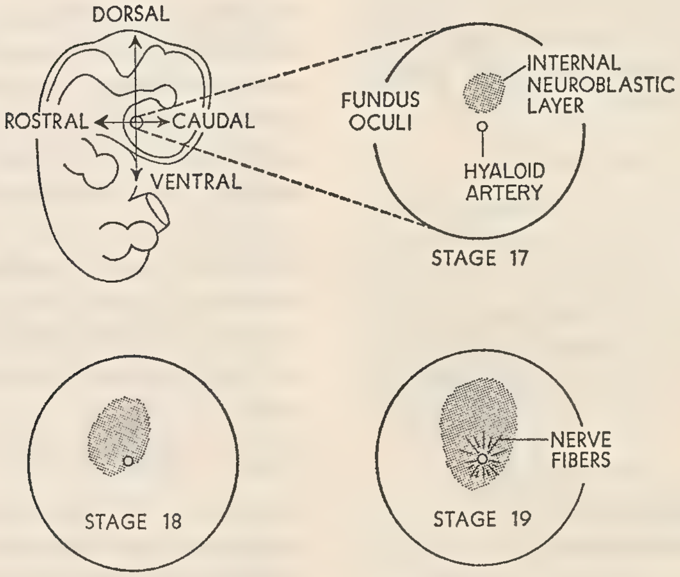

Fig. 12. Development of internal neuroblastic and optic nerve-fiber layers of retina during horizons xvii–xix. At horizon xvii, the dorsal portion of the inverted layer of the optic cup presents a cellular migration (shaded area) from the proliferative into the marginal zone of the retina. The migrated cells form the internal neuroblastic layer. At horizon xviii, the layer develops rostral and caudal limbs. At horizon xix, the internal neuroblastic layer surrounds the entrance of the hyaloid artery into the globe, and nerve fibers are present. Rostral, caudal, dorsal, and ventral here relate to the markedly curved neuraxis. The illustration is based partly on Mann (1964, her Fig. 109).

HORIZON XIX, ABOUT 16 TO 19 MILLIMETERS

SPECIMEN 9325, 17 MILLIMETERS
(PLATE 6, FIG. 43)

This is the most satisfactory specimen available at this stage.

Optic cup

The optic cup measures 800 × 767 μ. The uveocapillary lamina and the basal lamina of the uvea are evident, as they have been since their initial appearance. In the external layer of the cup, the crust of pigment is visible (Plate 6, Fig. 47), particularly behind the equator. The pigment cells no longer appear to be limited internally by a terminal bar net. Across the slitlike optic ventricle, the inverted layer of the cup comprises a terminal bar net, the future external limiting membrane; proliferative zone, containing mitotic figures; external neuroblastic layer; transient fiber layer; internal neuroblastic layer; and internal limiting membrane. The internal neuroblastic layer is most prominent dorsally, and it now surrounds the entrance of the hyaloid artery into the globe. The rostral side of the internal neuroblastic plaque is continuous, but the opposite, or caudal, side appears to be deficient in small areas. Many of the ganglion cells of this layer give rise to optic nerve fibers (Plate 6, Fig. 46) that form the beginning of a delicate layer in the retina and then proceed toward the optic stalk, where, in the absence of techniques based on silver, they become difficult to trace.

The cavity of the stalk is almost entirely closed. The retinal fissure is open only on the ventral aspect of the insertion of the optic stalk into the globe, where apparently an eversion of the inverted layer has occurred along the lips of the fissure (Plate 6, Fig. 45). The everted margins, which are covered by the transition from the internal limiting membrane to the basal lamina of the uvea, are almost devoid of pigment granules and form a sharp junction with the pigmented external layer of the cup. The everted lips allow the passage of the hyaloid artery into the globe and then fuse ventrally, forming a protuberance of nonpigmented cells.

Lens

The lens measures 350 × 338 μ in diameter. It shows a fairly spacious, perhaps artifactually enlarged, crescentic cavity in which cellular remnants are visible. Mitotic figures are evident in the lens epithelium. The lens capsule and the internal limiting membrane of the retina are attached to fine fibrils that traverse the vitreous body. The lens fibers are polygonal on cross section.

Future cornea

The plane of the sections is not favorable, but mesenchymal cells are present between the anterior epithelium and the lens.

SPECIMEN 9097, 21 MILLIMETERS

The optic cup measures 633 × 833 μ. Mitotic figures are seen in both layers of the cup. In the external layer, the crust of pigment is marked, especially behind the equator. The internal neuroblastic layer encircles the entrance of the hyaloid artery. It is most extensive dorsally (away from the lower limbs), where nerve fibers are easily found issuing from ganglion cells and proceeding toward the optic stalk. The lens measures 288 × 313 μ in diameter. Its cavity is a crescentic slit (Plate 6, Fig. 44), and it still contains nuclear remains. The lens epithelium contains about two rows of nuclei, whereas the lens body has approximately four. The axial fibers are straight; the younger fibers nearer to the equator are concave. In the future cornea, two rows of flat mesenchymal cells are found between the anterior epithelium and the lens. Eyelid folds are distinct.

SPECIMEN 9113, 18.5 MILLIMETERS

The internal neuroblastic layer, which is heavily stained in this specimen, encircles the hyaloid artery and is most dense dorsally. Optic nerve fibers are present. A few pigment granules are visible in some of the cells of the optic stalk.

SPECIMEN 8965, 19.1 MILLIMETERS

This is a suitable specimen for observing the distribution of pigment. The internal neuroblastic layer is well developed and nerve fibers, although poorly stained, can be seen. Eversion of the lips of the retinal fissure near the optic stalk is noticeable. The cavity in the stalk is virtually closed, and a few pigment granules are occasionally seen in some of the stalk cells. The future cornea resembles that of No. 9097.

SPECIMEN 5609, 18 MILLIMETERS

The lens cavity is probably completely closed, except for an artifactual shrinkage of the lens body in a few sections. Two layers of flat mesodermal cells line the anterior epithelium of the future cornea.

SPECIMENS 4501, 18 MILLIMETERS;
8092, 16.3 MILLIMETERS

No. 4501 is very weakly stained; No. 8092 is grossly overstained.

Comment on Horizon xix

The clavicle and mandible begin to ossify at this time or at one stage earlier or later.

Optic cup

The internal neuroblastic layer now surrounds the entrance of the hyaloid artery into the globe (Fig. 12). Some of the constituents of the internal neuroblastic layer, namely, the ganglion cells, give rise to optic nerve fibers, which proceed toward and reach the optic stalk. According to Bartelmez and Dekaban (1962), "no optic fibers have as yet reached the chiasma, but many nerve fibers are present in the postoptic component [of the optic stalk]. . . . Many fine fibers of the postoptic system are present on the caudal surface of the primordium chiasmatis; in the more advanced embryos of the group a few coarser retinal fibers have reached its rostral surface." Gilbert (1935) found optic fibers decussating beneath the chiasmatic plate at 18 mm. Ventral to the insertion of the optic stalk into the globe, the lips of the retinal fissure are everted and form a nonpigmented protuberance. This appearance is not seen in later stages; according to Mann, "the cells composing it rapidly become pigmented and by 20 mm no trace of it remains." The lumen of the optic stalk is practically closed along a considerable portion of its length.

The functional significance of the retinal fissure in relation to the optic nerve fibers is well summarized by Mann (1964): "If invagination of the cup had occurred symmetrically from its outer side, without formation of a cleft, there would have been no direct continuity between the inner (retinal) layer and the stalk, so that nerve fibers developing on the inner surface of the cup would have had no direct path back to the brain."

Lens

The slitlike cavity either is still noticeably open or is virtually closed.

Future cornea

About two layers of flat mesenchymal cells are located between the anterior epithelium and the lens. The formation of the mesothelium from these cells takes place during horizons xix–xxi (Plate 6, Fig. 44).

HORIZON XX, ABOUT 18 TO 23 MILLIMETERS

Specimen 8226, 18 Millimeters

This is the most satisfactory specimen available at this stage.

Optic cup

The optic cup, which is distorted, measures 1,067 × 800 μ. Mitotic figures are rare in the pigmented layer. The pigmented and inverted layers are in contact for most of their extent. The caudal side of the internal neuroblastic layer is deficient. The nerve fibers now occupy a definite layer but they remain a slight distance from the internal limiting membrane. Close to this membrane are radially arranged striations, presumably due now to the radial fibers of Müller. Tangential sections (12-2-5, 13-1-1, and 20-2-4) through the external limiting membrane show a netlike arrangement, although the precise structural components and possible contents are difficult to interpret.

As the hyaloid artery is traced medially, it becomes surrounded by the nerve-fiber layer of the retina. Medial to the termination of the internal neuroblastic layer, a few cells are seen in the nerve-fiber layer. Although their nuclei stain more lightly, these cells appear from their location to have been derived from the external neuroblastic layer of the retina. The cells remain sparse and do not yet form a cluster (Bergmeister's papilla) around the hyaloid artery. As a group, they are continuous with the cells found in the more central portion of the optic stalk. The cavity of the stalk is obliterated. A cellular sheath surrounds the stalk (Plate 7, Fig. 49).

Lens (Plate 7, Fig. 48)

The lens measures 413 μ in diameter. The lens cavity is closed. Retrolental blood vessels are well marked.

Vitreous body

In addition to blood vessels and blue fibrils, the vitreous body contains a number of cells, which present lightly staining oval nuclei containing one or two red nucleoli.

Future cornea

Two or three rows of more or less flat mesenchymal cells are present between the anterior epithelium and the lens (Plate 7, Fig. 48). At least the most deeply situated of these cells are those of the developing mesothelium of the future anterior chamber. All three layers—anterior epithelium, mesenchyme, and epithelium of lens—are essentially in contact. A thick cellular condensation around the optic cup is probably, at least in part, the developing sclera.

Specimen 5537, 22 Millimeters

Nerve fibers can, with some difficulty, be traced from the retina along the optic stalk and to the brain, as was done by Streeter (1951), who apparently managed this feat also in No. 6426, 21.5 mm.

SPECIMEN 4148, 21 MILLIMETERS

The eyes of this embryo show considerable shrinkage. According to Rones (1932), who described and illustrated the cornea, "a narrow space . . . filled with fine fibrillae" is present between the epithelium and the mesothelium. This slight interval in the developing cornea is presumably the postepithelial layer of Hagedoorn.

SPECIMEN 4059, 21.6 MILLIMETERS

The eyes of this embryo show considerable shrinkage. The cornea comprises anterior epithelium, postepithelial layer, and mesothelium. Flat mesenchymal cells from the periphery have begun to invade the postepithelial layer. They are presumably the so-called corneal corpuscles entering the *substantia propria.* Peripherally, the mesothelium is continuous with a mass of cells, the *amas stratifié* of Leplat (1912), or the so-called *endothélium stratifié* of Gabriélidès (1895), which appears in turn to be continuous with the scleral condensation. Behind the mesothelium, an interrupted line of mesodermal cells associated with some fibrils has been identified as "the beginning of the pupillary membrane" by Rones (1932), who described and illustrated the cornea of this embryo.

SPECIMENS 460, 21 MILLIMETERS; 462, 20 MILLIMETERS; 966, 23 MILLIMETERS; 5537, 22 MILLIMETERS; 6202, 21 MILLIMETERS; 7274, 18.5 MILLIMETERS; 7906, 19.5 MILLIMETERS; 8157, 20.8 MILLIMETERS

All these specimens, formerly graded "excellent," were examined for the cornea but were found to be of unsatisfactory quality.

COMMENT ON HORIZON XX

A subcutaneous vascular plexus is first noticeable grossly on the sides of the head at this stage.

Optic cup

The retina presents a definite nerve fiber layer, and the nerve fibers reach the brain. The cavity of the optic stalk and that of the lens are obliterated. The inverted layer of the retina (No. 5537) is about 115 μ thick. Mann records 190 μ at 21 mm and 200 μ in the adult, pointing out that "practically no increase in actual thickness of the retina occurs after the 21-mm stage, further growth being in area only."

With regard to the external limiting membrane, in a 21-mm embryo, Mann saw fine filaments "definitely reaching across the remains of the cavity of the primary optic vesicle" and was willing to identify them as "the outer limbs of the rods." As many filaments described by Mann are artifacts, however, judgment on this question is best reserved for the present. In the region of the internal limiting membrane, end feet, as drawn by Mann at 12 mm and at 17 mm, are not evident in No. 8226.

Lens

The formation of a lens suture appears to be beginning at this stage. In the French monograph, Dejean (Dejean *et al.,* 1958) illustrated a lens suture posteriorly at 22 mm, and Y sutures were found apparently both anteriorly and posteriorly at 30–31 mm. Yamasaki (1957) found the first sign of star formation posteriorly at about 25 mm and anteriorly not until after 32 mm.

Future cornea

Further sections of exceptional quality in the last five horizons (xix–xxiii) will be needed before a definitive account of the developing human cornea can be provided. In horizons xviii and xix, mesenchymal cells come to line the anterior epithelium. According to Streeter (1951), by horizon xx, "the cells on the internal surface begin to arrange themselves in the form of a mesothelium. [This becomes] a definite layer in the next group (xxi). . . ." The specimens available at present suggest that the looser mesenchyme seen at horizon xviii becomes, during horizons xix–xxi, "condensed" to form the mesothelium. A slender interval, the postepithelial layer, in which fine fibrillae may be seen, is generally found between the anterior epithelium and the mesothelium. This is the basis of the *substantia propria* of the cornea.

HORIZON XXI, ABOUT 22 TO 24 MILLIMETERS

SPECIMEN 9614, 22.5 MILLIMETERS

This is the most satisfactory specimen available at this stage. It was associated with maternal rubella.

Optic cup

The optic cup measures 1,033 × 900 μ. The cytological preservation leaves something to be desired, but the layers resemble those described for the previous stage. In this and in the next specimen, where the pigmented and inverted layers of the cup are separated from each other, it is difficult to decide to what degree the separation is artifactual, and it seems hazardous to attempt to identify structural specializations on the external surface of the inverted layer. The internal neuroblastic layer extends approximately to the equator of the globe. The optic stalk contains nerve fibers that reach the brain, but it no longer displays a cavity. Eversion of the inverted layer, as seen at the previous stage, is not observed in either this or No. 8553.

Lens

The lens measures 500 × 567 μ in diameter. It is surrounded by a distinct blue capsular membrane. Lens sutures seem to be present.

Cornea

The cornea comprises (1) the anterior epithelium; (2) the *substantia propria,* or postepithelial layer, now containing blue fibrils and mesenchymal cells (corneal corpuscles); and (3) the mesothelium, mostly a single layer of cuboidal and flat cells that is continuous with the stratified mass of cells at the periphery. The mass of cells is in turn continuous with the scleral condensation, which is thick and cellular, and is found particularly in the equatorial region and from there forward. At the central portion of the cornea, the postepithelial layer is still acellular. Behind the cornea are found (1) the beginning anterior chamber, (2) the blue and mostly acellular pupillary membrane, and (3) the capsule and the epithelium of the lens.

SPECIMENS 8553, 22 MILLIMETERS; 1358*F*, 23 MILLIMETERS; 2937, 24.2 MILLIMETERS

Most of the postepithelial layer of the cornea contains mesenchymal cells. The cornea of No. 2937 has been illustrated by Rones (1932), who adds that "this increase [in mesodermal cells] is the result both of the penetration from the peripheral mesodermal mass and of an actual proliferation of cells in situ, as can be proved by the mitotic figures seen."

SPECIMENS 7254, 22.5 MILLIMETERS; 7392, 22.7 MILLIMETERS; 7864, 24 MILLIMETERS

These remaining specimens, graded "excellent," were examined for the cornea but were found to be of unsatisfactory quality.

COMMENT ON HORIZON XXI

The changes between this and the previous stage are slight, at least externally.

Cornea

Cells begin to invade the postepithelial layer, thereby converting it into the *substantia propria corneae.* A cornea may be said to be present now that the anterior epithelium is lined by the *substantia propria* and the mesothelium. The *amas stratifié*—the peripheral continuation of the mesothelium—the anterior chamber, and the pupillary membrane are more easily recognizable than their precursors at the previous stage. Rones (1932) has pointed out that "the formation of the pupillary membrane is entirely independent of the development of the cornea."

HORIZON XXII, ABOUT 23 TO 28 MILLIMETERS

SPECIMEN 4339, 24.5 MILLIMETERS

This is the only Mallory-stained specimen at this stage. Unfortunately, considerable shrinkage has taken place.

Optic cup

The optic cup measures 1,017 × 1,150 μ. It has been mentioned already that the nerve fibers in the retina, as they move backward toward the optic stalk, leave free a narrow interval adjacent to the internal limiting membrane. Near the entrance of the hyaloid artery into the vitreous cavity, this narrow zone, free of nerve fibers, contains a cluster of nuclei. This aggregation of cells is known as Bergmeister's papilla.

Lens

The lens measures 438 × 476 μ.

Cornea

The anterior epithelium of the cornea includes a surface layer of flat nuclei, lying generally on a cuboidal and a columnar layer. The columnar layer rests on a distinct basement membrane. The *substantia propria* contains about eight rows of flat cells, in addition to numerous blue fibrils. The mesothelium, a single layer of mostly cuboidal cells, appears at least in places to be limited in front by a basement membrane. The pupillary membrane is associated with some cells derived apparently from those that line the back of the *amas stratifié* and that enter the vitreous cavity between the lens and the rim of the optic cup.

SPECIMEN 8394, 25.3 MILLIMETERS

The optic cup measures 1,400 × 1,433 μ. Mitotic figures are still plentiful in the proliferative zone of the inverted layer. At the optic disc, Bergmeister's papilla is present. The lens measures 600 × 700 μ in diameter. At the central portion of the cornea, the *substantia propria* has not yet been invaded by cells.

SPECIMEN 8120, 23.4 MILLIMETERS (PLATE 7, FIG. 50)

Optic cup

The optic cup measures 1,217 × 1,117 μ. As the hyaloid artery is traced medially, it becomes surrounded by a ring of cells (Bergmeister's papilla) located in the nerve-fiber layer.

Lens

The lens measures 567 × 600 μ in diameter. Lens sutures appear to be present.

SPECIMENS 1458, 27.5 MILLIMETERS; 4638, 23.4 MILLIMETERS; 6832, 25.8 MILLIMETERS

These remaining specimens, graded "excellent," were examined but were found to leave much to be desired as regards quality. Variation was noted in the extent of cellular spread into the *substantia propria* of the central portion of the cornea, and in the degree of development of the cells of Bergmeister's papilla. In one specimen (No. 4638), some blood vessels appeared to be associated with the pupillary membrane. In No. 6832, the paraxial lens fibers are concave toward the axis, so that a change in curvature is seen between the paraxial and the equatorial fibers. A similar appearance was noted in another embryo (No. 3681) at this stage, and a suggestion of the arrangement was seen in a specimen (No. 1358*F*) at the previous stage.

COMMENT ON HORIZON XXII

The eyelids, "which have been gradually thickening . . . are now rapidly encroaching upon the eyeballs" (Streeter, 1951).

Optic cup

The cells of Bergmeister's papilla are seen in some eyes at this stage. The formation of the papilla is accounted for by Mann (1964) as follows: "When the first nerve fibres appear these grow towards the epithelial papilla and pass through its substance into the inner layer of the optic stalk. Most of the cells of the primitive epithelial papilla disappear as the nerve fibres increase in number, but a few of them remain in the centre of the nervous papilla, separated by the nerve fibres from their fellows in the retinal layers around the papilla. . . . These sequestrated cells come to form a little cone-shaped mass of nuclei in the centre of the disc. This cone is known as Bergmeister's papilla." It is clear, however, that Mann's account needs to be modified because the nervous disc is present (at horizon xx) *before* Bergmeister's papilla develops (at horizon xxii).

The fate of Bergmeister's papilla is described by Mann: "The cells forming the papilla are glial in nature and proliferate during the 5th month to form the glial sheath of the hyaloid artery. . . . This sheath and the papilla of Bergmeister atrophy with the hyaloid before birth. The exact amount of atrophy determines the depth of the 'physiological cup' in the centre of the disc, this being the depression left by the absorption of the cone of cells." In the avian eye the cells of Bergmeister's papilla proliferate considerably and form most of the pecten oculi (O'Rahilly and Meyer, 1961).

Lens

Because the paraxial fibers are concave toward the axis, a change in curvature, the *Randwirbel* of Schwalbe, is seen between the paraxial fibers constituting the embryonic nucleus of the lens, and the equatorial or secondary fibers initiating the development of the fetal nucleus of the lens. The *Randwirbel* has been illustrated at 25 mm by Yamasaki (1957).

Cornea

The cellular invasion of the *substantia propria* is complete in some eyes at this stage; in others an acellular portion of the postepithelial layer is still present at the central part of the cornea.

Sclera

According to Streeter (1951), "the substantia propria of the cornea is continuous with a condensed band of mesenchyme which gradually spreads backward to enclose the eyecup. This primitive scleral condensation is present in embryos belonging to all the last five horizons," i.e., xix–xxiii. Actually, as can be seen clearly from Streeter's Fig. 6, the scleral band is continuous not with the *substantia propria* but with the *amas stratifié,* and hence with the mesothelium. Moreover, it is difficult to ascertain when first a scleral condensation is present. Its visibility depends partly on the thickness and staining of the section. Thus, in embryo 9247 of horizon xviii, little indication is seen in a thin section (42-3-5), but condensed tissue is evident in a nearby thicker section (43-1-1). Furthermore, much or most of the condensed mesenchyme around the eye is that for the developing muscles of the globe. Thus Gilbert (1957) found four peripheral condensations in horizon xiv, situated around the periphery of the optic cup. In later stages, the four rectus muscles grow toward these condensations "and eventually become inserted into them. It is believed that the peripheral condensations contribute to the formation" of the sclera. By horizon xxii, "the peripheral condensations into which the four rectus muscles insert have spread over the optic vesicle [cup] to form part of the sclera."

HORIZON XXIII, ABOUT 27 TO 31 MILLIMETERS

SPECIMEN 4570, 30.7 MILLIMETERS

Optic cup

The optic cup measures 1,933 × 1,867 μ.

Lens

The lens measures 567 × 733 μ in diameter. Lens sutures are present anteriorly and posteriorly.

The cornea of this embryo (Plate 7, Fig. 51); of No. 4525, 30 mm; and of No. 5725, 23 mm (illustrated by Rones, 1932), resembles that of No. 4289. The retinas of these embryos are of rather poor histological quality.

SPECIMEN 7425, 27 MILLIMETERS

The lens is surrounded by a narrow, refractile, eosinophil capsular membrane. The lens epithelium consists of one or two rows of cuboidal cells, and the lens fibers are numerous and well formed. Beginning behind the equator of the lens, the epithelial nuclei spread out into a broad nuclear band, convex forward. Posteriorly, the lens is loosely invested by perilental blood vessels and mesenchymal cells. The frontal bone has begun to ossify, although not yet in the roof of the orbit.

SPECIMEN 4289, 32.2 MILLIMETERS

The cornea comprises (1) the anterior epithelium, which consists of one or two rows of squamous cells, a cuboidal or columnar row, and a basement membrane; (2) the *substantia propria,* which includes many rows of flat mesenchymal cells, arranged in parallel rows in meridional sections but presenting a criss-cross pattern in tangential sections; and (3) the mesothelium, mostly a single row of flat or cuboidal cells, possibly resting anteriorly on a basement membrane. Peripherally, the mesothelium becomes continuous with the *amas stratifié.* No indication of the anterior (Bowman's membrane) or the posterior (Descemet's membrane) limiting lamina is observed. Behind the cornea, the pupillary membrane consists chiefly of flat mesenchymal cells and blood vessels. The eyelids have not yet fused.

SPECIMEN 9226, 31 MILLIMETERS

This Azan-stained specimen is included here under horizon xxiii, that is, at the termination of the embryonic period proper, because in neither humerus is the collar eroded completely through, even though small groups of cells are in the process of invading the bone collar. In other words, the embryo has not quite attained that stage when the onset of marrow formation in the humerus can be recognized, at which time such a "specimen is straightaway classed as a fetus, and this places it beyond the bounds of our embryonic horizons" (Streeter, 1949). A detailed description of the eye is provided not only because it marks the end of the embryonic period but also because of its exceptional histological quality.

Optic cup (Plate 8, Fig. 52)

The optic cup measures 1,533 × 1,767 μ. The uvea comprises the uveocapillary lamina and the basal lamina. The uveocapillaris extends forward to the rim of the cup, where the basal lamina becomes less noticeable but appears to be continuous with the internal limiting membrane of the retina. The external layer of the optic cup is heavily pigmented. The nuclei of the cells are basal in position, and the pigment is most dense internal to the row of nuclei. However, a pigment crust is also found, particularly in front of the equator. The pigment extends as far as the rim of the optic cup, where the granules become sparser. Except where artifactual separation has occurred, the cavity of the cup is obliterated. The inverted layer (Plate 8, Fig. 53) comprises the future external limiting membrane; the proliferative zone, which still contains mitotic figures both at the fundus and near the rim; the external neuroblastic layer; the transient fiber layer, ill defined; the internal neuroblastic layer; the nerve-fiber layer; and the internal limiting membrane (Plate 9, Fig. 56).

The internal neuroblastic layer extends only a short distance beyond the equator, and the nerve-fiber layer is narrow. The nuclei of the external neuroblastic layer are generally dark staining and oval, whereas those of the internal neuroblastic layer are mostly light staining and are either round or oval. Radial fibers of Müller can be detected in the retina, and it is possible that foot-pieces are present. Processes of visual cells, however, are not in evidence. At the junction of the retina and the optic nerve, the pigmented and the cellular layers end abruptly, but the external limiting membrane and the basal lamina are reflected posteriorly and become lost in the sheath of the optic nerve. At the optic disc, the internal limiting membrane is also reflected posteriorly, and it becomes lost in the sheath of the hyaloid artery. Bergmeister's papilla is noticeable (Plate 8, Fig. 54). Most of its nuclei are dark staining and oval, resembling those of the external neuroblastic layer. Where the optic nerve joins the optic cup, a few of the cells within the nerve appear to have a transverse orientation, thereby possibly presaging the development of the *lamina cribrosa.* The optic nerve is surrounded by a cellular sheath, which contains blue fibrils (Plate 8, Fig. 55).

Lens (Plate 9, Figs. 57–59)

The lens measures 833 × 1,000 μ in diameter. A distinct blue capsular membrane is present, and perilental blood vessels are prominent (Fig. 57, Plate 9). The lens epithelium is simple cuboidal in shape. Lens sutures are present anteriorly and posteriorly. The lens fibers are shown in Plate 9, Fig. 58.

Vitreous body (Plate 9, Fig. 56)

The vitreous body consists of numerous fine blue fibrils, blood vessels, and mesenchymal cells. Some indications of the secondary vitreous body can be seen.

At the angle between the equator of the lens and the optic cup, fibrils may be traced backward into the vitreous cavity (Plate 9, Fig. 57). These constitute the "marginal bundle," or *faisceau isthmique,* of Druault.

Cornea and sclera

The structure of the cornea (Plate 9, Fig. 59) resembles that already described in No. 4289. The anterior epithelium contains two to three rows of nuclei. The outermost cells are mostly squamous, the innermost generally columnar and resting on a distinct basement membrane. The fibrils of the *substantia propria* stain prominently with aniline blue. The blue coloration is more noticeable in the posterior two thirds of the *substantia,* as if the fibrils were thicker there. Up to about 15 rows of flat mesenchymal cells are present between the fibrils. Peripherally, the *substantia* becomes continuous with episcleral and scleral tissues. The mesothelium is typically a single row of squamous and cuboidal cells and seems to lie anteriorly on a basement membrane. The mesothelium is continuous peripherally with the *amas stratifié,* which is lined by loose tissue from which the pupillary membrane is derived. The pupillary membrane consists of flat mesenchymal cells and blue fibrils. Between the lens and the rim of the optic cup, mesenchymal cells and blood vessels escape into the vitreous cavity. The *amas* is continuous peripherally with uveal (choroid) or suprachoroid tissue. The sclera comprises numerous flat mesenchymal cells and fine blue fibrils. The eyelids have not fused centrally. The frontal bone is undergoing ossification in the roof of the orbit.

COMMENT ON HORIZON XXIII

This group marks the termination of the embryonic period proper. The embryo is about 30 mm in CR length and is approximately 56 postovulatory days in age (Olivier and Pineau, 1962). Streeter (1951) listed 47 days, a figure generally considered to be too low. The beginning of the fetal period is indicated, after horizon xxiii, by "an arbitrary boundary-line," namely, the onset of marrow formation in the humerus (Streeter, 1949).

An example of synophthalmia with two lenses and a common median wall for the two continuous optic cups has been described in a 25-mm embryo at this stage (Orts Llorca, 1955).

Optic cup

The heavy pigmentation in the external layer of the optic cup makes it difficult to assess the degree of cell division. It has been claimed, however, by Duke-Elder and Cook (1963) that "the mitotic activity is intensively maintained until about the end of the eighth week (30 mm.)...."

The development of the percipient elements has been reviewed recently by Duke-Elder and Cook (1963). Some workers believe that the optic ventricle is at first lined with cilia, which, "it seems possible, although it is not certain" (Duke-Elder and Cook), develop into the outer limbs of the rods and cones. Thus Mann (1964) identified cilia at 4.5 mm and at 21.0 mm, and claimed that these filaments "can be taken to represent the outer limbs of the rods." In the opinion of the present writer, the optic ventricle is lined by a terminal bar net, and the above account of the initial appearance of the processes of the visual cells is not convincing. In the more cautious presentation of Bach and Seefelder (1914), the processes are shown first appearing well within the fetal period. Electron microscopy should be of considerable aid in elucidating the early development of the rods and cones.

Vitreous body

The primary, or hyaloid, vitreous body forms at about horizon xiv. The secondary, or definitive, vitreous body develops as a finer though denser layer in contact with the internal surface of the retina. Its first appearance is illustrated by Dejean (his Fig. 261) at 32 mm, where it is continuous with the fibrils between the equator of the lens and the optic cup, the *faisceau isthmique* of Druault.

DISCUSSION

The relationship of the present findings to those of previous investigators has already been presented in the form of a series of comments after the description of each developmental stage. Hence only some general concluding remarks are needed here.

The foregoing detailed account of ocular development during the first two months of prenatal life has been made possible by (1) the examination of a large number of exceptionally well-preserved specimens, and (2) the employment of embryonic staging. In the opinion of the writer, staging provides an invaluable frame of reference in following the precise sequence in development of one organ throughout a series of embryos, in establishing the chronology of development, in assessing the development of one organ in relation to that of another, and in comparing a given embryo with other staged specimens already described. Furthermore, in experimental animals (Table 1), staging based on external characteristics leads to precise knowledge of the degree of both internal and external development—ophthalmic, for example—reached by a given embryo when an experimental procedure is applied. Moreover, the data are essential in determining which chemical substances may be related to specific morphogenetic phases of the eye. In summary, correlations between internal ophthalmic development and external embryonic staging are a necessary structural prelude to the experimental embryology, teratogenesis, and developmental histochemistry and ultrastructure of the eye.

The development of the eye presents a number of common basic features throughout various classes of vertebrates. The eye of the chick embryo has been investigated in considerable detail, and many similarities to, as well as some differences from, the conditions in the human visual organ can be found by examining Table 5. In later development, certain differences become more readily apparent—for example, the formation of the pecten in the avian eye.

The development of the human eye during the embryonic period proper is summarized in Table 6. It can be seen that, beginning at three postovulatory weeks of age, the eye over a period of eight weeks attains a high degree of development and by two prenatal months has acquired the main features characteristic of the adult organ. In the case of the following, however, development is largely, if not exclusively, confined to the fetal rather than the embryonic period: rods and cones, macula and *fovea centralis,* ciliary body, ciliary zonule, iris, *sinus venosus sclerae,* and anterior and posterior limiting laminae of the cornea.

TABLE 5. Comparative Sequential Development of Human Eye and Eye of Chick

Feature	Homo, horizon	Gallus,* stage
Cranial flexure	x	10
Optic primordium and optic sulcus	x	?
Optic vesicle	xi	9
Caudal limiting sulcus	xi	11
Closure of rostral neuropore	xi	11–12
Retinal and lens discs	xiii	12
Marginal zone in retinal disc	xiii	none
Uveocapillary lamina	xiii	before 16
Invagination of retinal and lens discs; optic cup and retinal fissure	xiv	14
Retinal pigmentation	xv	21
Lens vesicle closed	xv	17
Lens body; lens fibers	xv	17
Vessel in retinal fissure	xv	17
Perilental blood vessels	xvi	none
Closure of retinal fissure	xvi–xvii	*ca.* 25
Internal neuroblastic layer in retina	xvii	34 ?
Ganglion cells in retina	xvii–xviii	18–22
Nerve fibers in retina	xix	18
Annular lens pad	none	18–19
Mesothelium of anterior chamber	xix–xxi	21–22
Scleral condensation	*ca.* xix–xxii	24
Bergmeister's papilla	xxii	26

* Data are based mostly on O'Rahilly and Meyer (1959).

SUMMARY

More than 100 serially sectioned human embryos from 1½ to 32 mm CR in length served as the material for the study of the development of the eye during the first two months of prenatal life.

All the embryos studied were staged according to Streeter's developmental horizons (x–xxiii), and the importance of embryonic staging has been stressed throughout. The development is described at each horizon, and comments that include references to the relevant literature are provided after the description of each stage.

The optic primordium and the optic sulcus appear first at horizon x (three postovulatory weeks), the retinal and lens discs at horizon xiii (4 weeks), the optic cup at horizon xiv (4½ weeks), and the lens vesicle and the retinal pigment at horizon xv (5 weeks).

Other features are summarized in Table 6.

ACKNOWLEDGMENTS

The writer is indebted to Dr. James D. Ebert, Director of the Department of Embryology, Carnegie Institution of Washington, for facilities provided, and to both Dr. Ebert and Dr. Mary Rawles for their interest throughout the work.

The assistance of a Special Research Fellowship, BT–744, from the United States Public Health Service and of a Research Grant, NB–04426, from the National Institutes of Health is gratefully acknowledged.

TABLE 6. SUMMARY OF EARLY DEVELOPMENT OF HUMAN EYE

Horizon	Somites or Length, mm	Features
	Somites	
ix	1–3	Neural folds arise.
x	4–12	Optic primordium and optic sulcus appear in neural fold of forebrain at 8 somites. The two primordia meet at the *torus opticus* (primitive chiasma ridge).
xi	13–20	Rostral neuropore closes. Optic evagination is produced at optic sulcus at 14 somites. Cavity (optic ventricle) is continuous with that of forebrain. Lateral wall of evagination is at first in contact with surface ectoderm. Wall of optic evagination contributes neural crest to its mesenchymal sheath (from about 14–16 somites onward). Sheath then separates evagination from overlying ectoderm. Optic evagination constitutes optic vesicle (about 17–19 somites). Caudal limiting sulcus develops between optic evagination and brain.
xii	21–29	Optic neural crest formation reaches its maximum and optic vesicle becomes covered by a complete sheath.
	Mm	
xiii	4–6	Retinal disc (future inverted layer of optic cup) and lens disc appear and are in contact. Marginal zone appears in retinal disc. Optic vesicle is covered by a basement membrane, and surface ectoderm is lined by a basement membrane.
xiv	5–8	Uveocapillary lamina is defined. Retinal disc is invaginated to form optic cup, and retinal fissure is delineated. Inverted layer of cup comprises a terminal bar net (future external limiting membrane), mitotic phase (proliferative zone), intermitotic phase (primitive zone), marginal zone, and an internal limiting membrane. Lens disc becomes indented to form a lens pit, into which cell remnants are extruded.
xv	7–9	Primary vitreous body begins to form in lentiretinal space. Retinal pigment appears in external layer of cup. Lens pit has closed to form lens vesicle, surrounded by lens capsule. Lens body appears and consists of early lens fibers. Lens cavity more or less circular. Hyaloid artery enters lentiretinal space through retinal fissure.
xvi	7–13	Optic stalk is definite. Rim of optic cup is pentagonal. Lips of retinal fissure may be in contact or even fused.
xvii	11–14	Perilental blood vessels are prominent. Internal neuroblastic layer is formed by internal migration into marginal zone of retina. Latter then constitutes the transient fiber layer. Retina comprises the so-called proliferative zone, external neuroblastic layer, transient fiber layer, and internal neuroblastic layer. Cavity of lens vesicle becomes at first D shaped (xv–xvii), then crescentic (xvii–xviii). Lens nuclei form at first a circle (xv–xvii), then a D (xvii–xviii), and finally a nuclear bow (xvii–xxiii).
xviii	12–17	Internal neuroblastic layer is U shaped. Cavity of lens vesicle becomes obliterated by primary lens fibers. Mesenchyme invades interval between lens epithelium and surface ectoderm.
xix	16–19	Eyelid folds are distinct. Internal neuroblastic layer encircles entrance of hyaloid artery to globe. Ganglion cells give rise to optic nerve fibers. Lips of retinal fissure are temporarily everted near optic stalk.
xx	18–23	Mesothelium of future cornea begins to form (xix–xxi). Nerve fiber layer appears in retina. Nerve fibers reach brain. Cavity of optic stalk is obliterated. Lens cavity is obliterated. A lens suture begins to form. Future cornea comprises anterior epithelium, acellular postepithelial layer, and mesothelium.
xxi	22–24	Cells begin to invade postepithelial layer, converting it into *substantia propria.*
xxii	23–28	*Amas stratifié,* pupillary membrane, and anterior chamber develop (xx–xxi). Bergmeister's papilla is present in optic disc of some eyes. *Substantia propria* is cellular throughout in some eyes. Scleral condensation is more definite than in previous few stages.
xxiii	27–31	Secondary lens fibers are forming. Optic cup measures *ca.* 1.5–2.0 mm in diameter, and lens *ca.* 0.5–1.0 mm. Retina comprises pigmented layer, external limiting membrane, proliferative zone, external neuroblastic layer, transient fiber layer, internal neuroblastic layer, nerve fiber layer, and internal limiting membrane. Secondary vitreous body is forming. Frontal bone begins to ossify.

LITERATURE CITED

Arey, L. B. 1932. Retina, chorioid and sclera. In *Special Cytology,* E. V. Cowdry, ed., Hoeber, New York, 2nd edition, Vol. *3.*

Armstrong, P. B. 1962. *Stages in the Development of Ictalurus nebulosus.* Syracuse University Press, Syracuse, N. Y.

Atwell, W. J. 1930. A human embryo with seventeen pairs of somites. *Carnegie Inst. Wash. Publ.* 407, *Contrib. Embryol., 21,* 1–24.

Bach, L., and R. Seefelder. 1914. *Atlas zur Entwicklungsgeschichte des menschlichen Auges.* Engelmann, Leipzig, Germany.

Bartelmez, G. W., and M. P. Blount. 1954. The formation of neural crest from the primary optic vesicle in man. *Carnegie Inst. Wash. Publ.* 603, *Contrib. Embryol., 35,* 55–71.

Bartelmez, G. W., and A. S. Dekaban. 1962. The early development of the human brain. *Carnegie Inst. Wash. Publ.* 621, *Contrib. Embryol., 37,* 13–32.

Bartelmez, G. W., and H. M. Evans. 1926. Development of the human embryo during the period of somite formation, including embryos with 2 to 16 pairs of somites. *Carnegie Inst. Wash. Publ.* 362, *Contrib. Embryol., 17,* 1–67.

Brini, A., A. Porte, and M.-E. Stoeckel. 1962. Étude au microscope électronique de quelques problèmes d'embryologie oculaire chez l'embryon de poulet à des stades précoces. *Bull. Mem. Soc. Franc. Ophtalmol., 75,* 192–209.

Chanturishvili, P. S. 1958. The role of ectoderm in the development of the crystalline lens. *Trans. Ophthalmol. Soc. U.K., 78,* 411–438.

Cohen, A. I. 1961. Electron microscopic observations of the developing mouse eye. I. Basement membranes during early development and lens formation. *Develop. Biol., 3,* 297–316.

Corner, G. W. 1929. A well-preserved human embryo of 10 somites. *Carnegie Inst. Wash. Publ.* 394, *Contrib. Embryol., 20,* 81–101.

Da Costa, A. C. 1947. Sur quelques faits cytologiques de l'histogénèse de la rétine. *Acta Anat., 4,* 79–86.

Dandy, W. E. 1910. A human embryo with seven pairs of somites measuring about 2 mm. in length. *Am. J. Anat., 10,* 85–108.

Davis, C. L. 1923. Description of a human embryo having twenty paired somites. *Carnegie Inst. Wash. Publ.* 332, *Contrib. Embryol., 15,* 1–51.

Dejean, C. 1923. Rôle du feuillet moyen dans l'assemblage des premières ébauches de l'oeil. *Compt. Rend. Acad. Sci. (Paris), 177,* 220–222.

Dejean, C. 1934. La capsule du cristallin. Son développement—sa nature. *Compt. Rend. Assoc. Anat., 29,* 206–219.

Dejean, C., F. Hervouët, and G. Leplat. 1958. *L'embryologie de l'oeil et sa tératologie.* Masson, Paris.

Dufaure, J. P., and J. Hubert. 1961. Table de développement du lesard vivipare: Lacerta (Zoctoca) vivipara Jacquin. *Arch. Anat. Microscop. Morphol. Exptl., 50,* 309–327.

Duke-Elder, S., and C. Cook. 1963. Normal and abnormal development. In *System of Ophthalmology,* S. Duke-Elder, ed., Kimpton, London, Vol. *3.*

'Espinasse, P. G. 1962. The regeneration of the lens and its initial development. *Exptl. Eye Res., 1,* 466–467.

Fine, B. S. 1961. Limiting membranes of the sensory retina and pigment epithelium. *Arch. Ophthalmol., 66,* 847–860.

Froriep, A. 1906. Die Entwicklung des Auges der Wirbeltiere. In *Handbuch der Vergleichenden und experimentellen Entwicklungslehre der Wirbeltiere,* O. Hertwig, ed., Fischer, Jena, Germany, Vol. *2,* Part 2.

Gabriélidès, A. 1895. Recherches sur l'embryogénie et l'anatomie comparée de l'angle de la chambre antérieure chez le poulet et chez l'homme. Muscle dilatator de la pupille. *Arch. Ophtalmol. (Paris), 15,* 176–193.

Gallien, L., and O. Bidaud. 1959. Table chronologique du développement chez Triturus helveticus Razoumowsky. *Bull. Soc. Zool., 84,* 22–32.

Gallien, L., and M. Durocher. 1957. Table chronologique du développement chez Pleurodeles waltlii Michah. *Bull. Biol., 91,* 97–114.

Gilbert, M. S. 1935. The early development of the human diencephalon. *J. Comp. Neurol., 62,* 81–115.

Gilbert, P. W. 1957. The origin and development of the human extrinsic ocular muscles. *Carnegie Inst. Wash. Publ.* 611, *Contrib. Embryol., 36,* 59–78. .

Groth, W. 1939. Der Ursprung der Labyrinthplacode und des Ganglion statoacusticum im Vergleich zur Genese des Riechorgans beim Kaninchen. *Z. mikr.-anat. Forsch., 45,* 393–442.

Hamburger, V., and H. L. Hamilton. 1951. A series of normal stages in the development of the chick embryo. *J. Morphol., 88,* 49–92.

Heuser, C. H. 1930. A human embryo with 14 pairs of somites. *Carnegie Inst. Wash. Publ.* 414, *Contrib. Embryol., 22,* 135–153.

Heuser, C. H., and G. W. Corner. 1957. Developmental horizons in human embryos. Description of age group x, 4 to 12 somites. *Carnegie Inst. Wash. Publ.* 611, *Contrib. Embryol., 36,* 29–39.

Hunt, H. H. 1961. A study of the fine structure of the optic vesicle and lens placode of the chick embryo during induction. *Develop. Biol., 3,* 175–209.

Källén, B. 1955. Cell degeneration during normal ontogenesis of the rabbit brain. *J. Anat. (London), 89,* 153–161.

Keibel, F. 1912. The development of the sense-organs. In *Manual of Human Embryology,* F. Keibel and F. P. Mall, ed., Lippincott, Philadelphia, Vol. *2.*

Keibel, F., and C. Elze. 1908. Normentafel zur Entwicklungsgeschichte des Menschen. *Normentafeln zur Entwicklungsgeschichte der Wirbelthiere,* F. Keibel, ed., Fischer, Jena, Germany, Part 8.

Koecke, H.-U. 1958. Normalstadien der Embryonalentwicklung bei der Hausente (Anas boschae domestica). *Embryologia (Nagoya), 4,* 55–78.

Kopsch, F. 1952. *Die Entwicklung des brannen Grasfrosches (Rana fusca Roesel).* Thieme, Stuttgart, Germany.

Kornzweig, A. L. 1942. Development of human eye at five and five-tenths millimeter embryonic stage. *Arch. Ophthalmol. (New York), 28,* 670–678.

Krause, W. 1956. Zur Entwicklungsgeschichte der Arteria ophthalmica beim Menschen. *Z. Anat. Entwicklungsgeschichte, 119,* 311–334.

Laguesse, E. 1923. Les lamelles primitives de la cornée du poulet sont, comme le corps vitré, d'origine mésostromale ectodermique. *Compt. Rend. Soc. Biol. (Paris), 89,* 543–546.

Leplat, G. 1912. Recherches sur le développement et la structure de la membrane vasculaire de l'oeil des oiseaux. *Arch. Biol., 27,* 403–524.

Lindahl, C. 1912. Über die Pupillaröffnung des Augenbechers in früheren Entwicklungsstadien, mit besonderer Rücksicht auf die Bedeutung der Formverhältnisse derselben für unsere Auffassung von der Entstehung der Iriskolobome. *Arch. Augenheilk., 72,* 213–260.

Mall, F. P. 1917. Cyclopia in the human embryo. *Carnegie Inst. Wash. Publ.* 226, *Contrib. Embryol., 6,* 5–33.

Mann, I. 1964. *The Development of the Human Eye.* 3rd edition, British Medical Association, London.

McKay, D. G., E. C. Adams, A. T. Hertig, and S. Danziger. 1955. Histochemical horizons in human embryos. I. Five millimeter embryo—Streeter horizon xiii. *Anat. Record, 122,* 125–151.

McKay, D. G., E. C. Adams, A. T. Hertig, and S. Danziger. 1956. Histochemical horizons in human embryos. II. 6 and 7 millimeter embryos—Streeter horizon xiv. *Anat. Record, 126,* 433–463.

McKeehan, M. S. 1951. Cytological aspects of embryonic lens induction in the chick. *J. Exptl. Zool., 117,* 31–64.

Miller, D. C. 1939. A table for the normal development of Rana pipiens. *Proc. Indiana Acad. Sci., 48,* 209–214.

Mori, T. 1959. Histochemical studies on the distribution of alkaline phosphatase in early human embryos. II. Observations on an embryo with 13–14 somites. *Arch. Histol. (Okayama), 18,* 197–209.

Nieuwkoop, P. D., and J. Faber, eds. 1956. *Normal Table of Xenopus laevis (Daudin).* North-Holland Publishing Company, Amsterdam.

Okada, Y. K., and M. Ichikawa. 1947. A new normal table for the development of Triturus pyrrhogaster Boie. *Exptl. Morphol. (Tokyo), 3,* 1.

Olivier, G., and H. Pineau. 1962. Horizons de Streeter et âge embryonnaire. *Compt. Rend. Assoc. Anat., 47,* 573–576.

O'Rahilly, R. 1962. The initial membranes of the eye in staged human embryos (abstract). *Anat. Record, 142,* 263–264.

O'Rahilly, R. 1963. The early development of the otic vesicle in staged human embryos. *J. Embryol. Exptl. Morphol., 11,* 741–755.

O'Rahilly, R. 1965. The optic, vestibulocochlear, and terminal-vomeronasal neural crest in staged human embryos. In *Second Symposium on Eye Structure,* J. W. Rohen, ed., Schattauer-Verlag, Stuttgart, Germany.

O'Rahilly, R., and D. B. Meyer. 1959. The early development of the eye in the chick, *Gallus domesticus* (stages 8 to 25). *Acta Anat.,* 36, 20–58.

O'Rahilly, R., and D. B. Meyer. 1960. The periodic acid-Schiff reaction in the cornea of the developing chick. *Z. Anat. Entwicklungsgeschichte, 121,* 351–368.

O'Rahilly, R., and D. B. Meyer. 1961. The development and histochemistry of the pecten oculi. In *The Structure of the Eye,* G. K. Smelser, ed., Academic Press, New York.

Orts Llorca, F. 1955. Le cerveau et l'oeil de deux embryons humains cyclopes de 37 et 45 jours. *Acta Anat., 23,* 379–385.

Orts Llorca, F. 1957. Der Nervus opticus (Fasciculus opticus) und die Fissura chorioidea bei Zyklopie. *Acta Anat., 30,* 565–574.

Padget, D. H. 1948. The development of the cranial arteries in the human embryo. *Carnegie Inst. Wash. Publ.* 575, *Contrib. Embryol., 32,* 205–261.

Payne, F. 1925. General description of a 7-somite human embryo. *Carnegie Inst. Wash. Publ.* 361, *Contrib. Embryol., 16,* 115–124.

Politzer, G. 1928. Über einen menschlichen Embryo mit 18 Ursegmentpaaren. *Z. Anat. Entwicklungsgeschichte, 87,* 674–727.

Politzer, G. 1930. Über einen menschlichen Embryo mit sieben Urwirbelpaaren. *Z. Anat. Entwicklungsgeschichte, 93,* 386–428.

Pollister, A. W., and J. A. Moore. 1937. Tables for the normal development of Rana sylvatica. *Anat. Record, 68,* 489–496.

Porte, A., A. Brini, and M.-E. Stoeckel. 1962. La formation du vitré chez l'embryon de poulet. Étude au microscope électronique. *Compt. Rend. Soc. Biol. (Paris), 156,* 909–911.

Rones, B. 1932. Development of the human cornea. *Arch. Ophthalmol. (New York), 8,* 568–575.

Rosenbauer, K. A. 1955. Untersuchung eines menschlichen Embryos mit 24 Somiten, unter besonderer Berücksichtigung des Blutgefässsystems. *Z. Anat. Entwicklungsgeschichte, 118,* 236–276.

Sauer, M. E., and A. C. Chittenden. 1959. Deoxyribonucleic acid content of cell nuclei in the neural tube of the chick embryo: evidence for intermitotic migration of nuclei. *Exptl. Cell Res., 16,* 1–6.

Schulte, H. von W., and F. Tilney. 1915. Development of the neuraxis in the domestic cat to the stage of twenty-one somites. *Ann. N. Y. Acad. Sci., 24,* 319–346.

Shumway, W. 1940. Stages in the normal development of Rana pipiens. I. External form. *Anat. Record, 78,* 139–147.

Sondermann, R. 1949. Über die Entwicklung des Hornhautendothels. *Arch. Ophthalmol. (Berlin), 149,* 690–694.

Stewart, D. S. 1960. Further observations on regenerated crystalline lenses in rabbits, with special reference to their refractive qualities. *Trans. Ophthalmol. Soc. U.K., 80,* 357–372.

Streeter, G. L. 1942. Developmental horizons in human embryos. Description of age group xi, 13 to 20 somites, and age group xii, 21 to 29 somites. *Carnegie Inst. Wash. Publ.* 541, *Contrib. Embryol., 30,* 211–245.

Streeter, G. L. 1945. Developmental horizons in human embryos. Description of age group xiii, embryos about 4 or 5 millimeters long, and age group xiv, period of indentation of the lens vesicle. *Carnegie Inst. Wash. Publ.* 557, *Contrib. Embryol., 31,* 27–63.

Streeter, G. L. 1948. Developmental horizons in human embryos. Description of age groups xv, xvi, xvii, and xviii, being the third issue of a survey of the Carnegie collection. *Carnegie Inst. Wash. Publ.* 575, *Contrib. Embryol., 32,* 133–203.

Streeter, G. L. 1949. Developmental horizons in human embryos (fourth issue). A review of the histogenesis of cartilage and bone. *Carnegie Inst. Wash. Publ.* 583, *Contrib. Embryol., 33,* 149–167.

Streeter, G. L. 1951. Developmental horizons in human embryos. Description of age groups xix, xx, xxi, xxii, and xxiii, being the fifth issue of a survey of the Carnegie collection. Prepared for publication by Chester H. Heuser and George W. Corner. *Carnegie Inst. Wash. Publ.* 592, *Contrib. Embryol.*, *34*, 165–196.

Streiter, A. 1951. Ein menschlicher Keimling mit 7 Urwirbelpaaren. *Z. mikr.-anat. Forsch.*, *57*, 181–248.

Sundberg, C. 1924. Das Glykogen in menschlichen Embryonen von 15, 27 und 40 mm. *Z. Anat. Entwicklungsgeschichte*, *73*, 168–246.

Taylor, A. C., and J. J. Kollros. 1946. Stages in the normal development of Rana pipiens larvae. *Anat. Record*, *94*, 7–23.

Waterston, D. 1914. A human embryo of twenty-seven pairs of somites imbedded in decidua. *J. Anat. (London)*, *49*, 90–118.

Wen, I. C. 1928. The anatomy of human embryos with seventeen to twenty-three pairs of somites. *J. Comp. Neurol.*, *45*, 301–376.

West, C. M. 1930. Description of a human embryo of eight somites. *Carnegie Inst. Wash. Publ.* 407, *Contrib. Embryol.*, *21*, 25–35.

Yamasaki, Y. 1957. Über die Entwicklung der Linsensterne bei den menschlichen Embryonen. *Yokohama Med. Bull.*, *8*, 251–283.

Zacchei, A. M. 1961. Le sviluppo embrionale della quaglia giapponese (Coturnix coturnix japonica T. e S.). *Arch. Ital. Anat. Embriol.*, *66*, 36–62.

PLATES

PLATE 1, Figs. 13–19

The photomicrographs in the following plates were made by Richard Grill.

The photomicrographs are oriented in such a way that either the ventral or the rostral aspect is facing downward on the plate. Approximately ×200.

Fig. 13. The optic primordia appear (at bottom) as bilateral thickenings of the neural folds. Horizon x, No. 1201, section 4-1-3.

Fig. 14. The shallow optic sulcus (indicated by arrow) is visible at right. Horizon x, No. 5074, section 1-2-8.

Fig. 15. The optic sulcus (indicated by arrow) is visible in oblique section toward lower left corner. The neural groove at lower right corner indicates the median plane. Horizon x, No. 3707, section 1-1-13.

Fig. 16. Walls forming the optic sulci are in contact with the surface ectoderm. Upper half of the photomicrograph shows the midbrain, from which some neural crest cells are emerging. Optic sulcus is indicated by arrow. Horizon xi, No. 6344, section 2-5-5.

Fig. 17. The optic vesicles are now defined, and the rostral neuropore is evident. Optic neural crest cells are emerging from the caudal aspect of the optic vesicles. Horizon xi, No. 7611, section 1-3-11.

Fig. 18. The rostral neuropore has closed, although the neuroporal suture can be identified (at bottom). The preoptic forebrain, or telencephalon medium, is visible. The sheath of the optic vesicle separates the vesicle from the overlying ectoderm. A group of crest cells can be seen migrating laterally from the optic vesicle, at right. Horizon xii, No. 8943, section 2-3-2.

Fig. 19. The optic vesicle displays a well-marked caudal limiting sulcus. Horizon xii, No. 8941, section 2-7-7.

13

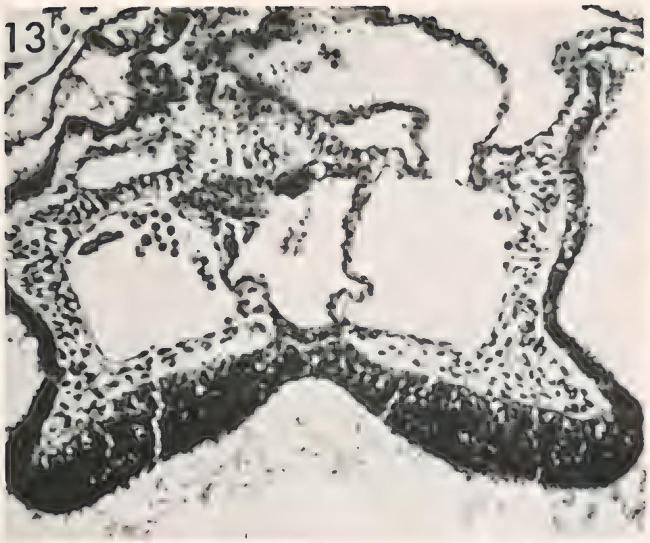

14

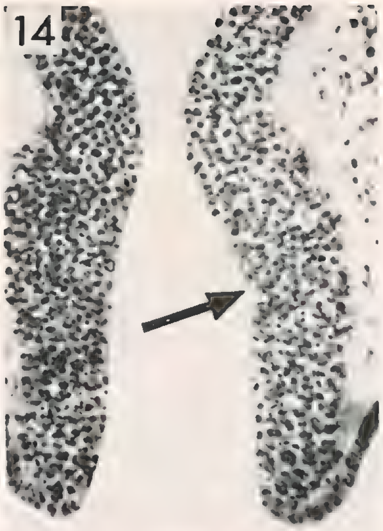

15

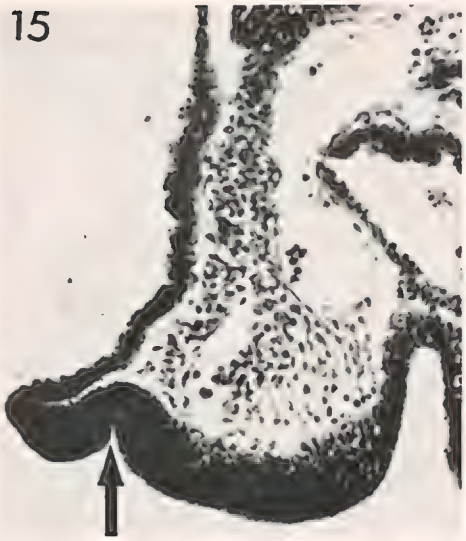

16

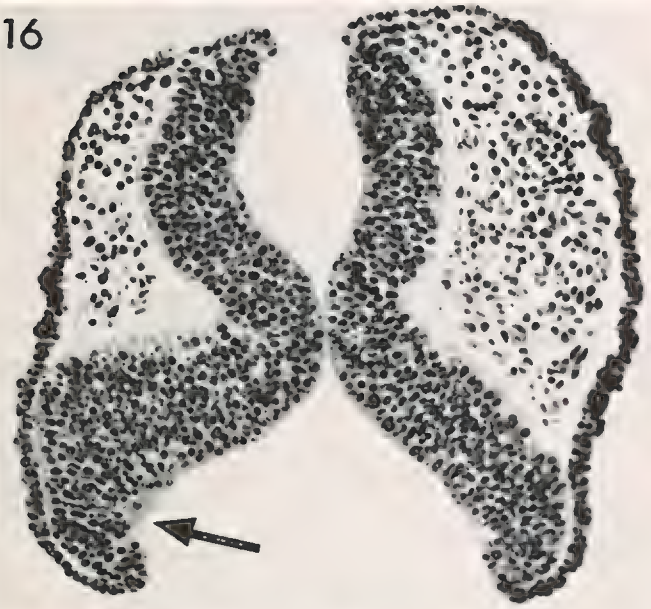

17

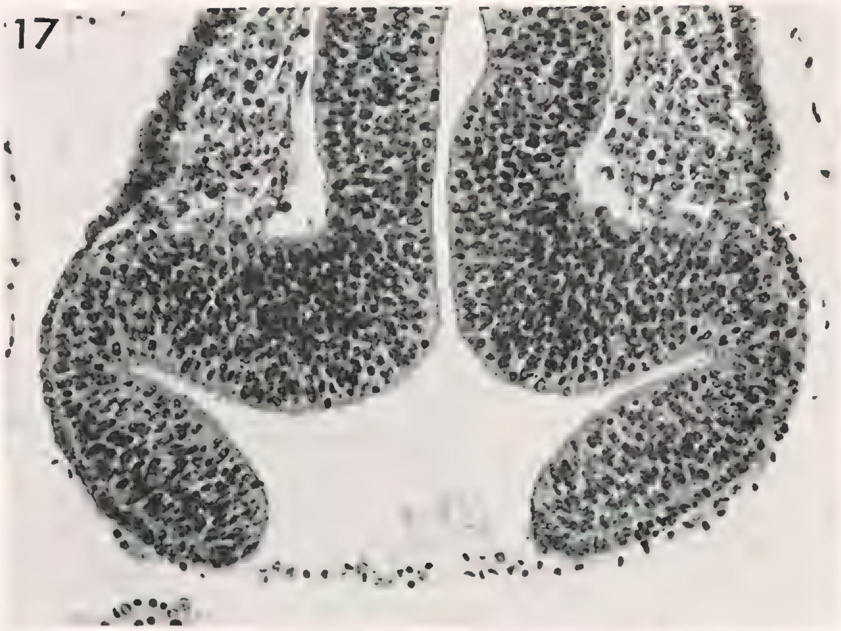

18

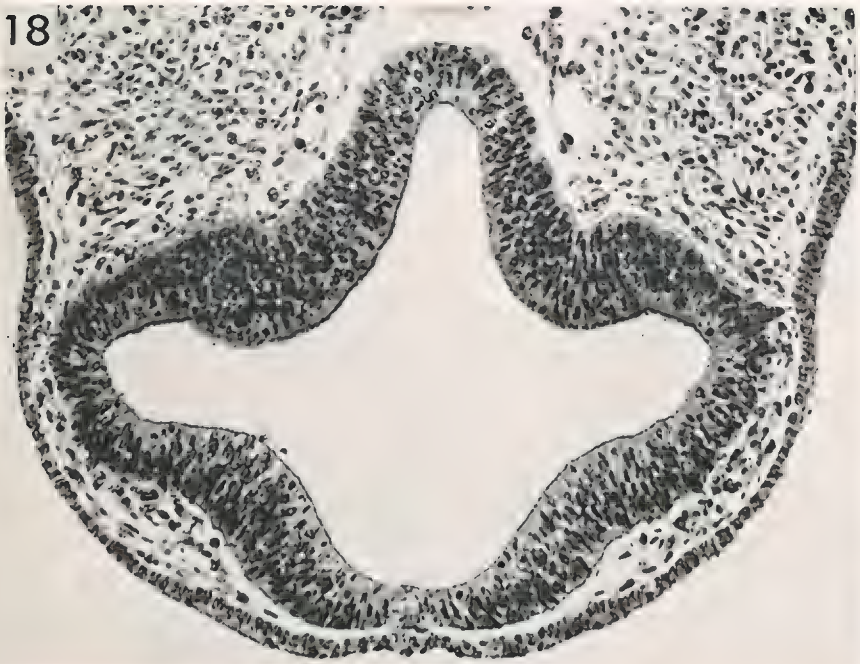

19

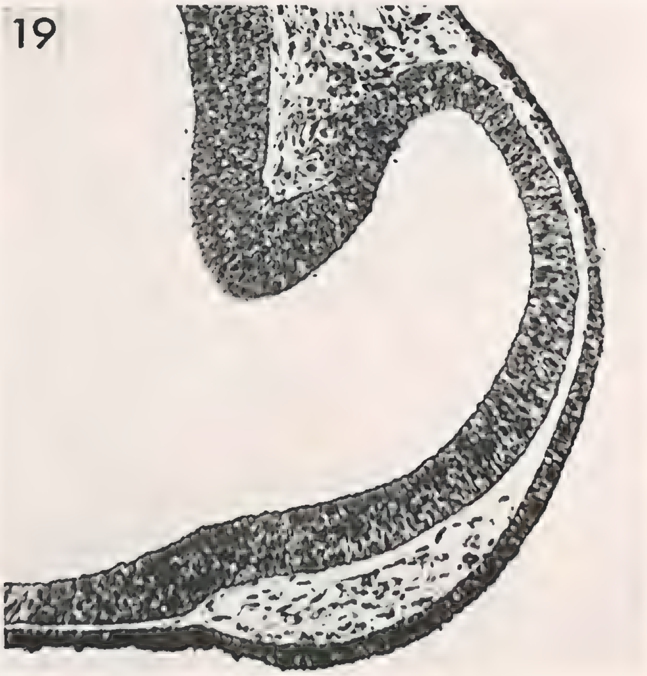

PLATE 2, Figs. 20–22

The optic vesicle at horizon xiii, about 4 weeks.

Fig. 20. The optic vesicles are larger, and show evidence of retinal and lens discs. Horizon xiii, No. 836, section 6-2-2; ×100.

Fig. 21. The retinal and lens discs are separated only by occasional degenerating sheath cells. Elsewhere, the discs make contact by their basement membranes. Horizon xiii, No. 7889, section 4-3-13; ×200.

Fig. 22. Slight indentation of both retinal and lens discs is beginning. The retinal disc shows a well-marked nucleus-free zone. Horizon xiii, No. 8372, section 3-5-5; ×200.

20

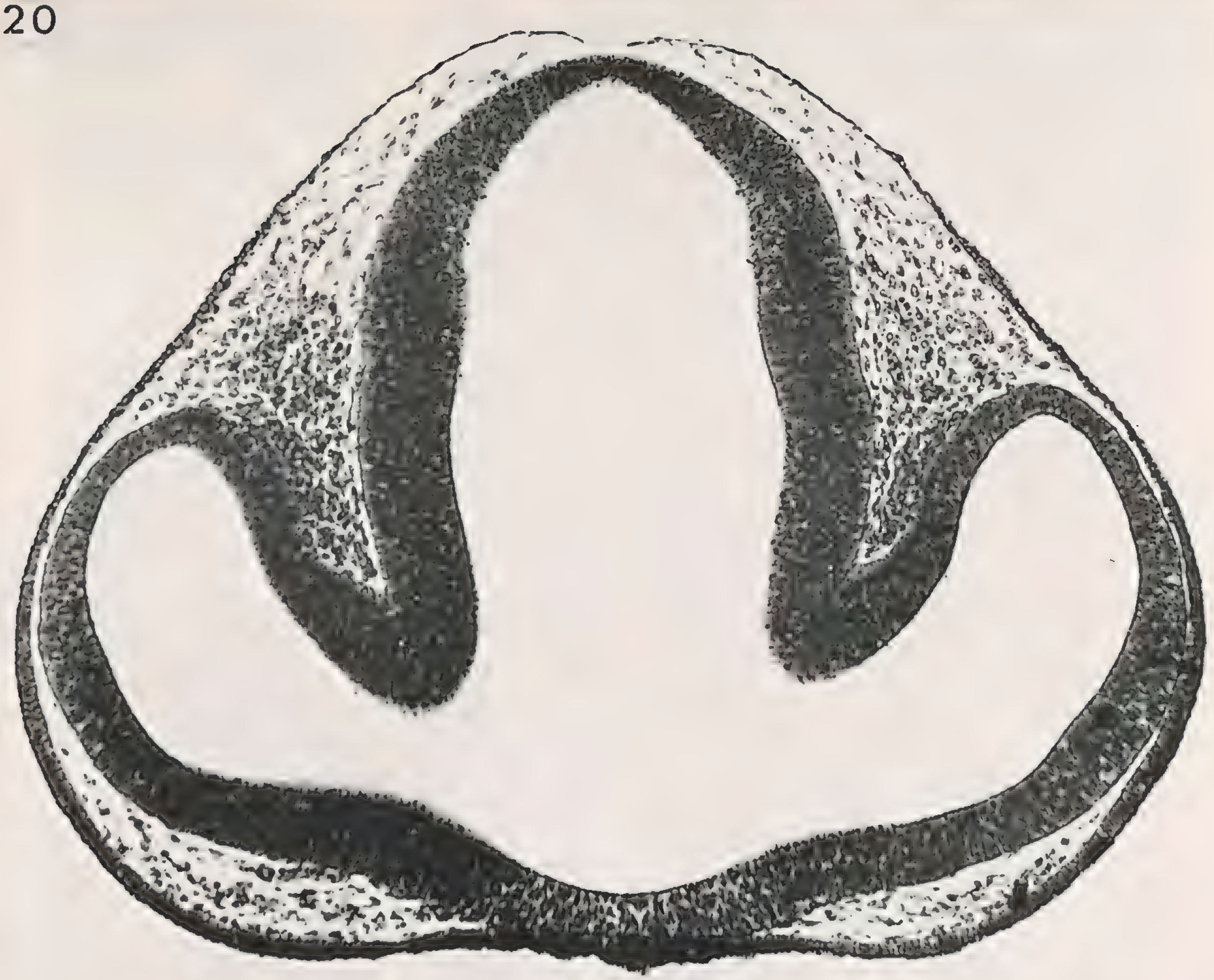

21

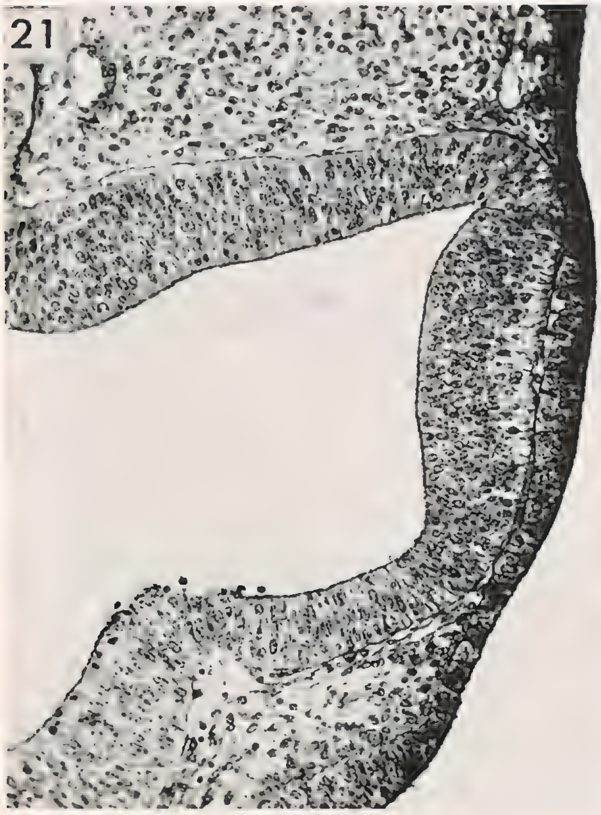

22

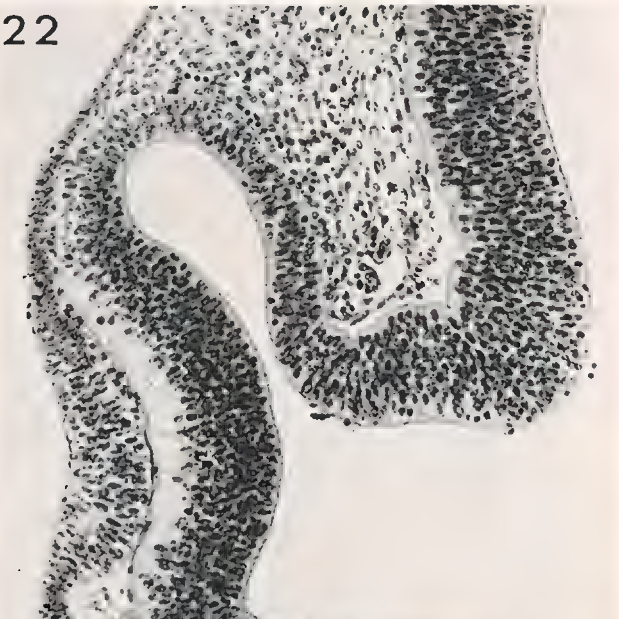

PLATE 3, Figs. 23–29

The optic cup at horizons xiv–xv, about 5 weeks.

Fig. 23. Optic cup, which has just been formed through indentation of the retinal disc. The cup now displays an inverted and an external layer. Note the optic ventricle and the nucleus-free zone of the retina. Horizon xiv, No. 8552, section 6-2-6; ×160.

Fig. 24. Lens pit, which has just been formed through indentation of the lens disc. Note the "unwanted" cell remnants in the pit. The developing lens capsule can be seen. Horizon xiv, No. 8552, section 6-2-6; ×320.

Fig. 25. Lens pit, sectioned at a right angle to the plane shown in Fig. 24. Note the unwanted cell remnants. The lentiretinal space is visible in lower portion of the photomicrograph. Horizon xiv, No. 8999, section 2-4-3; ×320.

Fig. 26. Inverted and external layers of the optic cup. The cavity between the two layers is lined by a terminal bar net. See Fig. 23 for orientation. Horizon xiv, No. 8552, section 6-2-6; ×320.

Fig. 27. General view of the optic cup and stalk. The proliferative, primitive, and marginal zones of the retina can be identified. Note the anterior epithelium of the future cornea. Horizon xv, No. 8997, section 7-1-2.

Fig. 28. Lens vesicle, showing early lens fibers. Note the unwanted cell remnants in the cavity. The primary vitreous body can be identified to the left, above and below the lens. See Fig. 27 for orientation. Horizon xv, No. 8997, section 7-1-2; ×280.

Fig. 29. Onset of pigmentation in the retina. The following layers are shown, from above downward: the uveocapillaris; the basal lamina of the uvea; the external (pigmented) layer, with two mitotic figures; terminal bars (external limiting membrane of retina); and the outermost part of the inverted layer, with two mitotic figures in the proliferative zone. The pigment appears as a number of minute black dots in the photomicrograph. See Fig. 27 for orientation. Horizon xv, No. 8997, section 7-1-2; ×800.

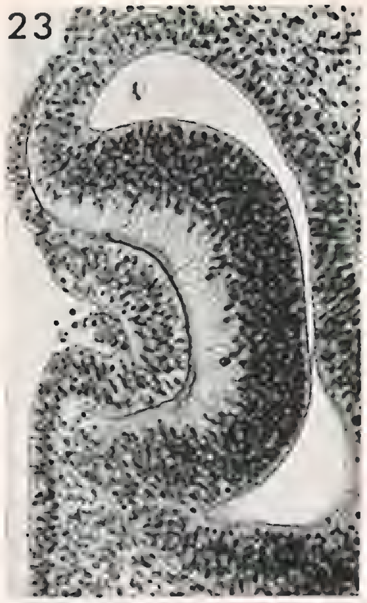
23

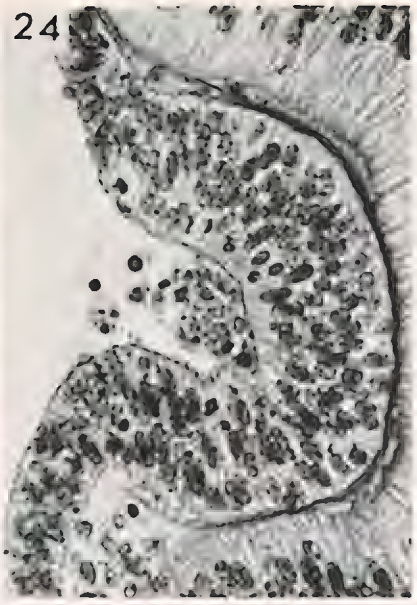
24

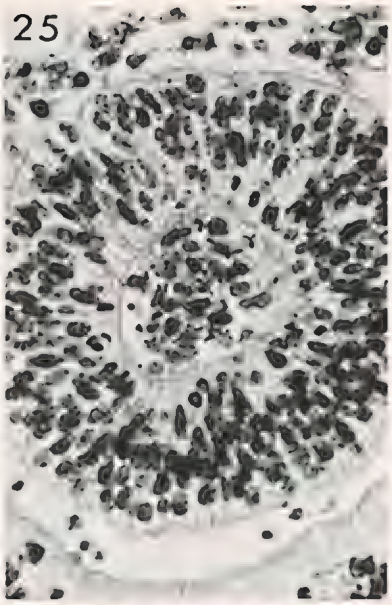
25

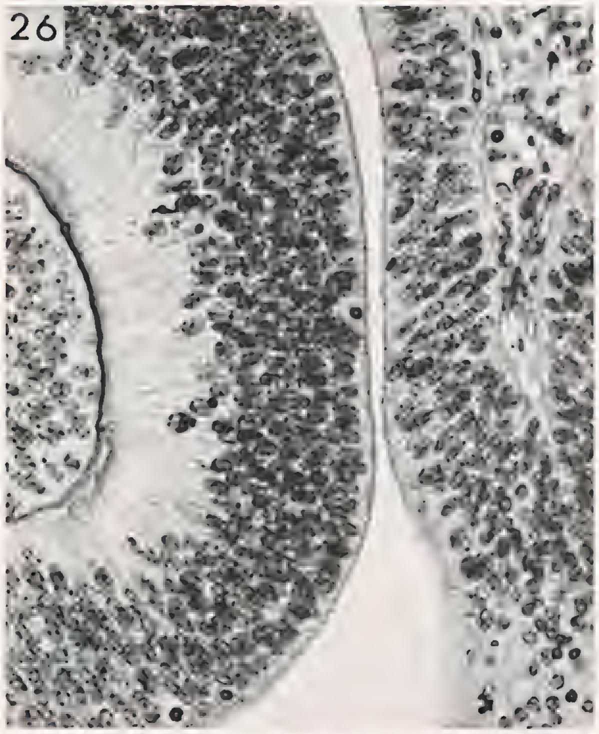
26

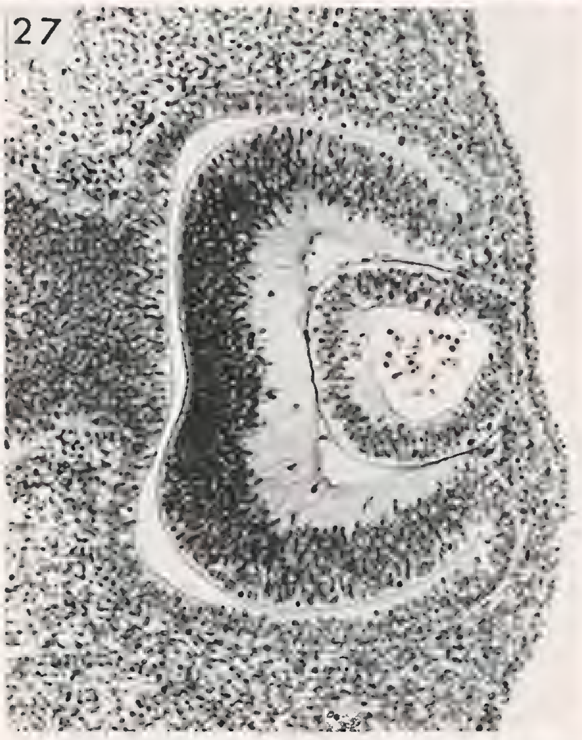
27

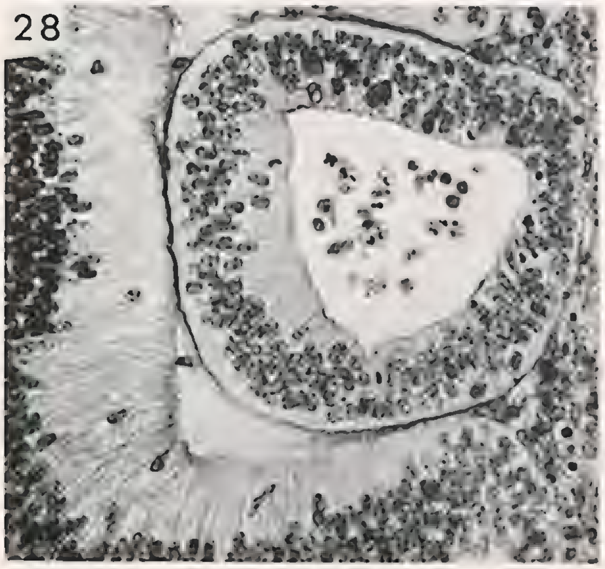
28

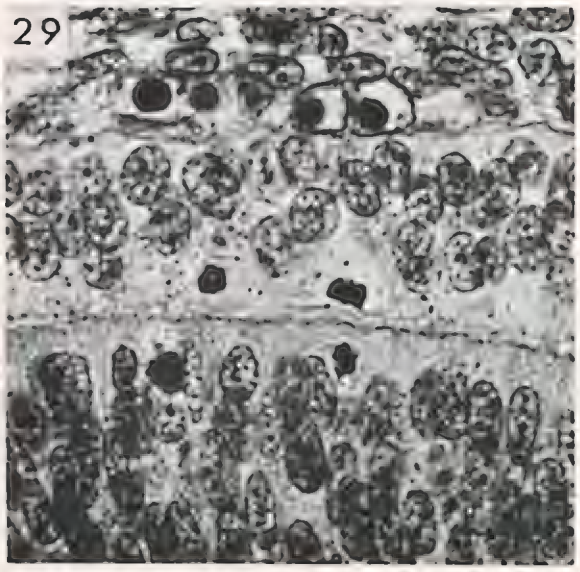
29

PLATE 4, Figs. 30–33

The optic cup at horizon xvi–xvii, about 6 weeks.

Fig. 30. General view of eye. Note increasing size of the lens body, which renders the lens cavity D shaped. Blood vessels can be seen in the lentiretinal space. Horizon xvi, No. 8773, section 12-1-1; ×200.

Fig. 31. General view of eye. The lens cavity still appears D shaped. Horizon xvii, No. 8998, section 13-3-7; ×200.

Fig. 32. General view of eye in a different plane of section. The retinal fissure is visible near lower right corner. The lens cavity appears crescentic. Horizon xvii, No. 8789, section 8-2-2; ×200.

Fig. 33. View of lens, showing lens fibers, lens capsule, and perilental blood vessels. The younger lens fibers are nearer the equator and show a concavity facing the equator. Horizon xvii, No. 8998, section 13-3-7; ×350.

30

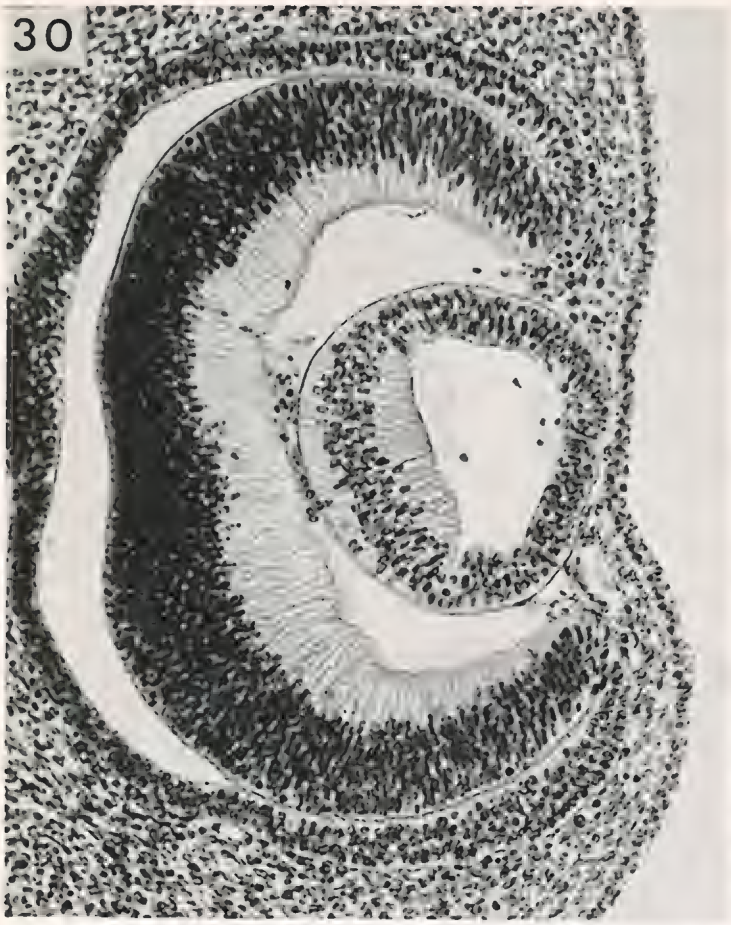

31

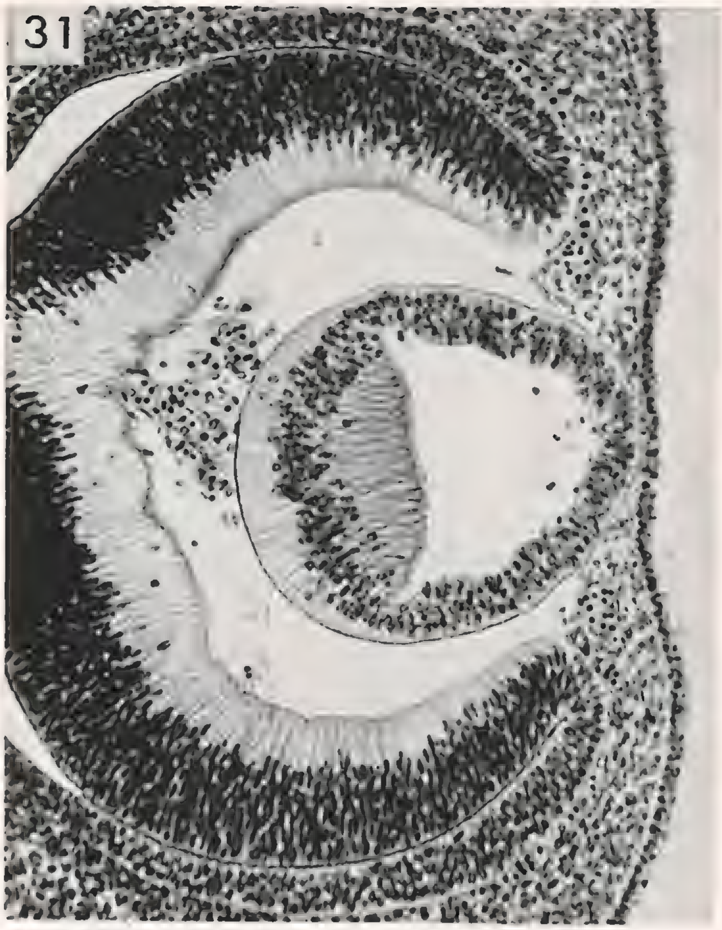

32

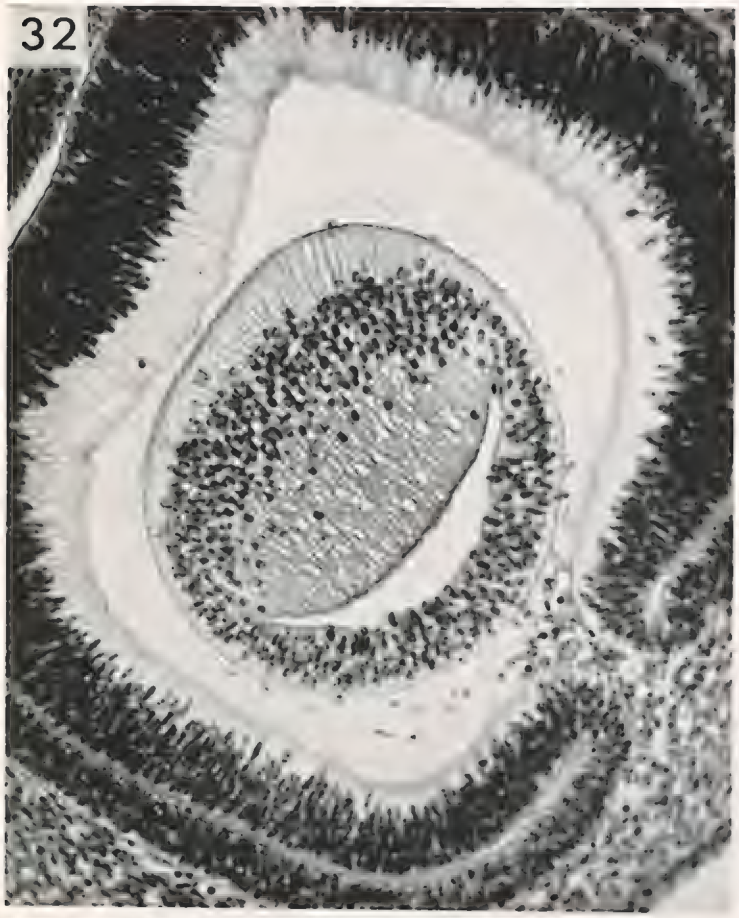

33

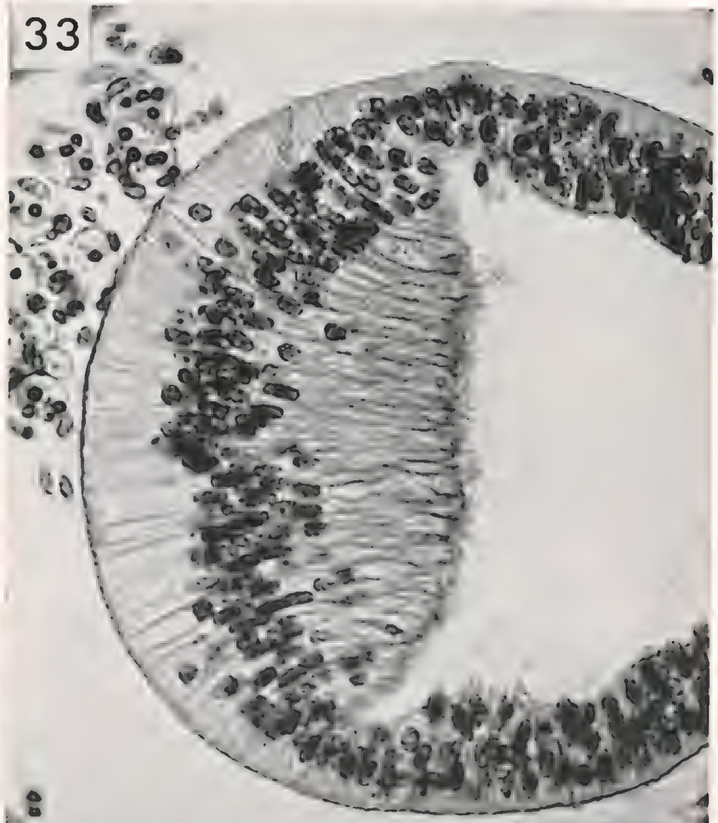

PLATE 5, Figs. 34–39

The optic cup at horizon xvii, about 6 weeks.

Figs. 34–37 illustrate the manner of closure of the retinal fissure at horizon xvii.

Fig. 34. Notch of the retinal fissure. Horizon xvii, No. 8789, section 28-2-2; ×180.

Fig. 35. Higher power view, one section farther medially. See Fig. 34 for orientation. Section 28-2-1; ×360.

Fig. 36. Junction between the notch and the closed portion of the retinal fissure, two sections farther medially. See Fig. 34 for orientation. Section 28-1-3; ×360.

Fig. 37. Commencement of the closed portion of the retinal fissure, one section farther medially. See Fig. 34 for orientation. Section 28-1-1; ×360.

Fig. 38. Formation of the internal neuroblastic layer of the retina. The dorsal portion (top) of the inverted layer shows a cellular migration from the proliferative into the marginal zone. Horizon xvii, No. 8789, section 27-1-4; ×180.

Fig. 39. Optic stalk. Owing to the presence of the retinal fissure, it appears crescentic in cross section. The concavity is occupied by the hyaloid artery. The inverted layer of the stalk is characterized by densely stained nuclei. Horizon xvii, No. 8789, section 25-2-1; ×360.

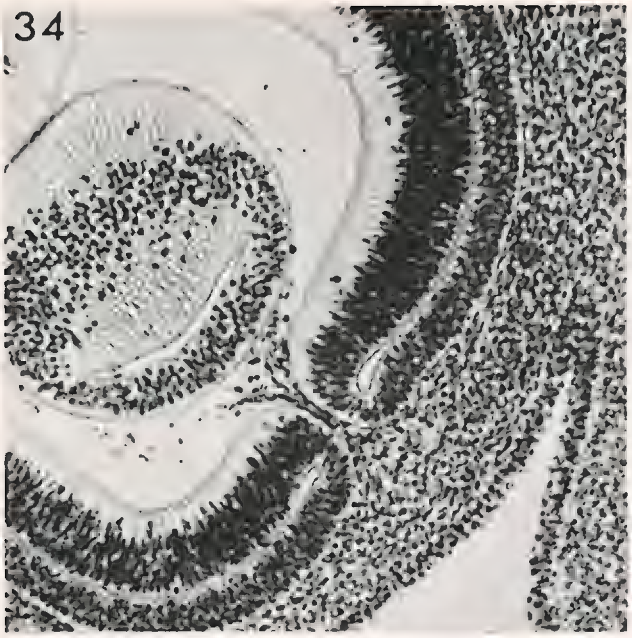
34

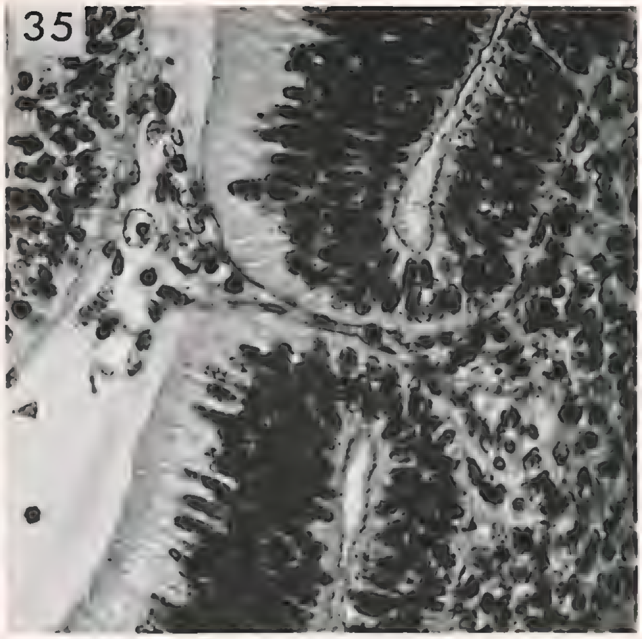
35

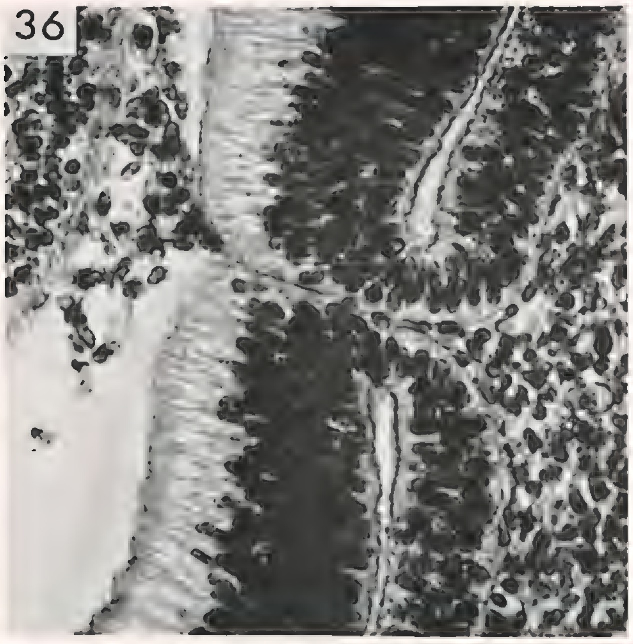
36

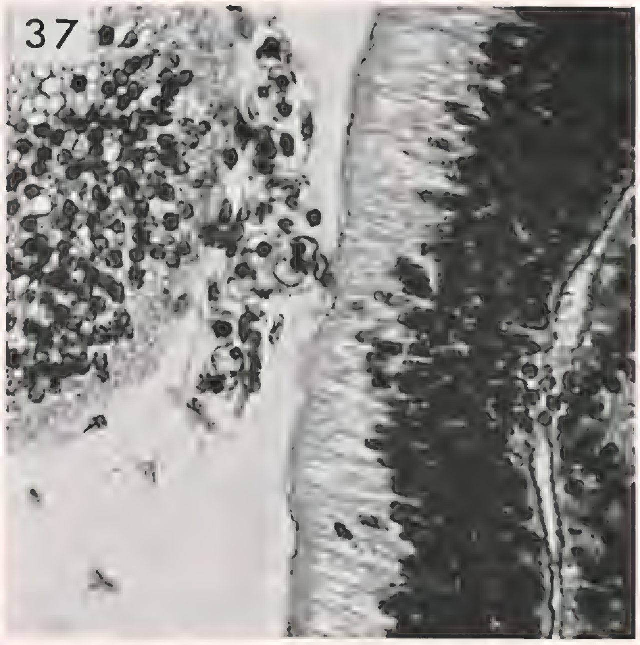
37

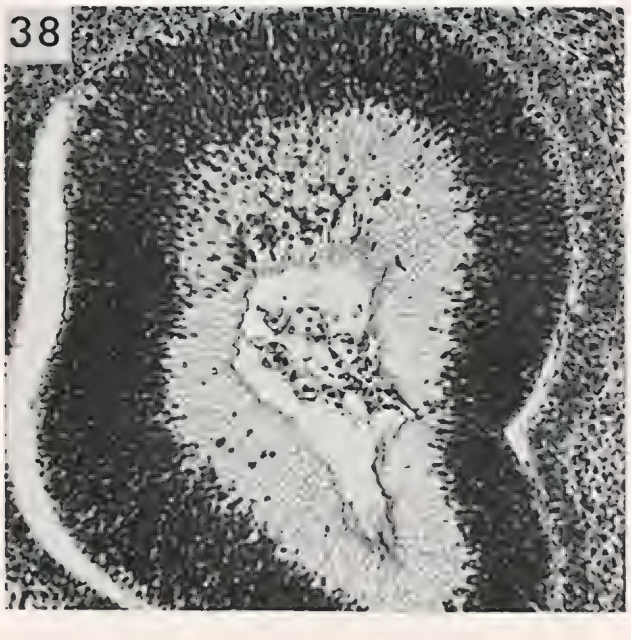
38

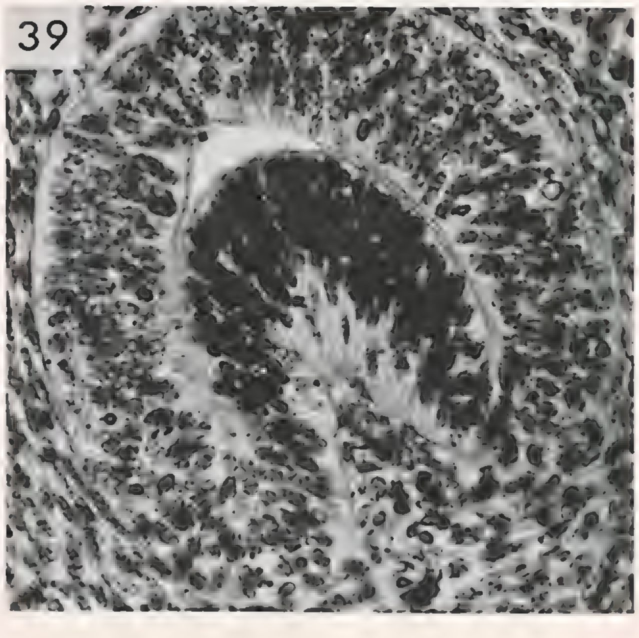
39

PLATE 6, Figs. 40–47

The eye at horizons xviii–xix, about 6–7 weeks.

Fig. 40. General view of eye. The annular vessel can be seen, sectioned twice, near the rim of the optic cup. Cellular remnants are noticeable in the lens cavity. Horizon xviii, No. 9247, section 13-3-1; ×100.

Fig. 41. Portions of the retina (left) and lens (right). The internal limiting membrane of the retina and the lens capsule can be seen. Horizon xviii, No. 9247, section 13-3-1.

Fig. 42. Pigmentation in the retina. The pigment granules in this section are chiefly internal to the nuclei. Below, two mitotic figures are visible in the proliferative zone of the inverted layer. Above, the uveocapillaris can also be seen. Horizon xviii, No. 9247, section 13-3-1.

Fig. 43. General view of eye. The internal neuroblastic layer of the retina is distinguishable. Horizon xix, No. 9325, section 13-2-7.

Fig. 44. Lens. The lens cavity is now reduced to a slit by the growth of the lens fibers. The axial fibers are straight; the younger fibers nearer the equator, concave. Marked nuclear bowing is present in the lens body. The perilental vessels are evident. Mesenchymal cells underlying the surface epithelium are becoming condensed to form the mesothelium of the anterior chamber. Horizon xix, No. 9097, section 14-1-3; ×200.

Fig. 45. Inverted layer of the optic cup, which appears to be everted (toward the left) along the lips of the retinal fissure. Because the everted margins are almost free of pigment, a sharp transition to the pigmented external layer of the cup is noticeable. Horizon xix, No. 9325, section 12-2-1; ×200.

Fig. 46. Nerve fibers as they traverse the retina. They are parallel with the internal limiting membrane. The internal neuroblastic layer shows at middle of right margin of the photograph. The hyaloid artery can be seen passing through the retinal fissure (at upper left corner) and passing (lower right corner) toward the lens. Horizon xix, No. 9325, section 12-2-3; ×350.

Fig. 47. Pigmentation in the retina. The pigment granules in this section are located chiefly internal to the nuclei but also form a crust externally. A uveal blood vessel can be seen above, and the external limiting membrane of the retina is visible in lower half of the photomicrograph. Horizon xix, No. 9325, section 13-2-7.

40

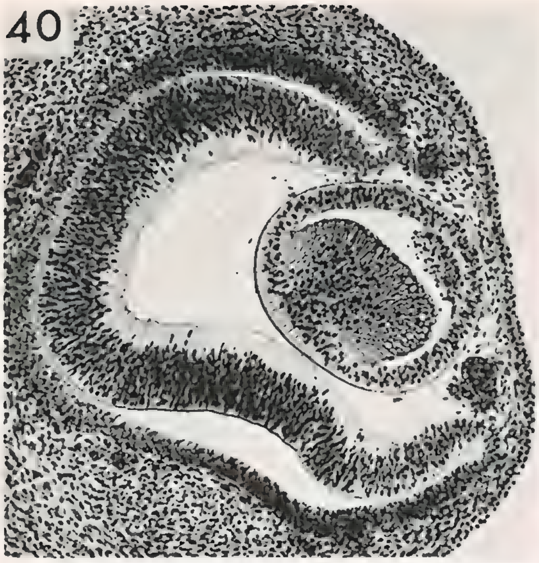

41

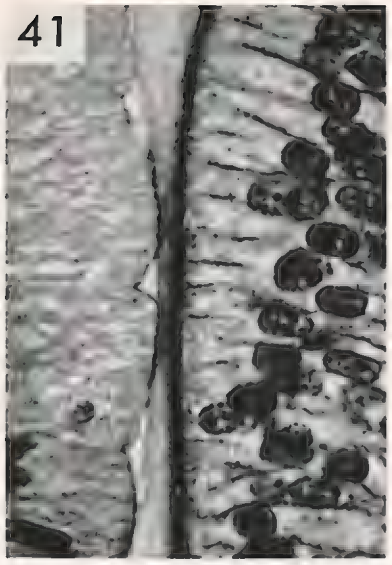

42

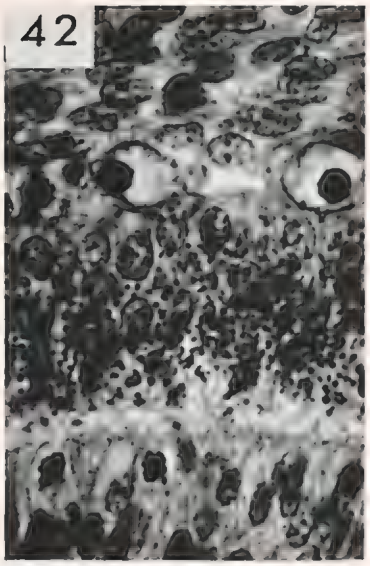

43

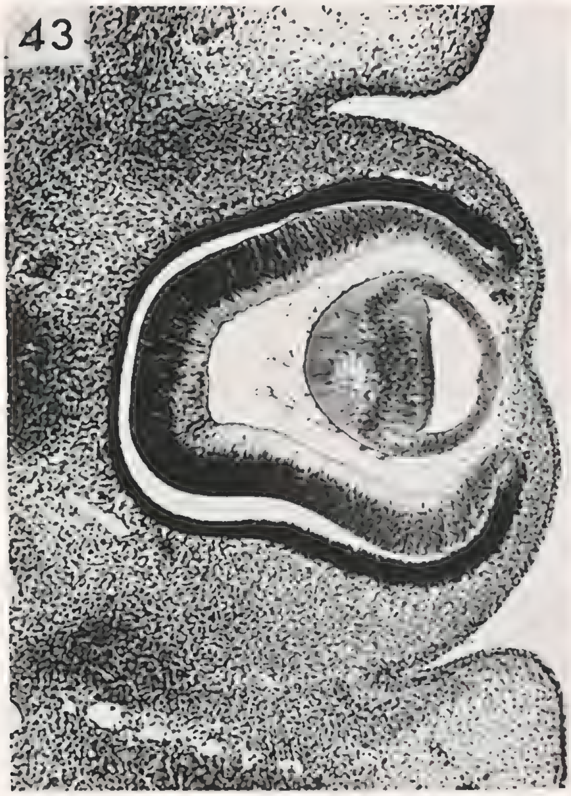

44

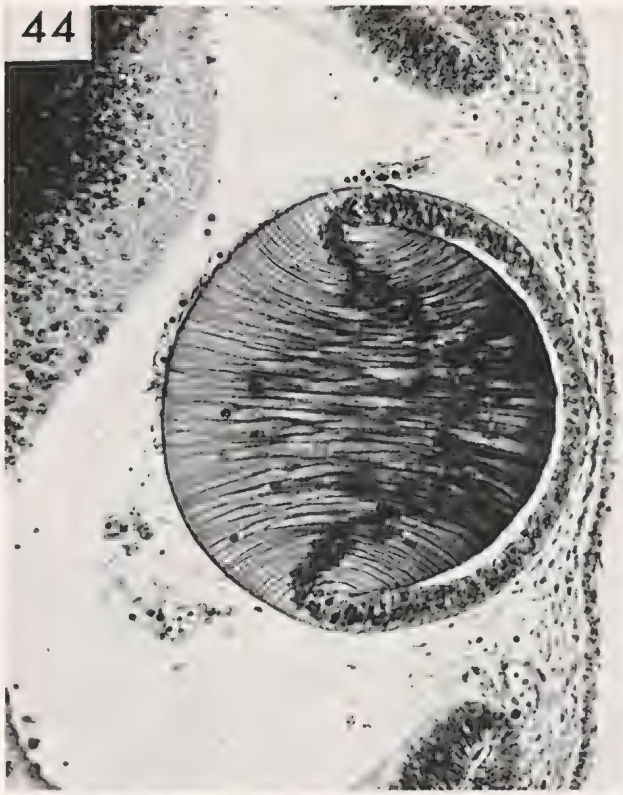

45

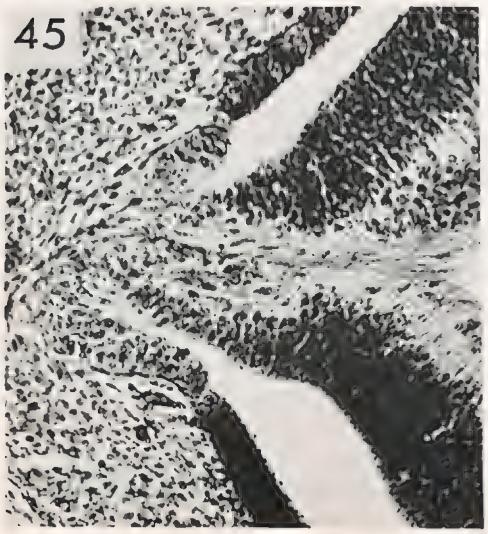

46

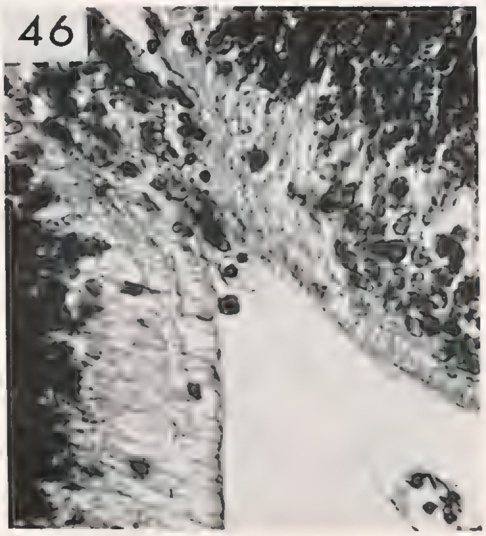

47

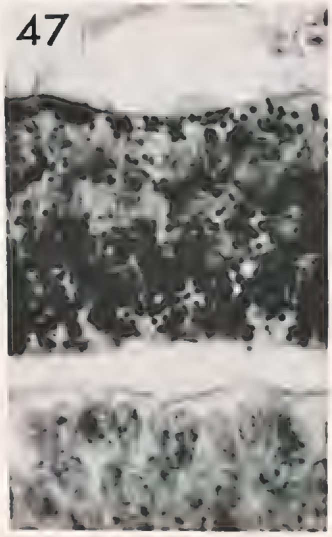

PLATE 7, Figs. 48–51

The eye at horizons xx–xxiii, about 7–8 weeks.

Fig. 48. Lens. The outlines of the lens fibers are clearly shown. The epithelium of the lens is on right side of the photomicrograph, where a portion of the future cornea can also be seen. Horizon xx, No. 8226, section 15-2-1; ×400.

Fig. 49. Optic stalk. The cavity of the stalk has been obliterated, although ependymal remnants are present. A cellular sheath surrounds the stalk. Horizon xx, No. 8226, section 21-1-1; ×400.

Fig. 50. General view of eye. The cornea is cut obliquely in this section. The mesothelium of the anterior chamber, the *amas stratifié,* and the scleral condensation form an almost continuous circle. The appearances at horizon xxi, not illustrated, resemble those at horizon xxii. Horizon xxii, No. 8120, section 36-2; ×60.

Fig. 51. Region of the cornea and the lens. The cornea comprises anterior epithelium, *substantia propria,* and mesothelium. The mesothelium can be traced peripherally into the *amas stratifié.* Behind the cornea, the pupillary membrane and the epithelium of the lens can be discerned. In front of the cornea, the conjunctival sac and the palpebral conjunctiva are evident. Horizon xxiii, No. 4570, section 70-2-2.

48

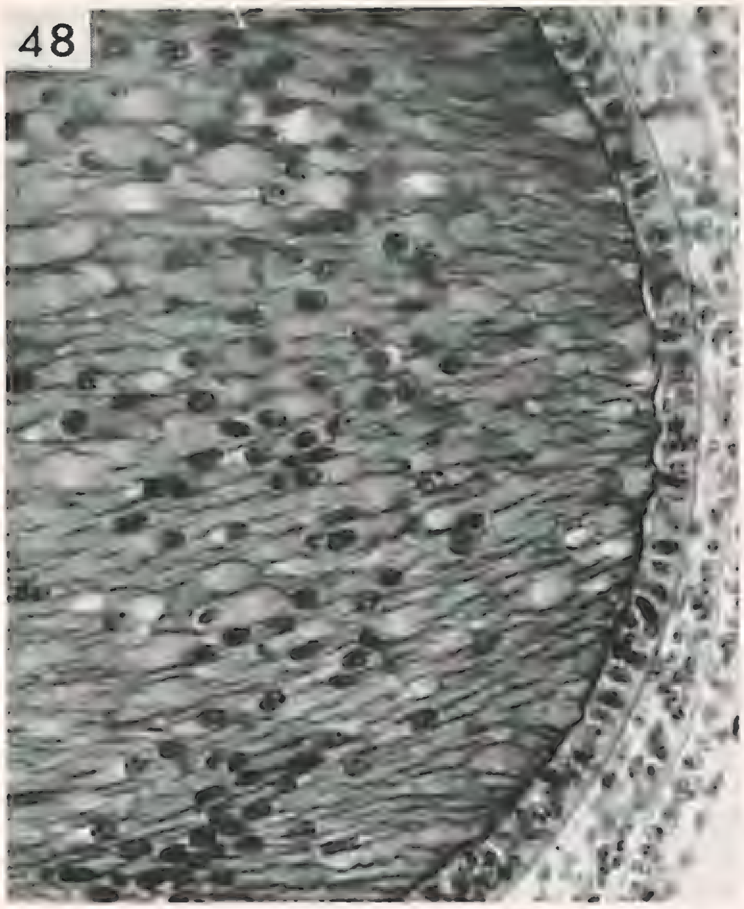

49

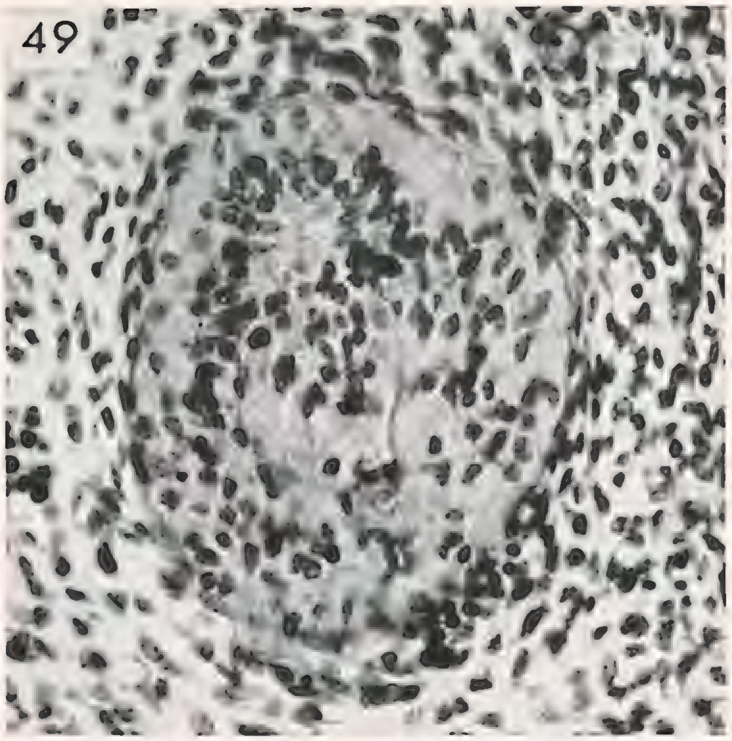

50

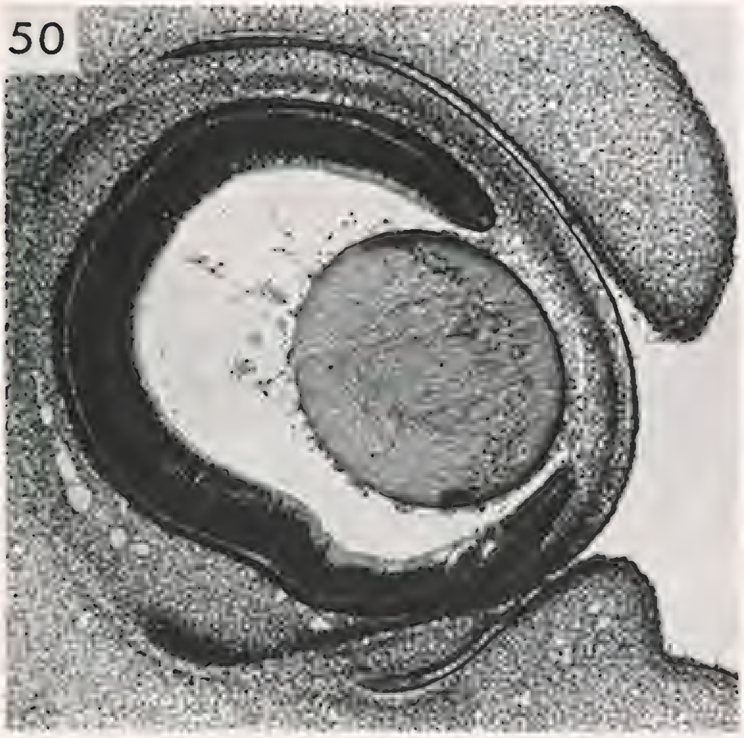

51

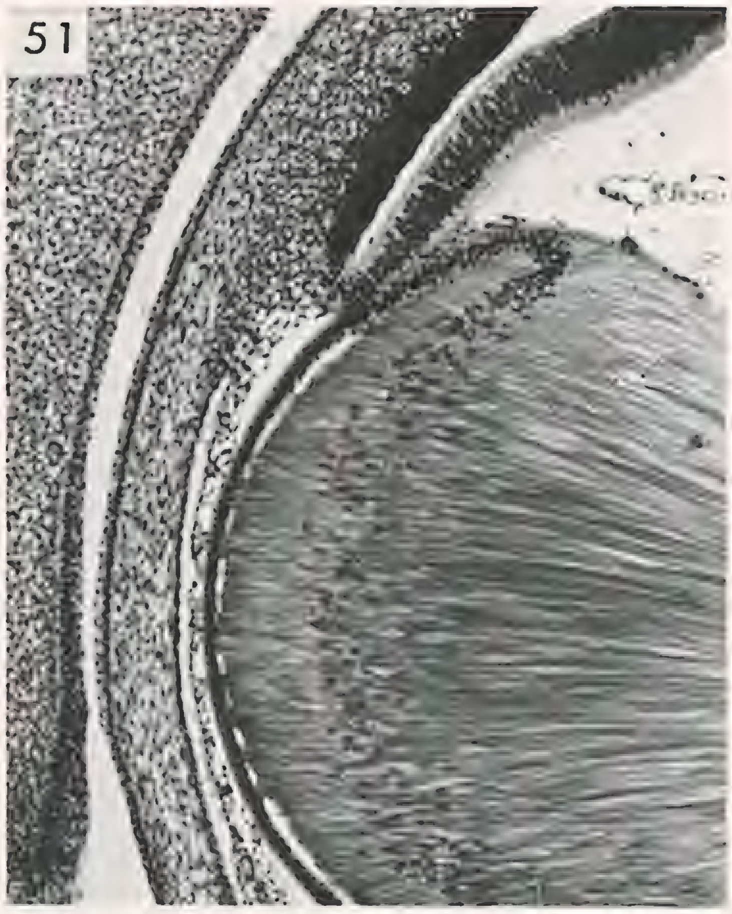

PLATE 8, Figs. 52–55

The eye at horizon xxiii, about 8 weeks.

Fig. 52. General view of eye at end of embryonic period proper. The primary vitreous body, the scleral condensation, and the fornices of the conjunctiva can be seen. The youngest (equatorial) fibers of the lens are lighter staining. Horizon xxiii, No. 9226, section 72-1-1; × 60.

Fig. 53. Retina. Internal to the pigmented stratum, the following layers can be seen: proliferative zone and external neuroblastic layer, internal neuroblastic layer, nerve fiber layer, and internal limiting membrane. Horizon xxiii, No. 9226, slide 72; × 400.

Fig. 54. Optic disc. The nerve fibers can be seen passing backward. The point of exit of the hyaloid artery is surrounded by a clump of cells known as Bergmeister's papilla. Horizon xxiii, No. 9226, section 67-3-2; × 400.

Fig. 55. Optic nerve. The stalk now consists almost entirely of nerve fibers. A cellular sheath is evident. Horizon xxiii, No. 9226, section 63-2-2; × 200.

52

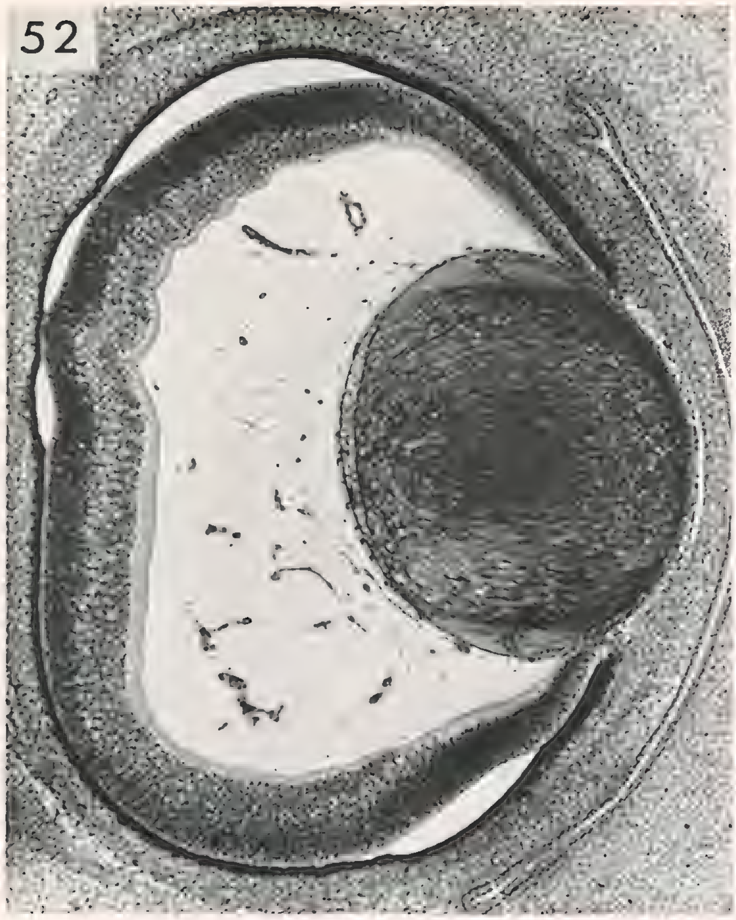

53

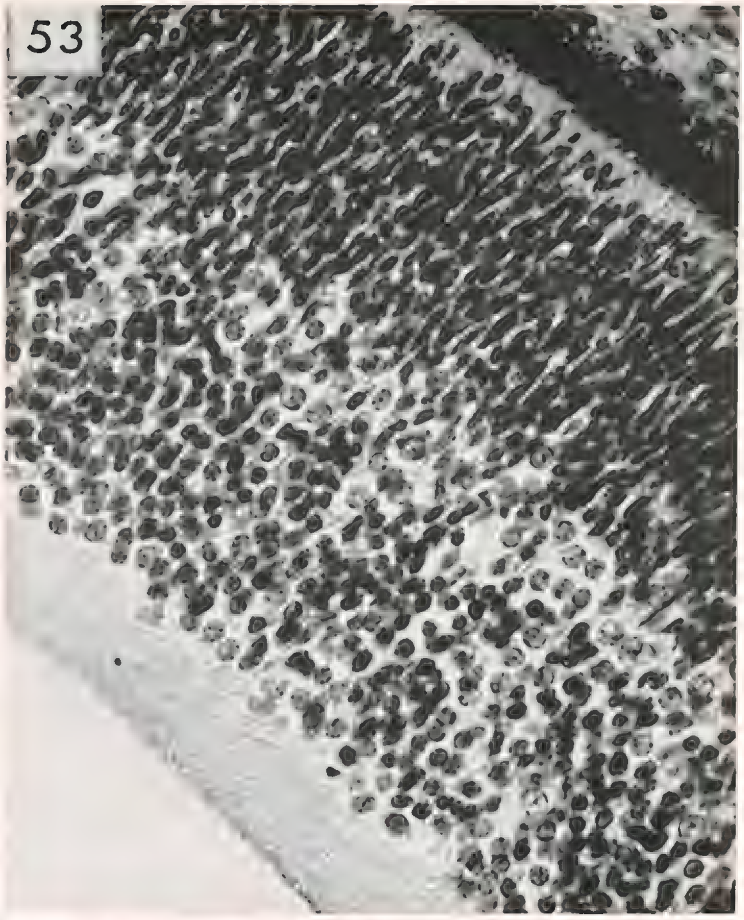

54

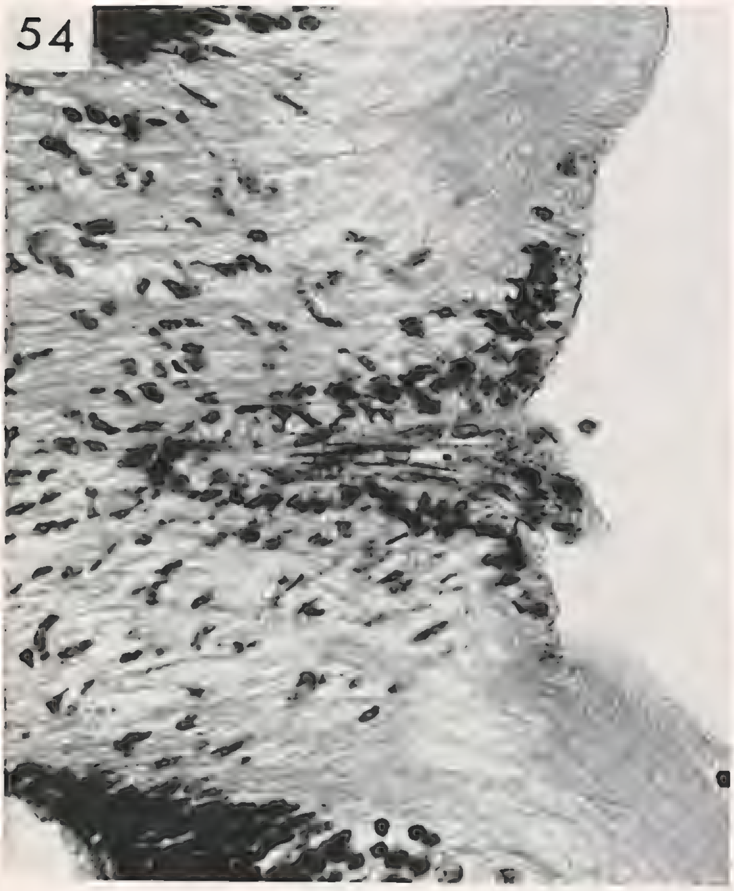

55

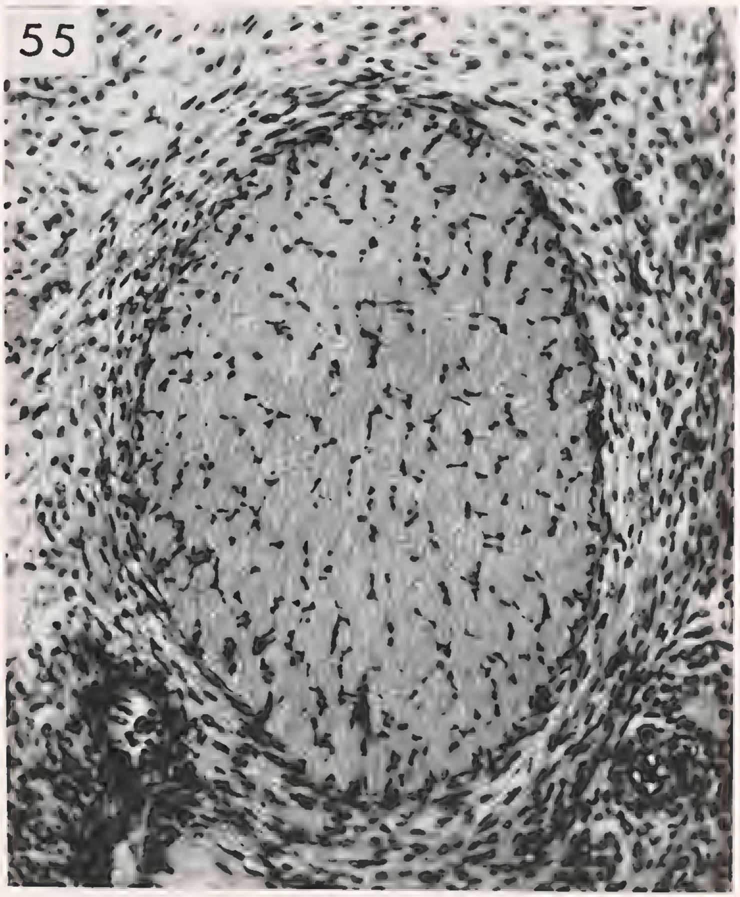

PLATE 9, Figs. 56–59

The eye at horizon xxiii, about 8 weeks.

Fig. 56. Vitreous body. Indications of the secondary or definitive vitreous body are present adjacent to the internal limiting membrane of the retina. Horizon xxiii, No. 9226, section 68-1-1; ×400.

Fig. 57. Fibrogenetic area of the lens. The conversion of the lens epithelial cells into lens fibers can be traced in this region. The prominent lens capsule, perilental vessels, and the "marginal bundle," or *faisceau isthmique,* of the vitreous body can be detected. Horizon xxiii, No. 9226, slide 72; ×400.

Fig. 58. Lens. Many cross sections of the lens fibers are visible here. Horizon xxiii, No. 9226, slide 72; ×400.

Fig. 59. Cornea. The following can be discerned from anterior to posterior; palpebral conjunctiva, conjunctival sac, anterior epithelium of cornea and its basement membrane, *substantia propria,* mesothelium, anterior chamber and cells of pupillary membrane, lens capsule, epithelium of lens, and lens fibers. Horizon xxiii, No. 9226, slide 72; ×400.

56

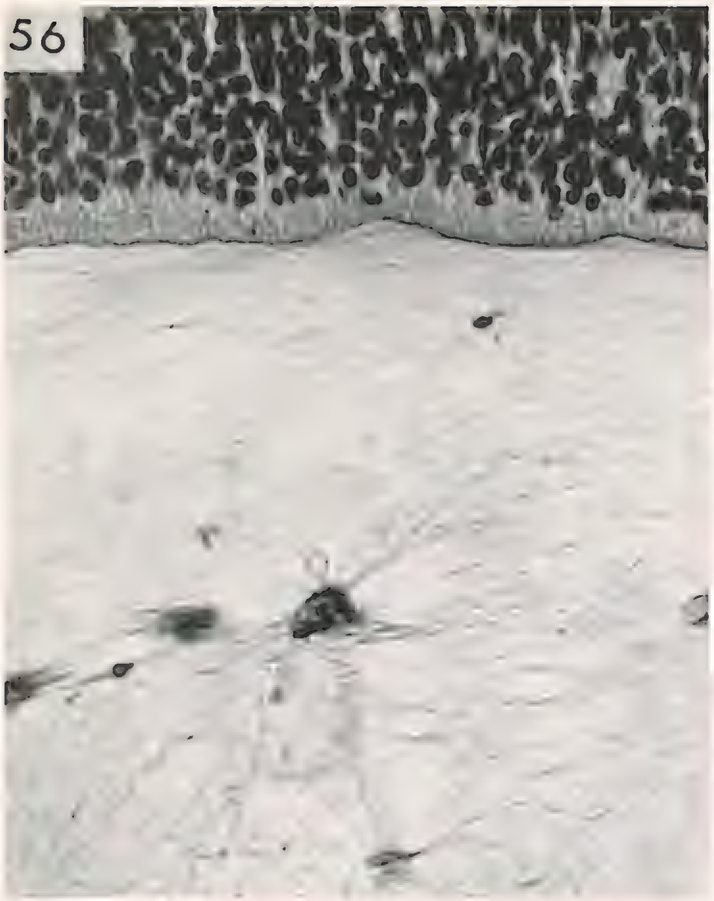

57

58

59

CONTRIBUTIONS TO EMBRYOLOGY, NO. 260

THE MORPHOLOGY OF HUMAN UTEROPLACENTAL VASCULATURE

JOHN W. S. HARRIS
Department of Anatomy, London Hospital Medical College, London, England

and

ELIZABETH M. RAMSEY
Department of Embryology, Carnegie Institution of Washington, Baltimore, Maryland

(With 13 plates)

CONTENTS

PAGE

PREVIOUS STUDIES 45

MATERIALS AND METHODS 46

DESCRIPTION OF SPECIMENS 47
  Presomite Stages 47
  Somite Stage 47
  Specimens 8306 and 8916 (About 28–30 Days) 48
  Specimens With Embryos of 13 to 17 Millimeters (38–46 Days) . . . 49
  Specimens With Embryos of 25 to 50 Millimeters (48–70 Days) . . 49
  Specimens With Fetuses of 60 to 73 Millimeters (12–14 Weeks) . . 50
  Specimens With Fetuses of 90 to 200 Millimeters (15–22 Weeks) . . 50
  Specimens With Fetuses of 200 to 310 Millimeters (24–40 Weeks) . . 51

DISCUSSION 51
  Uteroplacental Arteries 51
    Terminology 51
    Morphology 51
    Formation of the Lacunae 52
  Influence of Trophoblast on the Uteroplacental Vasculature 53
  Intravascular and Perivascular Cells 54
  Uteroplacental Veins 55
  Number of Arterial Openings 56

SUMMARY 56

ACKNOWLEDGMENTS 57

LITERATURE CITED 57

THE MORPHOLOGY OF HUMAN UTEROPLACENTAL VASCULATURE

The intimate involvement of uterine blood vessels in the formation and function of the placenta necessitates a full understanding of their arrangement, structure, and relationship with the trophoblast. Some years ago a systematic study of the uteroplacental vasculature in the rhesus monkey was carried out in the Carnegie Institution Department of Embryology, but no similar study has been made in man. In spite of the pronounced resemblance between the reproductive systems of monkey and man, species differences exist, and the validity of argument by analogy requires substantiation. Furthermore, because of an increasing number of investigations into the physiology of the uteroplacental circulation, it is desirable to establish observations on normal human material to provide a basis for comparison with experimental animals and for evaluating pathological changes. A study of the morphology and distribution of the arterial supply and venous drainage of the human placenta was therefore undertaken. Pregnant uteri with the placenta *in situ* were examined at all stages of pregnancy and, as far as possible, techniques were used comparable to those employed in studying the monkey.

PREVIOUS STUDIES

Previous descriptions of the uterine blood vessels and of the cyclic changes in the morphology of the endometrial arteries form an extensive literature that dates from the time of William Hunter (1774). Lundgren (1957) gives a comprehensive review of the subject that includes many papers of historic interest. Current descriptions of the uterine vasculature are largely based upon the work of Daron (1936), Hasner (1946), and Bartelmez (1931, 1933, 1957) who used injection techniques to study nonpregnant uteri of man and rhesus monkey, and upon the work of Markee (1940), who studied intraocular transplants of monkey endometrium.

There is general agreement among investigators that the endometrium is supplied by radially oriented arteries, which arise from arcuate arteries (Sampson, 1913) lying between the middle and outer thirds of the myometrium. The radial arteries pass medially, giving off lateral branches to the inner two thirds of the myometrium and basal branches, which terminate in the *stratum basalis.* Upon entering the endometrium the radial arteries are usually called "spiral" or "coiled endometrial" arteries, and at the time of ovulation they end in a capillary plexus in the *stratum compactum.* The distinction between spiral and radial arteries is one of distribution and as both undergo similar modification during pregnancy (to be shown later) they will be referred to together as coiled arteries. Constrictions of varying length are sometimes observed in the coiled arteries of nonpregnant uteri of man and monkey. The cause of the constrictions and the manner in which they develop are not clearly understood. Opinions differ over the presence of arteriovenous anastomoses in the endometrium, a subject fully discussed by Bartelmez (1956), who considers the claims unsubstantiated.

In a study of the uteroplacental vessels of rhesus monkeys, Ramsey (1949, 1954) noted the formation of terminal arterial sacs and a progressive uncoiling of the arteries as pregnancy advanced. Changes observed in the structure of arterial walls included epithelioid degeneration of the media and intimal fibrosis.

Knowledge of the initial relationship between the implanting human blastocyst and the endometrial blood vessels is based upon the specimens obtained and studied by Hertig and Rock. Details of their outstanding work appeared in several monographs, summarized in Hertig, Rock, and Adams (1956). In descriptions of four presomite implantation sites and of *in situ* placentas from the first three months of gestation, Hamilton and Boyd (1960) gave a detailed account of the uteroplacental blood vessels. In earlier contributions (Hamilton and Boyd, 1951; Boyd, 1956), based upon *in situ* specimens from later pregnancies, these authors commented on the occurrence of trophoblastic cells within the lumen of uteroplacental arteries and also on their inability to identify a marginal sinus (Spanner, 1935) in their specimens. The presence of trophoblastic cells in the walls and lumina of uteroplacental blood vessels had previously been described by Friedländer (1870) and Leopold (1877), who believed that affected vessels frequently became thrombosed in late pregnancy.

The radioangiographic studies of Borell *et al.* (1964, 1965*a, b*) in human subjects and of Ramsey *et al.* (1963, 1966) and others in rhesus monkeys, have demonstrated the circulation of blood through the intervillous space and how it may be influenced by uterine contractions. Further consideration of these experiments will be deferred until the results of the present study are discussed.

MATERIALS AND METHODS

Most of the pregnant uteri with placentas *in situ,* which form the subject of the present study, belong to the collection of the Carnegie Department of Embryology. The rest were made available through the kindness of Professor Richard J. Harrison of London. We are grateful to the colleagues who collected and prepared specimens for us. The increasing rarity of such specimens, particularly those from the second half of pregnancy, is the result of the dwindling number of indications for termination of pregnancy by hysterectomy. It is hoped that continuing cooperation between obstetricians and research workers will not only prevent the loss of such valuable material but also enable it to be preserved in a condition favorable for further examination.

From the material available to us, 31 specimens (Table 1) were selected as suitable for the present study. We also examined, for supplementary data, a large number of specimens from the Carnegie Collection, which were not included in the primary group either because of unsatisfactory preservation or because they came from women with medical conditions that may be associated with cardiovascular pathology. Thanks to the cooperation of our colleagues, we have information on the menstrual and medical histories relating to 25 of our 31 specimens, and consequently we have been able to confine our histologic studies to specimens from normotensive women.

In addition to the new material, the Hertig-Rock presomite implantation sites have been reexamined and serial sections prepared from the paraplacental uterine wall of some of these specimens to provide collateral information.

To facilitate the identification of arterial blood vessels, many uteri were injected via the uterine artery with a dilute solution of India ink, according to the

TABLE 1. Specimens Studied

Stage of Pregnancy	Approximate Developmental Age	Specimen No.	Crown-Rump Length of Embryo, mm	Recorded Menstrual Age, days	Number of Models
Early	20–30 days	9909	(12 somites)	34	1
		8306	5.3	unknown	1
		8916	5.5	43	
	40–46 days	8101	13	52	
		8689*a*	13 twins	60	
		b	16		
		9176	17	56	1
	48–70 days	8917	25	61	
		9380	30	63	1
		10119	48	83	
		9484	49	unknown	1
	12–14 weeks	8677	61	87	
		10117	62	85	
		9173	63	70	
		2328	65	69	
		8914	67	84	
		10120	70	100	
		9051	73	103	1
Middle	15–22 weeks	10122	94	107	
		8990	100	106	
		10118	109	104	
		8876	120	116	1
		8652	139	unknown	
		8991	172	139	1
		8593	177	unknown	
		10116	182	150	
		2606	198	162	
Late	24–40 weeks	8695	216	175*	
		9105	238	180	
		10121	257	unknown*	
		9124	275	unknown	1
		9033	310	Term + 3*	3

*Postmortem.

method of Rossman and Bartelmez (1957). Each injected specimen was suspended in three to four times its own volume of 10 per cent formalin or Bouin's solution, and undiluted fixative was introduced into the uterine cavity four to eight hours later, following the withdrawal of an equal volume of amniotic fluid. During the next two to three days, the specimen was rotated several times to assist distribution of the fixative by altering the position of the fetus. The uterus was then opened and the placental site was photographed to record gross relationships and to provide a means of locating the blocks of tissue removed for sectioning.

Initially, four or five such blocks, about 2 × 6 cm in size and including the full thickness of the placenta and uterine wall, were removed from various regions of the area of placental attachment. The blocks were embedded in celloidin and cut in series of 25–50 μ according to the menstrual age of the specimen. Every 5th section of the initial series of 100 was stained with hematoxylin and eosin and mounted for preliminary study. Subsequently, additional sections were cut from the same or an adjacent block to follow the entire course of a radial artery to its entry into the intervillous space. Intervening sections in the series were stained with orcein and hematoxylin, and some were counterstained with orange G, phloxine, or aniline blue and picric acid. Uteri selected for histologic study were sectioned through the placental site before fixation. Selected areas from these blocks of tissue were embedded in paraffin wax and cut in series of 8–10 μ. The sections were stained with hematoxylin and eosin, phosphotungstic acid hematoxylin, Azan, and Giemsa. Frozen sections were also prepared and stained with Oil Red O and hematoxylin.

Twelve models of representative vessels at various stages of pregnancy were prepared from the thick sections of ten specimens. Drawings of the sections were made either with the aid of a camera lucida or by projecting slides in a microscope at magnifications of 20, 25, or 50, according to the size of the specimen. The outlines of the outer wall and lumina of blood vessels and of neighboring structures were drawn on sheets of paper with ball-point pens of various colors. To assist in the orientation of the sheets, details from all regions of the projected image were incorporated in the drawings. After orientation by superposition, each sheet was marked with two intersecting guidelines to facilitate correct orientation of the sheets during the transfer of the outlines of the vessels onto 10 × 12-inch sheets of cellulose acetate. Special acetate inks were used for marking the plastic sheets, and calibrated cardboard frames were employed to give correct depth to each model.

DESCRIPTION OF SPECIMENS

Presomite Stages

We have prepared new models of blood vessels at the site of implantation of the youngest of the Hertig-Rock specimens (8020, 7½ days' postovulation), and also of the 11-day-old specimen (7699).

In 8020, the superficial stratum of the endometrium contains dilated capillaries, which pass parallel to the surface epithelium and are continuous with others that lie close to the basement membranes of adjacent uterine glands. In this, and in a slightly older specimen (8225), the course of several capillaries can be followed through the syncytiotrophoblast. The endothelial walls of the capillaries are intact to the point where each vessel enters and leaves the trophoblast, but between these points red blood cells can be seen to occupy a series of irregularly shaped spaces, which are in continuity with one another (Fig. 1*). The spaces are unlike the well-rounded vacuoles occasionally observed in syncytiotrophoblast and much smaller than the definitive lacunae present in the youngest of the 9-day specimens (8215).

In the 11-day specimen (7699), our reconstruction of the blood vessels confirms that the main connections between the lacunae and the maternal vasculature are by means of endothelium-lined sinusoids, which appear to be dilated derivatives of the capillary plexus of the surrounding stroma (Fig. 2). Continuity between the sinusoids and the endometrial veins can readily be demonstrated, but we could not establish incontrovertible evidence of the existence of direct connections with the coiled arteries of the type illustrated by Hertig and Rock (1941). Furthermore, we were unable to trace any open communications between adjacent arteries and the lacunar spaces, although several arterial branches are intimately related to this implantation site.

The endometrium adjacent to the early implantation sites is edematous, but the edema does not extend into the periarterial stroma. The coiled arteries and their branches reach the *stratum compactum* surrounded by a well-defined zone of closely packed stromal cells (columns of Streeter). The endometrial veins have no special covering of stromal cells and pass toward the myometrium in a tortuous and haphazard manner.

Somite Stage

Specimen 9909 (about 22 days) was sectioned in a plane tangential to the surface of the endometrium, which greatly facilitated the tracing of three coiled arteries from the outer third of the myometrium to their termination in the cytotrophoblastic shell. The endometrium at the site of implantation is 10 mm thick, and the trophoblast has penetrated to within 2 mm of the myoendometrial junction. Each coiled artery leaves the myometrium surrounded by a prolongation of muscle, and in the endometrium it lies within a column of a dense connective tissue. All three vessels are highly convoluted and each gives rise to a number of small branches that pass laterally to neighboring glands. Soon after entering the basalis, one artery divides in quick succession to form four vessels, which take independent courses. In the basalis there is a relatively abrupt disappearance of elastic fibers from the media of the arteries, but apart from this there is little change in their histologic appearance until they enter the transitional zone between the trophoblast and the decidua. Here, each vessel begins to dilate and the smooth muscle of the media is gradually replaced by cells that are morphologically indistinguishable from those of the cytotrophoblast. Slight variations occur in the thickness of the endothelium at various points along the arteries, but there is no evidence of endothelial proliferation or luminal obstruction. Breaks in the continuity of the endothelium in the terminal portions of the vessels are associated with the presence of red blood cells in the surrounding tissue. Distal to these points the vessel may end abruptly, or its lumen may be followed through several additional coils before it finally disappears. In the absence of leakage, the lumen of the vessel is frequently continuous with irregularly shaped spaces within the cytotrophoblastic shell.

---

* See end of text, Plates 1–7, for all figures.

As in the earlier specimens, venous sinusoids form the largest connections between the maternal vasculature and the intervillous space. There are many examples of the extension of syncytiotrophoblast along the walls of the sinusoids, and of multinucleate trophoblastic cells lying free in the lumen of veins several hundred microns from the intervillous space; only one of these cells was found in the lumen of a coiled artery (Fig. 4). Many of the uterine glands adjacent to the implantation site are dilated and some contain extravasated blood.

Specimens 8306 and 8916
(About 28–30 Days)

The sectioned material of 8306 does not include the whole thickness of the uterine wall, but the endometrium contains the terminal portions of two coiled arteries. A model of these vessels shows that each is continuous with a series of irregular spaces in the cytotrophoblastic shell. It is difficult to determine the precise point at which each vessel terminates, because the thin walls of the vessels are gradually replaced by cytotrophoblast. The endothelium, however, frequently remains intact until the last vestige of the arterial wall has disappeared. The model also shows that there is continuity between many of the irregular spaces in the cytotrophoblastic shell so that together they form a labyrinth within the shell, which communicates at intervals with the intervillous space. The openings from this labyrinth into the intervillous space are not always in direct relation to the terminal portions of the endometrial arteries (Fig. 3).

Specimen 8916, sectioned in a plane perpendicular to the decidual plate, provides further evidence of the spread of syncytium into the endometrial veins (Fig. 5). Syncytiotrophoblast enters the veins through their connections with the intervillous space; these connections extend over the whole of the basal plate. Table 2 shows that in this specimen the number of venous exits from the intervillous space is approximately twice the number of arterial openings. The significance of this and subsequent counts will be considered in the Discussion (p. 56). The diameter of the terminal

TABLE 2. Number of Arterial and Venous Openings Into the Intervillous Space

Specimen No.	Crown-Rump Length, mm	Area of Placenta Examined, mm²	Number of Openings		Approximate Number of Openings in 100 mm² of Placenta	
			Arterial	Venous	Arterial	Venous
8916	5.5	18	7	13	39	72
8101	13	100	11	10	11	10
9176	17	87	12	6	14	7
8917	25	105	10	8	9	7
9380	31	87	19	8	22	9
8677	61	125	16	6	13	5
9051	73	180	32	20	18	11
8876	120	200	22	12	11	6
8991	172	240	11	10	5	4
9124	275	200	4	3	2	<2
9033	310	1,326	25	10	<2	<1

portions of the larger coiled arteries varies between 20 and 25 μ, but in some, the lumen is reduced by cells that are continuous with the cells of the cytotrophoblastic shell. These accumulations of cytotrophoblast become increasingly apparent in later stages.

Specimens With Embryos of 13 to 17 Millimeters (38–46 Days)

In the four specimens in this age group, there are deep indentations in the contours of the uteroplacental junction. In consequence, the *decidua basalis* varies in thickness between 1.5 and 6.0 mm. Coincidental with the deeper penetration of trophoblast, there is a decrease in the number of veins draining the more central regions of the intervillous space, and this is reflected in a relative reduction in the number of venous openings recorded in two of the specimens. The appearance of a representative coiled artery from specimen 9176 is illustrated in Fig. 6. The complex coiling of the terminal portion of this vessel is produced by the entwining of two branches around the parent artery. The branches arise close together, and in between their origin and the myoendometrial junction the parent artery is less coiled and its lumen is distinctly smaller than in the adjacent portions of the vessel. Elastic fibers disappear from the wall of this artery just proximal to the origin of the branches. The terminal portions of the arteries in these specimens vary between 35 and 100 μ in diameter, and their lumina are reduced by accumulations of cytotrophoblast. There is no direct communication between the terminal parts of the arteries and the intervillous space. Blood still reaches the intervillous space via the intercommunicating spaces (labyrinth) within the cytotrophoblastic shell. The decidua adjacent to the shell contains discrete deposits of amorphous material known as fibrinoid.

Specimens With Embryos of 25 to 50 Millimeters (48–70 Days)

In this group the *decidua basalis* varies in thickness between 1.8 and 5.5 mm because of variation in the depth to which the trophoblast penetrates (Fig. 7). In consequence, the contour of the uteroplacental junction appears as a series of rounded prominences separated by clefts of varying dimensions; some of the smaller prominences contain the terminal portions of the coiled arteries (Fig. 8). The long axes of many of the dilated uterine glands in the *decidua basalis* are no longer perpendicular to the myoendometrial junction but are inclined toward the margin of the placenta. The veins are more numerous in the region where the *decidua basalis* merges with the *decidua capsularis* and, like the glands, they pass obliquely toward the myometrium. In one specimen (Fig. 9), there is a prominent venous sinus at the margin of the placenta, which communicates with the intervillous space through a wide slitlike opening, the largest diameter measuring 600 μ.

The thickness of the trophoblastic shell is very variable. In some regions it is reduced to a single layer of cells; in others it still contains intercommunicating spaces and forms a multicellular covering to the decidua. The amorphous deposits of fibrinoid are more plentiful but do not form a continuous layer beneath the trophoblastic shell. Some of the coiled arteries still terminate in continuity with remaining portions of the labyrinth within the shell (Fig. 10), while others (Fig. 11) communicate directly with the intervillous space through breaks in the continuity of a thin layer of cytotrophoblast. The distal portions of the arteries are dilated and the coils tend to be more loosely arranged than at earlier stages; the terminal openings are larger, with diameters ranging between 100 and 250 μ.

Fig. 32, a drawing of a model of three coiled arteries from specimen 9380, shows that the narrow segment distal to the myoendometrial junction is still present. The reduction in the size of the lumen appears to have no relation to the presence of elastic tissue in the wall of the vessel, since it occurs distal to the point at which elastic fibers cease to be histologically demonstrable in the walls of the arteries. The artery at the left side of the drawing has a prominent coil (indicated by an asterisk), which is illustrated in Fig. 12. Although the coil is some distance from the opening of the vessel, it lies at the edge of the trophoblastic shell. It appears likely that the attenuated wall of this part of the vessel will soon be breached by the cytotrophoblast, and as a result the portion of artery distal to this point will be undermined. Small sections of degenerating arteries can frequently be seen in the tips of the decidual prominences. In spite of the close proximity between the foregoing coil and the cytotrophoblast, there is little evidence of endothelial swelling, and unlike the terminal portion of this and other arteries, the lumen of the coil is not obstructed by an accumulation of cytotrophoblast. The artery is, however, dilated at this particular point, and the wall shows signs of degeneration.

A prominent feature of all the specimens in this group is the deep penetration of syncytiotrophoblast into the *decidua basalis,* where it appears as multinucleate cytoplasmic masses of variable length or occasionally in more bizarre forms (Figs. 13 and 14). The proximity of trophoblastic syncytium to the wall of a vein may be associated with a break in the continuity of the overlying endothelium (Fig. 15); in arteries it sometimes appears to cause focal degenerative changes in the media (Fig. 16).

SPECIMENS WITH FETUSES OF 60 TO 73 MILLIMETERS (12–14 WEEKS)

The seven specimens from this period of pregnancy present striking evidence of the invasive and destructive properties of the trophoblast. Continuing activity of the cytotrophoblastic shell causes a further reduction in the *decidua basalis,* which now varies in thickness between 0.4 and 3.0 mm with occasional extensions into fingerlike prominences. The multinucleate syncytial masses can now be found in the inner layers of the myometrium. In one specimen (9051) they have penetrated into the muscle to a depth of 400 μ. The presence of these cells appears to result in separation of the muscle bundles, especially where the muscle ensheathes the basal portions of the arteries. The basal coils of the arteries are now dilated and more loosely arranged, and their walls show degenerative changes.

The coiled arteries frequently terminate in groups as straight channels 200–350 μ in diameter, which are usually oriented in a vertical plane relative to the myometrium (Figs. 17, 18, and 33). The vertical channels often communicate directly with the intervillous space, but they may still terminate in continuity with the spaces within the cytotrophoblastic shell. Portions of degenerating vessel distal to an arterial opening are seen in all specimens. Most of the arteries are filled with cells (Figs. 17 and 18), which may extend down the vessel as far as the inner layers of the myometrium (Fig. 19). The cells are morphologically similar to the cells of the cytotrophoblast, and in the specimen illustrated in Fig. 19 there is continuity between the cytotrophoblastic shell and the cells that partially occlude the lumen of the myometrial portion of the artery; similar cells are never seen in the veins. The relationship between the intra-arterial cells and the endothelium varies in different parts of the vessel. In the terminal portions, the endothelium is absent, and the lumen is lined by several layers of intra-arterial cells. In the more proximal coils, although some cells lie in clumps within the endothelium, single cells may lie beneath it (Fig. 20). In the region adjacent to the myometrium, multinucleate trophoblastic cells are present in the walls of some arteries. The endothelial cells overlying these focal infiltrations of trophoblast show few signs of activity (Fig. 21).

In specimen 9051 (Figs. 33 and 22), the trophoblast has penetrated into the myometrium and opened up a large vein, which passes in a circumferential direction between muscle bundles lying beneath the basal plate. Although the lumen of the vein appears quite small, the communication between it and the intervillous space is over 4 mm wide. There are several examples of large centrally placed venous openings in the specimens in this group. The spread of trophoblast into the myometrium has interrupted the course of a myometrial artery, which now opens into the intervillous space.

SPECIMENS WITH FETUSES OF 90 TO 200 MILLIMETERS (15–22 WEEKS)

The *decidua basalis* in the six specimens from the fourth and fifth months of pregnancy is seldom more than 1.5 mm thick, but at intervals it extends into the intervillous space for 6–9 mm to form slender projections. Some of these projections contain the terminal portions of an artery that opens into the intervillous space at a variable distance above the general plane of the basal plate; other projections contain the degenerating remnants of an artery that has been undermined at a lower level. The openings of the arteries tend to be grouped together, but the projections of decidua that surround them remain discrete. The apexes of the projections end some distance below the chorionic plate, and villi are frequently attached to them. Groups of dilated uterine glands occur at intervals beneath the basal plate, and sometimes they are present in the decidual projections. The myometrium is frequently separated from the decidua by dilated veins that pass horizontally beneath the basal plate. Such veins communicate through short oblique channels with veins in the myometrium and also with the intervillous space. Several specimens have large veins draining the marginal region of the intervillous space, and often there are several communications between the space and a single vein. The appearance of representative arteries from two specimens in this group is illustrated in Figs. 34 and 35.

The terminal portions of many arteries are still grouped together in the form of vertically oriented channels, whose diameters vary between 200 and 500 μ. There is, however, considerable variation in the size of arteries in a given specimen, and the diameter of a single vessel may change at several points along its course. Fig. 35 shows that there is considerable variation in the size of the arterial communications with the intervillous space and also that there may be continuity between the branches of neighboring arteries.

Owing to the infiltration of trophoblastic cells into the inner third of the myometrium, it is often difficult to determine the position of the myodecidual junction. The arteries in the deeper parts of the myometrium have diameters of 120–300 μ, and their walls contain cells with radiating processes (Fig. 23). These stellate cells are frequently surrounded by deposits of an amorphous substance that is intensely basophilic. With the exception of the endothelium, the characteristic layers of the arterial wall are difficult to define, and there is a loss of elastic fibers from the media. The endothelium is often displaced into the lumen by small groups of cells that appear to originate in the disintegrating wall of the artery (Fig. 24). In frozen sections, the cytoplasm of these cells is seen to stain with Oil Red O (Fig. 25). Accumulations of the cells may be covered by endothelium, but some of them lie within the endothelial lining of the vessel. A few of these intravascular cells contain more than one nucleus, but most of them are uninuclear and closely resemble the intramural cells. Degenerative changes in the walls of some small branches of the main arteries may be associated with a marked reduction in the size of the lumen accompanied by the deposition of strands of material resembling fibrin beneath the endothelium (Fig. 26). Because of lack of uniformity in the distribution and severity of degenerative changes in myometrial arteries, collections of cells may occur proximal to apparently normal sections of the same vessel (Fig. 27).

Specimens With Fetuses of 200 to 310 Millimeters (24–40 Weeks)

The contour of the uteroplacental junction in the last four months of pregnancy is the reverse of that observed in earlier stages. In place of the deep indentations produced by the trophoblast, there are projections of decidua into the intervillous space of up to 15 mm in length. It is customary to describe these projections as septa but, as mentioned in the description of the earlier stages, they are separate structures and their apexes fall short of the chorionic plate; consequently they do not partition the intervillous space. Most of the projections contain the terminal portions of coiled arteries (Figs. 28 and 29). The openings of these arteries into the intervillous space are frequently above the general plane of the basal plate; see Fig. 37(A). Although many arteries end in a series of dilated coils within decidual projections of varying dimensions, some terminate as straight vessels, which lie almost parallel to the basal plate before passing obliquely through it to open into the intervillous space (Fig. 30). Drawings of representative arteries from specimens recovered in the 32nd and 40th weeks of pregnancy (Figs. 36 and 37) illustrate the enormous dilatation of the terminal coils, which are often 2–3 mm in diameter.

The decidua of the basal plate is usually less than one millimeter thick and is separated from the myometrium by very large veins. These veins communicate with the intervillous space through openings of varying dimensions, and together with the myometrial veins in the deeper portions of the myometrium they form a plexus that surrounds the arteries; see Fig. 37(B). The venous openings into the intervillous space frequently contain the terminal portions of fetal villi. Some specimens have large veins draining the marginal portion of the placenta, and groups of dilated and somewhat compressed uterine glands may still be present in the *decidua basalis* (Fig. 31).

DISCUSSION

Uteroplacental Arteries

Terminology

In the foregoing description of the uterine vasculature at various stages of pregnancy, we have referred to the branches of the uterine artery that supply the placenta as the uteroplacental arteries or simply as the coiled arteries. The customary division into radial and spiral arteries (p. 45), which may apply in the nonpregnant state, has no functional significance in pregnancy. Our findings show that after the third month of gestation both spiral and radial portions may open directly into the intervillous space. Furthermore, the boundary between the endometrium and myometrium, the usual line of division between radial and spiral portions, is irregular and may be difficult to identify in the latter half of pregnancy. An additional source of confusion in the literature is the use of the term "arteriole" to describe arterial vessels in the basal plate of the full-term placenta (Marais, 1962). Although there is no clearly defined transition between coiled artery and arteriole, the arterial supply to the intervillous space at this stage of pregnancy is derived from muscular arteries, which formerly had well-developed elastic laminae in their walls. In our material, and in the *decidua parietalis* of presomite conceptuses, the presence of elastic tissue cannot be demonstrated in the walls of the coiled arteries beyond the boundary of the *stratum basalis;* only distal to this point do the size and morphologic appearance of the vessel correspond to that of an arteriole.

Morphology

The endometrial portions of the uteroplacental arteries in the models of the four youngest specimens in our series exhibit varying forms of branching. In 9909 and in 9176 (Fig. 6), the trunk of the artery divides abruptly into two or more large branches soon after it enters the endometrium. In another specimen (9380, Fig. 32), the coiled artery divides in the myometrium into two trunks, which subsequently give rise to several branches in the *stratum spongiosum.* None of the vessels that we have modeled give rise to sizable basal branches within the endometrium, but from most of the large vertical branches small vessels originate that are distributed to neighboring glands. Some also supply branches to small clusters of lymphocytes, which are found in the *stratum basalis.* The myometrial portions of the coiled arteries frequently give rise to lateral branches, which pass through the deepest part of the myometrium to provide a link between neighboring arteries. From these circumferential branches arise small vessels, which pass into the endometrium to supply the *stratum basalis.*

All the arteries in these early models have constricted segments just distal to the myoendometrial junction and proximal to the origin of the large branches. We were unable to relate these constrictions to the presence of specialized muscle cells in the walls of the vessel of the type illustrated by Okkels and Engle (1938), and attempts to demonstrate a specific innervation of this region met with little success. It is unlikely that these constrictions are artifacts for they are clearly seen in well-injected specimens; furthermore, Bartelmez has observed constrictions in coiled arteries in the myometrium of nonpregnant human and monkey uteri, and Boyd (1956) described them in the *decidua basalis* of his material from human pregnancy. Ramsey (1949, 1958) noted their presence in the monkey, distal to the myoendometrial junction, at various stages of pregnancy; and Martin *et al.* (1964) demonstrated by radioangiography in monkeys that coiled arteries may function intermittently during periods of uterine relaxation in midpregnancy. The activity, when independent of myometrial contraction, is attributed by Martin *et al.* to vasomotion, occasioned by factors as yet unknown. Those that must be considered include local variations in the threshold response to impulses from autonomic nerves, and the presence of trophoblastic cells in the arteries. If vasomotion is dependent upon an intact arterial wall, then it is unlikely that constrictions will occur in those arteries that have been altered by the action of trophoblast. This applies equally to both human vessels and to those of the monkey (Ramsey, 1949).

In the specimens from the last three months of pregnancy, the terminal portions of the uteroplacental arteries are quite frequently located in the projections of the decidua into the intervillous space. As Becker and Jipp (1963) suggest, there appears to be little justification for calling these projections "placental septa," for there is no continuity between individual projections and the chorionic plate and consequently little reason for supposing that they subdivide the intervillous space. In our material, most of the decidual projections end midway in the intervillous space and are in general somewhat shorter than those illustrated by Bumm (1893).

Soon after the formation of the cytotrophoblastic shell, the uteroplacental arteries begin to dilate. At first, only the terminal parts of the vessels are affected, especially where they lie in contact with the cytotrophoblast. The dilatation gradually extends proximally until, in later stages, it extends into the myometrial segment where it is often very marked (Fig. 35). Vessels of this type are encountered with such regularity after the 20th week of pregnancy that they can hardly be regarded as resulting from a pathologic change in the vessel (Wigglesworth, 1964). Similar dilatation has been observed by Arts (1961), and it also occurs in the rhesus monkey (Ramsey, 1949), with the same progression proximally as gestation advances.

Formation of the Lacunae

The main object in reexamining the early implantation sites was to study the relationship between the trophoblast and the capillary plexus of the adjacent *stratum compactum.* In the youngest implanted human conceptus (8020, 7½ days) connections between the maternal capillaries and the syncytiotrophoblast are already established, although their functional significance is difficult to assess. The absence of extravasated blood and the uninterrupted transition between capillary endothelium and syncytium lend support to the assumption that the syncytium advances by a flowing movement that engulfs the blood vessels.

The presence of capillaries within the periphery of the syncytial plate and the demonstration of continuity between them suggest a possible stage in the formation of the lacunae. According to Streeter (1926), and Wislocki and Streeter (1938), the lacunae arise by the coalescence of vacuoles or fluid spaces within the trophoblastic plate. Of some interest is the great rapidity with which these spaces become confluent, for Hertig and Rock (1945) noted that the vast majority of the trophoblastic lacunae are in communication with one another by the ninth day of development. Of equal importance is the question of how the lacunae establish communication with the maternal capillaries. Hamilton and Boyd (1960) consider that there is no evidence that this results from a "disordered destruction of maternal tissue," and certainly the histologic appearance of early implantation sites suggests a state of orderly coexistence between the syncytiotrophoblast and the endometrium. It may be that the configuration of the early lacunae reflects, at least in part, the distribution of existing capillaries at the site of implantation and that the growing syncytium engulfs them *in situ.* Further early specimens are required to substantiate this suggestion, which offers an explanation for the rapid development of continuity between individual spaces and for their connection with the maternal circulation.

By the ninth day, the capillary connections with the trophoblastic lacunae have enlarged and are now usually referred to as sinusoids (Hertig and Rock, 1941). Most of the sinusoids can be traced to endometrial veins and subsequently to veins in the myometrium. We have followed several arteries in close proximity to the syncytiotrophoblast but have never found any evidence of direct communication with the lacunae, or of any reaction by the endothelium or by the vessel wall. This may be partly due to the presence of the perivascular stromal "cuffs" and partly because the lateral branches of the arteries are mainly distributed to the uterine glands. We agree with Bartelmez (1956) and Boyd (1956) concerning the absence of arteriovenous anastomoses in the *stratum spongiosum;* in our injected specimens, India ink does not spread directly from the arterial into the venous system.

Influence of Trophoblast on the Uteroplacental Vasculature

About the 12th or 13th day of development, the orderly relationship between the trophoblast and the endometrium starts to break down. Blood begins to appear in the uterine glands adjacent to the implantation site and may escape into the uterine cavity. Krafka (1941) has drawn attention to the frequency with which blood is present in uterine glands associated with early implantation sites, and Hamilton and Boyd (1960) consider that it is a normal feature of human implantation after the 12th day. Since this reaction occurs about the time of the first missed menstruation, Krafka (1941) considers that the appearance of blood in the glands is related to a pseudomenstruation and not to the erosive action of syncytium. Although agreeing with the latter statement, we consider that the appearance of extravasated blood around the implantation site coincides with the initial liberation of cells from the tips of the cytotrophoblastic columns into the maternal tissue. A chronological relation between these two events also occurs in the rhesus monkey, for, according to Wislocki and Streeter (1938), blood first appears in the glands on the 17th day, when the cytotrophoblastic shell is just beginning to form.

The formation of the trophoblastic shell disturbs the orderly relationship between the maternal and fetal tissues. There is hemorrhage into the lumina of neighboring glands and to a lesser extent into the intercellular spaces adjacent to the arteries. All elements of the endometrium appear to undergo gradual dissolution, and degenerating stromal cells are present in the boundary zone adjacent to the cytotrophoblast. It appears that the walls of the arteries are eroded from without, because the endothelium is frequently intact until the wall of the vessel has virtually disappeared. Initially, the thin walls of the terminal portions of the arteries offer little resistance to the cytotrophoblast, so blood escapes into spaces within the trophoblastic shell. While it is possible that there are some isolated spaces within the shell, we believe that many of them are linked together to form a labyrinth. Such an arrangement enables maternal blood to be distributed around the shell to areas not in immediate contact with the arteries. It does not seem that the spaces in the cytotrophoblastic shell are always situated in the wake of a degenerating artery; however, it is sometimes possible to demonstrate a fairly direct channel from the terminal part of the artery, through the shell, into the intervillous space.

During the first three months of development, the boundary between the trophoblast and the decidua is irregular. Some of the deep erosions into the decidua may result from the spread of trophoblast into and around the sinusoids, for there is a rapid reduction in the number of venous openings into the intervillous space. The presence of these deep penetrations has a marked effect upon the arteries. They expose the walls of the more proximal parts of the artery to dissolution by the cytotrophoblast and, in due course, blood leaks through the damaged wall of the vessel. As already mentioned, trophoblast may extend into the myometrium and breach the walls of arteries, which are not generally believed to open directly into the intervillous space.

The process of erosion and subsequent undermining of the arteries leads to a reduction and eventually to a cessation of the circulation through the distal parts of the affected vessel. The endothelium lining the nonfunctional portion of the artery becomes displaced toward the center of the lumen by exudate which may later undergo varying degrees of organization.

One such vessel is the basal artery illustrated in Fig. 26, which was in communication with two neighboring coiled arteries. A reconstruction of the vessel and its connections shows that on this occasion the reduction in circulation resulted from the leakage of blood through a breach in the wall of a connection between the affected vessel and one of the coiled arteries. The other coiled artery had a large opening into the intervillous space, and although the connection between this vessel and the basal artery was still patent, the histologic appearances suggest that little blood was diverted into it. As a result of observing several similar examples, we believe that the circulation through the arteries tends to follow a preferential path, and consequently blood is not readily diverted into branches of smaller caliber, particularly when the main vessel has become dilated. Furthermore, it seems likely that the cobweblike strands of subintimal fibrin deposition develop only if the wall of the affected artery is substantial enough to withstand collapse when the circulation finally ceases. This type of vascular response is seldom observed before the 12th week, but subsequently it occurs with increasing frequency, especially between the 4th and 5th months of pregnancy.

Intravascular and Perivascular Cells

Before discussing the nature of the cells found within and adjacent to the uteroplacental arteries, it is convenient to refer to the elements of the trophoblast, which spread into the *decidua basalis.* The migration of trophoblast commences during the formation of the cytotrophoblastic shell and continues in various forms throughout the remainder of pregnancy. At first it frequently occurs in the form of multinucleate cytoplasmic streamers, which are often several hundred microns in length (Fig. 13), but it may also assume more irregular shapes (Fig. 14). In later stages, the migrating trophoblast is composed of multinucleate and binucleate cells together with well-circumscribed multinucleate giant cells. We agree with Boyd and Hamilton (1960) and Schramm (1962) regarding the fetal origin of the migrating cells, but we are not altogether sure whether the origin and function of the early syncytial streamers correspond to those of the cells seen in older specimens. It may be that the syncytial streamers are eventually broken up into smaller units, but so little is known about their method of locomotion that their ultimate fate is open to speculation. There is no evidence in our sections to suggest that the streamers are specifically oriented toward the blood vessels, but undoubtedly some of them come into contact with the outer walls of arteries and veins. At such points of contact, the trophoblastic cells appear to insinuate themselves into the wall of the artery (Fig. 16), and fibrinoid material is deposited around them. We have no evidence that the syncytial streamers actually enter the lumina of the arteries, but independent multinucleate giant cells are quite frequently observed within the venous sinusoids.

By the 12th week of development, the more discrete elements of the migrating trophoblast begin to extend into the inner layers of the myometrium. When they are found in close proximity to blood vessels, their presence appears to induce degenerative changes in the walls of muscular arteries, but there is little evidence that they damage the walls of the veins. The changes in the walls of arteries consist of a loosening of the media and adventitia and a gradual dissolution of elastic fibers and muscle cells to form an amorphous layer around the endothelium. There is no subintimal deposition of fibrin or hyaline material and no evidence of endothelial proliferation. Large cells, which exhibit a stellate arrangement when stained with phosphotungstic acid hematoxylin, occur at intervals in the walls of affected muscular arteries (Fig. 23). We are not certain whether these cells originate from trophoblast. Their distribution is irregular, and they are larger and much less numerous than the enlarged muscle cells in the walls of similar arteries in the *decidua parietalis.* There is no histologic evidence to suggest that the stellate cells migrate into the lumen of the artery, and their presence in an attenuated form in later stages suggests that they eventually degenerate.

In addition to the stellate cells, smaller cells, which are occasionally binucleate, are found in the walls of arteries and beneath the endothelium (Figs. 20 and 24). We believe that these cells are derived from the cytotrophoblast, and because they are frequently found beneath the intact endothelium, it appears that they reach this position by passing through the damaged wall of the artery. It is very probable that most of these cells pass into the lumen, but we cannot distinguish them from cytotrophoblastic cells that migrate down through the open ends of the arteries. Intra-arterial migration commences soon after the formation of the cytotrophoblastic shell, but it becomes more evident when the thicker walls of the more proximal portions of the arteries take longer to disintegrate than the surrounding stromal tissue. Thus masses of cytotrophoblastic cells begin to occupy the terminal parts of most of the arteries, frequently causing a reduction in the lumina of affected vessels. Between the 12th and 14th weeks, the cytotrophoblast extends along many of the arteries and may reach as far as the deeper layers of the myometrium (Fig. 19). There is considerable variation in the extent of the intra-arterial migration in the different specimens in this age group and in the distribution of cells within the arteries of individual specimens. It is unusual to find continuous masses of intra-arterial cells after the 16th week of pregnancy although discrete collections of them are frequently present. The distribution of these collections suggests that the cells are deposited, possibly as the result of eddies, at places where the arteries make abrupt bends and near the origin of lateral branches. Such an explanation need not necessarily imply that the cells entered through the open end of the artery, for they could be deposited in these situations after passing through its wall. This may be the reason why quite substantial collections of cells may be found in a coiled artery within the inner layer of the myometrium, when only a few cells are present in the distal parts of the same vessel (Fig. 27). We do not know whether cells that have migrated into an artery are subsequently washed out into the intervillous space, but the fact that masses of them are still present in well-injected specimens suggests that they are not easily dislodged from the vessels.

We believe that in some instances a massive migration of cells may lead to a cessation of circulation in the affected vessel. Occasionally the deposition of fibrin around a small collection of cells leads to a reduction in the lumen of the artery. If this occurs near the origin of a branch, the circulation through the smaller vessel may be reduced and the lumen eventually obliterated. It must, however, be emphasized that the effects of such events on the arterial circulation may not be severe, for as Fig. 33 shows, the coiled arteries often have several openings into the intervillous space.

The occurrence of cells within the lumina of uteroplacental arteries and in the maternal tissues beneath the basal plate is not confined to human pregnancy. Key references to the relevant literature are to be found in the contributions of Wimsatt (1951), Orsini (1954), Björkman (1954), and Boyd and Hamilton (1960). In histochemical studies on the pregnant human uterus, McKay *et al.* (1958) have noted a similarity between the migratory cells of the placental site and the cytotrophoblast; they consider that both giant and intra-arterial cells are derived from the cytotrophoblast rather than from the syncytium. However, Brettner (1964) and other workers believe that some of the periarterial giant cells originate from smooth muscle cells in the media of arteries. He has identified sex chromatin in the periarterial giant cells from pregnancies with a male fetus. We find no similarity between the histologic appearance of smooth muscle cells in muscular arteries of the *decidua parietalis* and the giant and stellate cells that occur in similar vessels of the *decidua basalis*. Furthermore, we question whether dedifferentiation and subsequent redifferentiation of muscle cells can occur in close proximity to the erosive action of cytotrophoblast.

The distribution and appearance of the intra-arterial cells in the decidua of the pregnant rhesus monkey led Wislocki and Streeter (1938) and Ramsey (1949) to consider the possibility that they were derived from the endothelium of the vessel. Endothelial proliferation is minimal in our material and it is unlikely that it contributes to the cells within the arteries.

The presence of lipid within the intra-arterial cells (Fig. 25) is probably an indication of their senescence, for in the stromal cytotrophoblast its distribution is more discrete; we do not know whether there is any relationship between the lipid-laden intra-arterial cells and the foam cells described by Brosens (1964) in the uteroplacental arteries of hypertensive women.

Uteroplacental Veins

The venous drainage of the endometrium is not closely associated with the coiled arteries, and the veins do not lie within special columns of stromal cells. Because of the multiplicity of their interconnecting tributaries, they form a plexus that has wide and abrupt variations in caliber beneath the implantation site. Unlike the arteries, the efferent veins of the plexus are not convoluted. They tend to be oriented in a plane that is perpendicular to the surface epithelium, and they usually pass in an oblique and steplike manner toward the myoendometrial junction. The myometrial veins, which pass circumferentially between the muscle bundles, are interconnected at frequent intervals by short oblique vessels. This arrangement directs blood toward the large tributaries of the uterine veins in the *area vasculosa* of the myometrium. As Danesino (1957) has noted, it is often difficult to establish the boundary between the wall of a vein and the uterine muscle.

After the formation of the trophoblastic shell, the erosion of the decidua proceeds more quickly in the areas between the arterial columns. In consequence, the veins are opened up more rapidly than the arteries. Possibly this is related to the ease with which the trophoblast extends along the walls of the veins; large multinucleate giant cells are frequently encountered within the veins draining the early specimens, but they are seldom found in the arteries. As the trophoblast expands laterally and the course of both uterine glands and blood vessels becomes more oblique, venous openings occur with increasing frequency through the marginal portions of the basal plate (Fig. 9). By the 12th week, many of the openings from the intervillous space into veins in the central part of the *decidua basalis* are in the same plane as the most dependent parts of the space, which may be less than a millimeter from the inner surface of the myometrium. In one specimen that we examined (9051, Fig. 22), the trophoblast had opened up a vein in the myometrium, and at this point the wall of the vein actually formed the floor of the intervillous space.

At slightly later stages, large venous sinuses begin to appear beneath the basal plate, adjacent to and parallel with the muscle bundles in the deep layers of the myometrium. It is sometimes difficult to decide whether their size is an artifact, because only occasionally is the lumen of a venous sinus filled with blood cells. In view of the increasing frequency with which these sinuses are encountered after the 16th week of pregnancy, there is little doubt that they constitute an important route for the drainage of blood from the intervillous space. Moreover, it appears that they form a plane of cleavage, which facilitates the separation of the placenta from the wall of the uterus. The openings into this subdecidual venous plexus are distributed at random over the entire basal plate. The openings into the basal sinuses are either in the form of wide oblique fissures (Fig. 29) or of well-circumscribed vertical channels.

These channels may recur at intervals along a single sinus, forming the *Flötenrohrvenen* (flutelike veins) of Spanner (1935). In contrast to the arteries, the venous openings in the later specimens occur neither at the summits nor high up on the sides of the decidual prominences.

We have paid particular attention to the venous drainage of the marginal portion of the placenta in an endeavor to evaluate Spanner's (1935) concept of the marginal sinus. If, as Spanner suggested, the term implies the existence of a specific channel that is partially or completely separated from the intervillous space, such an arrangement is not a constant feature of our material. There is, however, no doubt that the marginal portion of the intervillous space is quite frequently drained by large venous sinuses (Fig. 31), and occasionally such sinuses arise from an area that is partially separated by a decidual partition from the intervillous space. The marginal venous sinuses drain blood away from the periphery of the placenta, and their superficial connections in the decidua may form a periplacental plexus of veins, which, when distended, is clearly visible to the naked eye.

Although trophoblastic giant cells are frequently found adjacent to the walls of veins in the latter half of pregnancy, we have no evidence that they penetrate the walls and enter the circulation. Terminal parts of villous stems, however, quite often pass through venous openings in the basal plate, but there is no morphological evidence to suggest that they cause serious obstruction.

In the full-term placenta, the uteroplacental veins surround the arteries forming a succession of layers, which are separated by strips of myometrium (Fig. 37). Blood flows between adjoining layers through the intervening myometrium in short oblique interconnecting veins that are devoid of valves. This arrangement of veins and muscle may enable myometrial contractions to influence the flow of blood through the veins, and indirectly the venous drainage of the intervillous space. Furthermore, the arrangement is without doubt of great importance in controlling hemorrhage from the veins after the separation of the placenta at parturition.

Number of Arterial Openings

Table 2 shows that the number of arterial openings into the intervillous space is subject to considerable variation at different stages of pregnancy. In early specimens, the number is largely determined by the pattern of branching from the coiled artery. Even at this stage there is some evidence of a tendency to form preferential pathways; our observations suggest that where several branches arise from the main vessel in close succession there is often a noticeable difference in their caliber.

As pregnancy proceeds, there appears to be a decrease in the number of openings. The penetration of cytotrophoblast into the decidua results in the undermining of some of the major terminal portions of the uteroplacental arteries, with consequent loss of other more peripheral branches. At the same time, some of the branches that are normally confined to the basal layer of the decidua now open into the intervillous space. It seems unlikely that these basal branches become major routes for arterial blood flow; they seldom become greatly dilated and, following the migration of cytotrophoblast into the arteries, many of them appear to be nonfunctional.

Between the 14th and 20th weeks, the presence of large amounts of intravascular cytotrophoblast probably leads to cessation of blood flow in some arteries; others may eventually be obstructed by deposition of fibrin around discrete collections of cytotrophoblastic cells at points along the vessel. After the 20th week, an important cause of further reduction in arterial openings is the breaching of arteries in the inner layer of the myometrium. It seems unlikely that this can be the sole reason for the abrupt reduction in the number of openings that occurred after the 16th week, and the decrease may be partly due to the onset of uterine stretching. Because of the virtual absence of branches in the full-term specimen, the count refers to the number of uteroplacental radial arteries, and it is similar to Boyd's (1956) average figure of one artery per 100 mm^2 of placental surface.

In describing the morphology of the uteroplacental vasculature, we are mindful of the fact that all our specimens come from women who had previously been pregnant on two or more occasions. This is mentioned because we do not know whether past pregnancies have any influence on the rate of decidual erosion, or on the depth to which cytotrophoblast extends into the arteries and penetrates the subplacental tissues.

SUMMARY

During the initial stages of implantation it appears that the syncytiotrophoblast engulfs the capillary plexus in the adjacent *stratum compactum*. It is suggested that part of the plexus remains within the trophoblastic plate as a series of small spaces, which maintain continuity with the maternal circulation and subsequently enlarge to form the lacunae. Before the development of the cytotrophoblastic shell, the most prominent vascular connections with the lacunae are dilated tributaries of endometrial veins. The apparently wellordered relationship between the syncytiotrophoblast and the surrounding maternal tissue is disturbed by the development of the cytotrophoblastic shell; blood appears in the lumina of uterine glands and, within the cytotrophoblastic shell, in a series of intercommunicating spaces, which form a labyrinth. On the maternal aspect of the shell the labyrinth is in continuity with the terminal portions of the coiled arteries and on the embryonic side it communicates with the lacunae, which coalesce to form the intervillous space. The labyrinth may enable blood to be distributed around the circumference of the trophoblast to regions not in contact with coiled arteries. This arrangement persists while the shell remains a multicellular layer but, when it becomes attenuated during the second month of development, arteries begin to open directly into the intervillous space and collections of cytotrophoblast appear in their lumina. Initially confined to the terminal portions, the cytotrophoblastic cells extend proximally and by the 16th week they are found in many of the arteries in the inner layer of the myometrium. During the same period, the coiled arteries become dilated; the dilatation extends proximally, affecting arteries in the inner third of the myometrium by the seventh month. Concomitant with the intra-arterial migration of trophoblast, the walls of arteries in the *stratum basalis* and inner myometrium contain large stellate cells and smaller cytotrophoblastic cells, some of which may also pass into the arterial lumen.

It is believed that intra-arterial accumulations of cytotrophoblastic cells may ultimately bring about a cessation of circulation through some of the affected vessels. The number of arterial openings into the intervillous space is gradually reduced, partly as a result of the intra-arterial accumulations of cytotrophoblast and partly by breaching of the walls of more proximal parts of arteries by deep penetrations of trophoblast through the decidua, which sometimes extend into the myometrium. Circulation ceases distal to the point at which such a breach occurs, but the walls of nonfunctional arterial segments remain until they are destroyed by the advancing trophoblastic shell. During the last three months of pregnancy, the terminal portions of many arteries lie in prominences of decidua, which project into the intervillous space but do not subdivide it.

The openings of uteroplacental veins are distributed throughout the decidual plate; large veins draining the marginal portion of the intervillous space into veins in the neighboring *decidua parietalis* have been observed in several specimens. After the 30th week a prominent venous plexus separates the *decidua basalis* from the inner layer of the myometrium and appears to function as a plane of cleavage for placental separation. The subdecidual venous plexus communicates with the myometrial veins through short oblique channels, which are surrounded by myometrium, an arrangement that appears likely to permit uterine contraction to influence venous blood flow.

ACKNOWLEDGMENTS

We wish to record our thanks to our American colleagues and to the staff of the Department of Obstetrics and Gynecology, the London Hospital, who collected and prepared specimens for us.

We are especially grateful to W. H. Duncan and the technical staff of the Carnegie Department of Embryology for the skill and enthusiasm they brought to the task of cutting and preparing large numbers of serial sections. We also wish to thank R. D. Grill for most of the photography, Dr. A. Boyde for his help with Fig. 6, and R. F. Birchenough, J. E. Lindner, and D. A. McBreaty for photographic and other assistance.

Particular acknowledgment is made to the artists, Ranice W. Crosby, Sharon N. Weilbaecher, and Frank B. Price, who have skillfully overcome the many difficulties inherent in illustrating the models.

John W. S. Harris wishes to acknowledge the award of a Rockefeller Foundation Fellowship by the British Medical Research Council and to express his gratitude for subsequent support as a Visiting Investigator of the Carnegie Institution.

LITERATURE CITED

Arts, N. F. Th. 1961. Investigations on the vascular system of the placenta. II. The maternal vascular system. *Am. J. Obstet. Gynecol., 82,* 159–166.

Bartelmez, George W. 1931. The human uterine mucous membrane during menstruation. *Am. J. Obstet. Gynecol., 21,* 623–643.

Bartelmez, George W. 1933. Histological studies on the menstruating mucous membrane of the human uterus. *Carnegie Inst. Wash. Publ.* 443, *Contrib. Embryol., 24,* 141–186.

Bartelmez, George W. 1956. Premenstrual and menstrual ischaemia and the myth of endometrial arteriovenous anastomoses. *Am. J. Anat., 98,* 69–95.

Bartelmez, George W. 1957. The form and the functions of the uterine blood vessels in the rhesus monkey. *Carnegie Inst. Wash. Publ.* 611, *Contrib. Embryol., 36,* 153–181.

Becker, V., and P. Jipp. 1963. Über die Trophoblastschale der menschlichen Plazenta. *Geburtsh. Frauenheilk., 23,* 466–474.

Björkman, N. 1954. Morphological and histochemical studies on the bovine placenta. *Acta Anat. (Basel),* 22, *Suppl. 22,* 1–92.

Borell, U., I Fernström, L. Ohlson, and N. Wiqvist. 1964. Effect of uterine contractions on the human uteroplacental blood circulation. An arteriographic study. *Am. J. Obstet. Gynecol., 89,* 881-890.

Borell, U., I. Fernström, L. Ohlson, and N. Wiqvist. 1965*a*. Influence of uterine contractions on the uteroplacental blood flow at term. *Am. J. Obstet. Gynecol., 93,* 44–57.

Borell, U., I. Fernström, L. Ohlson, and N. Wiqvist. 1965*b*. Arteriographic study of the blood flow through the uterus and placenta at mid-pregnancy. *Acta Obstet. Gynecol. Scand., 44,* 22–31.

Böving, B. G. 1963. Implantation mechanisms. In *Mechanisms Concerned with Conception,* C. G. Hartman, ed., Pergamon Press, New York, pp. 321–396.

Boyd, J. D. 1956. Morphology and physiology of the uteroplacental circulation. In *Gestation. Transactions of the Second Conference,* C. A. Villee, ed., Josiah Macy, Jr. Foundation, New York, pp. 132–194.

Boyd, J. D., and W. J. Hamilton. 1960. The giant cells of the pregnant human uterus. *J. Obstet. Gynaecol. Brit. Empire, 67,* 208–218.

Brettner, A. 1964. Zum Verhalten der sekundären Wand der Uteroplacentargefässe bei der decidualen Reaktion. *Acta Anat. (Basel), 57,* 366–376.

Brosens, I. 1964. A study of the spiral arteries of the decidua basalis in normotensive and hypertensive pregnancies. *J. Obstet. Gynaecol. Brit. Commonwealth, 71,* 222–230.

Bumm, E. 1893. Über die Entwicklung des mütterlichen Blutkreislaufes in der menschlichen Placenta. *Arch. Gynaekol., 43,* 181–195.

Danesino, V. 1957. The myometrial vasculature during gestation. *Arch. Ostet. Ginecol., 62,* 236-251.

Daron, G. H. 1936. The arterial pattern of the tunica mucosa of the uterus in Macacus rhesus. *Am. J. Anat., 58,* 349–419.

Friedländer, C. 1870. Physiologisch-anatomische Untersuchungen über den Uterus. Leipzig, Germany.

Hamilton, W. J., and J. D. Boyd. 1951. Observations on the human placenta. *Proc. Roy. Soc. Med., 44,* 489–496.

Hamilton, W. J., and J. D. Boyd. 1960. Development of the human placenta in the first three months of gestation. *J. Anat. (London), 94,* 297–328.

Hasner, Eivin. 1946. Endometriets vasculaere Cyklus. En anatomisk-histofysiologisk Undersøgelse. *Det Berlingske Bogtrykkeri,* Copenhagen.

Hertig, Arthur T., and John Rock. 1941. Two human ova of the pre-villous stage, having an ovulation age of about eleven and twelve days respectively. *Carnegie Inst. Wash. Publ.* 525, *Contrib. Embryol., 29,* 127–156.

Hertig, Arthur T., and John Rock. 1945. Two human ova of the pre-villous stage, having a developmental age of about seven and nine days respectively. *Carnegie Inst. Wash. Publ.* 557, *Contrib. Embryol., 31,* 67–84.

Hertig, Arthur T., John Rock, and E. C. Adams. 1956. A description of 34 human ova within the first 17 days of development. *Am. J. Anat., 98,* 435–494.

Hunter, W. 1774. Anatomia uteri humani grovidi tabulis illustrata.

Krafka, Joseph, Jr. 1941. The Torpin ovum, a presomite human embryo. *Carnegie Inst. Wash. Publ.* 525, *Contrib. Embryol., 29,* 167–193.

Leopold, G. 1877. Die Uterusschleimhaut während der Schwangerschaft und der Bau der Placenta. *Arch. Gynaekol., 11,* 443–500.

Lundgren, N. 1957. Studies on the vasculature of the corpus of the human uterus. *Acta Obstet. Gynec. Scand., 36, Suppl. 4,* 1–115.

Marais, W. D. 1962. Human decidual spiral arterial studies. *J. Obstet. Gynaecol. Brit. Commonwealth, 69,* 1–12.

Markee, J. Eldridge. 1940. Menstruation in intraocular endometrial transplants in the rhesus monkey. *Carnegie Inst. Wash. Publ.* 518, *Contrib. Embryol., 28,* 219-308.

Martin, C. B., Jr., H. S. McGaughey, Jr., I. H. Kaiser, M. W. Donner, and Elizabeth M. Ramsey. 1964. Intermittent functioning of the uteroplacental arteries. *Am. J. Obstet. Gynecol., 90,* 819–823.

McKay, D. G., Arthur T. Hertig, E. C. Adams, and M. V. Richardson. 1958. Histochemical observations on the human placenta. *Obstet. Gynecol., 12,* 1–36.

Okkels, H., and E. T. Engle. 1938. Studies on the finer structure of the uterine blood vessels of the Macacus monkey. *Acta Pathol. Microbiol. Scand., 15,* 150–168.

Orsini, M. W. 1954. The trophoblastic giant cells and endovascular cells associated with pregnancy in the hamster, *Cricetus auratus. Am. J. Anat., 94,* 273–331.

Ramsey, Elizabeth M. 1949. The vascular pattern of the endometrium of the pregnant rhesus monkey *(Macaca mulatta). Carnegie Inst. Wash. Publ.* 583, *Contrib. Embryol., 33,* 113–147.

Ramsey, Elizabeth M. 1954. Venous drainage of the placenta of the rhesus monkey *(Macaca mulatta). Carnegie Inst. Wash. Publ.* 603, *Contrib. Embryol., 35,* 151–173.

Ramsey, Elizabeth M. 1958. Vascular anatomy of the uteroplacental and foetal circulation. In *Oxygen Supply to the Human Foetus,* J. Walker and A. C. Turnbull, eds., Blackwell Scientific Publications, Ltd., Oxford, England, pp. 67–69.

Ramsey, Elizabeth M., George W. Corner, Jr., and M. W. Donner. 1963. Serial and cineradio-angiographic visualization of maternal circulation in the primate (hemochorial) placenta. *Am. J. Obstet. Gynecol., 86,* 212–225.

Ramsey, Elizabeth M., C. B. Martin, Jr., H. S. McGaughey, Jr., I. H. Kaiser, and M. W. Donner. 1966. Venous drainage of the placenta in rhesus monkeys: radiographic studies, *Am. J. Obstet. Gynecol., 95,* 948–955.

Rossman, I., and George W. Bartelmez. 1957. The injection of the blood vascular system of the uterus. *Anat. Record, 128,* 223–231.

Sampson, J. A. 1913. The influence of myomata on the blood supply of the uterus, with special reference to abnormal uterine bleeding. *Surg. Gynecol. Obstet., 16,* 144–180.

Schramm, B. 1962. Origine des cellules géantes de la caduque humaine. *Gynecol. Obstet., 61,* 423–433.

Spanner, R. 1935. Mutterlicher und kindlicher Kreislauf der menschlichen Placenta und seine Strombahnen. *Z. Anat. Entwicklungsgeschichte, 105,* 163–242.

Streeter, George L. 1926. The "Miller" ovum—the youngest normal human embryo thus far known. *Carnegie Inst. Wash. Publ.* 363, *Contrib. Embryol., 18,* 31–48.

Wigglesworth, J. S. 1964. Morphological variations in the insufficient placenta. *J. Obstet. Gynaecol. Brit. Commonwealth, 71,* 871–884.

Wimsatt, W. A. 1951. Observations on the morphogenesis, cytochemistry and significance of the binucleate giant cells of the placenta of ruminants. *Am. J. Anat., 89,* 233–282.

Wislocki, George B., and George L. Streeter. 1938. On the placentation of the macaque *(Macaca mulatta),* from the time of implantation until the formation of the definitive placenta. *Carnegie Inst. Wash. Publ.* 496, *Contrib. Embryol., 27,* 1–66.

PLATES

PLATE 1, Figs. 1–3

Fig. 1. Section through the implantation site of the 7½-day-old human conceptus described by Hertig and Rock. Part of the maternal capillary plexus in the *stratum compactum* has been engulfed by syncytiotrophoblast; the junction between the syncytium and the endothelium of a capillary is illustrated at *A.* The model prepared from this specimen shows the capillary at *A* is in continuity with the irregularly shaped space in the trophoblastic plate *B,* and that this communicates with the capillary *C,* at the opposite side of the implantation site. Erythrocytes and leucocytes are present in the capillary and in the space within the trophoblastic plate. Specimen 8020, section 7-1-3; ×300.

Courtesy Dr. Arthur T. Hertig

Fig. 2. Section through the implantation site of the 11-day-old human conceptus described by Hertig and Rock. The trophoblast is clearly differentiated into an inner layer of cytotrophoblast and a more peripheral syncytium that is in contact with the maternal tissues. At *A,* the cytotrophoblast has proliferated to form the rudiment of a primary villous stem. Within the syncytium are many intercommunicating lacunae, some of which contain maternal blood cells. Maternal venous sinusoids open into the lacunae at *B* and *C,* but there are no direct connections between the lacunae and the coiled artery at right. Specimen 7699, section 8-3-6; ×100.

Courtesy Dr. Arthur T. Hertig

Fig. 3. From a sagittal section through the uterus and *in situ* placenta of a 5.3-mm embryo. At *A,* the terminal portion of a coiled artery opens into a space within the multilayered cytotrophoblastic shell. A model prepared from this specimen shows that most of the spaces in the cytotrophoblastic shell are in continuity and that together they form a labyrinth, which communicates at intervals *(B)* with the intervillous space *(IVS).* The inner aspect of the shell is covered by syncytium, and multinucleate giant cells are present in some of the spaces. Specimen 8306, section 7-3-2; ×45.

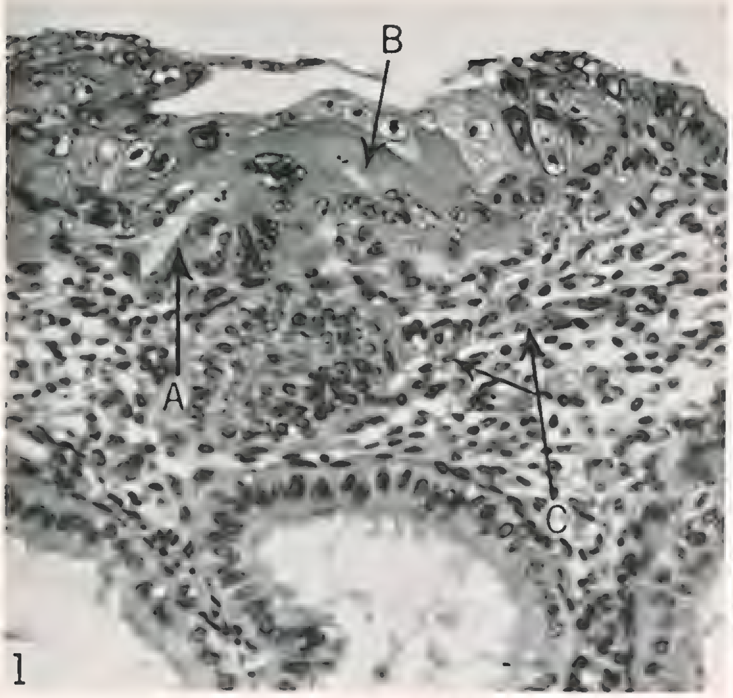
1

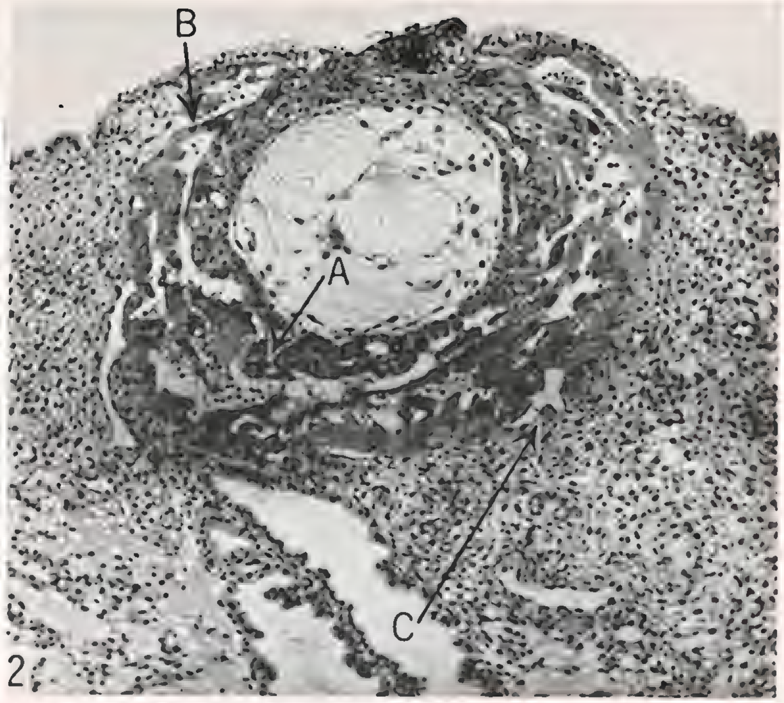
2

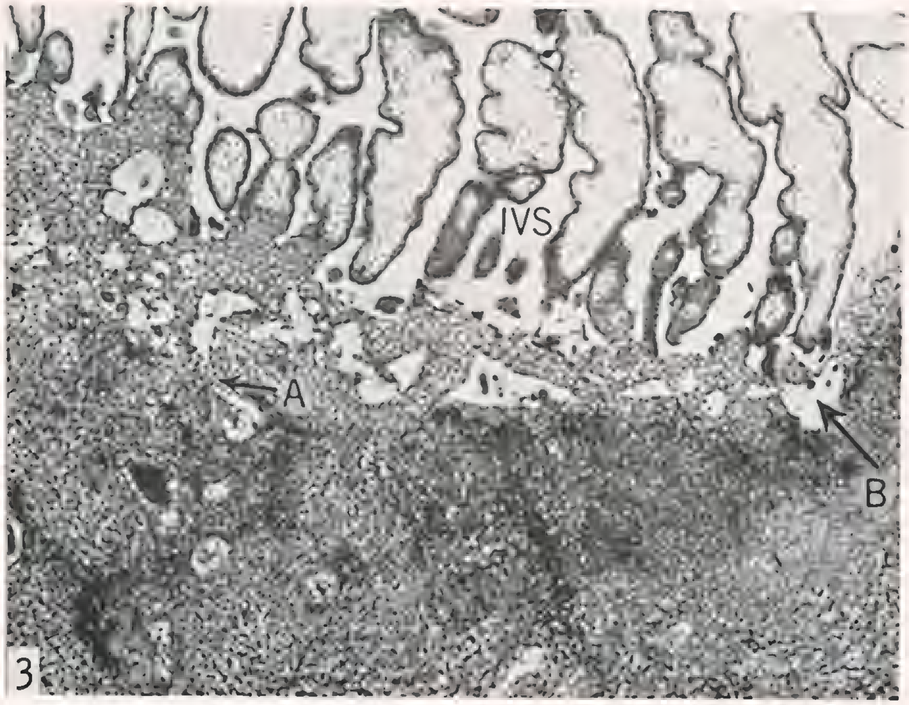
3

PLATE 2, Figs. 4–6

Fig. 4. From a horizontal section through the *decidua basalis* of a somite embryo showing a trophoblastic giant cell (indicated by arrow) lying free in the lumen of a uteroplacental artery. Specimen 9909; ×100.

Fig. 5. From a sagittal section through the *decidua basalis* of a 5-mm embryo showing a multinucleate giant cell in the lumen of a venous sinusoid. To the right, a multinucleate trophoblastic streamer lies partly in the wall of a tributary of the same sinusoid. The trophoblastic shell lies beyond the top of the picture. Specimen 8916; ×100.

Fig. 6. Stereoscopic photographs of part of the model of a uteroplacental artery from a pregnancy with a menstrual age of 56 days. The interrupted line marks the boundary between myometrium and decidua. The artery divides into three vessels, which open separately into the trophoblastic shell. Specimen 9176; ×20, ×10.

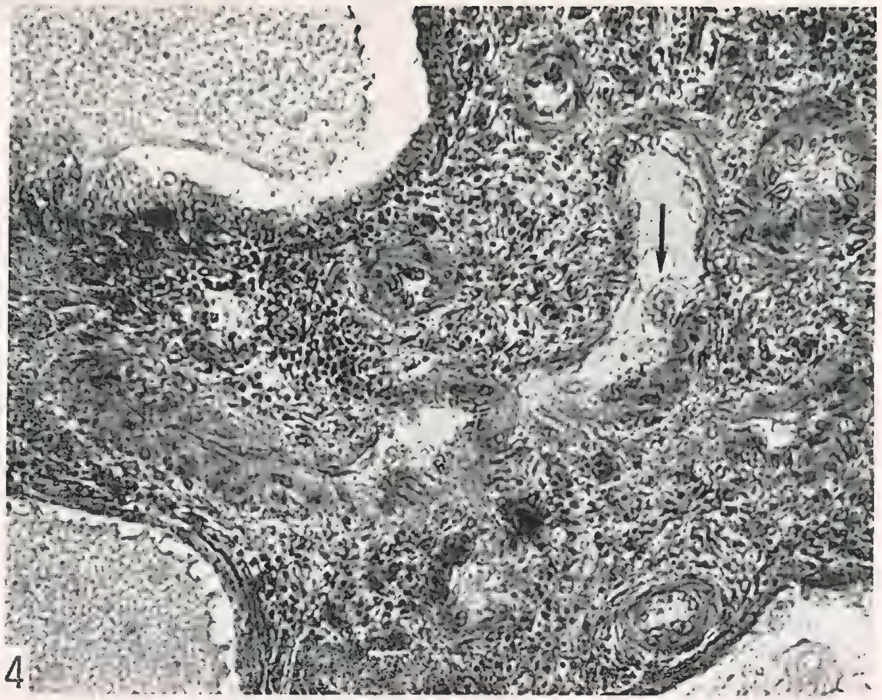
4

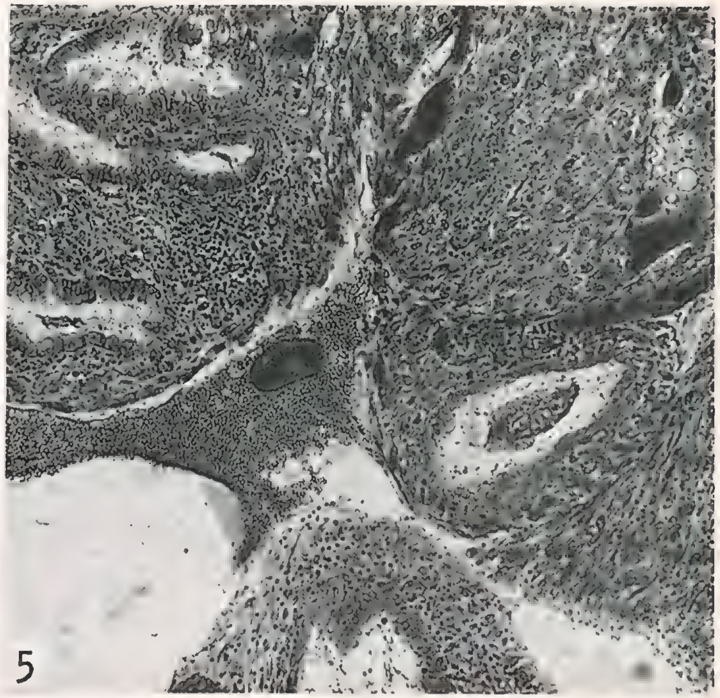
5

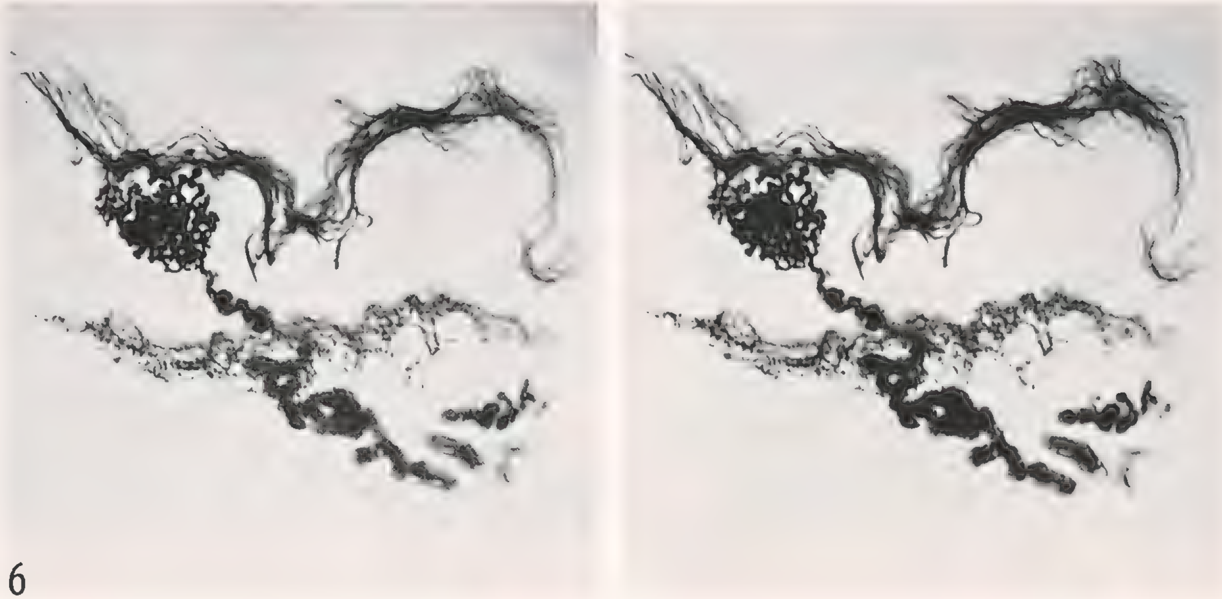
6

PLATE 3, Figs. 7–10

Fig. 7. From a sagittal section through the placenta and *decidua basalis* of a pregnancy with a menstrual age of 61 days, illustrating a deep penetration of trophoblast into the maternal tissue. The deep layers of the myometrium are visible in the lower part of the picture. Above and to the right are coils of a uteroplacental artery, one of which contains some cytotrophoblast. Trophoblast has extended along a tributary of the large venous sinus (indicated by asterisk). Specimen 8917; ×20.

Fig. 8. A slender decidual prominence from the same specimen (8917) as in Fig. 7, containing dilated terminal coils of a uteroplacental artery. One coil contains a cluster of cytotrophoblastic cells (indicated by arrow). Another coil, which lies proximal to the first, is in contact with the cytotrophoblastic shell. At this point (indicated by asterisk) the wall of the vessel shows signs of impending disintegration. Specimen 8917; ×45.

Fig. 9. Opening of a communication (indicated by arrow) between the intervillous space and a uteroplacental vein at the margin of the placenta of a 25-mm embryo. uc = uterine cavity. Specimen 8917; ×20.

Fig. 10. From a sagittal section through the basal plate of the same placenta (8917) as in Figs. 7, 8, and 9, illustrating the termination of a uteroplacental artery in the cytotrophoblastic shell. Cytotrophoblast lines the lumen of the terminal part of the artery and has almost completely destroyed the wall of the vessel, which lies in contact with the shell. Some cytotrophoblast has spread into an adjacent coil which has lost its endothelium. In the coils to the right, the endothelium has been displaced toward the center of the arterial lumen and some cytotrophoblast (indicated by arrow) is present beneath it. Specimen 8917; ×45.

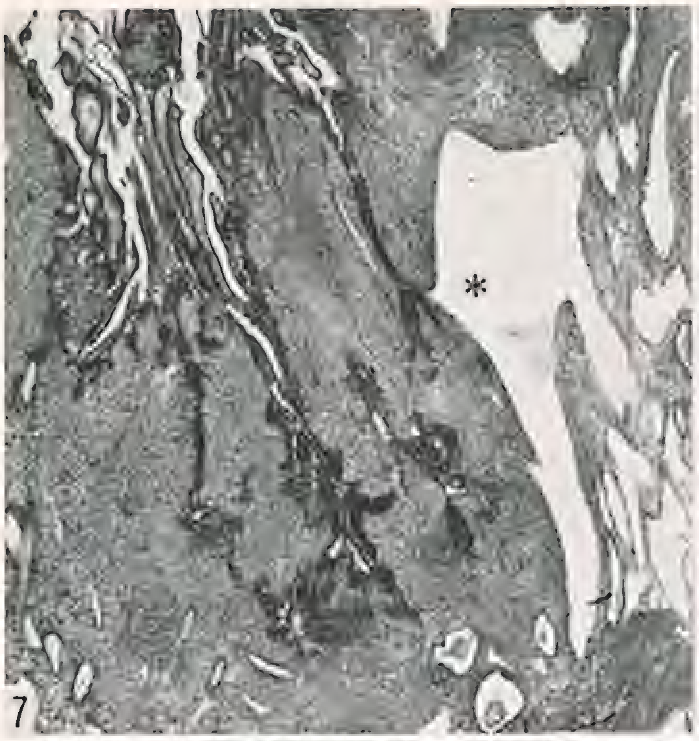

7

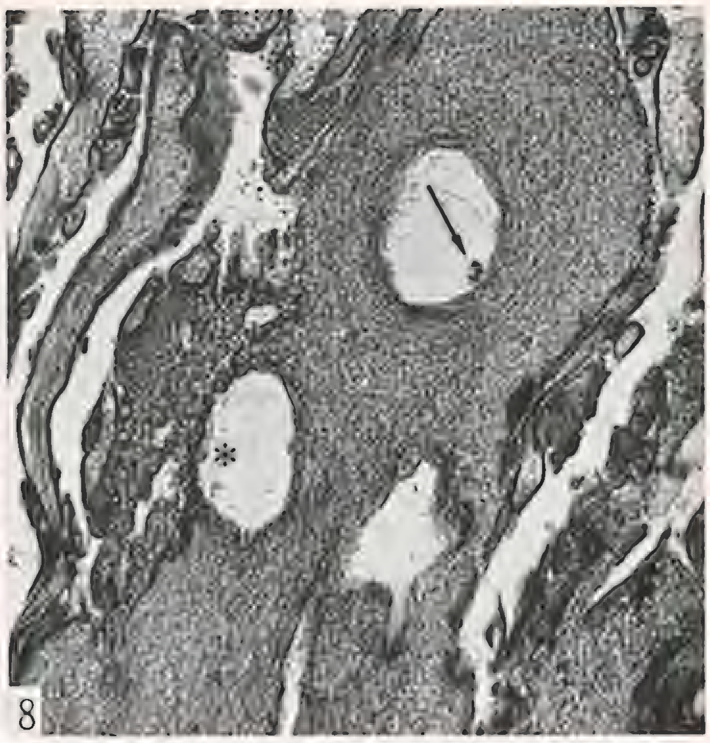

8

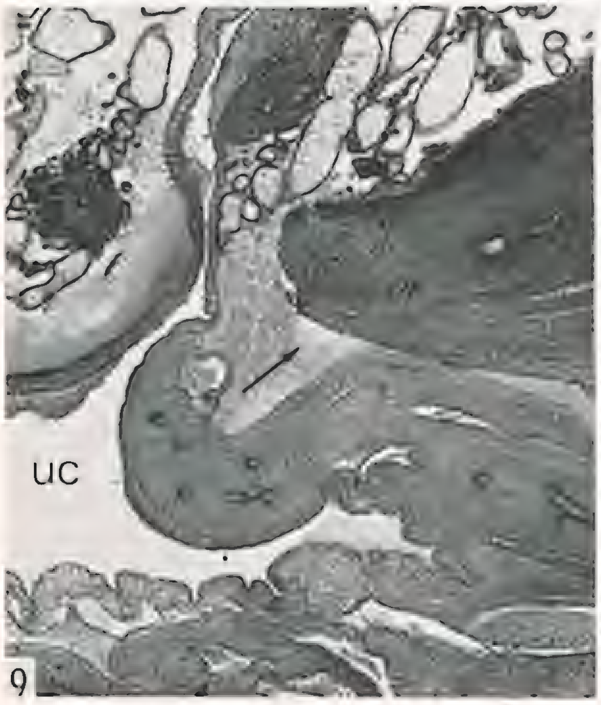

9

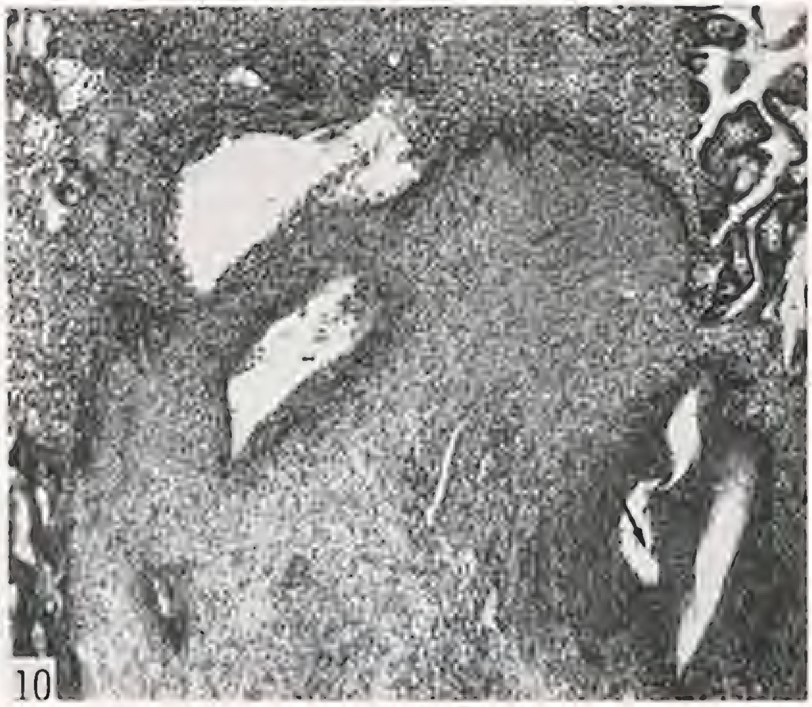

10

PLATE 4, Figs. 11–14

Fig. 11. Part of a sagittal section through the trophoblastic shell and adjacent decidua from a pregnancy with a menstrual age of 83 days. Cytotrophoblast has breached the wall of a uteroplacental artery and now almost completely lines the lumen of the vessel. Remnants of the arterial wall appear as dark strands. A fibrinoid deposit, part of Nitabuch's membrane, is visible on the left. Specimen 10119, stained with phosphotungstic acid hematoxylin; ×100.

Fig. 12. This section passes through the coil of a uteroplacental artery, indicated by asterisk in Fig. 32. The coil, which is more dilated than the succeeding portion of the vessel, is in contact with the cytotrophoblastic shell. Cytotrophoblast has penetrated through most of the wall of the lower part of the coil, but there is no evidence of endothelial swelling or other reaction to its destructive effect. Specimen 9380; ×45.

Fig. 13. Part of a trophoblastic streamer in the *decidua basalis* of a nine-week pregnancy. This particular streamer is 380 μ long. Muscle bundles in the deep layers of the myometrium are visible in the lower part of the picture. Specimen 10119; ×400.

Fig. 14. Another group of migrating trophoblastic elements from the same specimen as in Fig. 13. The cytoplasm of many of the streamers contains longitudinally oriented fibrils, and some elements end in thin "tails." The spermlike object at center is 105 μ long. Numerous lymphocytes are present in the intercellular spaces of the decidua. Specimen 10119, stained with phosphotungstic acid hematoxylin; ×400.

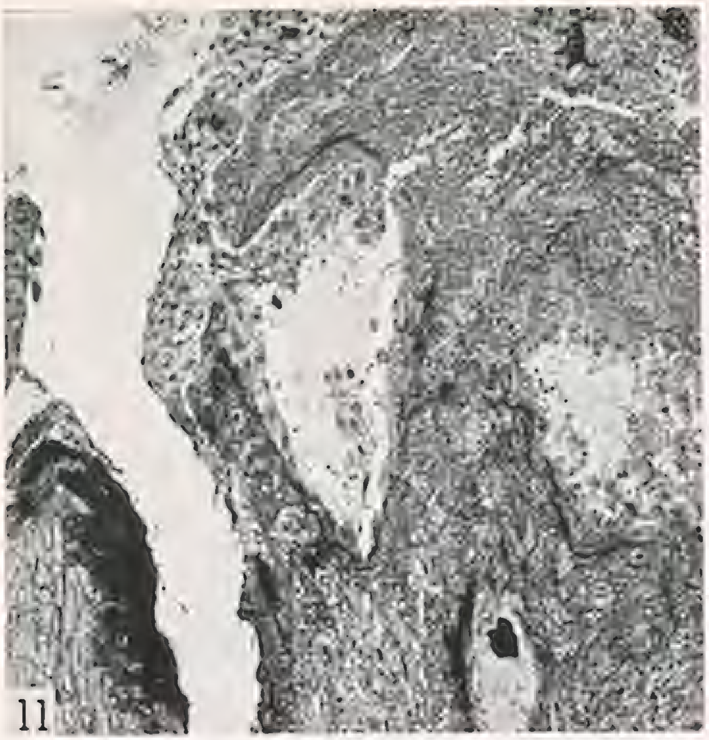
11

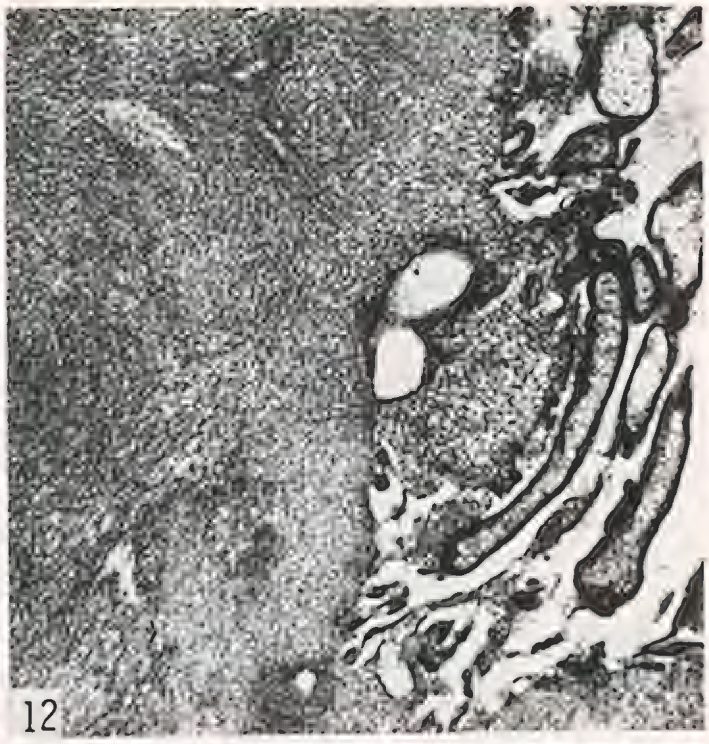
12

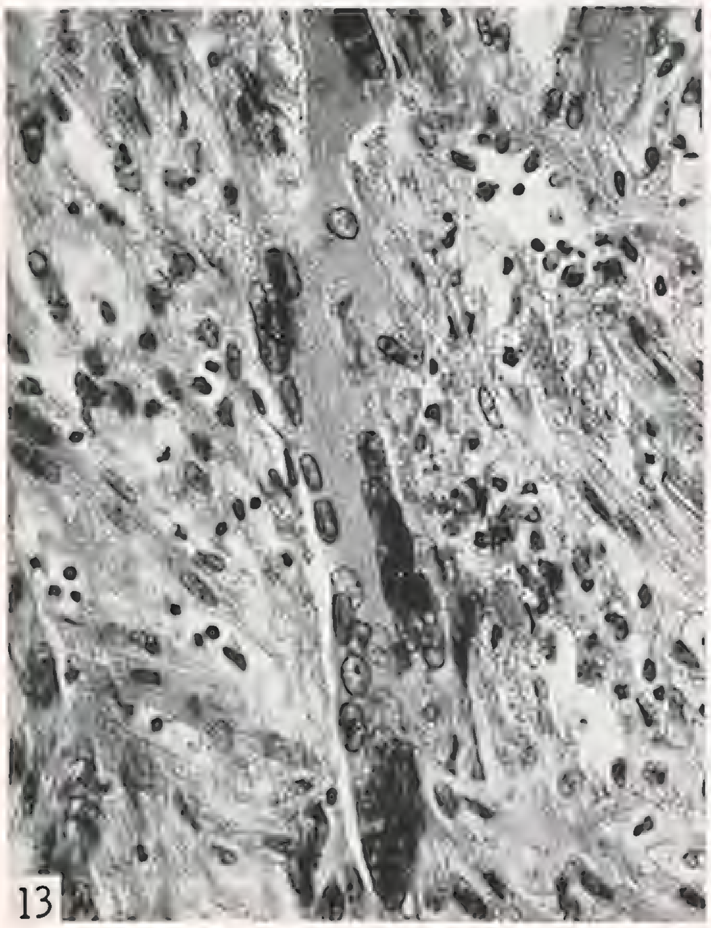
13

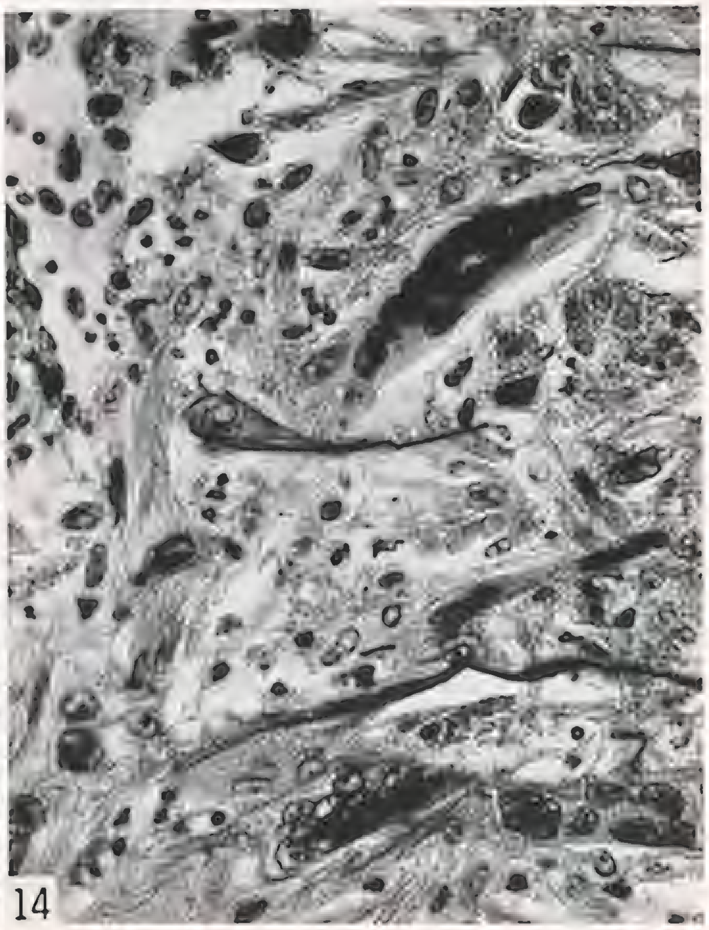
14

PLATE 5, Figs. 15–18

Fig. 15. Multinucleate trophoblastic giant cell 100 μ long, lying in contact with the wall of a venous sinusoid. The endothelium adjacent to the cell is not intact. This may represent a stage in the migration of giant cells into the vein. Specimen 10119; ×400.

Fig. 16. Part of a multinucleate trophoblastic streamer that has penetrated into the wall of a dilated uteroplacental artery close to the myodecidual junction. In an adjacent section, a small deposit of fibrinoid material is closely related to another part of this trophoblastic streamer. Specimen 10119; ×400.

Fig. 17. From a sagittal section through the *decidua basalis* and adjacent myometrium of a three-month pregnancy. The terminal part of the uteroplacental artery in the center of the picture is dilated and the lumen, indicated by India ink, is partly occluded by cytotrophoblast. Parts of a nonfunctioning branch of the artery are visible at left. Numerous trophoblastic giant cells, some of which are indicated by arrows, are present in the deep layers of the myometrium. Specimen 8914; ×20.

Fig. 18. Section through the large vertical termination of the uteroplacental artery illustrated at center of Fig. 33(A). The lumen of this vessel is lined by cytotrophoblast. A group of trophoblastic giant cells is visible in the myometrium in lower left corner. Specimen 9051; ×45.

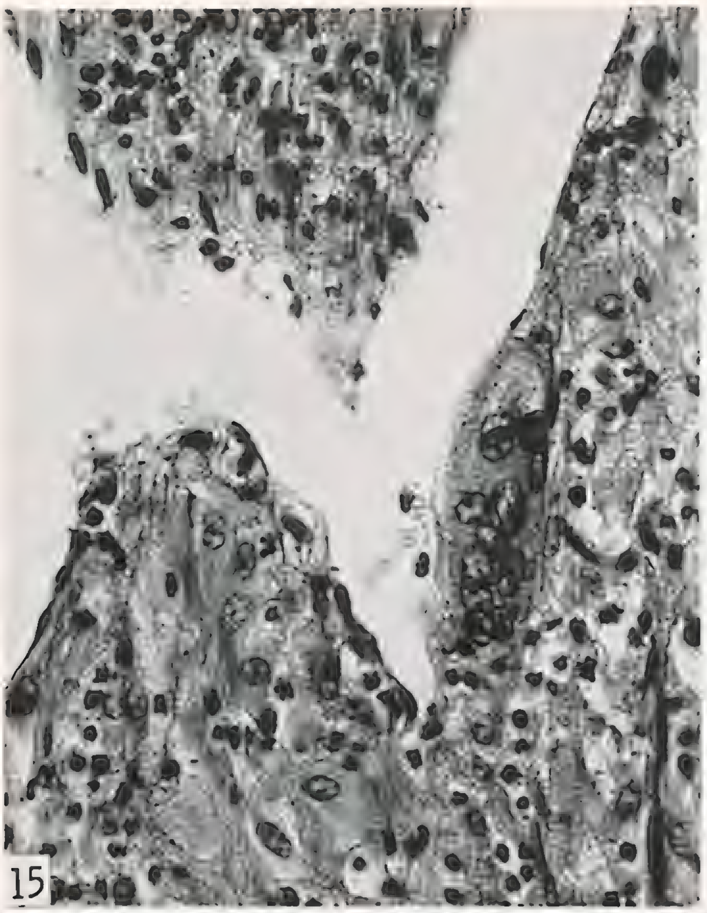
15

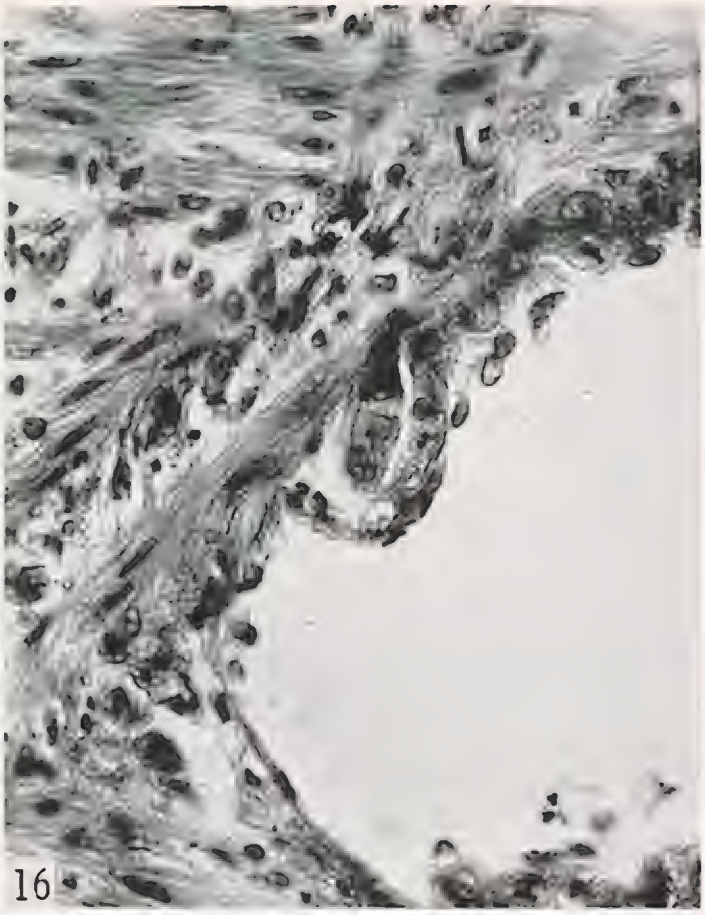
16

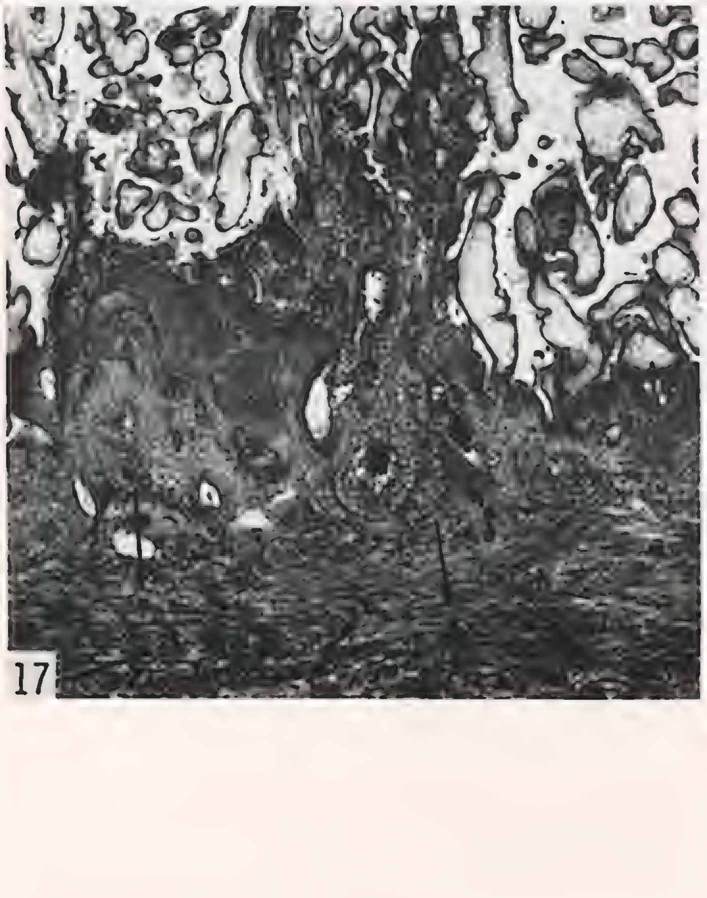
17

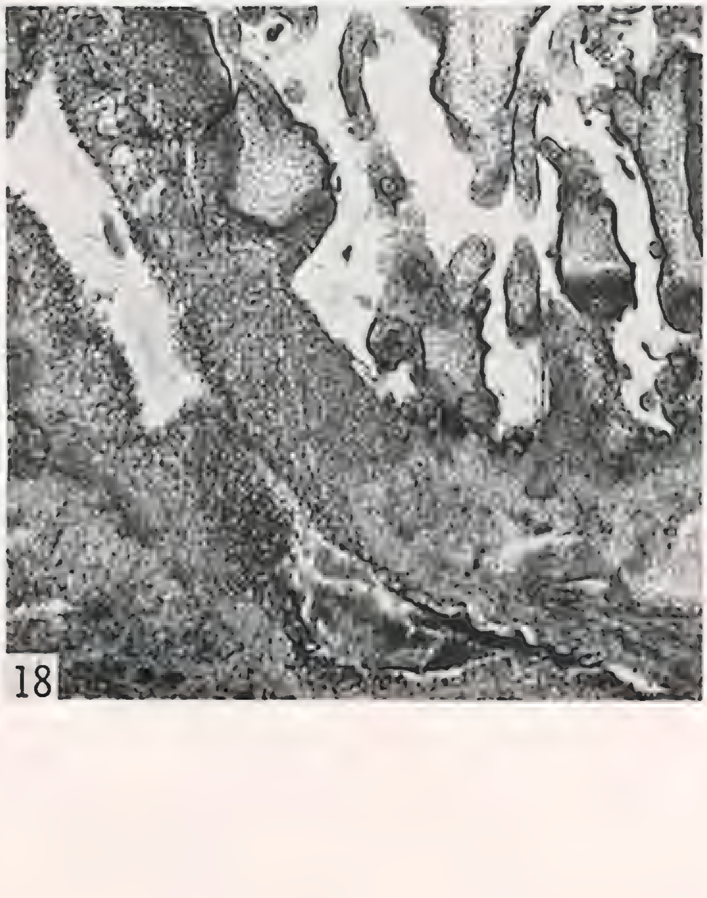
18

PLATE 6, Figs. 19–22

Fig. 19. Part of the myometrial portion of a uteroplacental artery showing the presence of cytotrophoblast within the lumen of the main vessel and some of its branches. Multinucleate giant cells can be seen between the muscle bundles (see Fig. 33). Specimen 9051; ×100.

Fig. 20. Group of intra-arterial cytotrophoblastic cells from the *decidua basalis* of a three-month pregnancy. Although most of the cells lie within the lumen, the single cell at the upper part of the vessel is covered by the endothelium, which is displaced toward the center of the artery. There is no evidence of endothelial proliferation. Specimen 2328; ×200.

Fig. 21. Portions of a uteroplacental artery in the *decidua basalis* of a 12-week pregnancy. Groups of cytotrophoblastic cells are situated around the wall of the artery, some surrounded by amorphous material. This change is observed only in the immediate neighborhood of cytotrophoblast. Specimen 10117; ×100.

Fig. 22. From a sagittal section through the *decidua basalis* and adjacent myometrium of a 14-week pregnancy. Trophoblast has penetrated into a myometrial vein and spread laterally to interrupt the course of a circumferentially oriented branch of a uteroplacental artery. This vessel is illustrated at right in Fig. 33 (B). The arterial orifice (indicated by arrow) is lined with cytotrophoblast and opens close to the most dependent part of the intervillous space, which in this area is formed by the wall of the eroded vein. Specimen 9051; ×45.

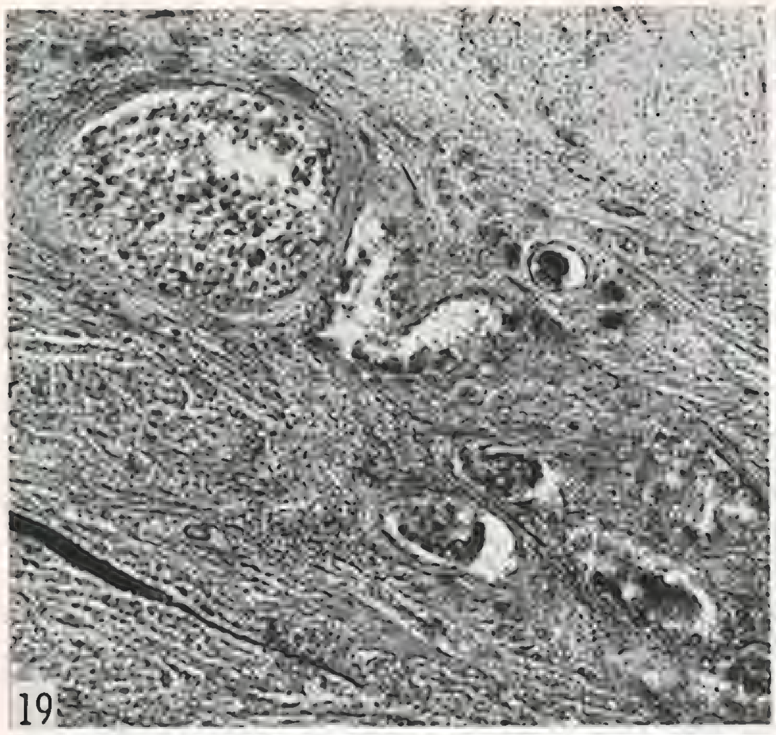
19

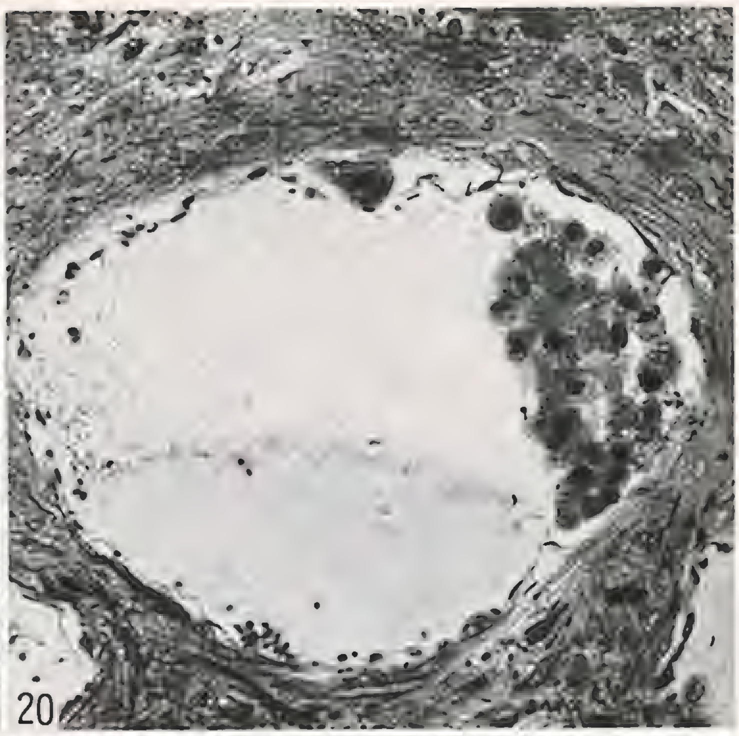
20

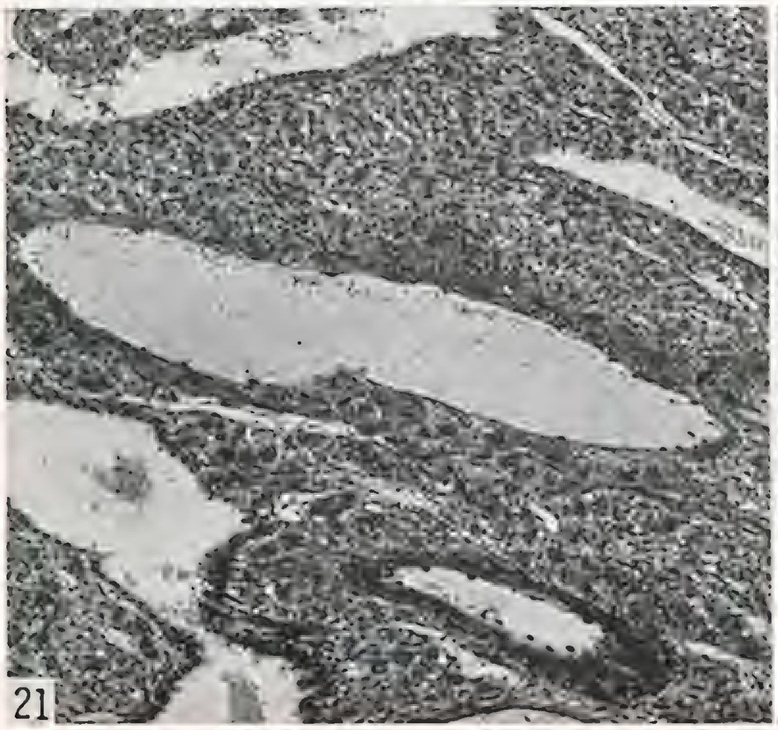
21

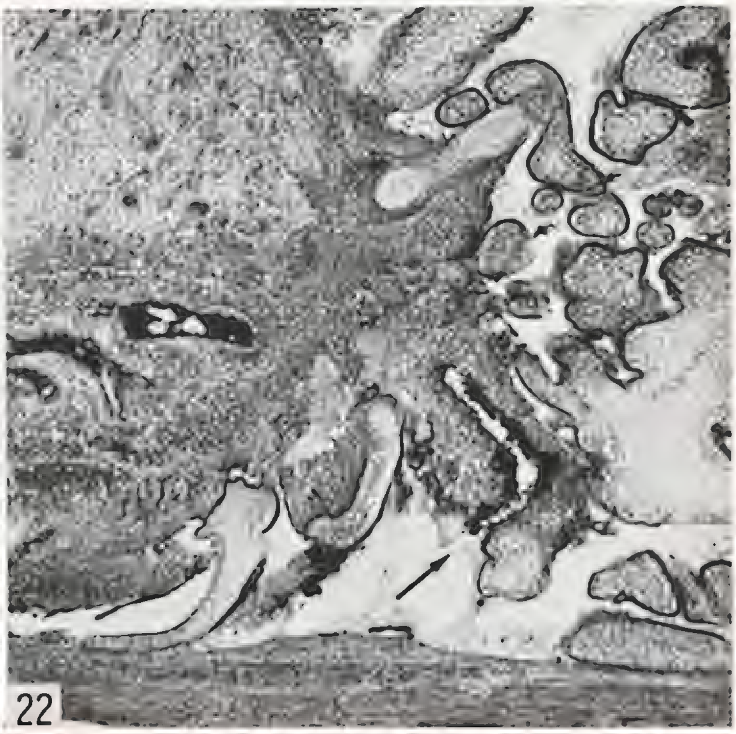
22

PLATE 7, Figs. 23–26

Fig. 23. Part of the wall of a uteroplacental artery in the *decidua basalis* of a 15-week pregnancy, showing a stellate cell 40 μ in diameter. The endothelium is displaced toward the center of the vessel. Specimen 10118; ×400.

Fig. 24. Section through a uteroplacental artery at the boundary between decidua and myometrium of a 15-week pregnancy. The characteristic layers of the arterial wall are no longer recognizable, and the whole region is heavily infiltrated with cells from the trophoblast. Collections of cytotrophoblast occur within the endothelial lining of the vessel, and small groups of similar cells are frequently encountered beneath it. One such group is indicated by arrow. Specimen 10118; ×100.

Fig. 25. Frozen section of the same specimen as in Fig. 24, stained with Oil Red O. Cells of cytotrophoblastic origin within the lumen and wall of the uteroplacental artery give a strongly positive reaction for fat. Some of the trophoblastic giant cells in the decidua and myometrium also give a positive but less intense reaction with this technique. Specimen 10118; ×90.

Fig. 26. Portions of a uteroplacental artery, *a*, and a branch arising from it, *b*, in the junctional area between decidua and myometrium. The endothelium of *b* is displaced toward the center of the vessel, and strands of fibrinlike material and a few cytotrophoblastic cells lie beneath it. Cytotrophoblast is also present in the reduced lumen of the vessel. The endothelium of artery *a* is also displaced, particularly on the left side where the vessel makes an abrupt turn and gives rise to another branch. The changes are thought to result from a reduction in circulation through the vessel. Specimen 10118; ×100.

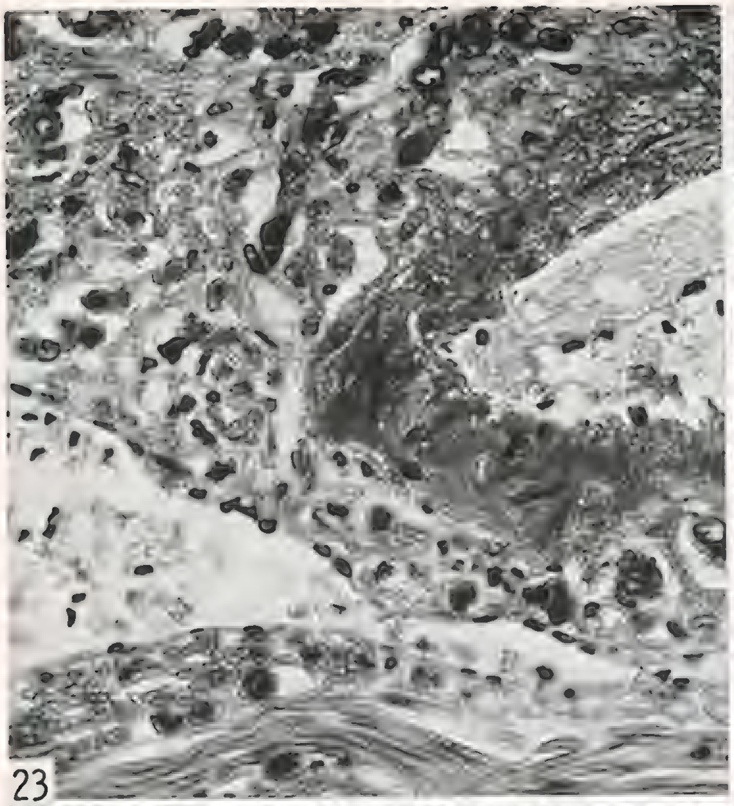

23

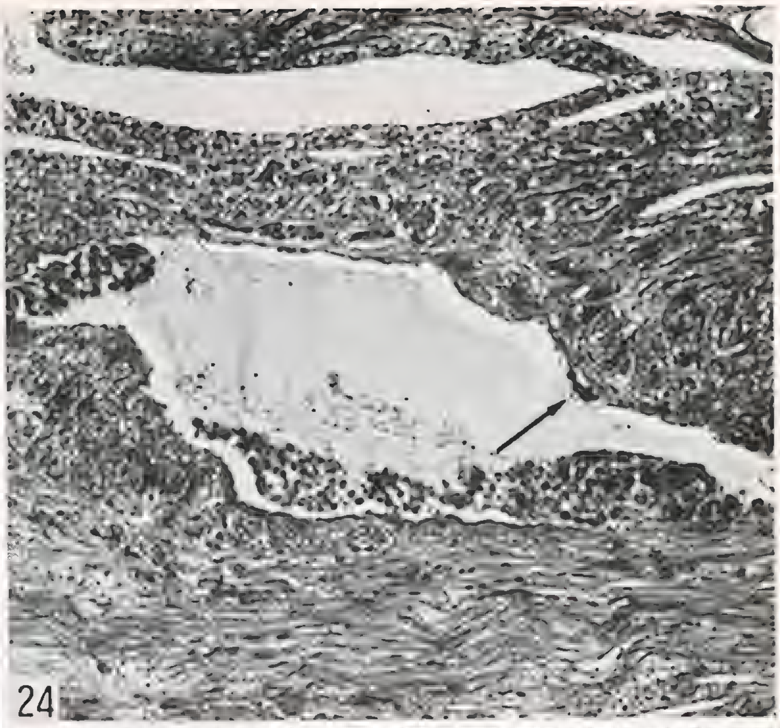

24

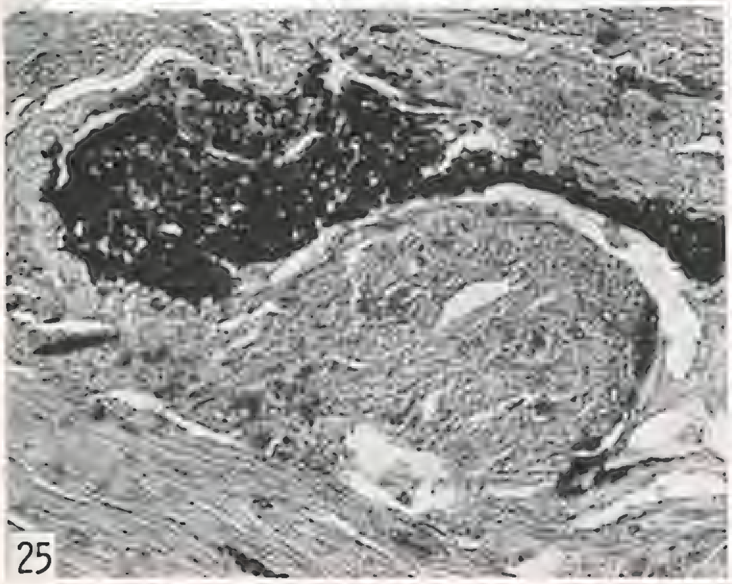

25

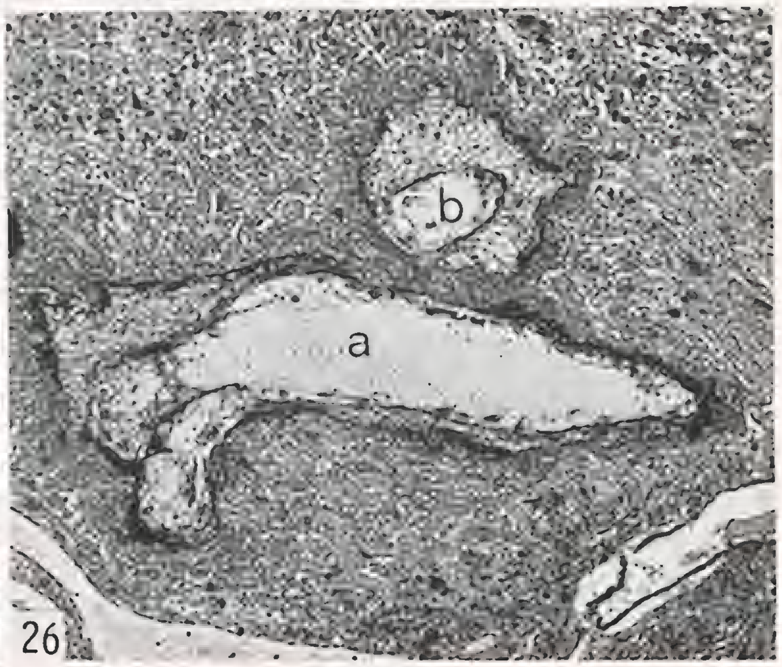

26

PLATE 8, Figs. 27–31

Fig. 27. *Decidua basalis* and adjacent myometrium of a 16-week pregnancy showing a collection of trophoblastic cells (indicated by arrows) within the lumen of a uteroplacental artery. The artery, which lies 1–2 mm from the myodecidual junction is more fully illustrated in Fig. 34. Very few cells are present in the arterial coils at left, which are distal to the affected segment. Specimen 8876; ×20.

Fig. 28. Dilated terminal coils of a uteroplacental artery from a 25-week pregnancy, injected with India link. The artery opens close to the apex of a decidual prominence. Numerous villi are attached to the sides of the projection. Specimen 8695; ×15.

Fig. 29. Example from a full-term placenta of a uteroplacental artery terminating in a decidual prominence, which lies above the large oblique orifice of a uteroplacental vein; other veins, injected with India ink, can be seen in the myometrium. Specimen 9033; ×20.

Fig. 30. Example of an arterial orifice (indicated by arrow) in a full-term placenta, which opens into the most dependent part of the intervillous space. The thin layer of *decidua basalis* and deeper parts of the myometrium are heavily infiltrated with trophoblastic giant cells. At right there is a communication between two veins that lie at different planes in the myometrium. Specimen 9033; ×20.

Fig. 31. Section through the margin of the placenta from a 32-week pregnancy showing a large venous sinus draining blood away from the peripheral portion of the intervillous space. Fetal villi encroach on the orifice of the sinus. Specimen 9124; ×20.

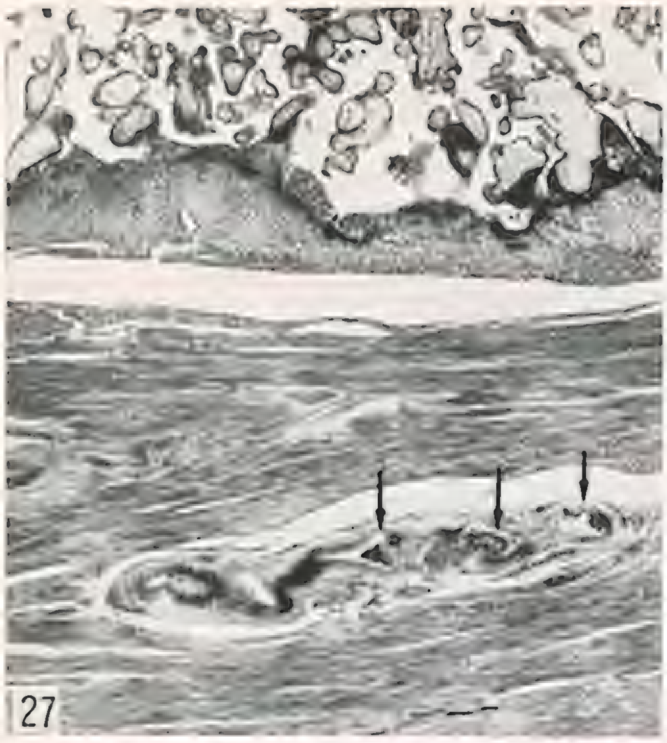
27

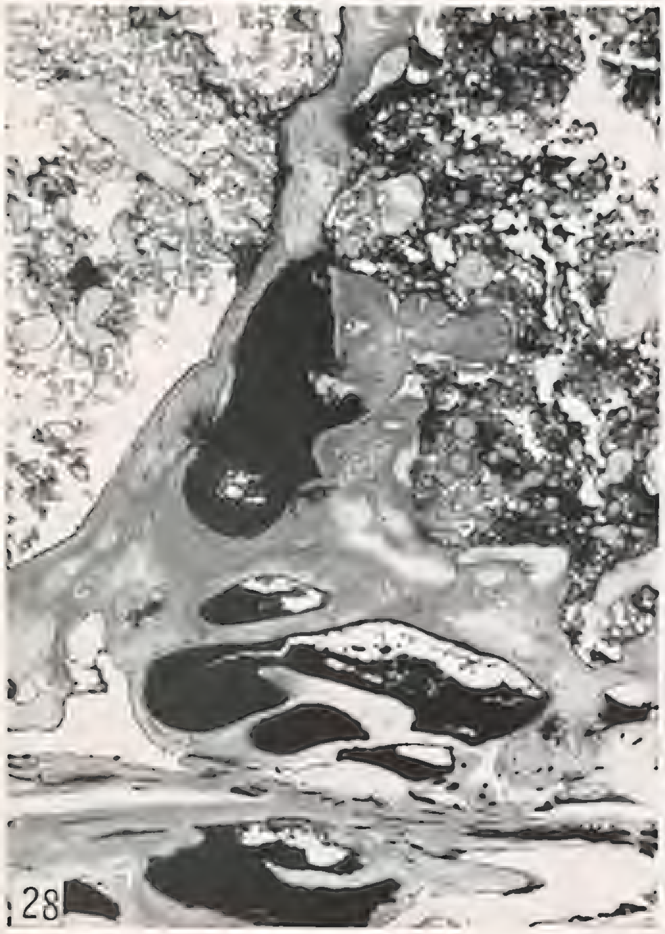
28

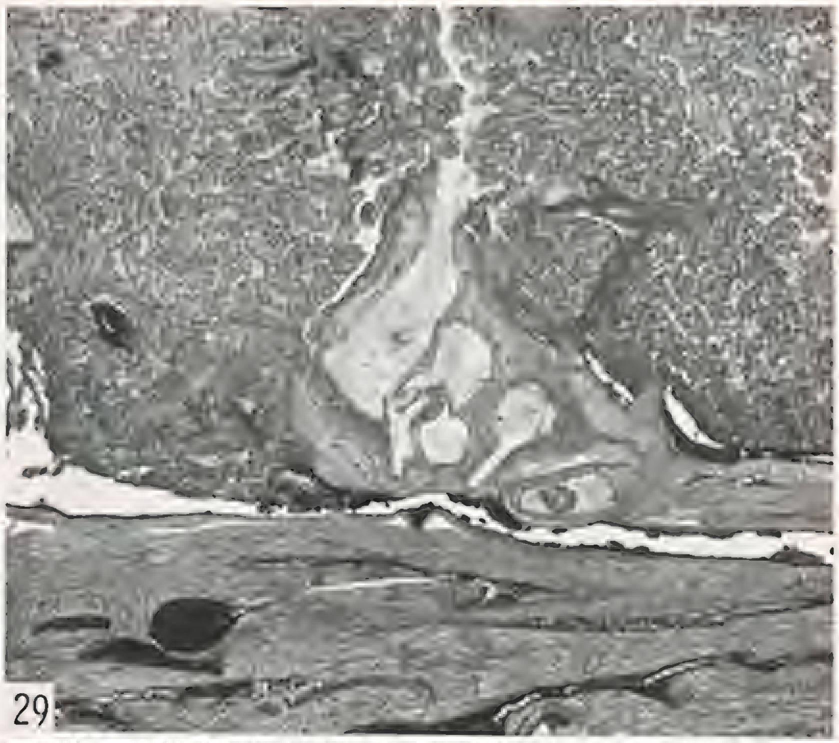
29

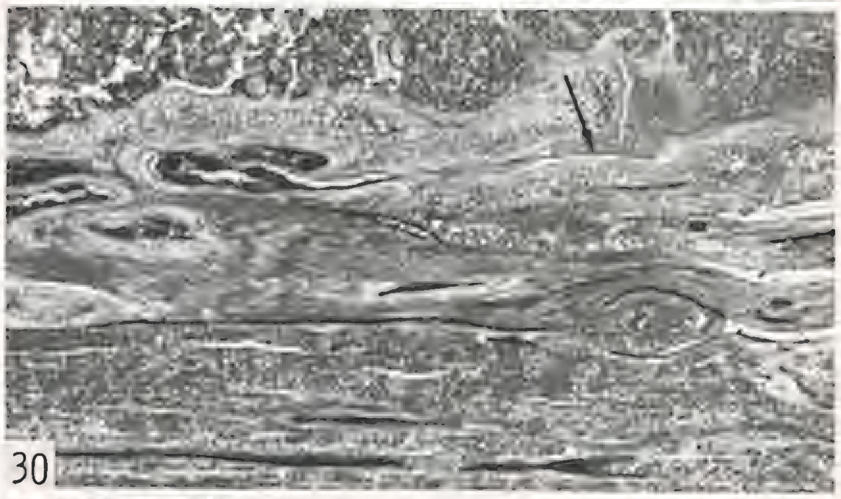
30

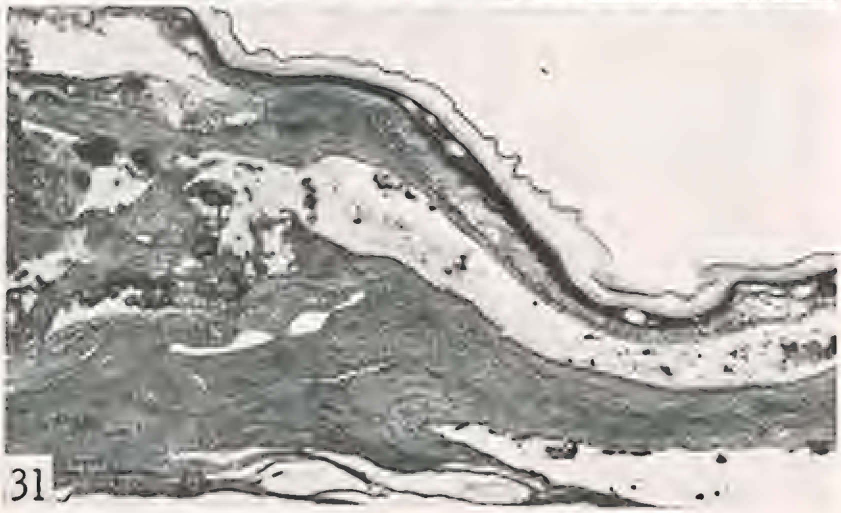
31

PLATE 9, Fig. 32

Fig. 32. Two uteroplacental arteries from a specimen with a menstrual age of 63 days. Only the lumen of the vessels is indicated in the drawing. The artery at left divides into two within the myometrium, and the left-hand stem gives rise to four vessels which open independently into the intervillous space. Only the two largest openings are shown. Arrows on the stem vessels indicate the point at which elastic tissue ceases to be demonstrable in the walls of the arteries. The coil marked by an asterisk is illustrated in Fig. 12. The scale indicates the relative thickness of the endometrium *E* and myometrium *M* in this specimen. Specimen 9380; model and drawing ×15, reduced $\frac{3}{5}$.

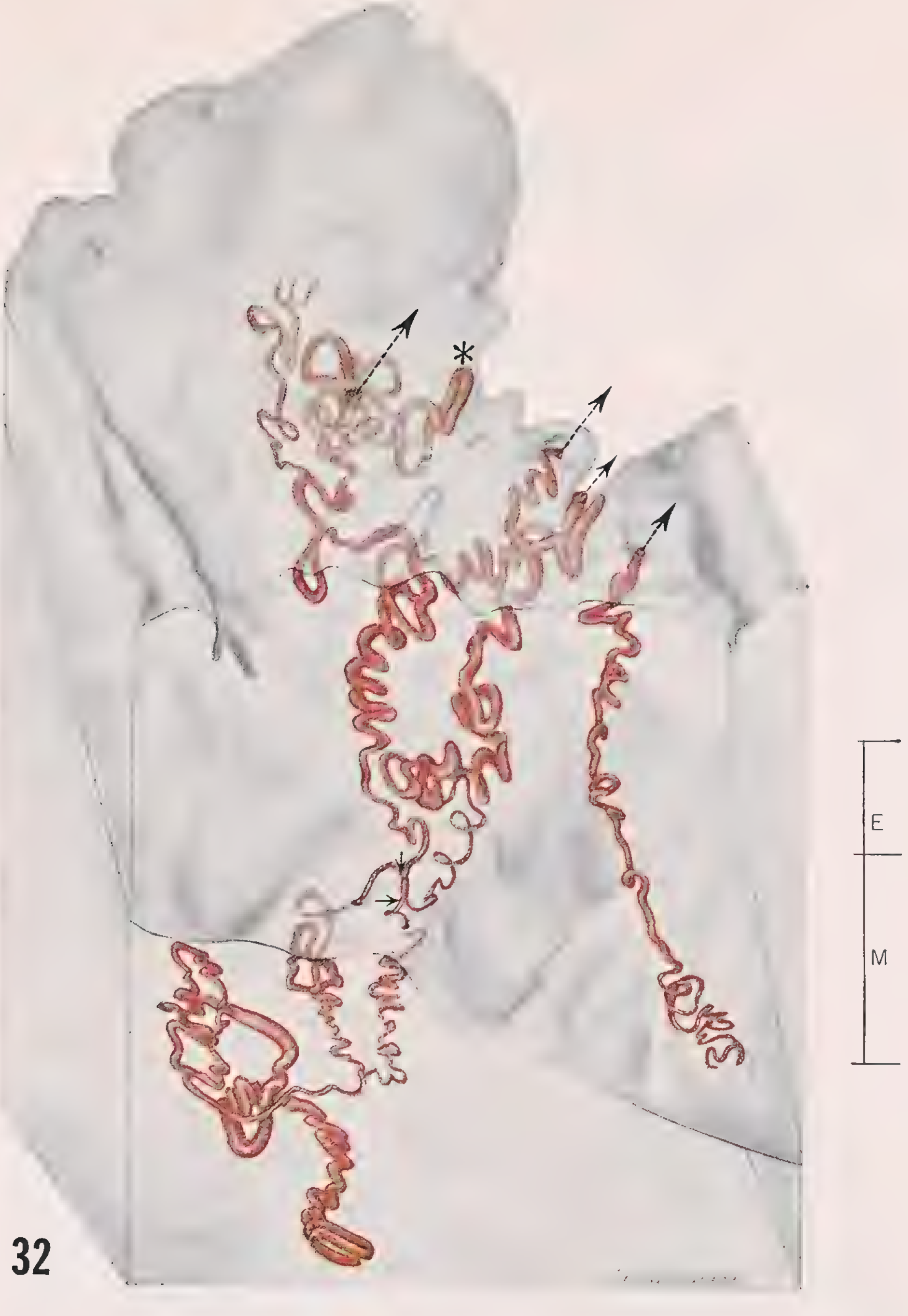

32

PLATE 10, Fig. 33

Fig. 33. Specimen with a menstrual age of 103 days. (A) Ten arterial openings come from a single uteroplacental artery, which is seen arising from an arcuate artery. The arcuate artery passes through the model in a plane at right angles to the surface of the paper. Only the lumen of vessels is indicated; the numerals mark points of continuity between the drawings. The terminal parts of most of the terminal vessels form vertical channels that, in this specimen, are dilated and thickly lined with cytotrophoblast. (B) At right, the penetration of trophoblast into a vein has opened up an artery that was passing through the myometrium parallel to the myodecidual junction. Variations in the degree of dilatation of the terminal vessels may be due to a tendency to establish preferential routes for the discharge of blood into the intervillous space. Photomicrographs from this specimen are illustrated in Figs. 18, 19, and 22. The scale indicates the relative thickness of the *decidua basalis E* and myometrium *M* in this specimen. Specimen 9051; model and drawings ×20, reduced $\frac{1}{2}$.

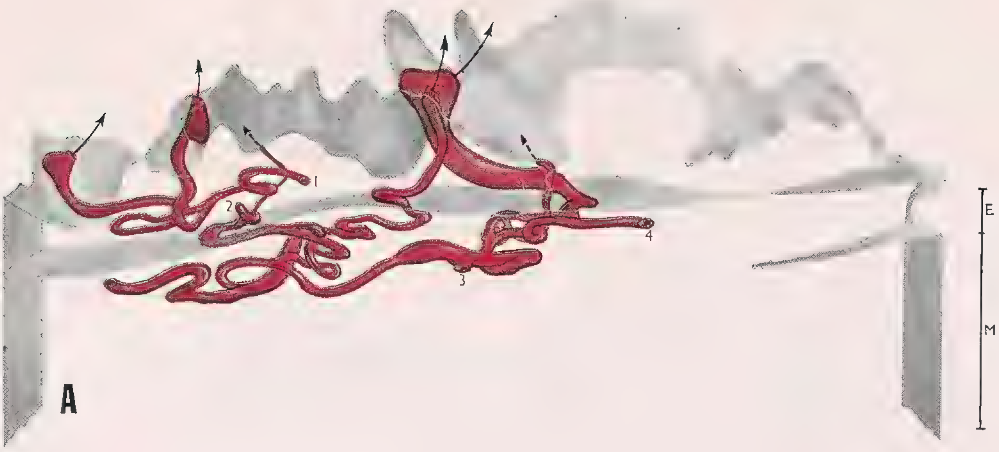

33 A

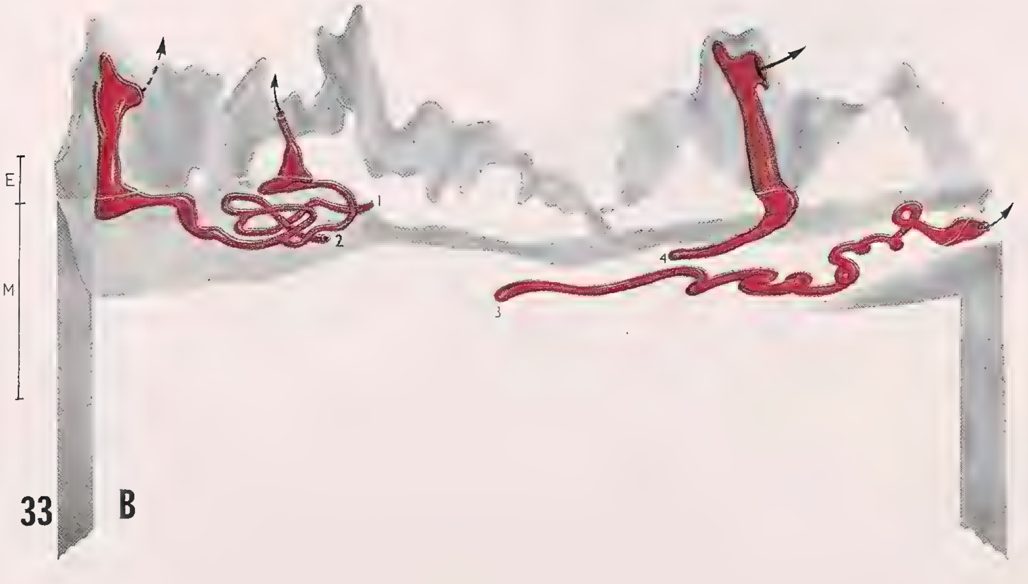

33 B

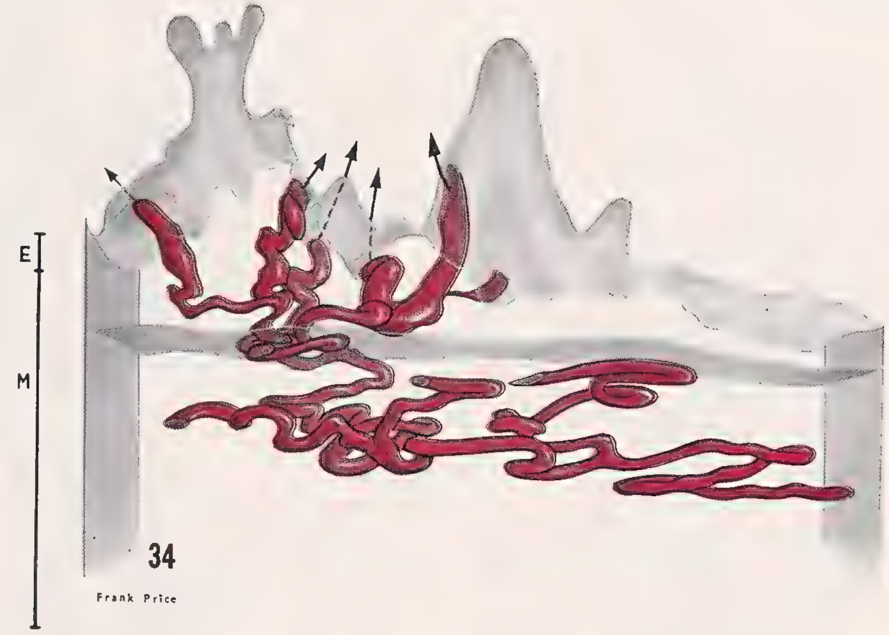

34

PLATE 11, Fig. 34

Fig. 34. Specimen with a menstrual age of 116 days. Only the lumen of vessels is indicated. An arcuate artery passes across the model from right to left and gives rise in succession to three uteroplacental arteries. Six terminal channels derived from the second and third uteroplacental arteries are illustrated, and, to avoid obscuring these branches, details of part of the stem of the second artery are omitted. Photomicrograph of a section showing collections of cytotrophoblastic cells within the lumen of the proximal part of the third artery is illustrated in Fig. 27. The terminal portions of most of the branches illustrated in the model form a group of dilated vertical channels, often heavily infiltrated with cytotrophoblast. The scale indicates the relative thickness of the *decidua basalis* E and myometrium *M* in this specimen. Specimen 8876; model and drawing ×20, reduced $\frac{1}{2}$.

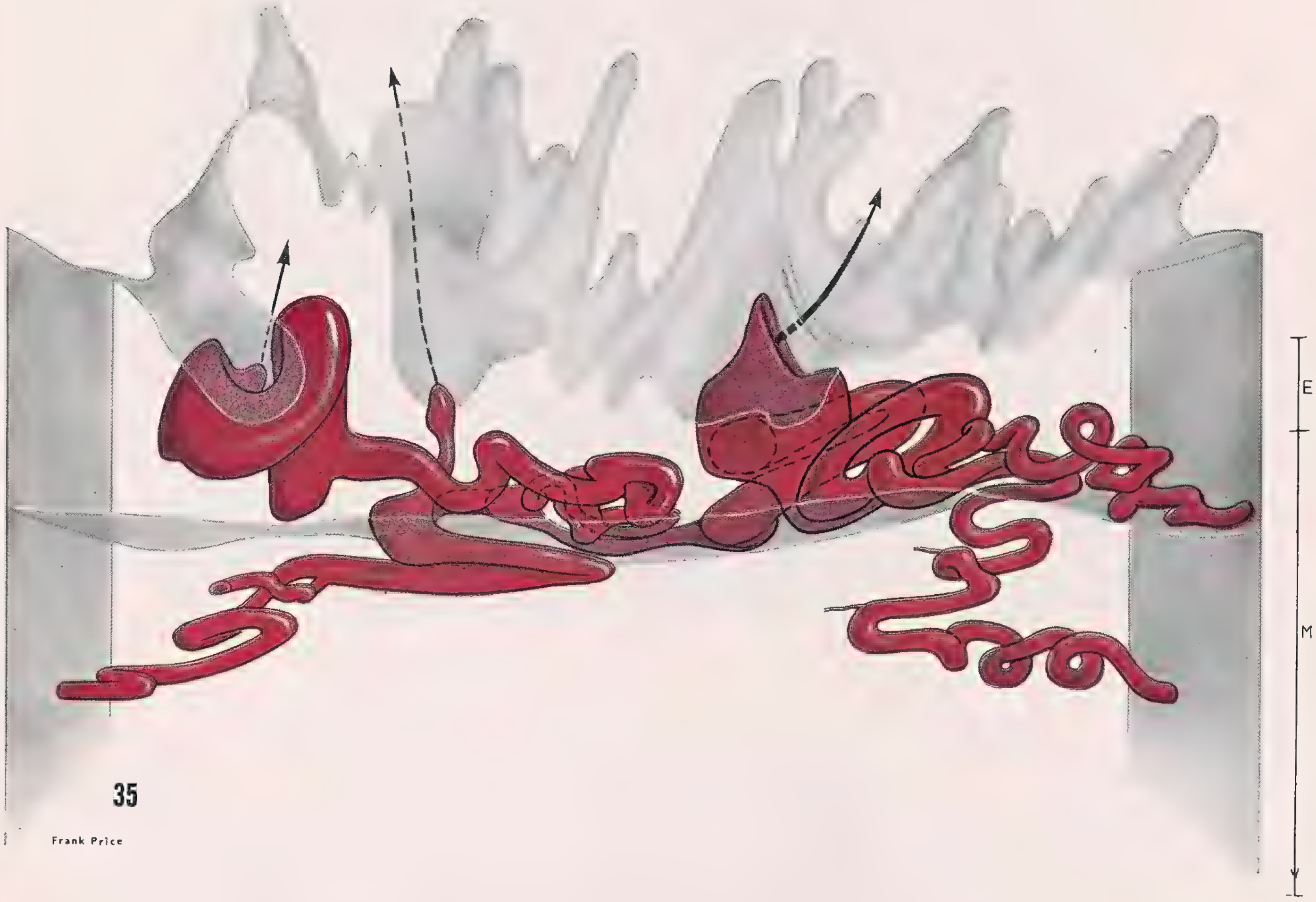

35

PLATE 12, Fig. 35

Fig. 35. Part of the model of a specimen with a menstrual age of 139 days (20 weeks). At left in the drawing, a uteroplacental artery gives rise to a myometrial vessel and later to a small branch, which opens into the intervillous space through a narrow vertical channel. The main artery continues toward the right and divides into two stems. One of these becomes dilated and after a tortuous course moves to the left to open into the intervillous space. The terminal part of the vessel is grossly dilated and the vertical portion of the final coil is 3.0 mm long. The second stem moves farther to the right in the deep layers of the myometrium to join a large terminal dilatation that is also in communication with the uteroplacental artery at right in the drawing. The combined terminal opening of these two vessels is a slitlike aperture, 1.75 mm long. Another branch from the right uteroplacental artery opens into the intervillous space some distance in this drawing, especially at places where the vessels make abrupt turns. The scale indicates the relative thickness of the *decidua basalis E* and myometrium *M* in this specimen. Specimen 8991; model and drawing ×20, reduced $\frac{1}{2}$.

PLATE 13, Fig. 36

Fig. 36. Uteroplacental artery from a specimen with an estimated menstrual age of 32 weeks. The symbols + and * indicate points of continuity between drawings (A) and (B). After leaving the myometrium, the artery moves to the left, and then forms a series of three clockwise coils, the last of which communicates with the intervillous space through the large openings. This terminal coil has a diameter of 0.525 mm. In contrast to earlier specimens, there are comparatively few cytotrophoblastic cells within the dilated coils of the vessel. The scale indicates the relative thickness of the *decidua basalis E* and myometrium *M* in this specimen. Specimen 9124; model and drawings ×20, reduced $\frac{1}{2}$.

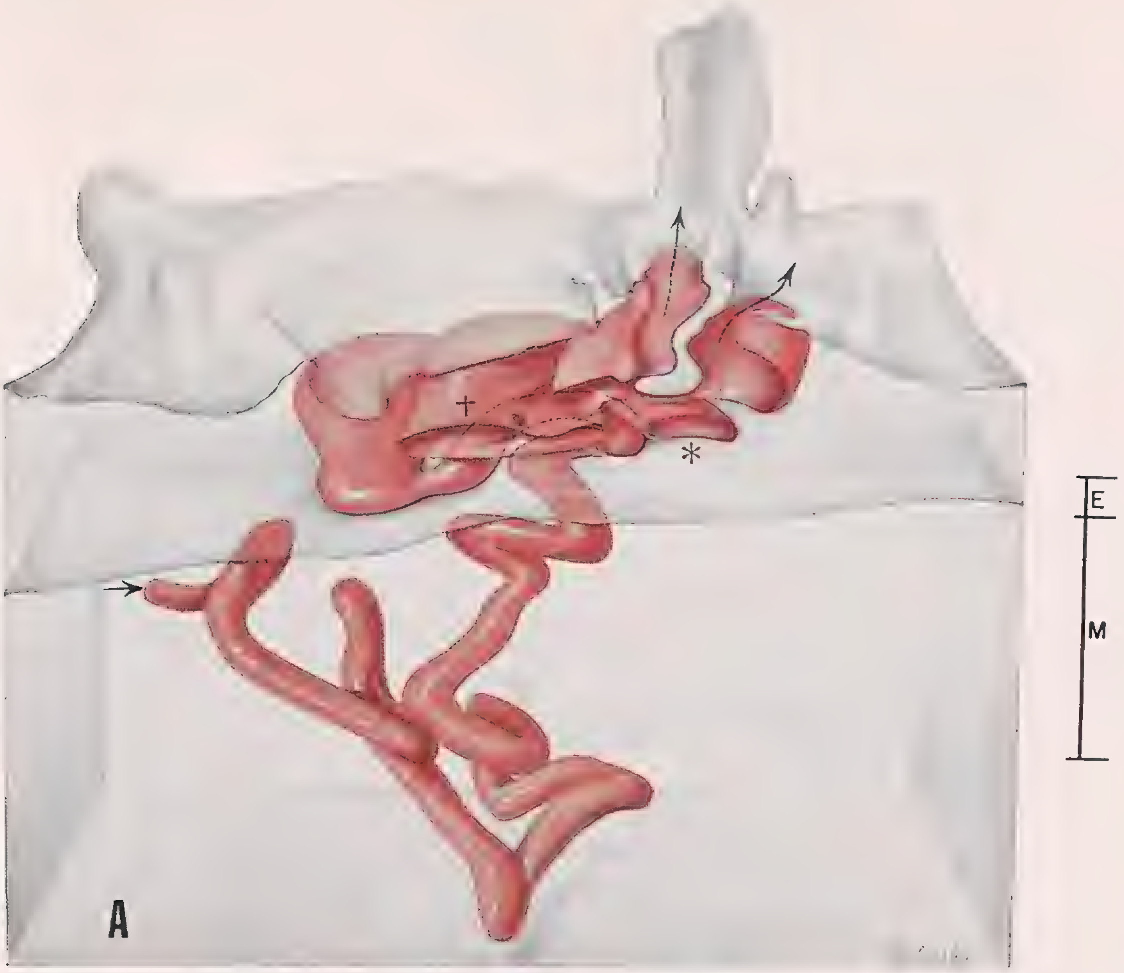

36 A

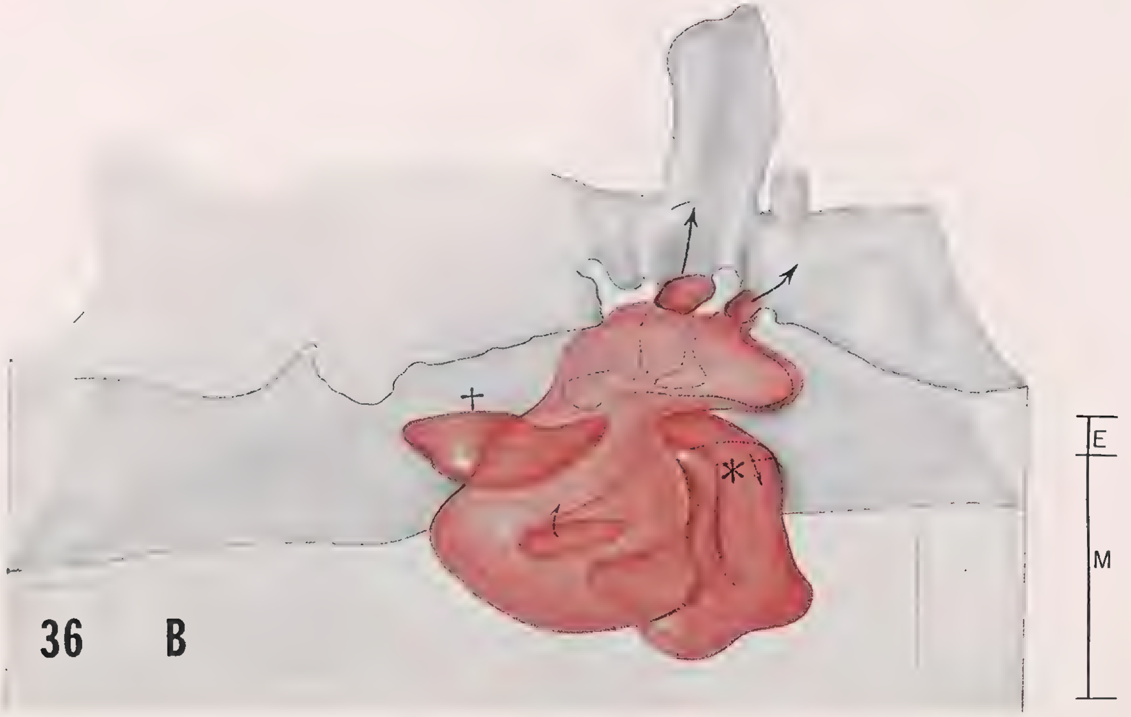

36 B

PLATE 14, Fig. 37

Fig. 37. Uteroplacental artery and surrounding venous plexus from a full-term specimen. (A) The artery gives origin to a myometrial branch and soon after leaving the myometrium terminates in a large funnel-shaped channel. The terminal portion of the artery is raised above the general plane of the basal plate, and the largest diameter of the outlet measures 2.4 mm. Part of another artery lies at left and opens into the most dependent part of the intervillous space. (B) The same artery is shown in relationship with the surrounding venous plexus. Arrows indicate the position of communications between the plexus and the intervillous space; some of these are shown in (A). Photomicrographs of this specimen are illustrated in Figs. 29 and 30. The scale indicates the relative thickness of the *decidua basalis E* and myometrium *M* in this specimen. Specimen 9033; model and drawings ×20, reduced $\frac{1}{2}$.

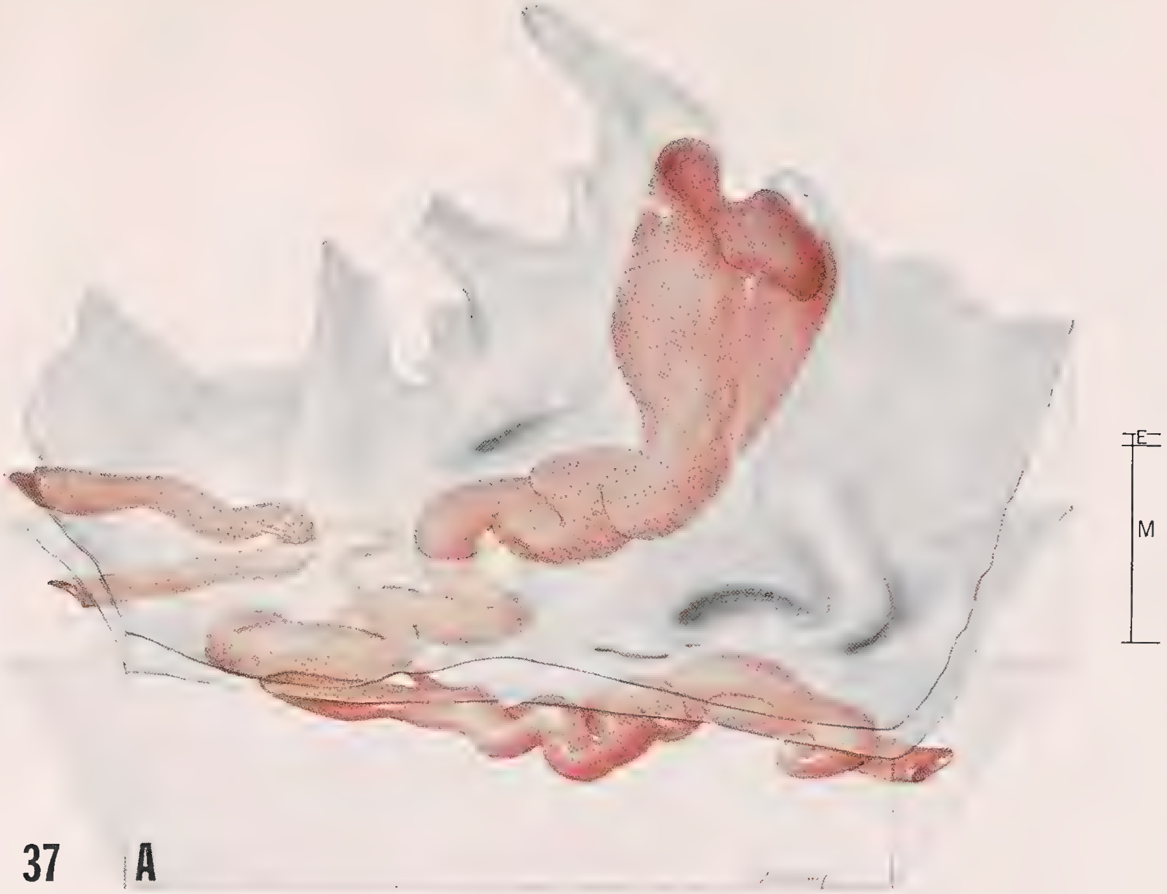

37 A

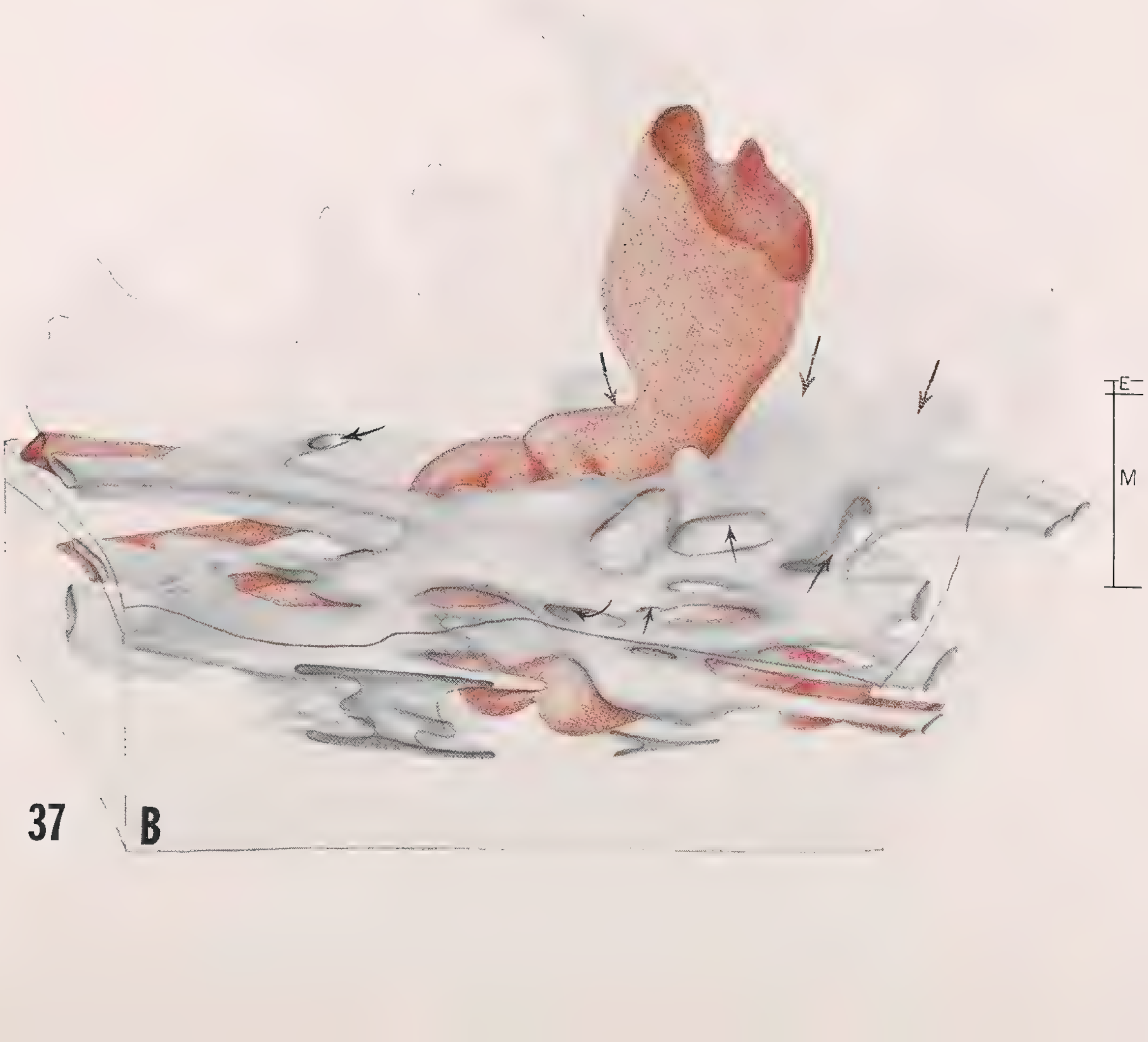

37 B

CONTRIBUTIONS TO EMBRYOLOGY, NO. 261

COMPARISON OF UTEROPLACENTAL VASCULATURE AND CIRCULATION IN THE RHESUS MONKEY AND MAN

Elizabeth M. Ramsey
Department of Embryology, Carnegie Institution of Washington, Baltimore, Maryland
and
John W. S. Harris
Department of Anatomy, London Hospital Medical College, London, England

(With 7 plates)

CONTENTS

PAGE

MORPHOLOGY 61
  Material and Methods 61
  Comparison of Findings in Monkey and Man 62
    Implantation 62
    Development of Trophoblastic Shell 62
    Action of Trophoblast on Uteroplacental Vessels 63
    Vascular Connections With the Intervillous Space 64
    Effect of Observed Differences 65

MYOMETRIAL ACTIVITY 65
  Material and Methods 65
  Comparison of Findings in Monkey and Man 66

RADIOANGIOGRAPHY 66
  Material and Methods 66
  Comparison of Findings in Monkey and Man 67
    Arterial Inflow: Basic Pattern and Effect of Uterine Contractions . . 67
    Venous Drainage: Basic Pattern and Effect of Uterine Contractions . 67

SUMMARY 68

LITERATURE CITED 68

COMPARISON OF UTEROPLACENTAL VASCULATURE AND CIRCULATION IN THE RHESUS MONKEY AND MAN

A comprehensive study of uteroplacental vasculature and circulation has been in progress in the Carnegie Department of Embryology for some years. The study has comprised four separate but related investigations. The first and fourth have dealt with vascular morphology in the rhesus monkey and man, respectively, and the second and third with myometrial activity and radioangiography of placental circulation, both in the monkey. Detailed reports of each phase of the study have been published (Ramsey, 1949, 1954; Corner *et al.,* 1963; Donner *et al.,* 1963; Ramsey *et al.,* 1966; Harris and Ramsey, 1966).

It is now appropriate to review the findings from a broad point of view, synthesizing the information already available and laying out some of the avenues along which future investigations may profitably proceed. Because of the increasing use of the monkey as an experimental model in the study of the physiology of pregnancy it is important to determine to what extent monkey and human placental vasculature and circulation are similar. In particular, an attempt must be made to answer two basic questions: (1) Are "arguments by analogy," comparing monkey and man, valid? (2) Do observed differences between the two species necessitate revision of any of the existing general theories based on findings in the monkey?

The recently completed study of the morphology of uteroplacental vasculature in man (Harris and Ramsey, 1966) provides the first opportunity to make a comparison of this aspect of the circulation in the two species. Previously no systematic study directly comparable with that in the monkey (Ramsey, 1949, 1954) was available in the human. The situation is different with respect to the investigations of myometrial activity (Corner *et al.,* 1963) and of circulatory pattern demonstrated radiographically (Donner *et al.,* 1963; Ramsey *et al.,* 1966), for the studies in rhesus monkeys have their counterparts in the studies carried out on women in a number of clinical institutions (Caldeyro-Barcia, 1957; Hendricks, 1958; Borell *et al.,* 1958, 1965*a* and *b*; Bieniarz *et al.,* 1964). The Carnegie Institution findings in monkeys can therefore be compared with those in human beings, as established by these investigators.

No attempt will be made to summarize all the observations made in our own studies and the comparable ones of other workers. Attention will be focused rather upon the observed differences and fundamental similarities between monkey and man.

MORPHOLOGY

Material and Methods

Except for modifications necessitated by inherent circumstances, the methods used to investigate the uteroplacental vasculature in man were the same as those previously developed for studies in the monkey.

The monkey material consisted of 29 pregnant animals of the Carnegie colony distributed throughout pregnancy, as shown in Table 1. The human material, obtained and prepared through the kind cooperation and expert skill of colleagues in the United States and Britain, comprised 31 pregnant uteri with placentas *in situ,* removed at operation or necropsy, and representing all stages of pregnancy (Table 1). Besides these two series, which were especially designed for investigation of uteroplacental vasculature, additional monkey and human specimens were available for study in the general Carnegie collection. This supplementary material was segregated from the primary series because of technical inadequacies or clinical histories suggestive of uterine, placental, or cardiovascular pathology.

In the monkey, colored material was introduced directly into the systemic circulation of the anesthetized animal, and the injected uterus was promptly removed and fixed (Ramsey, 1949, 1954, 1958*a* and *b*). Large series of thick sections were prepared from selected areas, and representative vessels were modeled by the plastic-sheet method. The entire placenta was serially sectioned in most of the specimens recovered before the 125th day of pregnancy. In the human, the extirpated uterus was prepared, immediately after its removal, by injection with India ink via the uterine artery (Rossman and Bartelmez, 1957). The subsequent fixation, sectioning, and construction of models

TABLE 1. Distribution of Placentas Studied

	Early Pregnancy	Mid-pregnancy	Late Pregnancy	Total
Monkey	9	16	4	29
Human	10	16	5	31

followed the technique employed for the monkey in all respects except that the size of the human placenta made serial sectioning of the whole organ impractical after the first trimester. To compensate, numerous sample areas were serially sectioned. In both species the thick sections upon which the models were based (25–50μ) were augmented by series of even thicker sections (up to 500μ) for overall survey of entire placentas and by series of thin sections (7–10μ) stained for special histologic studies.

Comparison of Findings in Monkey and Man

Implantation

When the earliest stages of implantation in the monkey, as described by Wislocki and Streeter (1938), are compared with the same stages in the human (Hertig, Rock, and Adams, 1956; Harris and Ramsey, 1966), it appears at once that there are certain conspicuous differences in the mechanism of implantation (Table 2), some of which may influence the development of the uteroplacental circulation. The lack of a decidual reaction in the endometrial stroma in the monkey is perhaps the most fundamental of these differences (Figs. 1, 3, and 5),* in contrast with the pronounced decidual reaction in the human endometrium (Fig. 6). This is offset by the appearance of a transitory epithelial plaque that has no counterpart in the human (Figs. 1 and 2). Whether as a consequence of these two conditions or coincidentally, implantation in the monkey is superficial (Figs. 1 and 2), and a secondary placenta forms on the uterine wall opposite the primary implantation site. The secondary placenta closely resembles the primary one. It tends to be smaller, but it lacks no constituent parts. The umbilical cord is inserted in the primary placenta, and interplacental fetal vessels connect the two discs. In a small percentage of pregnancies there is only one placenta, apparently the result of fusion of the primary and secondary discs.

A great deal has been written (see review in Böving, 1963) about the superficial implantation in the monkey versus the interstitial implantation in man. Attempts have been made to relate the condition in the monkey to the barrier action of the epithelial plaque and the inadequate pabulum provided by the nondecidual, glycogen-poor stromal cells. Other authors (Böving, *loc. cit.*) have read a different meaning into the evidence, considering the glycogen-rich plaque as a highly nutritive tissue inviting trophoblastic invasion in preference to the nonnutritional stroma. These authors point out that lateral rather than deep extension of the implantation site is thus favored and that secondary trophoblastic attachment occurs where the secondary epithelial plaque has formed. Studies of uteroplacental vasculature have little to contribute to this phase of the subject; more light can be shed on the problem by investigations specifically designed to study the mechanism of implantation (Böving, *loc. cit.*).

Development of Trophoblastic Shell

More directly allied to the mechanism by which uteroplacental vascular connections are established is the behavior of the trophoblast. In both human and

TABLE 2. Chief Differences Between Human and Monkey Placentation

Monkey	Man
Implantation	
Superficial	Interstitial
No decidual reaction	Pronounced decidual reaction
Transitory epithelial plaque	No epithelial reaction
Secondary placenta	No secondary placenta
Trophoblast	
Boundary between maternal and fetal tissues—straight	Boundary between maternal and fetal tissues—very irregular
No penetration of myometrium by trophoblast	Penetration of inner third of myometrium by trophoblast
No trophoblastic wandering cells	Trophoblastic wandering cells prominent
Arteries	
Intravascular cells very early—17th day	Intravascular cells later—peak at 12th week
Migration of intravascular cells in lumen only	Walls also traversed by intravascular cells
Elastic tissue extending halfway up in endometrium	Little elastic tissue beyond myoendometrial junction
Multiple openings to intervillous space from single stems—infrequent	Multiple openings—common
Terminal sac and progressive dilatation	More pronounced general dilatation; no terminal sac
Loss of tortuosity toward term	Coils looser but still present at term

---

* See end of text, Plates 1–7, for all figures.

monkey implantation the earliest maternal vessels that open into the spaces in the trophoblastic plate are superficial segments of the subepithelial capillary network. The endometrial veins open next, and finally the coiled arteries. The spaces, or lacunae, in the trophoblastic plate into which maternal blood first enters, are the forerunners of the intervillous space. Wislocki and Streeter (1938) assumed that these lacunae in the monkey arose from coalescence of fluid spaces within the trophoblast, and Hertig, Rock, and Adams (1956) made the same assumption with regard to man. The finding in the recent studies of human uteroplacental vasculature (Harris and Ramsey, 1966) have shown that some of the spaces in the trophoblastic plate, which contain blood, can be linked with maternal capillaries at the margin of the plate, suggesting that the lacunae may arise through engulfment of part of the capillary plexus by the trophoblast. This suggestion accords with the further observation that early vascular connections are established before there is any marked extravasation of blood or general disintegration of maternal tissue. The demonstration in future studies of persisting endothelium in the spaces within the trophoblastic plate would establish the process of engulfment as one of the basic factors in the formation of placental vascular connections. Studies in the monkey so far (Heuser and Streeter, 1941) have yielded no additional information on this point.

The development of the cytotrophoblastic shell is characterized by disorganization in its zone of junction with the decidua. Degeneration of maternal tissue, erosion of arterial walls, and extravasation of blood occur, the blood accumulating in the lumina of the endometrial glands as well as in the stroma. It is noteworthy that these processes are much less pronounced in the monkey than in man (Figs. 3 and 4). Human trophoblast penetrates the maternal tissues more deeply and irregularly and has a greater effect upon the endometrial arteries. In the monkey the more superficial and restricted action of the trophoblast causes erosion of only the tips of the coiled arteries, whereas in man the far-ranging trophoblastic cells breach the walls of the arteries and their branches as far as the basalis or even the inner layer of the muscularis. Segments of an artery distal to such a breach of its wall may become nonfunctional with partial or complete obliteration. The arterial wall may be breached in many places, effecting multiple openings into the intervillous space from a single arterial stem (the *Mündungsstücke* of Spanner, 1935). Multiple openings are uncommon in the monkey; indeed, in this species, two or more arteries not infrequently open together into the intervillous space via a common terminal sac (Fig. 15).

Endometrial projections into the intervillous space, often called "septa," are seen in both monkey and man. These septa extend no more than halfway to the chorionic plate, except occasionally in the monkey, when they form the margins of maternal cotyledons or lobules. Thus they do not subdivide the intervillous space and lack the importance attributed to them by Bumm (1893) and Spanner (1935). Arterial openings frequently occur at the sides of these projections. Brosens (1965) has recently completed a detailed study of the septa, preparing models and sketches to show their character and distribution and the relation of arterial and venous orifices to them. His findings are in accord with those of Harris and Ramsey. He emphasizes that the incompleteness of the septa and the frequent occurrence of perforations in them allow free intercommunication among all parts of the intervillous space. He also notes that "every sizable septum has one or more spiral arteries opening at its base."

In the monkey the cytotrophoblast forms neat compact columns that interlace to form a well-demarcated trophoblastic shell (Fig. 3). At early stages syncytium borders the cytotrophoblast on the decidual side of the shell and lines the lacunae, as it does in man. Later the monkey syncytium becomes less prominent, though it continues to line the intervillous space. Monkey trophoblast does not typically form wandering cells within the maternal tissue, in contrast to the human, where large numbers of trophoblastic cells throughout the endometrium and in the myometrium are a conspicuous feature of the placental bed (Fig. 14).

Action of Trophoblast on Uteroplacental Vessels

Arteries

Figs. 7–14 show representative human and monkey arteries at successive stages of pregnancy. The photographs illustrate the changes that take place in the vessels communicating with the intervillous space. In general the changes fall into two groups: accumulations of cells within the lumina of the arteries, and cellular infiltration of the arterial walls.

The nature and origin of the cells taking part in these changes have been subjects of prolonged debate (see reviews in Mossman, 1937; Wislocki and Streeter, 1938; Ramsey, 1949; Hamilton and Boyd, 1960; and reports of recent investigations by Klinger and Ludwig, 1957; McKay *et al.*, 1958; Schramm, 1962; Brettner, 1964). Basically the question is whether these cells are of maternal or fetal origin, and up to now no unequivocal answer has been found. The cells' histologic resemblance to cytotrophoblast is usually marked, but such evidence is inconclusive. Sex chromatin studies may be expected to supply a definitive answer in due course, but none of the studies published so far fit all the technical requirements, nor have cells in all the various locations been examined. It may be noted, however, that the preponderance of the available evidence points to a trophoblastic origin of the cells. Trophoblastic origin is also suggested by the recent Carnegie Institution studies in which the appearance of the cells is traced in slow, closely seriated time steps; in this way continuity between the cells and the cytotrophoblast can frequently be demonstrated.

In the monkey, the intra-arterial cells appear in profusion very early (Fig. 7). They reach their peak in the human somewhat later, at about 12 weeks (Figs. 8 and 10). In both species the cells are first seen close to the placental base and gradually extend into the myometrial portion of the vessels. Medial changes commence shortly after the appearance of the intra-arterial cells and, in both monkey and man, consist of an infiltration of cells, most of which resemble cytotrophoblast. In addition, in the human, multinucleate giant cells of bizarre shape appear in the arterial walls and in the perivascular stroma. Such cells are uncommon in the monkey. Histologic appearances strongly suggest that the human giant cells enter the wall from the surrounding endometrial stroma.

The effect of these cells upon the tissue of the vessel wall is essentially degenerative although degeneration may not occur at once. Thus, the intra-arterial cells of the monkey only gradually replace the vascular endothelium and slowly destroy the media and replace it (Figs. 7, 9, and 11). This action occurs from within the lumen. The action in human arteries takes place in two directions: from within as in the monkey, and from without by transmural migration of the cytotrophoblast-like cells. Fig. 12 provides an example of such migration.

Fig. 13 shows the last of the changes in the arterial wall as it occurs in the monkey. It is characterized by extensive narrowing of the vessel's lumen as a result of the deposition of fibrin in its wall, plus the accumulation of trophoblast-like cells and some proliferation of fibrous connective tissue. A similar change occurs in human arteries, commencing between the 12th and 16th weeks, but it varies in certain respects, as may be seen in Fig. 14. There is obstruction of the lumen by masses of cells and by deposits of fibrin upon the cells. The endothelium is sometimes displaced toward the center of the lumen by deposits of fibrin beneath it, as shown in Fig. 14. In both species this change commences at the placental base and extends proximally. This physiologic change is also noted by Brosens (1965). It is important to differentiate it from vascular changes associated with pathologic conditions.

Veins

The reaction in human and monkey veins is quite similar, consisting essentially of a passive response to external compression. This causes obliteration of many of the more delicate channels. Consequently the remaining channels distend to accommodate the increasing volume of blood from the developing intervillous space. Throughout pregnancy, orifices in all regions of the basal plate communicate with endometrial veins. In neither species is there preferential drainage of the placental margin nor any demarcated "sinus" separated from the intervillous space (Spanner, 1935; Fish, 1955). Drainage of the margin is often by way of large channels that form a wreath of conspicuous veins around the placenta. Much of the drainage of the central portion of the basal plate is effected by slender veins pursuing an oblique course toward the myometrium; but occasionally, particularly in the monkey, a wide, sluicelike channel will proceed directly from the placental outlet to a myometrial arcuate vein.

In the mature placenta, the uteroplacental veins in monkey and man form a network around the arteries. Muscle fibers penetrate the meshes of the network, separating it into layers connected by short oblique stems. The veins lack valves. In the early weeks of human pregnancy, trophoblastic giant cells may be found in the lumina of veins, and trophoblast appears to migrate along their outer walls as it penetrates the decidua. There is no evidence in either species, however, that the trophoblast evokes changes comparable to those occurring in the arteries. Fragments of villi, or even whole villi, are occasionally seen in the veins, often at some distance from the base of the trophoblastic shell. They do not appear to produce occlusion, although they may function as physiologic ball valves.

Unanswered questions

Various unresolved problems have been noted in the foregoing. The more important may be summarized as follows:

What is the nature of the intra-arterial cells? Conclusive evidence of their trophoblastic origin is still lacking.

What controls the extent of migration of the trophoblast-like cells, intra-arterially, in the vessel walls, and in the uterine tissue?

Why are only arteries involved in the migration with no similar occurrence in veins?

Does transmural migration of trophoblast-like cells in human arteries occur in both directions?

Vascular Connections With the Intervillous Space

The number of connections between uterine vessels and the intervillous space has been determined in several mature midterm monkey placentas *in situ* by direct count in serial sections through the entire organ (Ramsey, 1958*a*). The number in human placentas has only been estimated on a sampling basis, since the size of the organ precludes total serial sectioning. Even when multiple openings into the intervillous space from a single stem are discounted, a marked discrepancy is found between monkey and man. In the monkey, approximately 20 arteries and 40 veins connect with the intervillous space of the placenta at midpregnancy. They are distributed fairly equally between primary and secondary placentas. The general accuracy of these figures, at least for the arteries, is substantiated by counts of entries in placentas visualized by radiography after injection with radiopaque dye (Martin *et al.,* 1964).

Recent estimates for the human placenta (Harris and Ramsey, 1966), which are in essential agreement with Boyd's estimated averages (Boyd, 1956), indicate that the number of communications is appreciably higher than in the monkey at a comparable stage, even when the difference in placental size is taken into account. Boyd estimated one entry per 100 square millimeters of placenta. Harris and Ramsey estimated two arterial and one to two venous orifices per 100 square millimeters of placenta, in placentas approximately 6–8 cm in diameter. Brosens (1965) modeled two fifths of a term placenta and counted 48 arterial entries. Calculated on the basis of this sample, he set the total number of entries at 120, or one entry for each 200 square millimeters of basal plate. None of these arteries had more than one opening into the intervillous space.

The study by Harris and Ramsey indicated considerable variation in the number of communications as gestation progresses. The number of arterial openings into the intervillous space increases up to midpregnancy and then falls off sharply. This may reflect the dual action of the trophoblast in breaching the main trunk of some arteries in several places and in occluding branches of others. No data on variation throughout pregnancy are available for the monkey.

Effect of Observed Differences

The gross morphologic effects of these differing histologic phenomena are remarkably similar in the two species. Figs. 15 and 16 are semidiagrammatic drawings based on models reconstructed from serial sections. They show the morphologic changes in representative monkey and human uteroplacental arteries at selected stages throughout pregnancy. Data in the legends provide an approximate comparison of the ages of the pregnancies selected, assuming that the length of the gestation period in the monkey is three fifths of that in the human. The probable variation in developmental rate is disregarded.

The outstanding feature is the progressive dilatation of the uteroplacental arteries. In the monkey, this commences early with the formation of a terminal sac close to the base of the placenta and gradually extends proximally until all parts of the vessel greatly exceed their nonpregnant dimensions. That the distention is somewhat less striking in the monkey than in the human may perhaps be related to the persistence of elastic tissue in the walls of the monkey arteries as far as the middle layer of the endometrium during the early period when the dilatations are formed. Elastic tissue is absent in human arteries beyond the myoendometrial junction. In man, dilatation is gradual until the 12th week. Then, coincident with the intra-arterial migration of trophoblast, the terminal portions of the arteries form vertically oriented channels that may correspond to the terminal sacs of the monkey. Formation of these sacs coincides with the beginning of intra-arterial migration of trophoblast-like cells. The greater enlargement of human arteries may also be related to the more intense action of human trophoblast upon the arterial walls from without.

In both species, the dilatations may be expected to have important physiologic effects in that they provide a kind of antechamber to the intervillous space, in which the linear velocity and hence the force of the blood flow is reduced.

The greater degree of uncoiling of uteroplacental arteries in the monkey as gestation advances probably bears no relation to trophoblastic action but is rather a reflection of the relatively greater stretching and thinning of the uterine wall. A related factor may be the extreme sponginess of the remaining portion of the monkey endometrium, which may supply less support to the vessels than is provided in the human uterus.

MYOMETRIAL ACTIVITY

Material and Methods

In contrast with the study of vascular morphology, in which the investigation of the monkey came first, the study of myometrial activity in the monkey followed the pioneering work of Alvarez and Caldeyro-Barcia (1954) and Caldeyro-Barcia (1957) in women, and it employed as nearly as possible the technique devised by them. Very few alterations in procedure were necessary. In both man and monkey the observations could be made in vivo, although for purposes of handling it was necessary to anesthetize the monkey. Initially laparotomy was performed to facilitate insertion into the monkey's amniotic cavity of the catheter to which the pressure transducer and the recording system are attached. Later, however, it was found possible to insert the catheter percutaneously, just as in the human subject. Although psychological and social factors limit, to some extent, the admissible time and frequency of hysterocentesis in pregnant women, such studies in cooperative patients have a significant advantage over studies in the monkey, for the conscious monkey, unless restrained in a primate chair or by similar means, invariably removes the catheter. Determination of intrauterine pressure on successive days thus requires reinsertion under anesthesia. On the other hand, the interruption of pregnancy in the monkey is a cause of less concern, so that earlier and more frequent examinations can be carried out. In the monkey studies all experiments followed by abortion within three days were considered "impending abortions" and studied separately.

In the series designed specially to study myometrial contractility in the monkey (Corner *et al.*, 1963), 137 determinations of intrauterine pressure were made at various stages in 87 pregnancies: 41 in early pregnancy, 67 in midpregnancy, 26 in late pregnancy, and 3 in labor. In addition, intrauterine pressure was routinely monitored and analyzed in 68 radioangiographic studies at midpregnancy or late pregnancy. In the group at midpregnancy, uterine activity was spontaneous; in the late-pregnancy group, contraction was frequently induced with oxytocin. The induced contractions had the same characteristics as those of late pregnancy or spontaneous labor.

Comparison of Findings in Monkey and Man

Comparison of Figs. 17 and 18 shows the resemblance between the patterns of myometrial activity in the monkey and in man. The tracings should be analyzed in terms of the three fundamental parameters of the contraction wave that indicate myometrial state: intensity, frequency, and pattern. The most significant feature shown by the tracings is the trend, from midpregnancy onward, toward increased intensity and frequency of contractions with progressive simplification and coordination of the wave pattern as labor approaches. This trend is essentially the same in the two species, and the labor wave itself is quite similar in them.

Although the human uterus is active to some extent at all stages, the high degree of strong but uncoordinated activity shown by the monkey in early pregnancy is not duplicated in the human. Indeed, in early pregnancy the human uterus is relatively quiescent and the occurrence of a compound wave as distinctive and consistent as that in the monkey is rare (Hendricks, 1958). Several possible causes of the difference may be recognized. The two placental discs of the monkey, providing two foci of local progesterone formation (Csapo, 1963), may supply a source of incoordination not present in the human placenta, though this remains speculative until it is determined whether monkeys with a single placenta display a coordinated contraction pattern. The proportionately greater thickness of the monkey myometrium may be another factor. In addition, it has been shown (Short and Eckstein, 1961) that the progesterone production by the monkey placenta, relative to placental weight, is many times less than the production by the human placenta. The generally similar physiologic response of the human and monkey myometrium to oxytocic drugs (Scoggin *et al.*, 1963) suggests, however, that fundamentally similar mechanisms regulate myometrial contractions in the two species.

RADIOANGIOGRAPHY

Material and Methods

The early clinical work of Borell and his co-workers provided the impetus for radioangiographic studies in pregnant monkeys (Borell *et al.*, 1958), and the technique they described needed little modification (Ramsey *et al.*, 1963*a* and *b;* Donner *et al.*, 1963). In studies employing roentgenography, use of the monkey has distinct advantages over the human patient in whom radiation hazard limits the number and duration of permissible exposures. This fact makes it especially important to determine the suitability of the monkey as a model.

In the monkey, injections of radiopaque dye were made in 76 animals at stages of pregnancy ranging from 59 to 158 days. In 44 animals, injection was made into the femoral artery to demonstrate arterial inflow to the placenta (Ramsey *et al.*, 1963*a*), and in 32 animals the injection was made into the intervillous space to demonstrate venous drainage (Ramsey *et al.*, 1966). Visualization was achieved either by rapid serial radiography or cineradiography. Intrauterine pressure was monitored simultaneously in 68 animals to permit dye injection at specific stages of the contraction cycle and observation of the effects of myometrial contraction upon placental circulation. Oxytocin was employed as needed to induce contractions. As in the myometrial studies, it was necessary to anesthetize the monkeys; the only other important variation from the Borell technique was the necessity for open insertion of the arterial catheter, because the femoral artery lies deeper in the monkey than in the human and is acutely susceptible to constriction when touched. In the experience of Ramsey and co-workers, visualization of placental drainage channels in the monkey could be achieved with dependable distinctness only when the contrast medium was injected directly into the intervillous space because of the dilution of dye injected intra-arterially by the blood in the space. The catheter for this injection was inserted at laparotomy after localization of the placenta by transillumination.

Borell and his co-workers have studied uteroplacental blood flow in 22 women at midpregnancy and in 3 women at term, employing rapid serial roentgenography (Borell *et al.*, 1964, 1965*a* and *b*). All injections were made intra-arterially. The time of appearance of dye at various points in the uteroplacental circuit was determined, but no attempt was made to map the course of drainage channels. Particular attention was focused upon the effects of uterine contractions induced by intravenous administration of oxytocin or intra-amniotic injection of hypertonic saline. In the studies of human subjects, as in those of monkeys, certain technical points have proved to be of great importance, among them the amount of dye used, the rapidity and pressure of injection, and the time in the contraction cycle when the dye is introduced. It is significant that the effects of these factors appear to be the same in the monkey and in man.

In other radiologic studies of the human uteroplacental circulation, including those of Nelson *et al.* (1961), Richart *et al.* (1964), Bieniarz *et al.* (1964), and Benson *et al.* (1963), techniques essentially similar to those of Borell were employed.

COMPARISON OF FINDINGS IN MONKEY AND MAN

Arterial Inflow: Basic Pattern and Effect of Uterine Contractions

Rather than uncovering fundamental differences between monkey and human uteroplacental circulation, these studies have revealed a striking similarity. Comparison of the monkey radiograph in Fig. 19 with the human radiograph in Fig. 20 shows the similar course pursued by the arteries through the uterine wall to the point where they discharge their contents into the intervillous space in fountainlike "spurts" of identical configuration. The manner in which these spurts grow and coalesce is also identical. With uterine contractions, inflow of blood is halted or curtailed (Figs. 21 and 22). In the monkey, abolition of all spurts has been observed with intrauterine pressure no higher than 36 mm Hg. In other animals, or in other injections in the same animal, some spurts may persist at higher pressures. Similar variability occurred in Borell's studies. In 12 of the 22 patients examined at midpregnancy, total abolition of spurts occurred with pressures between 50 and 57 mm Hg, and in the remainder, filling of the intervillous space was partial and faint. In the three patients at term, complete absence of entries was never found, though injection pressure was the same, but marked reduction in number of spurts and delay of entry was demonstrated. Evidence of segmental variation in the inhibitory effect was noted in the human uterus. Data on this point are not available for the monkey.

In the monkey, the pattern of spurts into the intervillous space is variable (Martin *et al.*, 1964), even under constant conditions of myometrial activity and maternal blood pressure (Fig. 23). This suggests the possibility of intrinsic vasomotor activity of the arteries or sharply localized myometrial contractions and is in accord with the findings of morphologic studies of nonpregnant human and monkey uteri (Bartelmez, 1957*a* and *b*; Markee, 1940), that coiled arteries undergo constrictions just before they cross the myoendometrial border. Ramsey (1958*a*), using histologic techniques, demonstrated similar constrictions in uteroplacental arteries in the monkey.

Borell (1965*a*) examined the outlines of human uteroplacental arteries in illuminating detail, producing radiographic evidence that coiled arteries may become smoothly narrowed even to the point of occlusion. The site of the narrowing is not apparent. Borell's radiographs show, in addition, examples of asymmetric vascular constrictions that are considered the result of external compression. None of the studies to date, in monkey or in man, throw light upon the primary cause of the constrictions.

Venous Drainage: Basic Pattern and Effect of Uterine Contractions

Radiographs made after injection of dye into the intervillous space in monkeys (Ramsey *et al.*, 1966) show the network of veins in the uterine wall and their connection with the extrauterine channels (Fig. 24). The ovarian veins constitute the major routes of drainage to the systemic circulation in this animal, the uterine veins playing a minor role. During uterine contractions, dye disappears to a greater or lesser degree from the mural and extrauterine veins, although the size of the pool of dye in the intervillous space remains constant (Fig. 24). Borell and associates (1965*b*) observed that no dye could be seen in human mural veins when intrauterine pressure was high (55 mm Hg), though partial filling of channels (38 per cent) occurred when the contraction was of lesser intensity. Thus it appears that exit of dye from the intervillous space is wholly or partially suspended during uterine contractions.

From their observations of the monkey, Ramsey and co-workers (1966) conclude that the observed inhibition of drainage during a contraction, as well as the overall retardation of blood flow, depends basically upon the reduction or halting of arterial inflow. The disappearance of dye from mural veins is regarded as the result of direct action of the myometrial contraction upon the veins at a time when they are not being refilled from the intervillous space. Borell *et al.* (1965*a*) reserve judgment in this matter. Although agreeing that this mechanism may be one of those involved, and citing the role of local arterial constrictions, they note the possibility that back pressure, resulting from myometrial compression of mural veins, may also play a part. However, in the monkey experiments it was found that drainage persists if injection into the intervillous space at low pressure is continued throughout the contraction (Ramsey *et al.*, 1966). This finding casts some doubt upon the role of back pressure.

SUMMARY

From the foregoing it seems clear that an affirmative answer may be given to the first of the two questions posed at the beginning of this paper and a negative answer to the second. The "argument by analogy" from monkey to man *is* valid; and the observed variations between monkey and man do *not* necessitate revision of theories based upon the analogy.

By emphasizing the similarities between human and monkey uteroplacental circulation, it is not intended, however, to minimize the differences which, as shown above, are numerous and appreciable. In the areas of difference, each of the two species must be considered separately. Thus, generalizations about trophoblastic behavior can only be made for man upon the basis of human studies and for the monkey upon the basis of monkey studies. Similarly, to cite but one more among many examples, studies of decidua formation can only be made in man, as no decidua forms in rhesus. Nevertheless, if the differences between monkey and man are analyzed, it is found that those specifically related to the operation of the circulatory mechanism are not numerous, and they appear to be essentially quantitative variations upon a qualitatively similar scheme.

The most significant morphologic variation is the greater dilatation of human uteroplacental arteries, possibly resulting from the paucity of elastic tissue in the endometrial portion of the vessel wall and the more severe trophoblastic challenge to the integrity of the wall. However, despite the greater dilatation in human arteries, the important fact is that pronounced dilatation occurs in both monkey and man. Such specifically human features as multiple openings of the intervillous space from a single arterial stem, which may be a result of the different patterns of branching and the deeper trophoblastic invasion in man, cannot be regarded as capable of modifying the basic circulatory mechanism, particularly as the situation is largely redressed in later pregnancy by occlusion of branches and establishment of single preferential pathways of flow.

The differences in myometrial activity pattern are superficial rather than substantive when viewed in the light of their effect upon uteroplacental circulation. Further information is needed before the full extent of the differences is clear.

The final justification for regarding the species differences as physiologically of minimal importance lies in the data supplied by radioangiography. Here the most fundamental of the phenomena are found to be common to both species: fountainlike entry of arterial blood into the intervillous space (so-called spurts); intermittent functioning of individual arteries; reduction or halting of blood flow through the placenta during uterine contractions.

Thus it is possible to visualize uteroplacental circulation in both man and monkey in the following terms, as illustrated in the composite drawing reproduced in Fig. 25: Maternal blood enters the intervillous space of the placenta in well-demarcated, fountainlike spurts produced by the force of maternal pressure in the uteroplacental arteries. This *vis a tergo* drives the blood in discrete streams toward the chorionic plate until the head of pressure is reduced. Lateral spread then occurs. Continuing inflow of arterial blood exerts pressure upon the existing content of the intervillous space, pushing the blood toward the orifices of exit in the basal plate through which it is drained into uterine and pelvic veins. During uterine contractions, both inflow and outflow are curtailed or even halted, although the volume of blood in the intervillous space appears to be maintained, thus providing for continued (though reduced) maternal–fetal exchange.

LITERATURE CITED

Alvarez, H., and R. Caldeyro-Barcia. 1954. Fisiopatología de la contracción uterina y sus aplicaciónes en la clínica obstetrica. *Segundo Congreso Latinoamericano Obstet. Ginecol.*, and *Cuarto Congreso Brasilero de Obstet. Ginecol.*, São Paulo, Brazil.

Bartelmez, George W. 1957*a*. The form and the functions of the uterine blood vessels in the rhesus monkey. *Carnegie Inst. Wash. Publ.* 611, *Contrib. Embryol., 36,* 153–181.

Bartelmez, George W. 1957*b*. The phases of the menstrual cycle and their interpretation in terms of the pregnancy cycle. *Am. J. Obstet. Gynecol., 74,* 931–955.

Benson, R. C., C. T. Dotter, and K. R. Straube. 1963. Percutaneous transfemoral aortography in gynecology and obstetrics. *Am. J. Obstet. Gynecol., 85,* 772–791.

Bieniarz, J., J. J. Crottogini, and E. Curuchet. 1964. Angiographic study of arterial and venous uterine circulation in advanced human pregnancy. In *Symposium on Effects of Labor on the Fetus and the Newborn,* Montevideo, Uruguay, Oct. 1–3, 1964. In press.

Borell, U., I. Fernström, L. Ohlson, and N. Wiqvist. 1964. Effect of uterine contractions on the human uteroplacental blood circulation. An arteriographic study. *Am. J. Obstet. Gynecol., 89,* 881–890.

Borell, U., I. Fernström, L. Ohlson, and N. Wiqvist. 1965*a.* Influence of uterine contractions on the uteroplacental blood flow at term. *Am. J. Obstet. Gynecol., 93,* 44–57.

Borell, U., I. Fernström, L. Ohlson, and N. Wiqvist. 1965*b.* Arteriographic study of the blood flow through the uterus and placenta at mid-pregnancy. *Acta Obstet. Gynecol. Scand., 44,* 22–31.

Borell, U., I. Fernström, and A. Westman. 1958. Eine arteriographische Studie des Plazentarkreislaufs. *Geburtsh. Frauenheilk, 18,* 1–9.

Böving, B. G. 1963. Implantation mechanisms. In *Mechanisms Concerned with Conception,* C. G. Hartman, ed., Pergamon Press, New York, pp. 321–396.

Boyd, J. D. 1956. Morphology and physiology of the uteroplacental circulation. In *Gestation, Transactions of the Second Conference,* C. A. Villee, ed., Josiah Macy, Jr. Foundation, New York, pp. 132–194.

Brettner, A. 1964. Zum Verhalten der sekundären Wand der Uteroplacentargefässe bei der decidualen Reaktion. *Acta Anat. (Basel), 57,* 366–376.

Brosens, I. A., 1965. The placental bed. Thesis. Faculty of Medicine, University of London.

Bumm, E. 1893. Über die Entwicklung des mütterlichen Blutkreislaufes in der menschlichen Placenta. *Arch. Gynaekol., 43,* 181–195.

Caldeyro-Barcia, R. 1957. In *Physiology of Prematurity, Transactions of the First Conference,* J. T. Lanman, ed., Josiah Macy, Jr. Foundation, New York, pp. 20–25, 128–135.

Corner, G. W., Jr., E. M. Ramsey, and H. M. Stran. 1963. Patterns of myometrial activity in the rhesus monkey in pregnancy. *Am. J. Obstet. Gynecol., 85,* 179–185.

Csapo, A. I. 1963. Model experiments and clinical trials in the control of pregnancy and parturition. *Am. J. Obstet. Gynecol., 85,* 359–379.

Donner, M. W., E. M. Ramsey, and G. W. Corner, Jr. 1963. Maternal circulation in the placenta of the rhesus monkey; a radioangiographic study. *Am. J. Roentgenol., 90,* 638–649.

Fish, J. S. 1955. *Hemorrhage of Late Pregnancy.* Charles C. Thomas, Springfield, Illinois.

Hamilton, W. J., and J. D. Boyd. 1960. Development of the human placenta in the first three months of gestation. *J. Anat. (London), 94,* 297–328.

Harris, J. W. S., and E. M. Ramsey. 1966. The morphology of human uteroplacental vasculature. *Carnegie Inst. Wash. Publ.* 625, *Contrib. Embryol.,* this volume, pp. 43–58.

Hendricks, C. H. 1958. The hemodynamics of a uterine contraction. *Am. J. Obstet. Gynecol., 76,* 969–982.

Hertig, Arthur T., J. Rock, and E. C. Adams. 1956. A description of 34 human ova within the first 17 days of development. *Am. J. Anat., 98,* 435–494.

Heuser, C. H., and G. L. Streeter. 1941. Development of the macaque embryo. *Carnegie Inst. Wash. Publ.* 525, *Contrib. Embryol., 29,* 15–55.

Klinger, H. P., and K. S. Ludwig. 1957. Sind die Septen und die grosszelligen Inseln der Placenta aus mütterlichem oder kindlichem Gewebe aufgebaut? *Z. Anat. Entwicklungsgeschichte, 120,* 95–100.

Markee, J. Eldridge. 1940. Menstruation in intraocular endometrial transplants in the rhesus monkey. *Carnegie Inst. Wash. Publ.* 518, *Contrib. Embryol., 28,* 219–308.

Martin, C. B., Jr., H. S. McGaughey, Jr., I. H. Kaiser, M. W. Donner, and Elizabeth M. Ramsey. 1964. Intermittent functioning of the uteroplacental arteries. *Am. J. Obstet. Gynecol., 90,* 819–823.

McKay, D. G., Arthur T. Hertig, E. C. Adams, and M. V. Richardson. 1958. Histochemical observations on the human placenta. *Obstet. Gynecol., 12,* 1–36.

Mossman, H. W. 1937. Comparative morphogenesis of the fetal membranes and accessory uterine structures. *Carnegie Inst. Wash. Publ.* 479, *Contrib. Embryol., 26,* 129–246.

Nelson, J. H., Jr., R. L. Bernstein, J. W. Huston, N. A. Garcia, and G. Gartenlaub. 1961. Percutaneous retrograde femoral arteriography in obstetrics and gynecology. *Obstet. Gynecol. Survey, 16,* 1–19.

Ramsey, Elizabeth M. 1949. The vascular pattern of the endometrium of the pregnant rhesus monkey *(Macaca mulatta). Carnegie Inst. Wash. Publ.* 583, *Contrib. Embryol., 33,* 113–147.

Ramsey, Elizabeth M. 1954. Venous drainage of the placenta of the rhesus monkey *(Macaca mulatta). Carnegie Inst. Wash. Publ.* 603, *Contrib. Embryol., 35,* 151–173.

Ramsey, Elizabeth M. 1958*a.* Vascular anatomy of the uteroplacental and foetal circulation. In *Oxygen Supply to the Human Foetus,* J. Walker and A. C. Turnbull, eds., Blackwell Scientific Publications, Ltd., Oxford, England, pp. 67–69.

Ramsey, Elizabeth M. 1958*b.* Vasculature of the endometrium and the placenta: A progress report. In *Factors Regulating Blood Flow, Proceedings of the Third Microcirculatory Conference,* Am. Physiol. Soc., Washington, D. C., pp. 73–77.

Ramsey, Elizabeth M., George W. Corner, Jr., and M. W. Donner. 1963*a.* Cineradioangiographic visualization of the venous drainage of the primate placenta *in vivo. Science, 141,* 909–910.

Ramsey, Elizabeth M., George W. Corner, Jr., and M. W. Donner. 1963*b.* Serial and cineradiographic visualization of maternal circulation in the primate (hemochorial) placenta. *Am. J. Obstet. Gynecol., 86,* 213–225.

Ramsey, Elizabeth M., C. B. Martin, Jr., H. S. McGaughey, Jr., I. H. Kaiser, and M. W. Donner. 1966. Venous drainage of the placenta in rhesus monkeys: radiographic studies. *Am. J. Obstet. Gynecol., 95,* 948–955.

Richart, R. M., G. B. Doyle, and G. C. Ramsay. 1964. Visualization of the entire maternal placental circulation in the rhesus monkey. *Am. J. Obstet. Gynecol., 90,* 335–339.

Rossman, I., and George W. Bartelmez. 1957. The injection of the blood vascular system of the uterus. *Anat. Record, 128,* 223–231.

Schramm, B. 1962. Origine des cellules géantes de la caduque humaine. *Gynecol. Obstet., 61*, 423–433.

Scoggin, W. A., H. S. McGaughey, Jr., W. L. Johnson, and W. N. Thornton, Jr. 1963. Uterine contractility in primates: a comparative study. *Surg. Forum, 14*, 384–385.

Short, R. V., and P. Eckstein. 1961. Oestrogen and progesterone levels in pregnant rhesus monkeys. *J. Endocrinol., 22*, 15–22.

Spanner, R. 1935. Mütterlicher und kindlicher Kreislauf der menschlichen Placenta und seine Strombahnen. *Z. Anat. Entwicklungsgeschichte, 105*, 163–242.

Wislocki, George B., and George L. Streeter. 1938. On the placentation of the macaque *(Macaca mulatta)*, from the time of implantation until the formation of the definitive placenta. *Carnegie Inst. Wash. Publ.* 496, *Contrib. Embryol., 27*, 1–66.

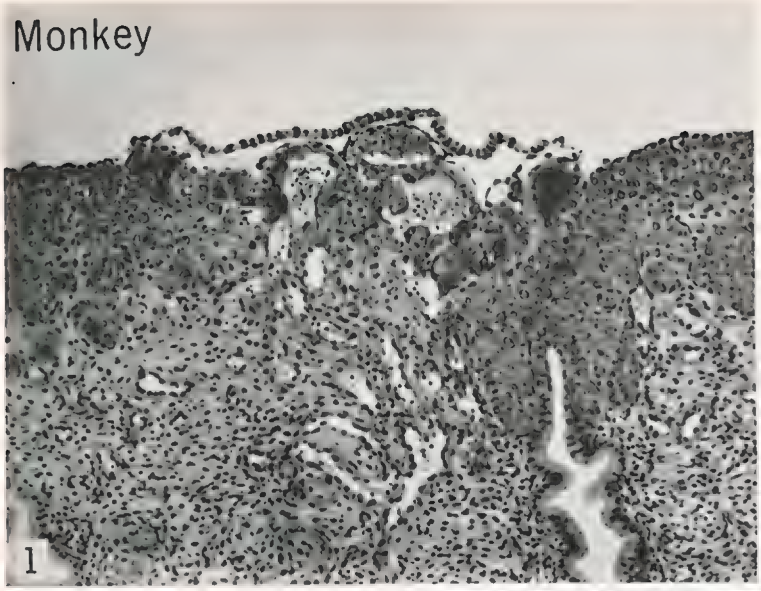

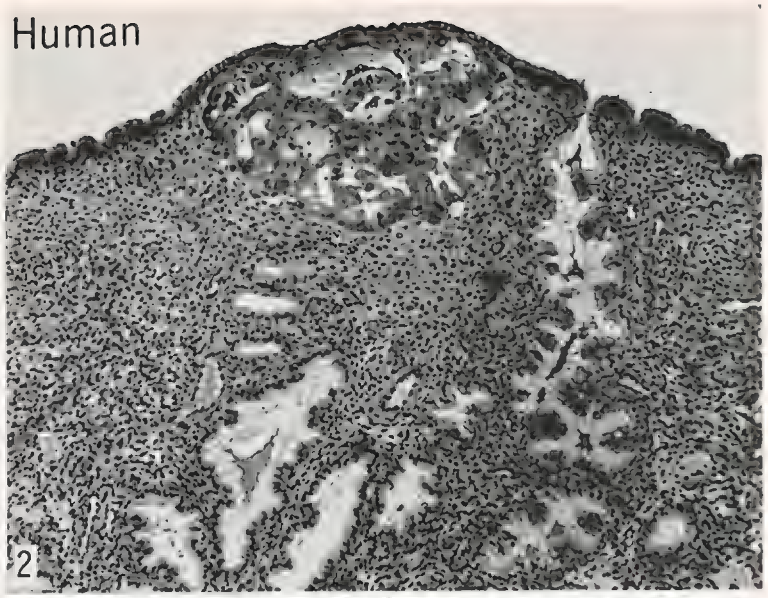

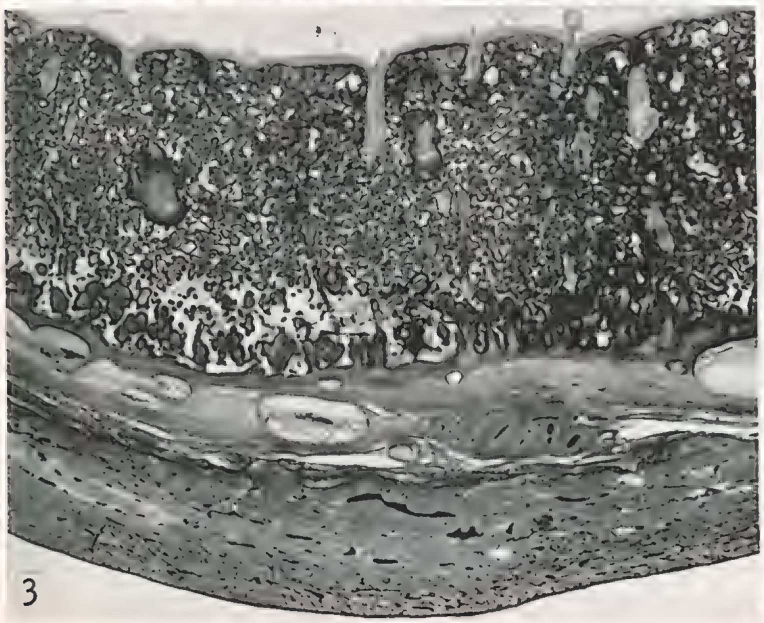

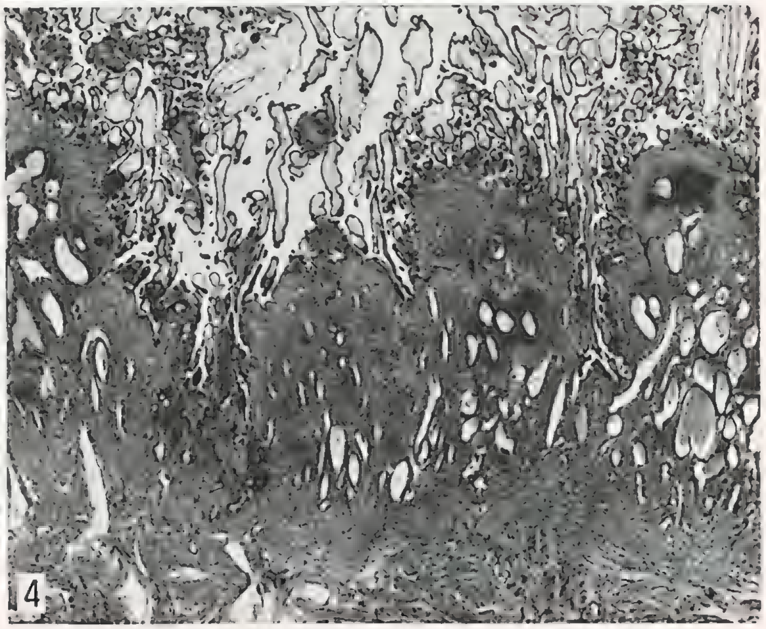

PLATE 1, Figs. 1–4.

Unless otherwise specified, the duration of pregnancy in the monkey is expressed as ovulation age; that in the human as menstrual age. Ovulation is assumed to occur on the 12th day of the menstrual cycle.

Fig. 1. Section through a monkey blastocyst shortly after its attachment to the endometrium. The superficial implantation is apparent, as well as the marked proliferation of the surface epithelium forming the epithelial plaque characteristic of the monkey. Dilated capillaries lie beneath the implantation site, some of them communicating with the trophoblastic lacunae. The endometrial stroma shows no evidence of decidual reaction. Monkey C-524, 10th day after ovulation; section 3-3-10; × 105.

Fig. 2. Section through a newly implanted human blastocyst showing the interstitial implantation, lack of an epithelial plaque, and early evidences of decidua formation. The section shown does not include many segments of the capillary network, but the presence of maternal blood cells in the trophoblastic lacunae is evidence that capillary connections have been established. Human specimen 8004, 8th day after ovulation; section 11-4-4; × 85.

Fig. 3. Section through the full thickness of the uterine wall and attached placenta of a monkey in early pregnancy. The smoothness of the base of the trophoblastic plate at its junction with maternal tissue is striking. There are no irregular projections of trophoblast into the endometrium. Traces of injected India ink can be seen in the maternal vessels and the intervillous space. Monkey C-629, 53rd day of pregnancy; section 32; × 8.

Fig. 4. Section through the base of an attached human placenta in early pregnancy. The irregularity of the junction between trophoblast and endometrium is in striking contrast with the condition in the monkey, as seen in Fig. 3. Note that in some areas the trophoblast penetrates nearly to the myometrium. Human specimen 10129, 61st day of pregnancy; section 2; × 8.

PLATE 2, Figs. 5–10

Fig. 5. High-powered view of the endometrial stroma in a monkey, showing absence of decidual reaction. The area photographed lies just beneath the trophoblastic attachment. Monkey C-658, 38th day of pregnancy; section S1; ×100.

Fig. 6. Characteristic decidual reaction seen in an area of human endometrium adjacent to the base of the trophoblast. Human specimen 9742, 2nd month of pregnancy; ×100.

Fig. 7. Terminal portion of a uteroplacental artery close to its communication with the intervillous space. Note the piling up in the lumen of cells, probably of trophoblastic origin. The endothelium has been destroyed in the main stem, but some cells are still present in the branch at upper right. Monkey C-477, 29th day of pregnancy; section A2; ×150.

Fig. 8. Sagittal section through the basal plate of an attached placenta in an area where a uteroplacental artery is approaching its entry to the intervillous space. The lumen of the artery contains trophoblastic cells, but these are not as abundant as in the monkey specimen of comparable age shown in Fig. 7. Human specimen 9057, 9th week of pregnancy; section 64; ×45.

Fig. 9. Uteroplacental artery, its lumen filled with injected India ink, seen at the point of entry to the intervillous space. There are fewer trophoblastic cells in the lumen than at 29 days, but trophoblast is becoming apparent in the wall. The endothelium is missing. No trophoblast is present in the perivascular stroma. Monkey C-658, 38th day of pregnancy; section 35; ×60.

Fig. 10. Cross section of a uteroplacental artery seen just at the myoendometrial junction. Comparing this photograph with Fig. 8, it is evident that there are now more trophoblastic cells in the arterial lumen than previously. The series of figures 7 through 10 shows that the peak of cell accumulation occurs earlier in the monkey than in the human. Human specimen 9051, 14th week of pregnancy; section 27; ×45.

Monkey

Human

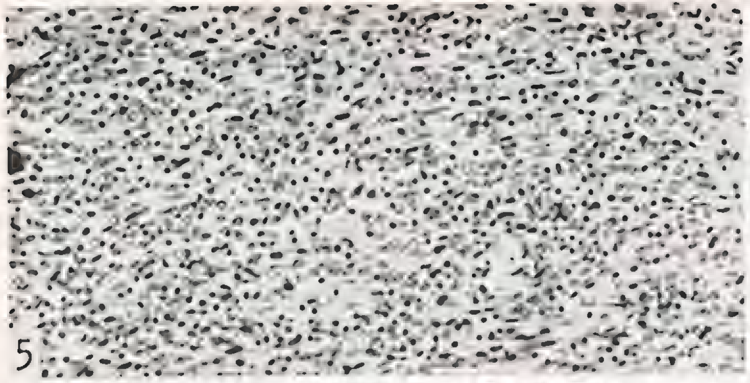

5

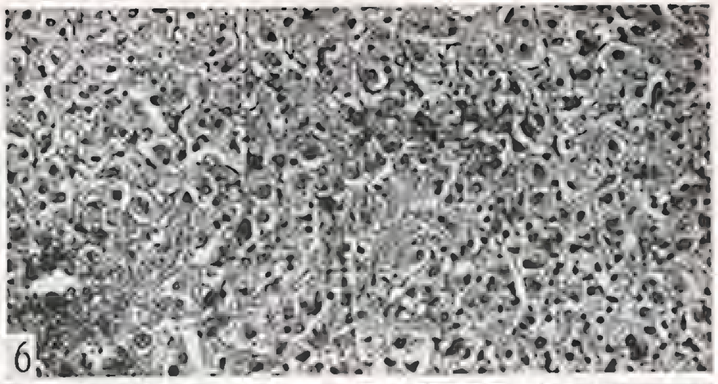

6

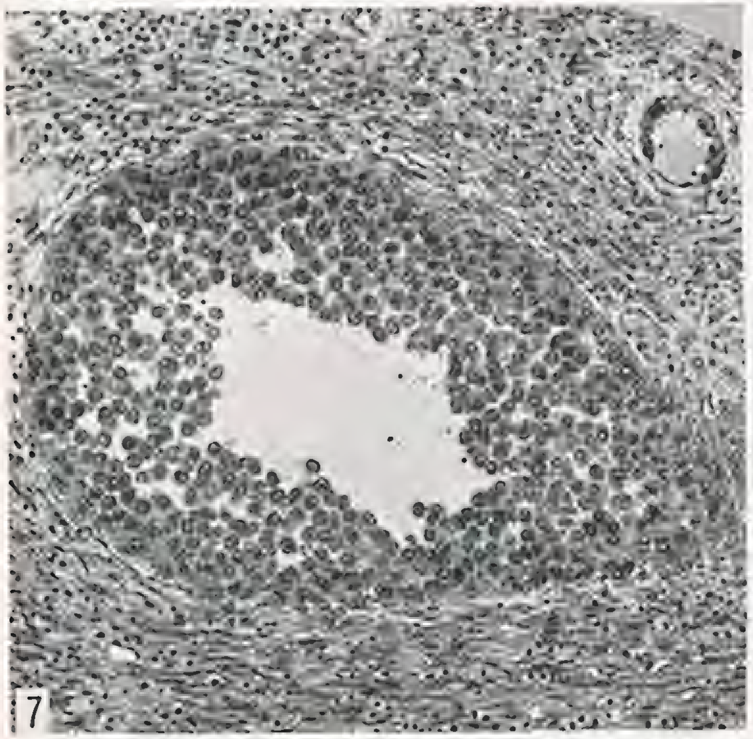

7

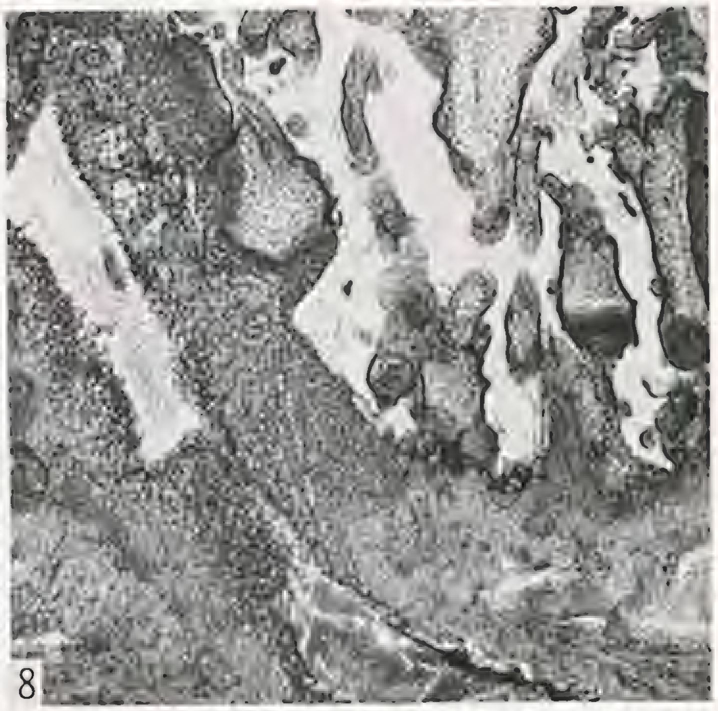

8

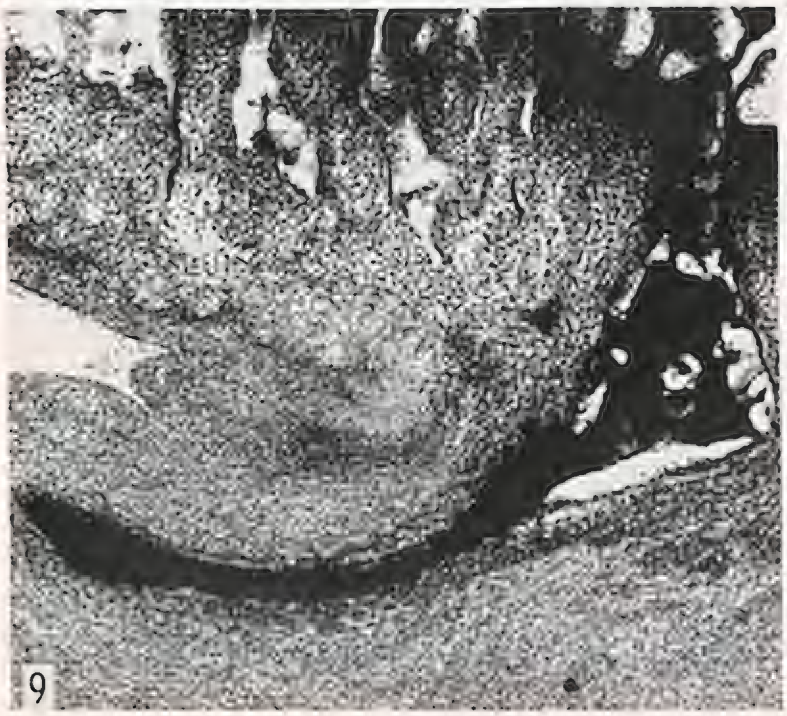

9

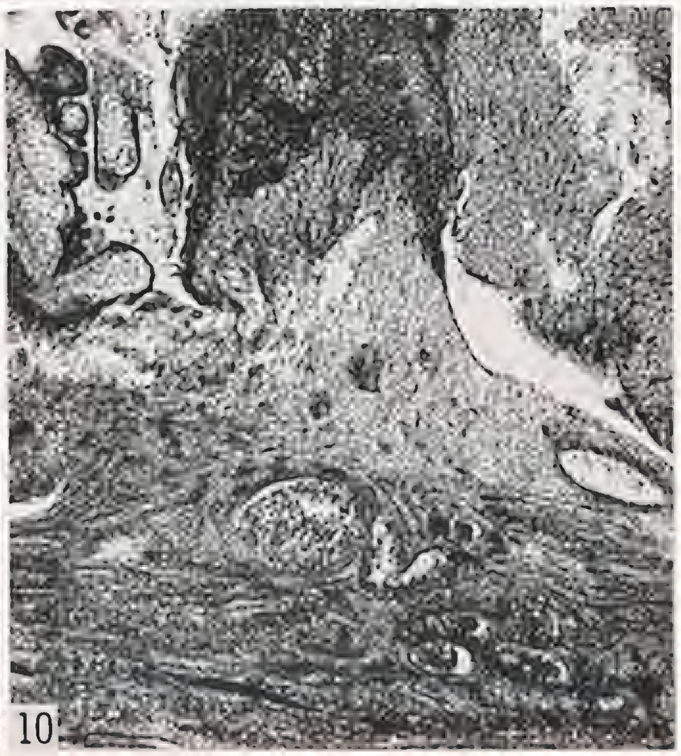

10

PLATE 3, Figs. 11–14

Fig. 11. Uteroplacental artery near the placental base showing disappearance of trophoblast from the vessel's lumen, but a prominent accumulation of similar cells replacing the media. Note the absence of trophoblastic invasion of the stroma either in connected strands or in isolated cells. India ink is present in the vessel's lumen. Monkey C-629, 53rd day of pregnancy; section 106; × 100.

Fig. 12. Uteroplacental artery close to the myoendometrial junction. Trophoblast-like cells have penetrated the wall. The endothelium is largely intact. Note trophoblastic invasion of the perivascular stroma. Human specimen 10118, 16th week of pregnancy; × 400.

Fig. 13. Section of a uteroplacental artery midway in its course through the endometrium. Fibrous connective tissue proliferation has become a prominent feature in many vessels at this stage. Here the process has caused marked narrowing of the lumen. Trophoblastic cells are present in the outer portion of the vessel wall together with small deposits of fibrin. Note, however, that there is no trophoblast outside the vessel wall. Monkey C-679, 102nd day of pregnancy; section B100; × 60.

Fig. 14. Cross sections through the stems and branch of a uteroplacental artery in which subendothelial fibrosis has markedly narrowed the lumen. There is widespread infiltration of the stroma by trophoblastic wandering cells. Human specimen 10118, 16th week of pregnancy; × 100.

Monkey

Human

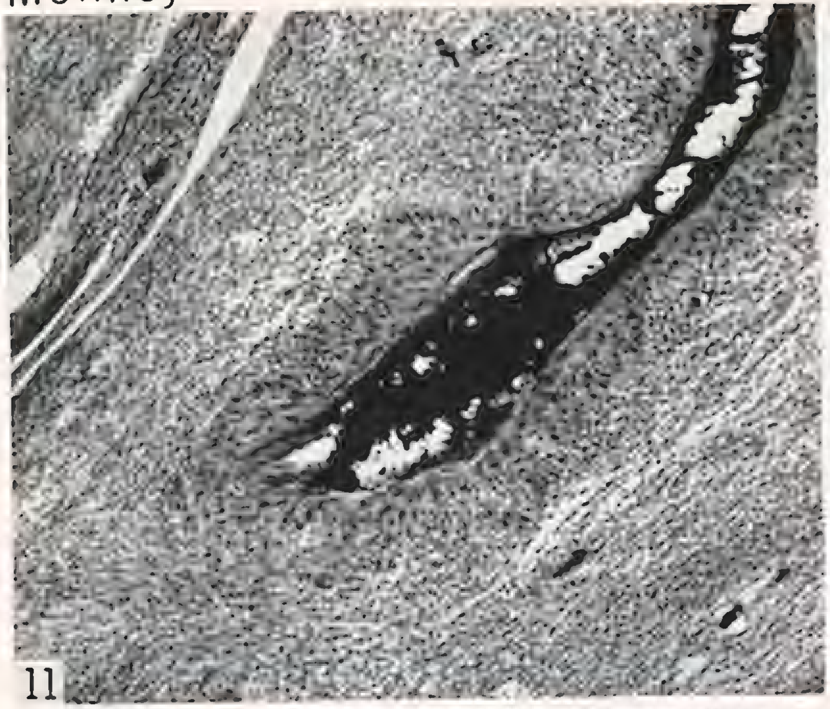

11

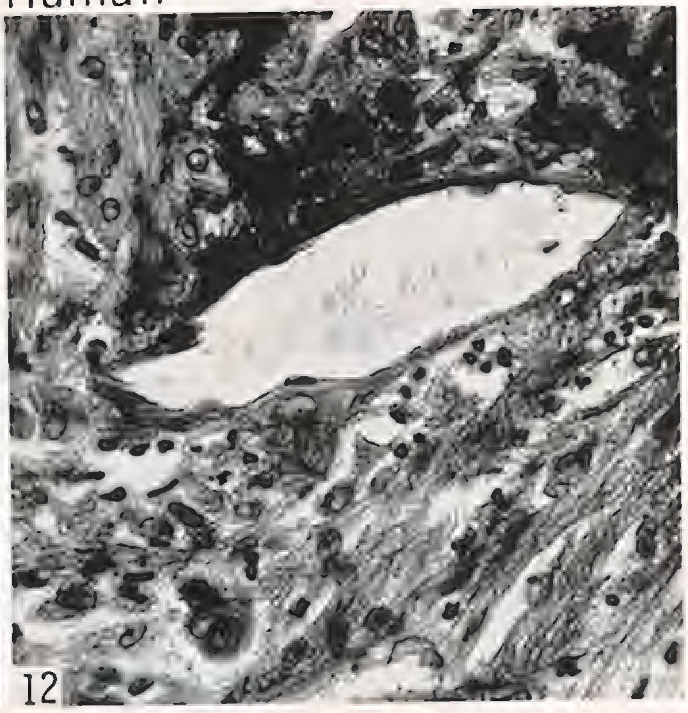

12

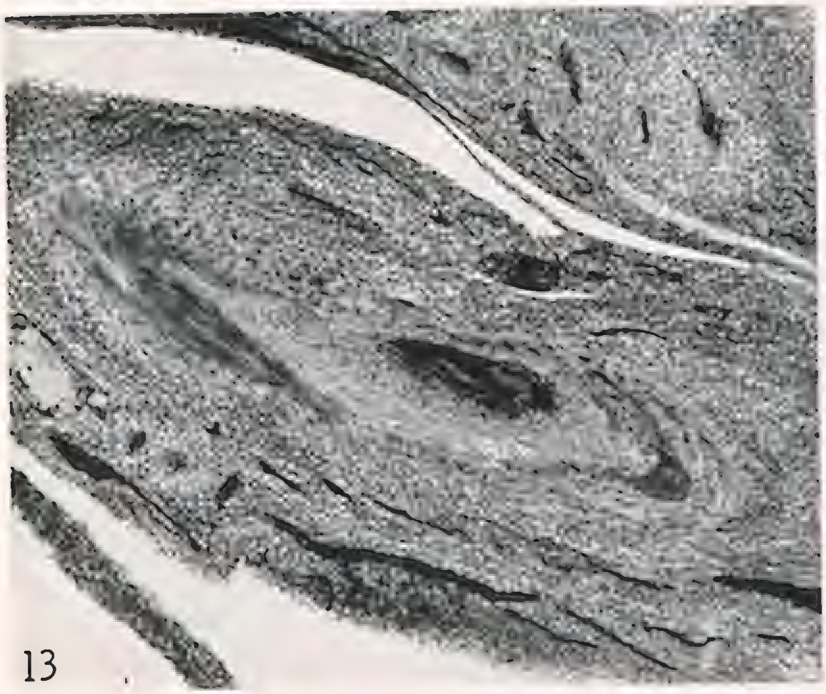

13

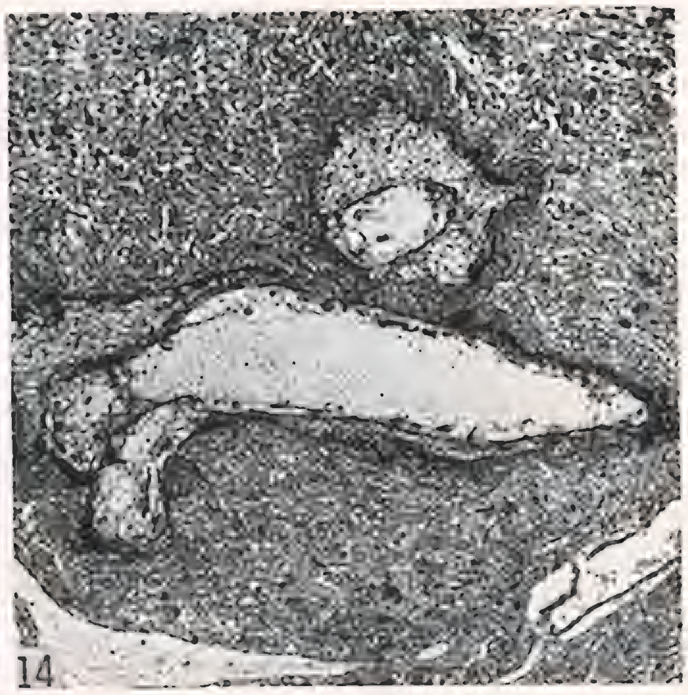

14

PLATE 4, Figs. 15, 16

Fig. 15. Diagrammatic representations of the course and configuration of the uteroplacental arteries in the rhesus monkey at various stages of pregnancy, based on three-dimensional models constructed from serial sections. The base of the placenta, myoendometrial junction, and peritoneal surface are artificially represented as smooth planes. The relative thickness of endometrium and myometrium is accurately portrayed.

Drawn by James F. Didusch for Ramsey (1949)

Monkey–Human Gestation Age Equivalents, weeks

Monkey:	3	6	8	15	19
Human:	5	10	13	25	32

Fig. 16. Diagrammatic representations of the course and configuration of human uteroplacental arteries at various stages of pregnancy, based on three-dimensional models constructed from serial sections. The base of the placenta and the myoendometrial junction, when shown, are realistically portrayed. These drawings do not include the myometrium, but the scale to one side indicates the relative thickness of the endometrium and the myometrium.

Drawn by Frank B. Price

Human–Monkey Gestation Age Equivalents, weeks

Human:	8	16	20	32	40 (term)
Monkey:	5	9	12	18	24

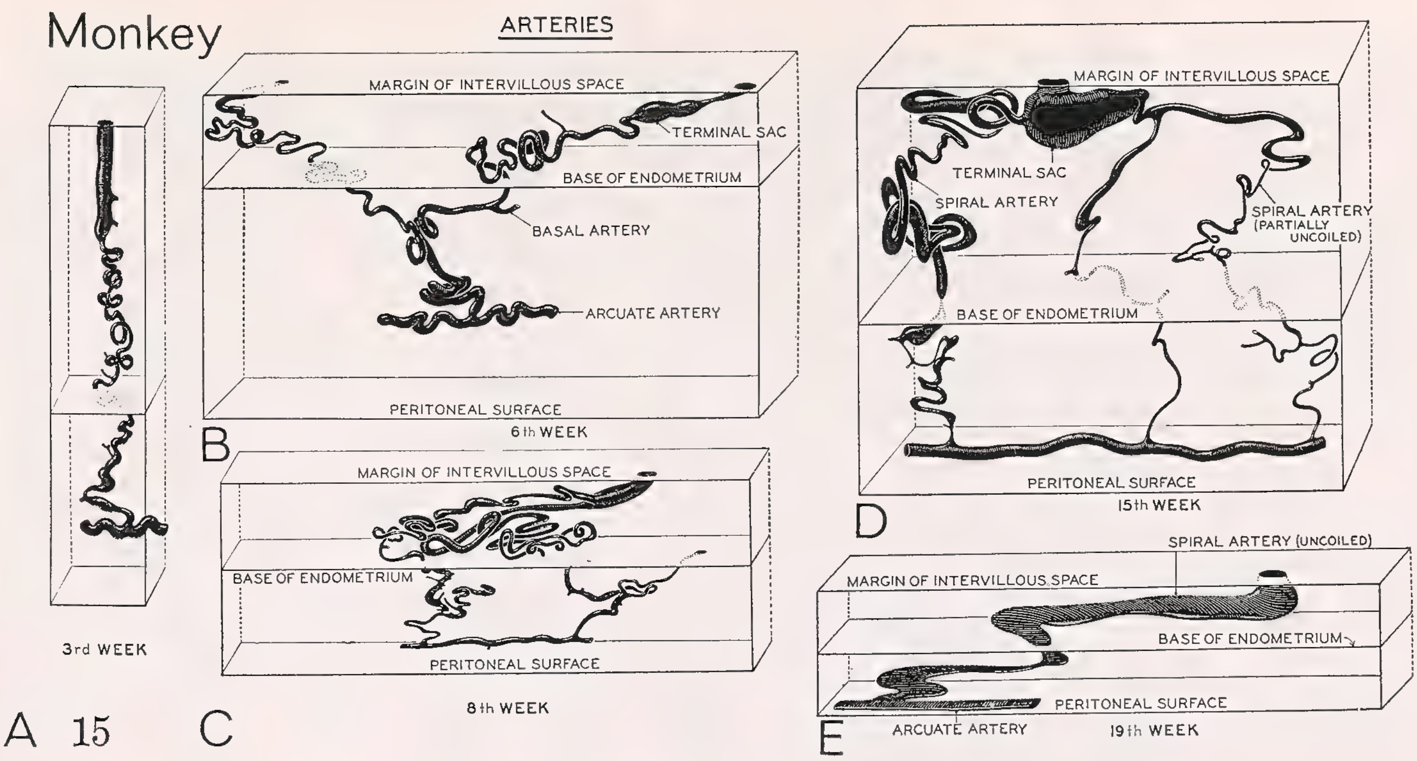

15

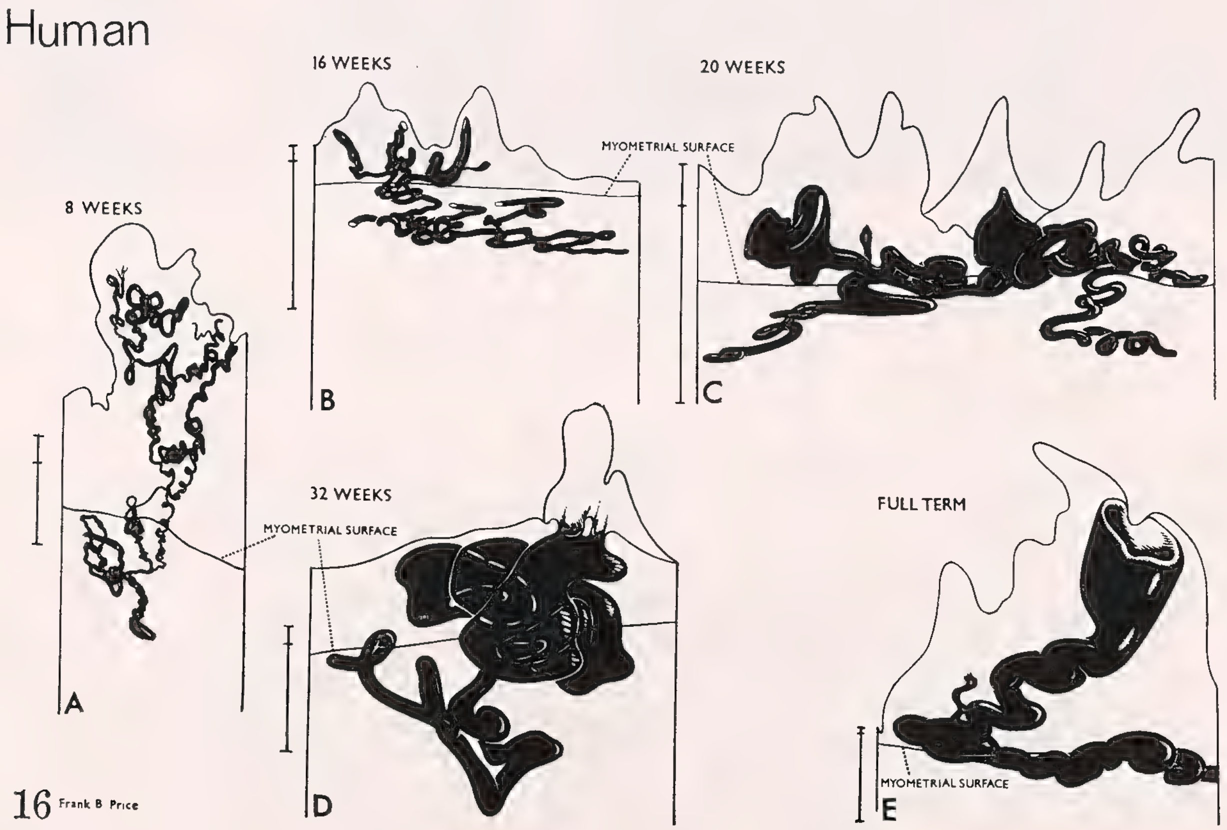

16 Frank B Price

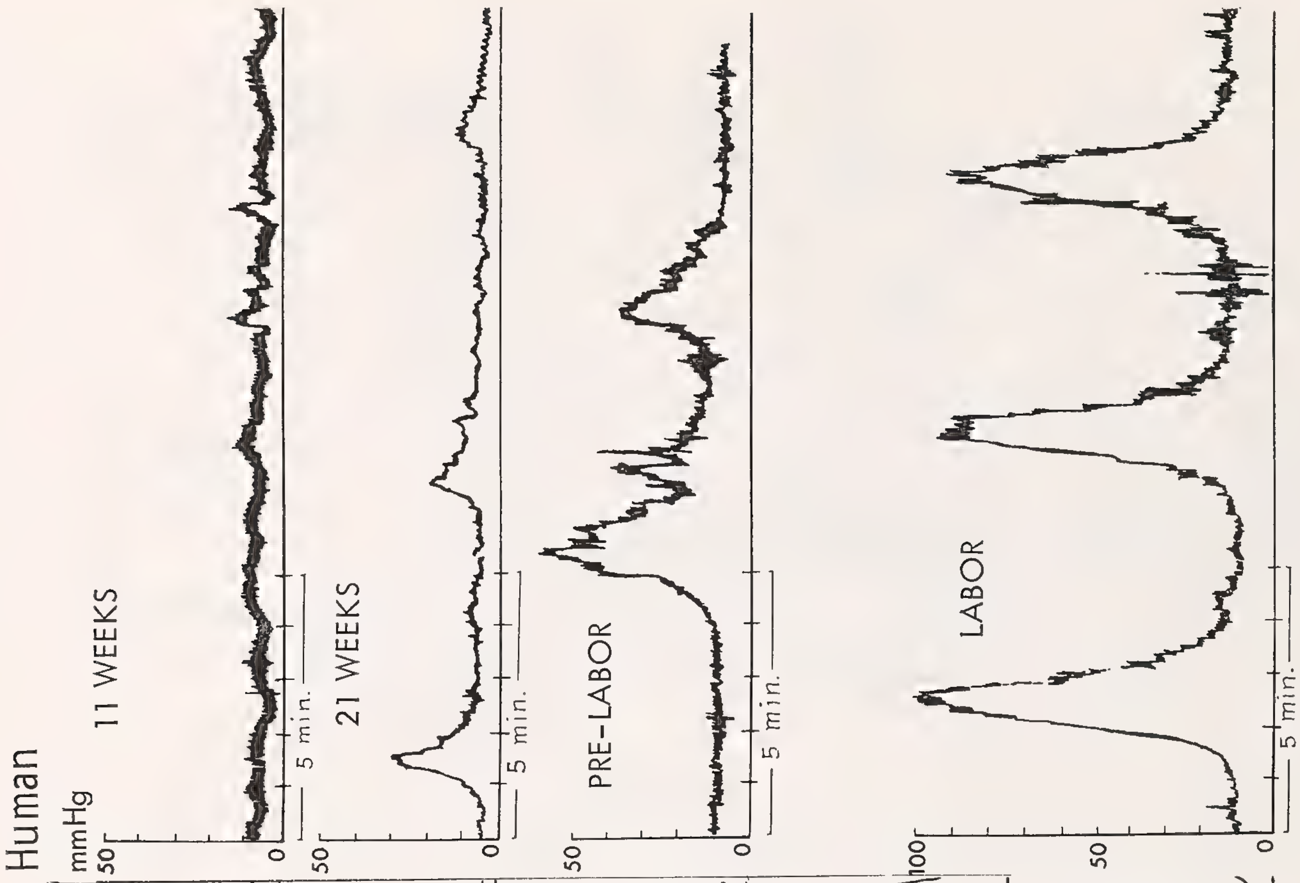
Human
mmHg
50
0
11 WEEKS
5 min.
50
0
21 WEEKS
5 min.
50
0
PRE-LABOR
5 min.
100
50
0
LABOR
5 min.

18

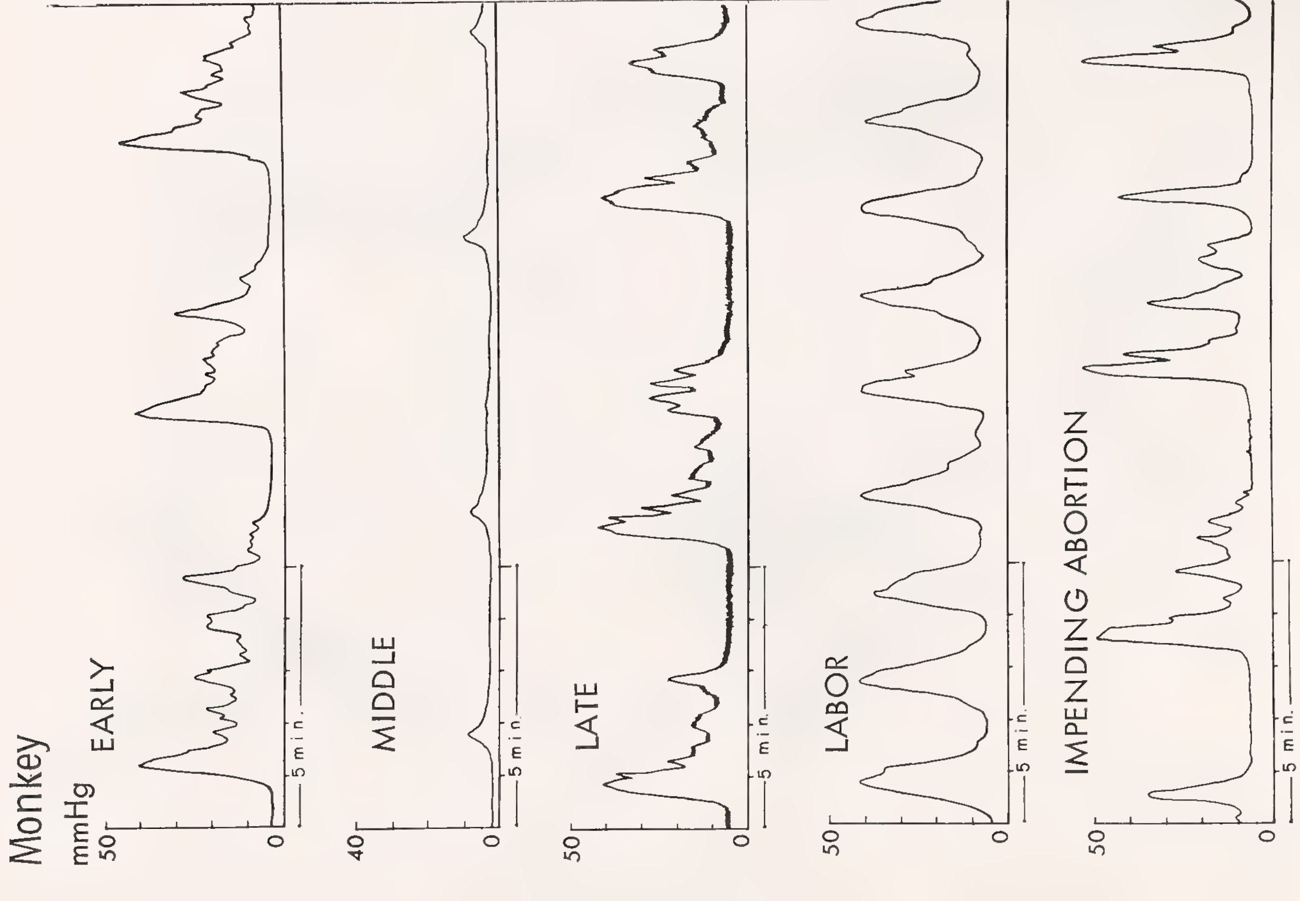
Monkey
mmHg
50
0
EARLY
5 min.
40
0
MIDDLE
5 min.
50
0
LATE
5 min.
50
0
LABOR
5 min.
50
0
IMPENDING ABORTION
5 min.

17

Monkey

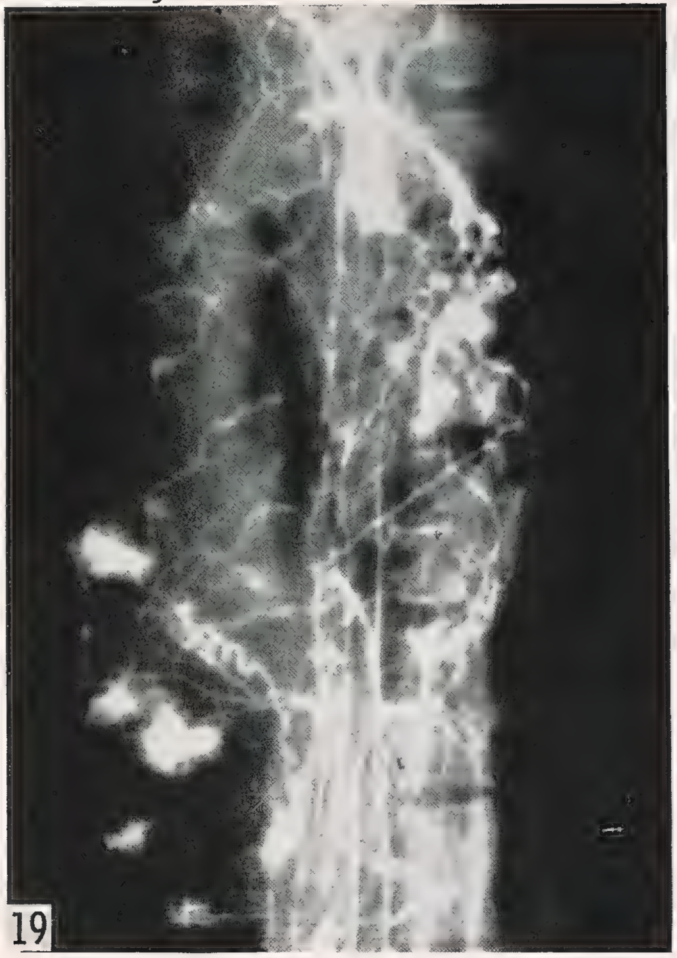

19

Human

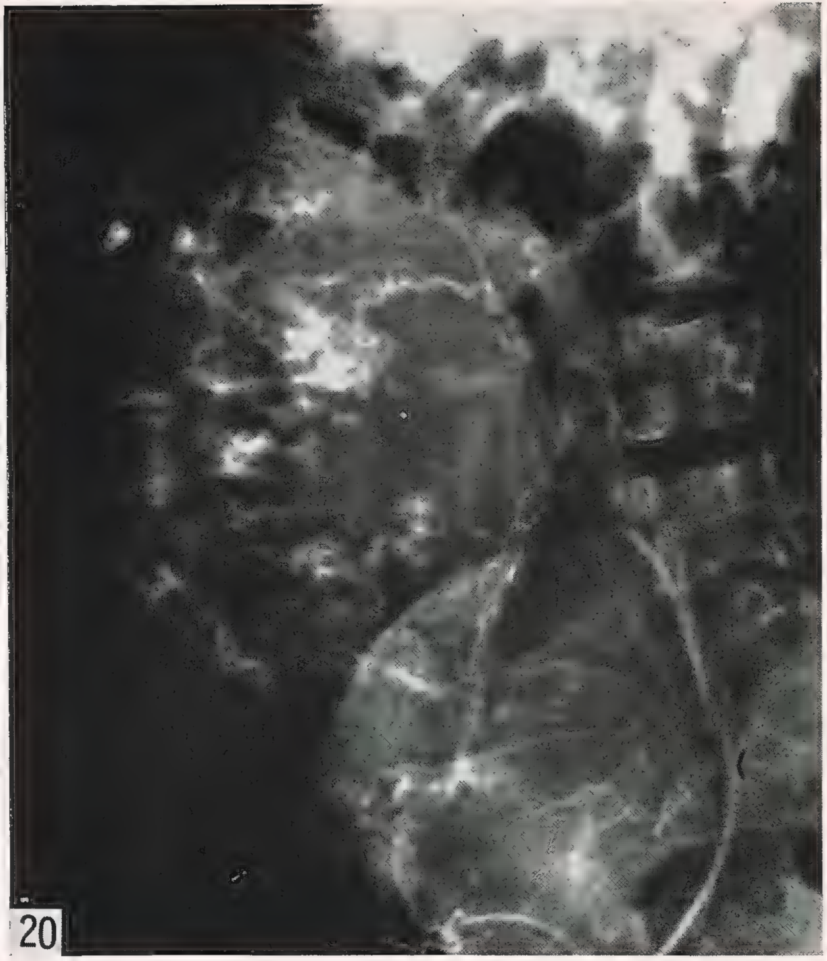

20

PLATE 5, Figs. 17–20

Fig. 17 (opposite). Representative recordings of intrauterine pressure in the monkey at three stages of pregnancy, in labor, and when abortion is imminent. Monkeys 16A at 66 days; L53 at 119 days; 6B at 153 days; 940 at 148 days; and 8A at 140 days.

From Corner, Ramsey, and Stran (1963)

Fig. 18 (opposite). Representative recordings of intrauterine pressure in three pregnant women at stages comparable to those of the first four monkey tracings shown in Fig. 17. The prelabor and labor recordings were made in the same patient with an interval of 6 hours between them.

Courtesy Dr. Charles H. Hendricks

Fig. 19. Radiograph made $4\frac{1}{2}$ seconds after injection of radiopaque dye into the femoral artery of a monkey on the 117th day of pregnancy. Dye fills the arteries of the uterine wall, including the endometrial arteries whose spiral course is apparent. Spurts of dye at the end of the arteries mark the entry of dye into the intervillous space. Monkey 1B, 117th day of pregnancy.

Fig. 20. Radiograph made in a human patient 32 weeks pregnant. Dye fills the uteroplacental vessel just as in the monkey (Fig. 19). Similar spurts of dye into the intervillous space are seen. Univ. of Virginia No. 372656, 32nd week of pregnancy.

Courtesy Dr. H. S. McGaughey, Jr.

PLATE 6, Figs. 21–24

Fig. 21. Radiograph made 10 seconds after injection of a radiopaque dye into the femoral artery of a monkey during relaxation. Spurts are seen in both placental discs. Monkey 980, 87th day of pregnancy.

Fig. 22. Radiograph made 10 seconds after injection of radiopaque dye into the femoral artery of the same monkey as in Fig. 21. This time the dye was injected during a uterine contraction, and no spurts into the intervillous space are seen. Monkey 980, 87th day of pregnancy.

Fig. 23. Lateral radiographs of the pregnant uterus made 6 seconds after injection of dye during uterine relaxation, with outline tracings identifying the various entries. In the first injection *A*, 15 entries appear; in the second injection *B*, 14; and in the third injection *C*, 13. Identification of 17 different arteries can be made: 12 appear in all the injections; 1 is seen twice; and 4 others appear only once. Monkey 64/65, 92nd day of pregnancy. BL = bladder; ED = extravasated dye.

From C. B. Martin, Jr., et al. (1964)

Fig. 24. Three selected frames from a cineradiograph made immediately after completion of a slow injection of radiopaque dye into the intervillous space. The first and third frames come from two successive periods of relaxation; the second frame, from a contraction that occurred between the two relaxations. Note the appearance and disappearance of the mural veins connecting the pool of dye in the intervillous space with the extrauterine drainage channels. The ovarian vein forms an arc on the right. Monkey 62/29, 99th day of pregnancy.

Monkey

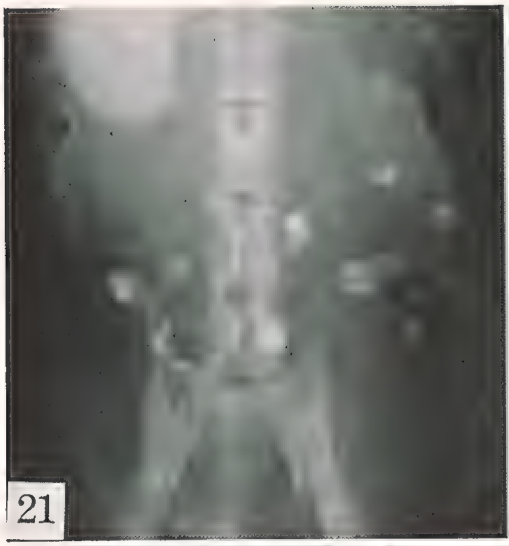

21

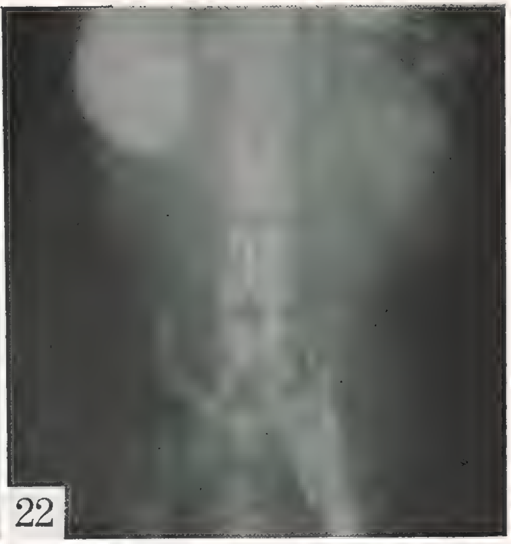

22

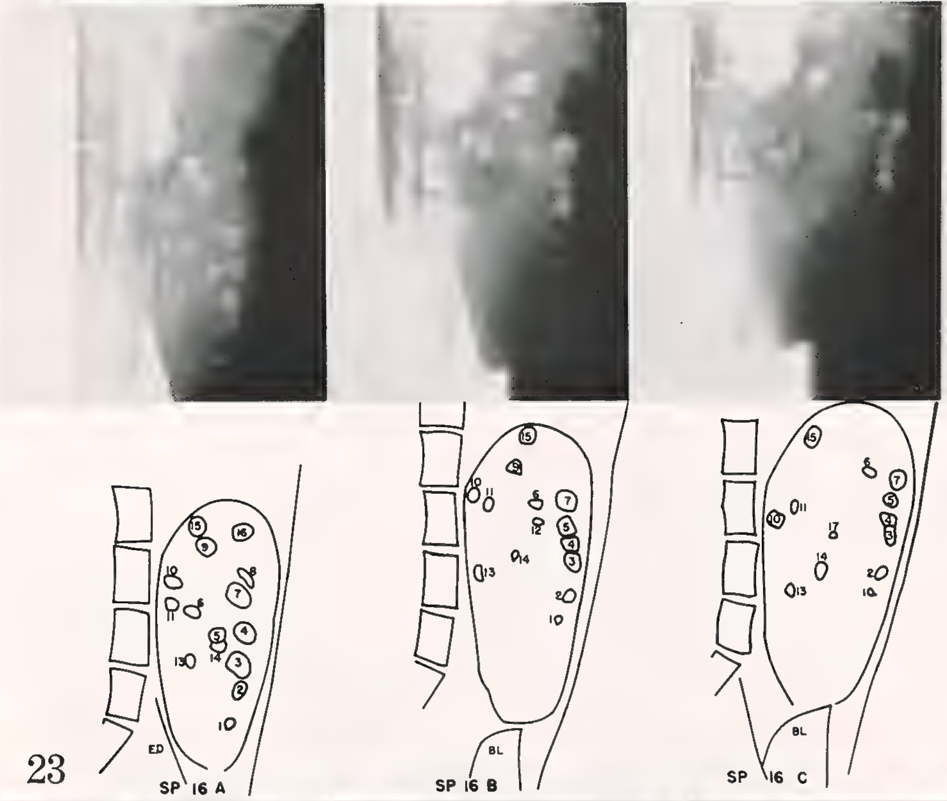

23

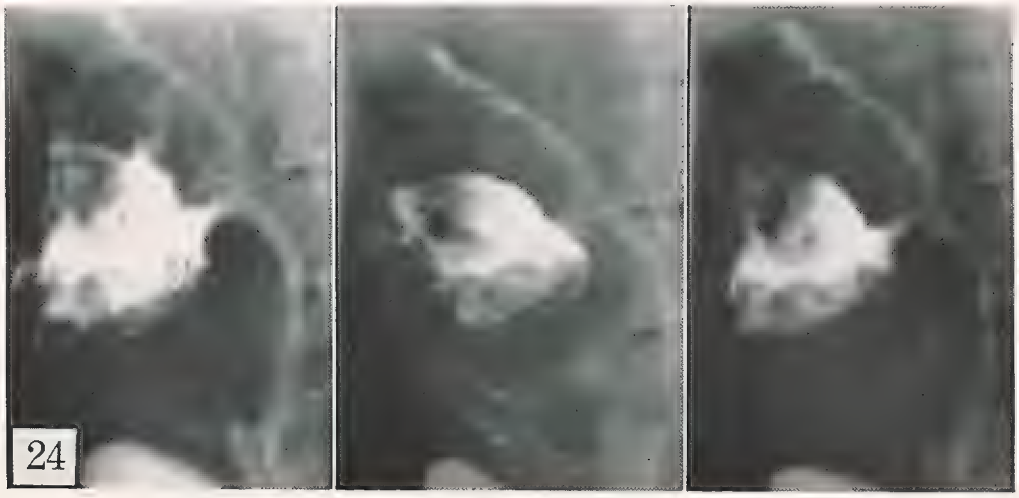

24

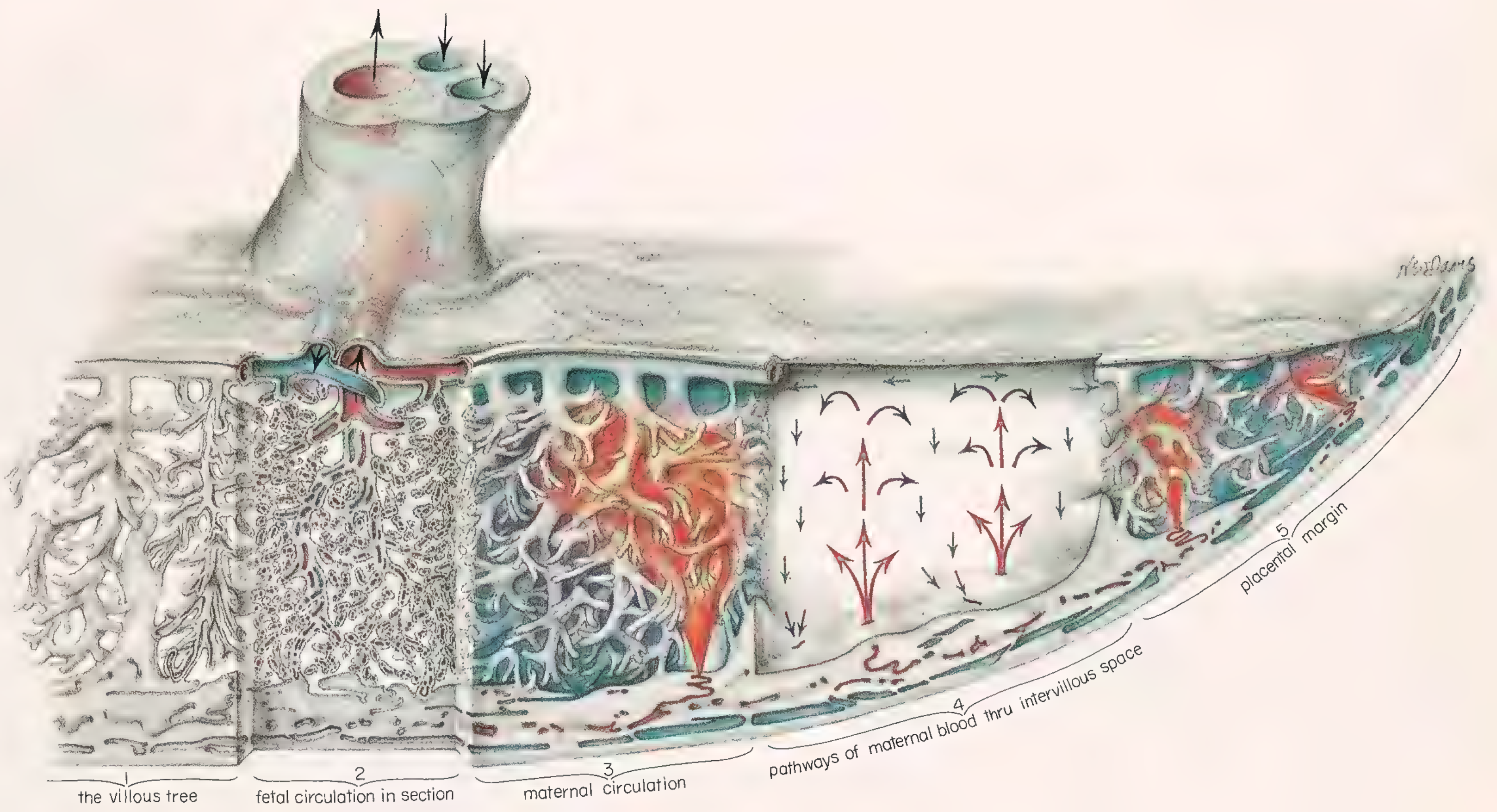
1
the villous tree
2
fetal circulation in section
3
maternal circulation
4
pathways of maternal blood thru intervillous space
5
placental margin

Fig. 25. Placenta, showing structure and circulation. The head of maternal blood pressure drives entering blood toward the chorionic plate in fountain-like streams ("spurts"). As the head of pressure is dissipated, lateral dispersion of blood occurs. Inflowing arterial blood pushes venous blood out into the endometrial veins.

Drawing by Ranice Davis Crosby; engraving by W. B. Saunders Co.

CONTRIBUTIONS TO EMBRYOLOGY, NO. 262

A RADIOAUTOGRAPHIC STUDY OF LABELED GRAFTS IN THE CHICK BLASTODERM

DEVELOPMENT FROM PRIMITIVE-STREAK STAGES TO STAGE 12

GLENN C. ROSENQUIST

Department of Embryology, Carnegie Institution of Washington,
Baltimore, Maryland

(With 12 plates and 19 figures)

CONTENTS

PAGE

METHODS 73
  Epiblast-Dorsal Streak Grafts 73
  Endoderm-Mesoderm Grafts 74
  Locating the Grafted Cells 74
  Classification of Grafts 75
  Labeling Effects 75

RESULTS 76
  Epiblast-Dorsal Streak Grafts 76
    Grafts Twenty-one Hours Before Stage 5 77
    Grafts Eighteen Hours Before Stage 5 79
    Grafts Fifteen Hours Before Stage 5 81
    Grafts Twelve Hours Before Stage 5 85
    Grafts Nine Hours Before Stage 5 86
    Grafts Six Hours Before Stage 5 88
    Grafts Three Hours Before Stage 5 90
    Grafts at Stage 5 91
  Endoderm-Mesoderm Grafts 92
    Movements of the Grafts 92
      Mesoderm Squares 92
      Endoderm Squares 95

DISCUSSION 99
  Organization of Blastoderm 100
      Epiblast at Stage 5 100
      Epiblast at Stage 3+ to 4 100
      Mesoderm at Primitive-Streak Stages 101
      Mesoderm at Head-Process Stages 102
      Endoderm at Primitive-Streak Stages 102
      Endoderm at Sage 5 104
  Movements of Cells 104
      Epiblast-Ectoderm Cells 104
      Mesoderm Cells 105
      Endoderm Cells 106
  Function and Organization of the Streak 106
SUMMARY 108

ACKNOWLEDGMENTS 109

LITERATURE CITED 109

A RADIOAUTOGRAPHIC STUDY OF LABELED GRAFTS IN THE CHICK BLASTODERM

The problems of how germ layers form within the pellucid area of the chick embryo at early primitive-streak stages—Hamburger-Hamilton (H-H) 3+ to 4—and how the areas of the blastoderm undergo the convolutions that lead to gastrulation and early morphogenesis have been favored subjects of investigation by embryologists for almost a century. Nonetheless, detailed information about these processes at a cellular level is surprisingly deficient, largely because of inadequacies of techniques.

Investigation has been primarily in two fields: determination of the fate of cells in the intact germ layers, and testing of the organ-forming capacities of blastodermal regions.

In the first field, in order to determine the fate of cells, small regions of the embryo were marked with vital dyes, particulate matter, or restricted cell damage, or the movement of cells was observed with time-lapse cinematography. By these methods, the following have been explored: formation of the germ layers and primitive streak (Wetzel, 1929; Pasteels, 1937; Spratt, 1946; Malan, 1953; Vakaet, 1962); localization of gut (Hunt, 1937*a;* Bellairs, 1953*a, b*); nervous tissue (Spratt, 1952; Pasteels, 1937); and heart (DeHaan, 1963*a*). However, because vital dyes readily diffuse from one cell or layer into another, a single layer of cells cannot be labeled; the marker is therefore not permanent. Since carbon or carmine particles are rarely engulfed by cells, it is not certain whether their movements will conform to those of the tissue onto or into which they have been placed. Wounds in the embryo of sufficient size to produce permanent marks seldom permit completely normal development of the tissues surrounding the wound. With time-lapse cinematography there is no histologic verification of either the cells or the layer(s) involved in the movements observed.

In the second field of investigation, organ-forming capacities of blastodermal regions at various stages were tested by transplanting fragments to suitable nutritive environments to permit differentiation of the explanted tissue in isolation. With this method, the following fields have been localized in the primitive-streak or head-process-stage blastoderm: nervous tissue (Hunt, 1932; Rawles, 1936); eye (Butler, 1935; Clarke, 1936); gut (Rudnick and Rawles, 1937); thyroid (Rudnick, 1932; Butler, 1935); heart (Rawles, 1936, 1943; DeHaan, 1963*a*); and other structures. However, the differentiation of small tissue explants gives, at best, only gross delineation of organ-forming regions, which, moreover, may be misleading. Groups of cells that form a given tissue when explanted from the embryo at an early stage may lose that potential in the intact embryo as a result of new tissue relationships brought about by morphogenetic movement.

Labeling specific cells of the embryo with a durable marker that is nontoxic and nondiffusible would obviate many of the difficulties mentioned. A step in that direction was taken when Abercrombie and Causey (1950) used radioisotopes for tracing morphogenetic movements in chick embryos. Using similar methods, but with the substantial advantages offered by H^3 (tritiated) thymidine as a label, Weston (1963) was able to trace the migration of neural crest cells by grafting blocks of labeled neural tube from one chick to another.

The present paper records a radioautographic study of epiblast or endoderm-mesoderm grafts labeled with tritiated thymidine as they participate in the normal development of chick embryos from primitive-streak stages to the stage of 16 somites (stages 3+ to 12, Hamburger and Hamilton, 1951).

METHODS

Fertile DeKalb eggs were incubated 10–22 hours and explanted, hypoblast side up, in watch glasses, according to the method of New (1955). Donor embryos were labeled by placing 1 μc (microcurie) of tritiated thymidine in 0.037 cc chick Ringer's saline solution on the hypoblast surface. The explanted embryos were then reincubated to the stage of the recipient embryos (1–5 hours), washed six times with 1–2 cc saline at room temperature, and blotted dry. Two types of grafts were made: those to the epiblast-dorsal streak layer and those to the endoderm-mesoderm layer.

Epiblast–Dorsal Streak Grafts

The endoderm-mesoderm layer and ventral streak were stripped from primitive-streak and head-process-stage donor embryos with tungsten needles; see Plate 1(a). Grafts were first cut from the underlying epiblast of right side or central regions; next transferred one by one to separate recipient embryos of visually similar stages—Plate 1(b)—whose endoderm-mesoderm layer had been dissected from the ectoderm and folded back but not removed—Plate 1(c); and finally fitted into the corresponding site of the recipient embryo from which the homologous epiblast fragment had been excised and discarded. The endoderm-mesoderm flap was then replaced; see Plate 1(d).

Because the donor blastoderm can have slightly different dimensions from those of the recipient, the grafts were placed according to their relation to the streak and the edges of the *area pellucida* rather than by measurement of their distance from any single landmark. Each graft position was identified as the percentage of an anatomical distance—for example, centered 35 per cent of the distance between the node and the caudal limits of the *area pellucida* and 50 per cent of the distance between the streak and the right *area pellucida* margin. Photographing each recipient embryo after grafting was helpful in checking these dimensions. Host embryos were then placed in covered Petri dishes and reincubated at 37.8°C in sealed cans containing room air without regulation of humidity. Dissection of the endoderm-mesoderm flap delayed development slightly, but in 1–1½ hours of reincubation the flap had reexpanded to its original size and met the edges of the *area opaca;* see Plate 1(e) and Plate 2(a). Graft sites were occasionally visible for 2–4 additional hours. In this event, imperfect healing was suspected—Plate 2(b), (c)—and was also suggested by the discovery of labeled cells in peripheral *area vasculosa* on the right side, which were always separated from the main distribution and showed no evidence of ever having reached the streak. Their distribution always gave the effect of their having separated from a poorly healed corner of the epiblast graft and migrated into mesoderm. Such cases are noted in the descriptions of individual grafts beginning on p. 77. In preparing the summarizing maps, shown in Figs. 1(d–k) and 7, such doubtful marks have been neglected. The pre-endoderm-premesoderm zones have been reconstructed exclusively either from grafts placed in the dorsal primitive streak (which automatically moved to bilateral endoderm-mesoderm) or from unilateral grafts contributing to both right and left endoderm-mesoderm.

Endoderm–Mesoderm Grafts

The hypoblast surface of stage 5 donor embryos was flooded with a thin layer of chick Ringer's saline, after which the endoderm-mesoderm layer of the right side was subdivided with a tungsten needle into a grid of 25 squares; see Plate 3(a); the grid is also shown in Fig. 1(a). Each square was dissected from the underlying ectoderm, floated free of the donor bed, and transferred with a capillary pipette to the surface of a recipient embryo, where the homologous square was removed and the donor piece fitted in; see Plate 3(b). Squares adjacent to the *area pellucida* margin were usually cut to include a small piece of *area opaca* endoderm and mesoderm. This not only increased the size of the grafts and made them easier to orient in the recipient position but hastened their healing time, as grafts wedged into a yolky bed were less likely to float away. Grafts containing mesoderm as well as endoderm attached to the recipient bed more readily than those containing only endoderm. For example, squares 1, 2, and occasionally 3 (from which mesoderm is typically absent) contract into folds with reincubation and fail to expand into the recipient bed. Removing all sub-blastodermal fluid to make the edges of the graft lie flat on the bed and chilling the preparation reduced this tendency but did not completely resolve the problem. After being photographed, the embryos were reincubated at 37.8°C in closed Petri dishes in airtight containers of either room air or a mixture of 40 per cent oxygen, 5 per cent carbon dioxide, and 55 per cent nitrogen. Since the cans were not continuously gassed, humidity was not regulated. Within an hour of reincubation, the donor square had spread on its recipient bed to meet the edges of the host tissue. In two hours or less, the grafts had healed completely; see Plate 3(c).

After incubation to the desired stage (stages 5–12 for epiblast-dorsal streak grafts, stages 6–12 for endoderm-mesoderm grafts; *cf.* Table 1), all host embryos were again photographed. They were then fixed in 10 per cent neutral formol in chick Ringer's solution, and trimmed, embedded in paraffin, and sectioned. The 10-μ sections were coated with Kodak NTB-2 emulsion according to the methods of Messier and LeBlond (1957); the sections were developed, fixed after 5–18 days of exposure, and stained through the emulsion with hematoxylin and eosin, or nuclear fast red and picric acid.

Locating the Grafted Cells

Distribution of the labeled cells in the recipient embryos was determined by recording the location of the labeled cells for each section, transferring the information to a scale drawing of each embryo, and comparing the drawings or reconstructions of embryos fixed at various stages with the graft location. The morphogenetic movements of the various areas or squares could then be determined.

In the reconstruction of grafted embryos, the following landmarks were particularly useful: (1) *Area pellucida–area opaca* boundary, determined as the transition from a coherent endoderm layer containing a minimum of yolk particles to a layer where thick yellow yolk was present with its large endoderm nuclei; this boundary is characterized by fluctuations and inconsistencies in both photographs and sections. (2) First section of foregut. (3) First and last sections of oral plate. (4) Appearance of single heart tube. (5) Anterior intestinal portal (AIP). (6) First and last somites. (7) Cephalic end of streak; since primitive groove and Hensen's node are not applicable as landmarks of the cephalic end of the streak after stages 7–8, the cephalic end of the streak was located in embryos of stages 8–12 as the section where the bulb of the notochord first wedges apart the dorsal epiblast layer, partially dividing right from left preneural tube cells. In this paper the section will be termed the bulb-wedge (BW) level.

Classification of Grafts

The 208 epiblast-dorsal streak grafts were divided into eight groups depending upon their stage at the time of operation (Table 1). For the New explanted embryo, reliance upon dimensions alone (length of primitive streak or ratio of streak length to total *area pellucida* length) is not satisfactory, because dimensions vary with the amount of tension placed on the embryo as the vitelline membrane is stretched over the glass ring. Therefore, primitive-streak embryos were staged according to their temporal relationship to stage 5. In this study, stage 5 was defined as a stage in which the head process extends one fourth to one third the distance between the node and the cephalic end of the *area pellucida;* see Plate 3(a), (b), and Fig. 1(h). This stage has the advantage of lasting normally no more than one hour of incubation, and it was easier to recognize at a glance than the definitive primitive-streak stage, which precedes it. The youngest embryos operated upon required 15–25 hours of reincubation to reach stage 5, and they are considered equivalent to H-H stage 3+ in general appearance (length and width of primitive streak and size of *area pellucida*). Those that required 3–15 hours span stage 4.

Time after stage 5 was calculated in the following way: stages 5–7, approximately seven hours; addition of somites, approximately one hour per somite. Time spent in the various stages was calculated from actual observations of some embryos, and retrospective calculations were made for others. As an example of the retrospective calculations, an embryo grafted at primitive-streak stages but fixed eighteen hours later at the 6-somite stage would retrospectively be classified as operated upon six hours before stage 5, as it required five hours of reincubation to add 5 somites, seven hours between stages 5 and 7, and six hours between stages 4 and 5. These incubation times differ from H-H staging (*in ovo,* 1951) and even from Vakaet's staging (in vitro, New technique, 1962). Some of this delay may be due to the insult of grafting, but similarly incubated control embryos were also retarded in their development. However, their morphogenesis was normal, and many of the embryos that were reincubated to stage 12 developed extraembryonic circulation.

The 175 endoderm-mesoderm grafts were divided into seven groups, the classification depending upon the stage fixed. Each embryo carried one of the 25 squares of the grid. The first group of 25 embryos was fixed at stage 6, three to five hours after grafting, the next group at stage 7, and so on; thus all the grafted embryos were fixed between stages 6 and 12 (Table 1).

Labeling Effects

Though 90–100 per cent of the cells could be labeled if the donor had been exposed to tritiated thymidine for 8–10 hours—Plate 12(f, g)—for practi-

Table 1. Classification of Grafts

	Type of Graft									
Stage	Epiblast-Dorsal Streak									Endoderm-Mesoderm
	Number of hours before stage 5									
At grafting	21+	18	15	12	9	6	3	0	...	...
	Number of embryos								Total	
At fixation										
5	0	0	0	0	2	2	2	0	6	...
6	0	0	1	4	3	1	5	3	17	25
7	1	0	0	0	3	0	0	0	4	25
8	0	2	3	7	6	11	1	4	34	25
9	1	0	5	8	15	14	9	5	57	25
10	2	1	2	10	13	6	7	5	46	25
11	1	3	0	2	8	7	6	3	30	25
12	0	0	1	10	1	0	1	1	14	25
Total Embryos	5	6	12	41	51	41	31	21	208	175

cal purposes most of the donor embryos were pulsed for 1–5 hours, which labeled 50–70 per cent of the cells. This ratio was observed as long as the graft remained in the epiblast; see Plate 2(a), (b). But once the labeled cells from the graft mix at the streak during invagination with the unlabeled cells from the host, the percentage falls; see estimated percentage of labeling in Results. After the cells reach the endoderm-mesoderm layer, there is little if any mixing of labeled cells from the graft with unlabeled cells from the hosts, at least between stages 5 and 12 (see Rosenquist and DeHaan, 1966, their Table 2). The photomicrographs of Plate 2, and Plates 4–12 illustrate how the cells retain their label up to 40 hours after grafting. However, because of the dilution of the label among the descendants of the grafted cells, a graft reincubated for 40 hours required a longer exposure to the emulsion to obtain satisfactory radioautographs.

Table 2 summarizes the results of a control study that showed that not only were labeled embryos indistinguishable from unlabeled embryos in size and configuration but that the number of cell divisions was not diminished in the presence of the beta radiation of the 1 μc tritiated thymidine, nor was there selective disappearance of any particular cell type. Fifteen New explanted unlabeled control embryos and 15 embryos labeled by applying 1μc tritiated thymidine in 0.037 cc chick Ringer's saline were washed six times with Ringer's saline at stage 5 (described on p. 73); they were reincubated to stages 10, 11, and 12, fixed, photographed, and then sectioned. The 15 labeled embryos were indistinguishable from matched unlabeled embryos in size and general configuration. Average endoderm, mesoderm, and ectoderm populations of labeled vs. unlabeled embryos were compared in 10-μ sections taken at three levels of the embryo by counting the number of nuclei in three successive sections of each level: (1) through head at tip of foregut—total head mesoderm, ectoderm (epithelium); (2) through trunk at a level three fourths the length of gut caudal to the tip of the foregut—mesoderm (myocardium), endoderm (gut); (3) 60 sections caudal to the AIP—mesoderm (homologous right or left somite), ectoderm (neural tube). Each entry in Table 2 represents the average number of nuclei counted in a given area of three successive sections of five embryos. The labeling percentage of labeled embryos was comparable to that reported for grafted squares (see above), varying between 50 and 100 per cent.

TABLE 2. GROWTH RATES OF TRITIATED THYMIDINE-LABELED VERSUS UNLABELED CONTROL CHICK EMBRYOS
(Nuclei per section)*

	10-Somite Stage†		13-Somite Stage†		16-Somite Stage†	
Population	Labeled‡	Unlabeled (Control)	Labeled‡	Unlabeled (Control)	Labeled‡	Unlabeled (Control)
Mesoderm						
Head	246	171	495	427	782	794
Myocardium	139	119	181	185	226	252
Somite	97	94	86	87	130	128
Endoderm						
Gut	161	111	165	183	204	202
Ectoderm						
Head	306	244	307	290	351	380
Trunk	82	97	67	69	78	90

* Each entry represents average number of nuclei counted in 3 successive sections in homologous areas and levels of five embryos.

† At fixation. Five labeled and five unlabeled embryos were fixed.

‡ 1 μc H^3 (tritiated) thymidine was applied for 1–5 hours.

RESULTS

The epiblast-dorsal streak and the endoderm-mesoderm grafts were placed in different layers of the blastoderm and will therefore be reported separately.

EPIBLAST–DORSAL STREAK GRAFTS

The grafts to be described in this section are the 208 tissue squares placed in the epiblast of stage 3+ to 5 embryos. These are discussed according to stage of operation; see Table 1. After study it was seen that the epiblast at each of these stages could be divided into eight zones or areas, whose general locations are shown in the drawing of epiblast in Fig. 1(a), and in the cross-sectional drawings of reincubated embryos in Fig. 1(b), (c). In this study the prefix "pre" is applied to cells of the zones that will invaginate (*E, F, G,* and *H*) and to the zones that remain in the ectoderm (*A*, *B*, *C*, and *D*) until they reach their final destination. The changes in the size and shape of these zones, which parallel growth of *area pellucida* and changes in streak length (Figs. 1 (d–k), 2–5, and 7), are due to morphogenetic movements. The preectoderm cells remain in the dorsal layer, but the preendoderm, premesoderm and prenotochord cells move into the endoderm-mesoderm layer where they form the endoderm and mesoderm portions of the embryo.

Grafts Twenty-one Hours Before Stage 5

At 21 hours before stage 5, the blastoderm looks like that described at stage 3+ (Hamburger and Hamilton, 1951). There is a well-formed rod-shaped streak. The distance from the node to the cephalic end of the *area pellucida* is between two thirds and one streak length; see Fig. 1(d). The following observations may be made:

1. Though often tremendously elongated, the grafts retain their identities as single areas with sharp outlines. Unlabeled host cells do not invade the graft at its boundaries. See case reports below.

2. A graft to cephalolateral epiblast contributes to both epidermis and neural tube—case report below; Figs. 1(d) and 2.

3. Presomite mesoderm derives from a graft to the cephalic end of the streak, and *area vasculosa* mesoderm from a graft to the caudal end of the streak—case report below; Figs. 1(d) and 2.

4. None of the cells from grafts placed in the streak and its environs remain in the streak. Migration is ventral, then in ventral layers from the streak in all directions. The most prominent movement is cephalolateral—case report below; Figs. 1(d) and 2.

5. Perhaps the most striking observation was that two grafts placed in the streak were later found completely or partly in endoderm. The preendoderm zone, though poorly outlined, is at least one graft in width, and probably two thirds the streak in length; see Fig. 1(d).

6. The zones represented (*B*, *C*, *E*, *F*, *G*, and *H*) agree with the zone arrangement in Fig. 1(a). This suggests that the blastoderm at stage 3+ is subdivided like the blastoderm at stages 4 and 5 but on a smaller scale.

Graft to zones B and C—Fig. 1(d); labeling time,

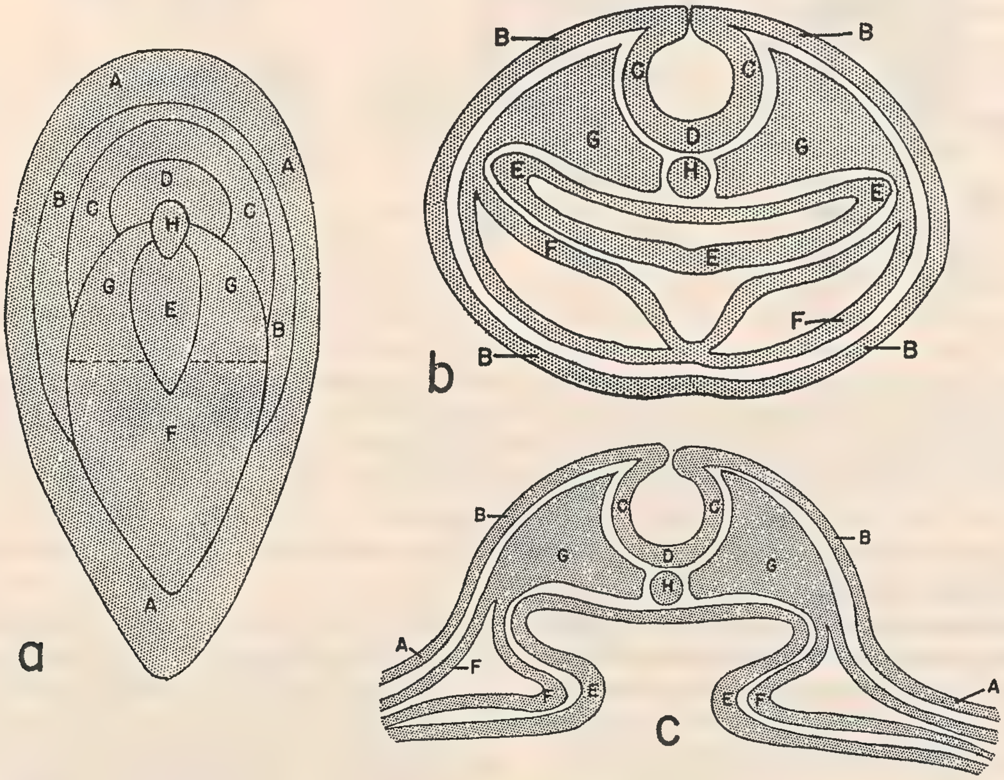

Artwork by Judith Baer.

Fig. 1(a–c). The epiblast-dorsal streak zones at stages 3+ to 5. (a) Ventral view of the dorsal surface of a typical stage 3+ to 5 blastoderm upon which are superimposed the following eight zones: *A*, preextraembryonic ectoderm; *B*, preepidermal ecotoderm; *C*, predorsal neural tube ectoderm; *D*, preventral neural tube ectoderm; *E*, preendoderm; *F*, prelateral plate mesoderm; *G*, preparaxial mesoderm; and *H*, prenotochord.

After 17 hours of reincubation, these eight zones have moved to their definitive positions as shown in a cross section (b) through the head and (c) just caudal to the AIP. AIP = anterior intestinal portal.

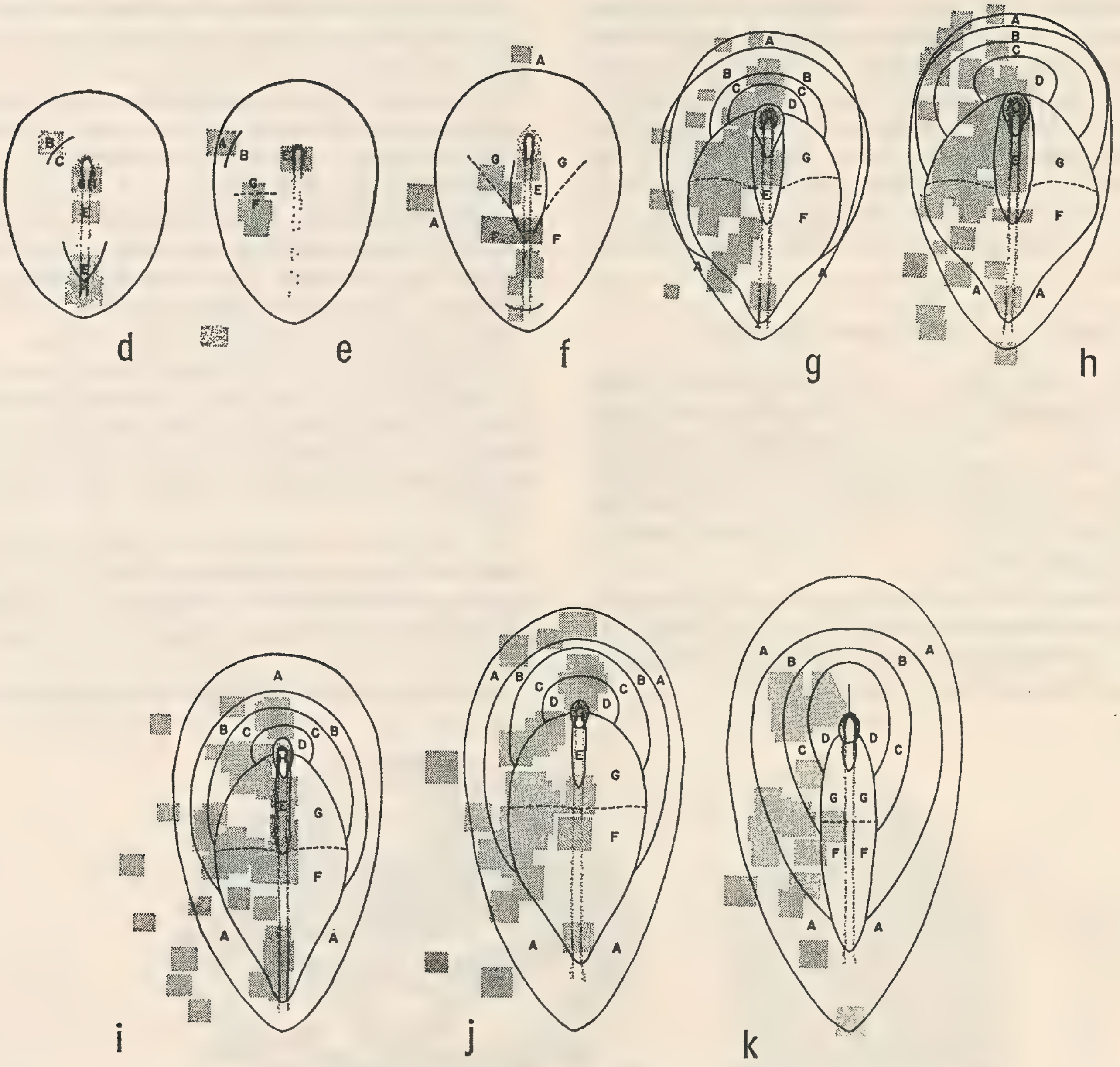

Fig. 1(d–k). The eight zones were found in most of the stages studied (H-H stages 3+ to 5), and resulted from the reconstructions of the 208 grafts placed at the following stages, determined as the number of hours' reincubation required to reach stage 5 (see Table 1, and text, p. 73): (d) 21 hours, 5 grafts; (e) 18 hours, 6 grafts; (f) 15 hours, 12 grafts; (g) 12 hours, 41 grafts; (h) 9 hours, 51 grafts; (i) 6 hours, 41 grafts; (j) 3 hours, 31 grafts; and (k) 0 hours or stage 5, 21 grafts.

2½ hours; estimated labeling 41 hours later, 50–70 per cent. When the recipient embryo was fixed at the 12-somite stage, labeled cells from this graft were distributed to an elongated oval area of epidermal ectoderm on the dorsal surface of the head fold and in adjacent dorsal neural tube at the approximate level of the AIP (areas labeled 1 in Fig. 2). Labeled cells from the medial half of the graft moved medially as the neural tube folded, while the lateral half moved cephalad in relation to the medial half.

Graft to region of Hensen's node—Labeled *GH* in Fig. 1(d); labeling time, 3 hours; estimated labeling 40 hours later: notochord, 5 per cent; mesoderm, 5–10 per cent. When fixed at the 11-somite stage, cells from this graft were distributed to the notochord beginning at a level 18 sections cephalic to the AIP and extending caudally into the bulb at the cephalic end of the streak, and to the medial half of the first to the tenth somites on the right side (Fig. 2, area 2). Labeled cells therefore moved ventrally into notochord and mesoderm and cephalically in relation to Hensen's node, some retaining contact with Hensen's node at the bulb.

Graft to cephalic end of zone E—Fig. 1(d); labeling time, 3 hours; estimated labeling 40 hours later,

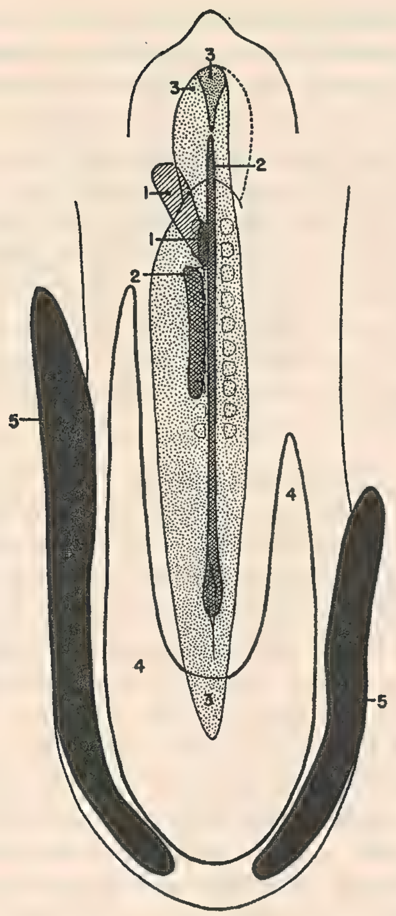

Fig. 2. Distribution of labeled cells in five stage 3+ recipient embryos 21 hours before stage 5 (ventral view), reincubated to foregut stages. Numbers refer to text descriptions (pp. 77–79). Location of grafts shown in Fig. 1(d).

20–40 per cent. At the 6-somite stage, cells from this graft were distributed to the midline ventral gut, and to the dorsal gut (mostly to the right side), its continuation into yolk-sac endoderm extending laterally halfway to the *area pellucida* margin and caudally to a level 83 sections caudal to the BW level. The labeled area ends at the midline of the streak (Fig. 2, area 3). Labeled cells from this graft moved ventrally and cephalolaterally into endoderm. At stage 6, the cephalic portion of the labeled endoderm was folded ventrally into the midline ventral gut.

Graft to caudal end of zone E—Fig. 1(d); labeling time, 3 hours; estimated labeling 40 hours later, 30 per cent. At the 10-somite stage, labeled cells from this graft were distributed to two lateral columns of *area pellucida* endoderm, beginning at the level of the AIP, which converge to the midline 45 sections below the BW level; to the medial half of endoderm from the level of convergence caudally to a level 15 sections from the caudal end of the *area pellucida* (Fig. 2, area 4); and to the right *area vasculosa* mesoderm in a very limited area at a level where the head begins. The graft is shown in Fig. 1(d) as located mostly in zone *E* but with a corner straddling prelateral plate mesoderm in zone *F*. Labeled preendoderm cells from this graft therefore moved ventrally, laterocephalically, and laterocaudally. Labeled premesoderm moved cephalically and slightly to the right. It is not certain whether premesoderm went to the midline streak before descending to the ventral layers.

Graft to midline caudal streak, zone F—Fig. 1(d); labeling time, 3 hours; estimated labeling 40 hours later, 10–20 per cent. At stage 7—, labeled cells from this graft were distributed to two oval areas in right and left lateral plate mesoderm (Fig. 2, areas 5). The most cephalic tip of the right oval extended into the *area vasculosa* of the *area opaca,* while the caudal ends of both right and left ovals approached the medial *area pellucida* but did not meet. Labeled cells from this graft therefore moved ventrally and laterocephalically away from the dorsal streak.

Grafts Eighteen Hours Before Stage 5

At 18 hours before stage 5, the difference between this and the previous stage is one of increase in blastoderm size and streak length. However, for the purposes of this study, the distinction made between this stage and the previous one (also H-H stage 3+) is based on the amount of reincubation necessary to reach stage 5 rather than on the change in dimensions. The locations of the six grafts to this stage are illustrated in Fig. 1(e). With one exception they are different areas of the epiblast from those of the five grafts placed at the previous stage. The distribution of five of the six grafts in the definitive embryo is seen in Fig. 3. The following observations may be made:

1. A graft to the boundary of the *area pellucida* or in the *area opaca* contributes cells to extraembryonic ectoderm. There is no evidence that this peripheral region of epiblast moves to the streak.
2. Grafts to the *area pellucida* epiblast lateral to the streak contribute cells to both right and left mesoderm. The method of crossover is not indicated.
3. One of the grafts mentioned in (2) contributed cells to both paraxial and lateral plate mesoderm, while the others (placed slightly caudal to the first) contributed cells to lateral plate mesoderm only. This suggests that the premesoderm is already spatially organized; see Fig. 1(e), *G* and *F*.

Grafts to zones A and B—Fig. 1(e); labeling time, $3\frac{1}{2}$ hours; estimated labeling 41 hours later, 50–60 per cent. At the 10-somite stage, cells from this graft were distributed to extraembryonic ectoderm at the edge of the *area pellucida,* beginning 67 sections cephalad to the head and extending caudally in an elongated oval 154 sections in length. At a level 16 sections caudal to the AIP, the ectoderm ended at the neural tube boundary. The graft was not involved in the head fold (Fig. 3, area 1).

Graft to zone E—Fig. 1(e); labeling time, 3 hours; estimated labeling 28 hours later, 30 per cent. At the 3-somite stage, labeled cells from this graft were distributed to the median *area pellucida* endoderm and to the midline ventral and dorsal gut. The first group of labeled cells moved to the endoderm, beginning at a level halfway between the cephalic limit of the *area pellucida* and the top of the head and extending caudally to the AIP, where the endoderm divided into two columns; the columns extended caudally over the yolk sac lateral to the somites, ending on the right side near Hensen's node at a spot two thirds the distance to the *area pellucida* margin, and on the left side at approximately the third somite. The cells that migrated to the midline ventral and dorsal gut became a continuation of yolk-sac endoderm folded into the AIP (Fig. 3, areas 2). Labeled cells therefore moved ventrally and cephalolaterally into an arch-shaped region of endoderm. At stage 6, the apex of the arch was folded ventrally, internalizing labeled cells to ventral and dorsal gut.

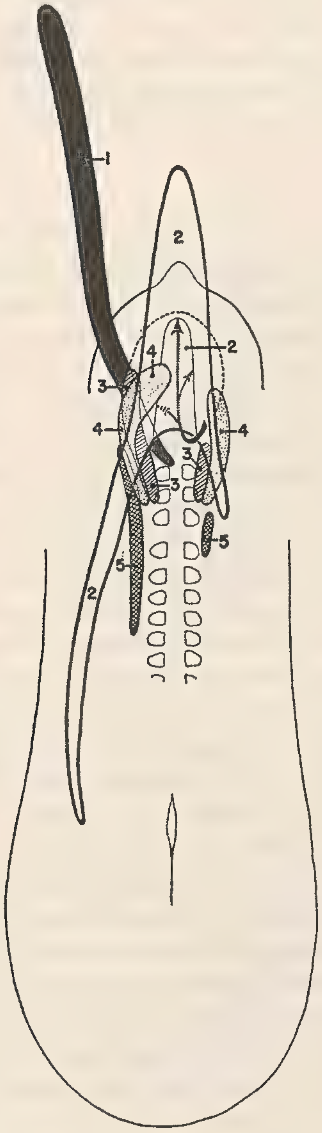

Fig. 3. Distribution of labeled cells in five of the six grafts placed in stage 3+ recipient embryos 18 hours before stage 5 (ventral view), and reincubated to foregut stages. Numbers refer to text descriptions (pp. 79–81). Location of grafts shown in Fig. 1(e). The graft to epiblast in *area opaca* zone *A* is not shown.

Graft to zones G and F—Fig. 1(e); labeling time, 3 hours; estimated labeling 36 hours later: right side, 10–30 per cent; left side, 10 per cent. At the 12-somite stage, labeled cells from this graft were distributed to two oval areas: distal paraxial and proximal lateral plate mesoderm at the nephrotome, beginning on the right at a level halfway between the top of the head and the AIP and on the left at a level just caudal to the AIP (Fig. 3, areas 3). These two columns extended caudally to a level 47 sections caudal to the AIP, where they ended at the nephrotome. Labeled cells therefore moved medially to streak, ventrally, and cephalolaterally into mesoderm.

Most cephalic of two grafts exclusively in zone F—Fig. 1(e); labeling time, 3½ hours; estimated labeling 35 hours later: right side, 50–70 per cent; left side, 10–20 per cent. At the 15-somite stage, labeled cells from this graft were distributed to mirror image areas of nephrotome and its attached somatic and splanchnic folds, beginning on the right at the conus region of the heart and on the left at the level of the ventricle. From here they extended caudally to a level 30 sections below the AIP. The movements of cells from this graft were therefore medial to streak, ventral, and cephalolateral into mesoderm (Fig. 3, areas 4). Photographs and a radioautographed section of this embryo appear in Contribution 263 (Rosenquist and DeHaan, 1966).

Most caudal of two grafts exclusively in zone F—Fig. 1(e); labeling time, 3½ hours; estimated labeling 35 hours later: right side, 50 per cent; left side, 5 per cent. At the 12-somite stage, labeled cells from this graft were distributed to two oval areas of proximal somatic and splanchnic mesodermal folds. The right oval began directly caudal to the AIP and extended caudally to the end of the 100th section caudal to the AIP. The left oval began on the 50th section caudal to the AIP and ended at the 60th section caudal to the AIP (Fig. 3, areas 5).

Labeled cells therefore moved medially to the streak, ventrally, and cephalolaterally into mesoderm. The left oval was much smaller than the right and contained fewer labeled cells.

Graft to caudolateral zone A—Fig. 1(e); labeling time, 3 hours; estimated labeling 27 hours later: ectoderm and epithelial vesicle, 50 per cent. At the 3-somite stage, labeled cells from this graft were distributed to an epithelial vesicle 25 sections in diameter extending into the space dorsal to the *area opaca* ectoderm, beginning at a level 93 sections caudal to the caudal end of the *area pellucida.* The vesicle was attached to a pedicle connected to a well-circumscribed area of ectoderm beginning 97 sections caudal to the caudal limits of the *area pellucida,* and ending on the 104th section. Labeled cells from this graft therefore moved caudolaterally, away from the streak and their original position. The distribution of cells from this graft is not shown in Fig. 3.

Grafts Fifteen Hours Before Stage 5

At 15 hours before stage 5, the blastoderm size and streak length have both increased, but the configuration is still much like H-H stage 3+. The 12 grafts to this stage are scattered throughout the epiblast; see Fig. 1(f). Some areas are covered by grafts for the first time, and the following observations may be made:

It has become increasingly clear that the epiblast is divided into an area in which the cells remain on the homolateral side and into areas from which cells are distributed to both homolateral and heterolateral sides. The former are all preectoderm cells—case reports below; Figs. 2, 3, and 4, the latter all premesoderm or preendoderm cells—case reports below; Fig. 5.

The preectoderm grafts at this stage happened to be limited to regions that contribute to extraembryonic ectoderm. The three grafts to zone *A* retain their position in *area opaca* despite migration to the streak or adjacent areas (Fig 4); move peripherally from the streak and from the *area pellucida* margin; and elongate into rod-shaped areas radiating like the spokes from the axle of a wheel. The graft elongation with growth suggests that the growth of ectoderm in the *area opaca* is a spreading or stretching over the vitelline membrane.

The grafts that moved to both heterolateral and homolateral sides appeared to do so by crossing over at the streak. Wherever the crossover occurred, the homolateral mesoderm (1) was more concentrated than heterolateral mesoderm (the percentage of labeling was higher); (2) was seen at more cephalic (or peripheral) levels than heterolateral mesoderm; and (3) in most cases disappeared from the labeled region at approximately the same level as the heterolateral mesoderm—case reports 4, 5, 6, and 7 below; graft 4 in Fig. 5(b). The result of this crossover was also seen in endoderm for the first time—case report below; Plate 4, graft 3. Graft 3 was originally unilateral, that is, its medial side was not placed in the streak. Yet labeled cells appeared bilaterally in endoderm as well as in mesoderm, suggesting that preendoderm, like premesoderm, enters the streak from the right epiblast, mingles with unlabeled cells from the left epiblast, and migrates from the streak to both right and left endoderm.

In this study, there were numerous examples of bilateral mesoderm distribution from unilateral grafts;

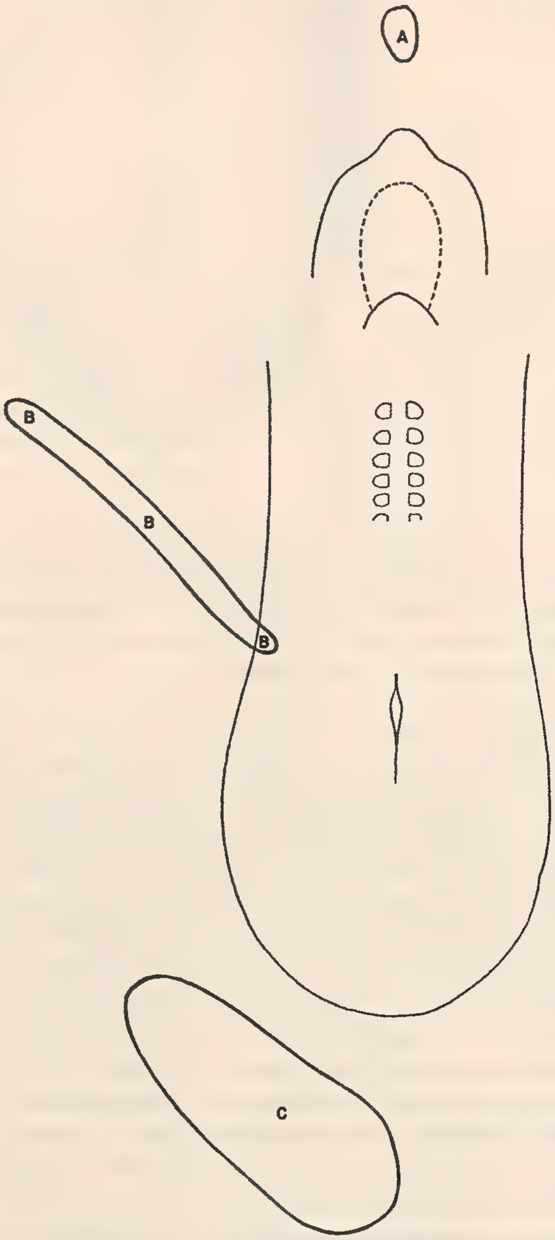

Fig. 4. Distribution of labeled cells in three stage 3+ to 4− recipient embryos 15 hours before stage 5 (ventral view), reincubated to foregut stages. Grafts were originally located in extraembryonic ectoderm zone *A*, Fig. 1(f) (described also on pp. 82–83).

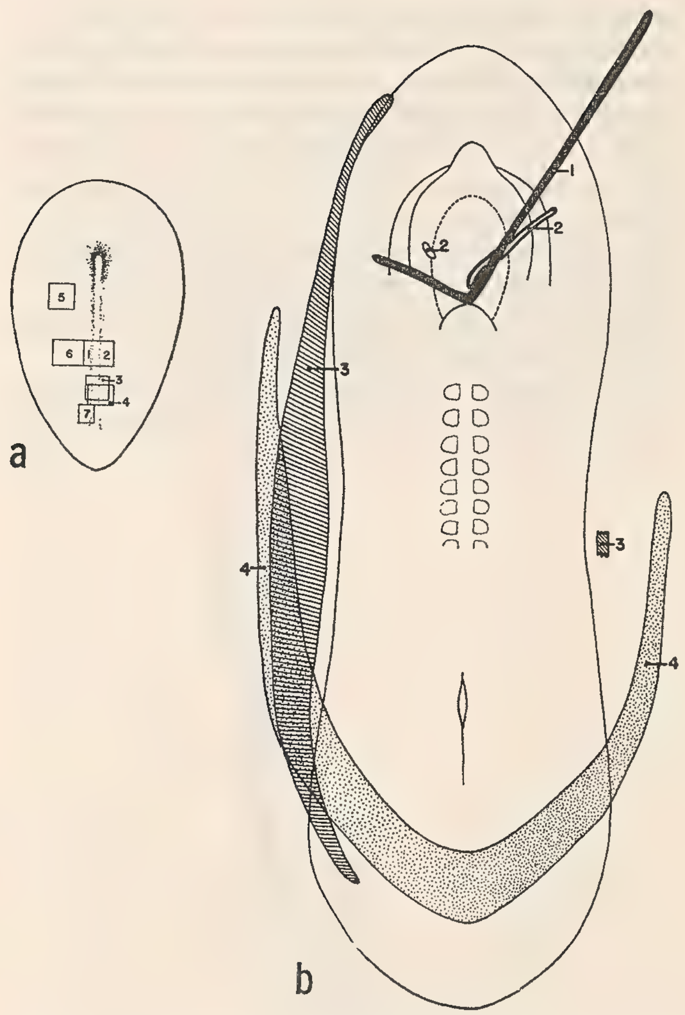

Fig. 5. (a) Location and numbering of seven grafts to zone *F* of stage 3+ to 4− recipient embryos 15 hours before stage 5 (ventral view), Fig. 1(f). (b) Distribution of labeled cells from grafts 1–4 (text descriptions, pp. 83–84) after reincubation to foregut stages.

the point was not as well illustrated for endoderm, however, because most of the grafts containing preendoderm were those placed in the midline streak or with the medial border of the graft at the midline. Though these grafts were invaluable in mapping the limits of the preendoderm zones of epiblast and preendoderm zones of the streak, only unilaterally placed grafts prove that endoderm, like mesoderm, crosses over at the streak. This was one of three grafts in the present series that illustrate this point.

The streak cannot be termed a blastema, but can be considered a modified blastopore. Cells neither from grafts to the streak itself nor from grafts to the regions lateral to the streak remain in the streak—case reports at previous stages and below.

For the first time, cells from the unilateral grafts have been discovered in the process of invaginating at the streak—see case report below for graft position shown in Fig. 5(a). When this occurs, the lateral epiblast cells approach the streak, where they lose their epithelioid structure, descend ventrally, mixing with unlabeled host cells from the heterolateral side and perhaps with some unlabeled host cells from the homolateral side.

The preinvaginating area of the streak appears to be divided into two areas: preendoderm invaginating area and premesoderm invaginating area (described below). The transition between the two areas is located by studying the reconstructions of two embryos in which labeled grafts were placed at a level halfway down the streak—case reports below; grafts 1 and 2 in Fig. 5(a). Cells from these grafts were distributed to caudal *area pellucida* endoderm and to cephalic mesoderm of *area vasculosa* and endocardium, the latter shown in Fig. 5(b).

The preendoderm invaginating area of the streak is divided so that grafts placed in the most cephalic area move to cephalic *area pellucida* and gut—case reports below; 4(a), grafts placed in the middle of the zone move to central *area pellucida,* and grafts placed in the caudal limits of the zone move to caudal *area pellucida*—graft locations seen in Fig. 1(f).

The premesoderm invaginating zone of the streak is also divided into three sectors: cephalic, middle, and caudal. Through the cephalic sector are invaginated prechordal mesoderm (axial and paraxial)—case reports below; grafts 1 and 2 in Fig. 5(a), (b)—followed by axial and paraxial head mesoderm and axial and paraxial presomite mesoderm. Through the middle sector is invaginated extraembryonic mesoderm to the ala (or wing) of the *area vasculosa*—case reports below; graft 3 in Fig. 5(a), (b)—followed by the embryonic mesoderm, nephrotome, dorsal mesentery, and heart—case report below. Through the caudal sector is invaginated extraembryonic *area vasculosa* mesoderm to laterocaudal *area opaca*—case report below; graft 4 in Fig. 5(a), (b). Through all sectors is invaginated endothelium, which may take one of the following three forms: blood islands (*area vasculosa*), endocardium (cephalolateral *area pellucida*), or subendodermal plexus (remaining central *area pellucida*). Whether these three endothelial cell types took these forms because of position (association with endoderm, peripheral mesoderm, ventrality), because of method of invagination at the streak, or because of inherent factors cannot be determined from this study.

Graft to midline zone A, cephalad to anterior limit of area pellucida—Fig. 1(f); labeling time, 3 hours; estimated labeling 26 hours later, 40–50 per cent. At the 6-somite stage, labeled cells from this graft were distributed to a well-circumscribed area of midline proamnion at the cephalic end of the *area pellucida,* where they extended through nine sections of *area opaca* and 16 sections into *area pellucida* (Fig. 4, area *A*). Labeled cells from this square appeared to move as a unit into the *area pellucida* margin.

Graft to zone A in lateral area opaca—Fig. 1(f); labeling time, 3¼ hours; estimated labeling 25 hours later, 50–70 per cent. At the 5-somite stage, labeled cells from this graft were distributed to *area opaca* ectoderm, beginning at a level 50 sections caudal to the AIP at a distance half the width of the *area pellucida* into the *area opaca* and extending as a narrow circumscribed oval to the *area pellucida* margin at a level 130 sections caudal to the AIP (Fig. 4, area *B*). Labeled cells were stretched cephalolaterally from the original location of this graft. In addition, the graft as a unit moved cephalad in relation to the streak.

Graft to zone A in caudal area pellucida, most caudal graft—Fig. 1(f); labeling time, 4 hours; estimated labeling 31 hours later, 30 per cent. At the 10-somite stage, cells from this graft were distributed to a well-circumscribed elongated oval area of yolk-sac endoderm, beginning at a level 20 sections cephalic to the posterior limits of the *area pellucida* and ending near the midline 99 sections caudally (Fig. 4, area *C*). Labeled cells from this graft therefore moved laterocaudally from their original position.

Graft to cephalic end of zone E—Fig. 1(f); labeling time, 2½ hours; estimated labeling 27 hours later, 30 per cent. At the 5-somite stage, cells from this graft were distributed to the midline yolk-sac endoderm, beginning at a level 90 sections above the head and extending over the medial half of the *area pellucida* to the AIP, where the labeled region divided into two columns. These columns extended cephalically into the lateral gut as far as the foregut and caudolaterally to the somites as far as a level 10 sections caudal to the BW level on the right side, 8 sections cephalic to the BW level on the left. Though the drawing in Fig. 1(f) does not so indicate, this graft contributed a labeled cell to the notochord at the sixth and seventh sections cephalic to the AIP. Labeled cells from the graft therefore moved ventrally, cephalically (notochord), and cephalolaterally (endoderm). As the foregut was formed, the cephalic limits of the arch-shaped area on the yolk-sac surface were folded ventrally into the lateral gut wall. This graft is shown as graft 2 in Plate 4(a). A radioautographed section from the embryo is shown in Plate 4(c).

Graft to zones E and G—Fig. 1(f); labeling time, 3 hours; estimated labeling 18½ hours later: right side, 20–30 per cent; left side, 5–10 per cent. At stage 6—, labeled cells from this graft were distributed to oval areas of right and left mesoderm, beginning at a level 34 sections cephalic to Hensen's node and ending at Hensen's node, and to right and left endoderm, beginning 25 sections cephalic to Hensen's node and ending at Hensen's node. Though amniocardiac vesicles are not present in the stage 6 embryo, the results of the ectoderm-mesoderm grafts indicate that the mesoderm of this graft is located in the preparaxial zone. Movements of the cells in the graft were medial to streak, ventral, and cephalolateral into right and left mesoderm and endoderm layers. The graft is shown as graft 3 in Plate 4(a). A radioautographed section from the embryo is illustrated in Plate 4(d).

Graft to zones E and F—Fig. 1(f), also seen as grafts 1, 2 in Fig. 5(a); labeling time, 3 hours; estimated labeling 27 hours later: endoderm, 30–50 per cent; mesoderm, <10 per cent. At the 6-somite stage, labeled cells from this graft were distributed to two columns of yolk-sac endoderm, beginning on the right just caudal to the AIP and on the left 36 sections caudal to the AIP. From here they extended caudally about halfway to the *area pellucida* margin, meeting at the midline halfway between the BW level and the caudal edge of the *area pellucida.* Labeled cells were then found in the medial half of the *area pellucida* endoderm for 46 additional sections before they disappeared at the midline 20 sections cephalic to the caudal edge of the *area pellucida.* The cells were distributed to mesoderm of *area opaca* and *area pellucida,* beginning on the left 50 sections above the head and on the right in yolk-sac mesoderm of the *area pellucida* at a level just cephalic to the AIP. These two columns of labeled mesoderm extended caudomedially into the subendodermal endothelial plexus between the two primitive heart tubes, meeting just cephalad to the AIP; see Fig. 5(b). Movements of cells from this graft were therefore ventral, caudolateral into endoderm, and cephalolateral into mesoderm. As the gut fold formed, the mesoderm was pulled ventrally into the space between the gut and the yolk-sac endoderm (Fig. 6).

Graft to zones E and F—Fig. 1(f); same position as graft 1; labeling time, 3 hours; estimated labeling 27 hours later: endoderm, 30–60 per cent; mesoderm, 5–20 per cent. At the 5-somite stage, labeled cells from this graft were distributed in very much the same way as those in graft 1, that is, to two columns of the yolk-sac endoderm, beginning on the left at the level of the AIP and on the right 16 sections caudal to the AIP. From here the two

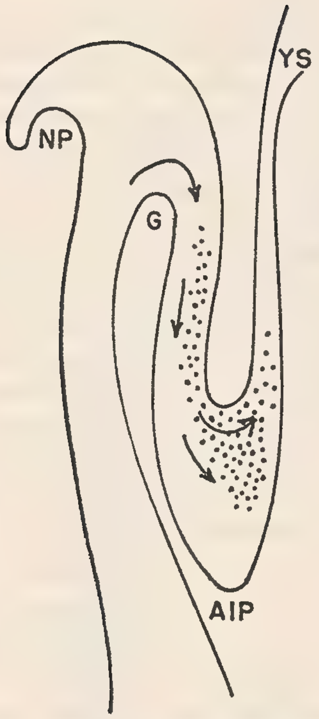

Fig. 6. Midsagittal section of chick embryo of 9–10 somites. As foregut forms, the most cephalic midline mesoderm is folded ventrally into the space between ventral gut and yolk-sac endoderm, where it contributes cells to endocardium and ventral mesocardium. Arrows indicate the direction in which mesoderm migrates between endoderm and ectoderm. NP = neuropore, G = foregut, YS = yolk sac. Dorsal surface of blastoderm is on the left.

columns extended caudally over the somites to meet at the midline 20 sections cephalic to the BW level. The labeled endoderm was then distributed to the medial half of the *area pellucida* to a level 115 sections caudal to the BW level, where it ended near the caudal edge of the *area pellucida.*

Mesoderm was also distributed to areas similar to those of graft 1, beginning in yolk sac on the left halfway between the top of the head and the AIP and on the right at a level just cephalic to the AIP. Mesoderm from the left extended caudomedially into the endothelial plexus ventral to the gut. However, mesoderm on the right extended through only four sections and thus was not seen in endocardium; see Fig. 5(b). Labeled endoderm therefore moved ventrally and peripherally in all directions, but most prominently in a caudal and laterocephalic direction. Mesoderm migrated ventrally and laterocephalically. As the gut folded, this mesoderm was pulled ventrally into the space between the gut and the yolk-sac endoderm (Fig. 6).

Graft to zone F—Fig. 1(f); also seen as graft 3, Fig. 5(a); labeling time, 3 hours; estimated labeling 28 hours later, 40–60 per cent. At the 8-somite stage, labeled cells from this graft were distributed to lateral plate mesoderm, beginning at the right edge of the *area pellucida* 21 sections cephalic to the top of the head and extending caudally as a narrow strip of *area vasculosa* mesoderm to a level 259 sections caudal to the AIP, just medial to the edge of the *area pellucida.* The left *area vasculosa* was inadvertently trimmed so close that labeled mesoderm was distributed on the left side in only three sections, at a level just cephalic to the BW level; see Fig. 5(b), areas 3. Labeled cells moved medially, ventrally, and cephalolaterally.

Graft to zone F—Fig. 1(f); also seen as graft 4, Fig. 5(a); labeling time, 3 hours; estimated labeling 22 hours later, 5–10 per cent. At the 9-somite stage, labeled cells from this graft were distributed to *area vasculosa* mesoderm, beginning on the right a short distance into the *area opaca* at the level of the AIP and on the left 65 sections caudal to the AIP. From here the labeled cells extended as two narrow strips of *area vasculosa* mesoderm down the flanks of the embryo, crossing medially into the *area pellucida* at approximately 40 sections caudal to the BW level, meeting in the midline 80 sections caudal to the BW level. Labeled cells then extended through 40 additional sections of midline *area pellucida,* ending 10 sections caudal to the last section of the *area pellucida;* see Fig. 5(b), areas 4. Movements of the labeled cells in this graft were therefore medial to the streak, ventral, and caudolateral into *area vasculosa.*

Descriptions of the three grafts to nonstreak areas of zone *F* follow:

Most cephalic of the three grafts straddling zones F and G—Fig. 1(f); also seen as graft 5 in Fig. 5(a). Definitive position: bilateral proximal splanchnic and somatic mesoderm from dorsal mesentery of the heart just cephalic to the AIP, extending to the streak where the two columns meet. Nephrotomal and paraxial mesoderm are also included.

Graft to lateral zone F—Fig. 1(f); also seen as graft 6 in Fig. 5(a). Definitive position: bilateral proximal somatic and splanchnic mesoderm from the level of the conus to 30 sections caudal to the AIP, contributing to the heart in a stage 12 embryo.

Graft to caudal zone F—Fig. 1(f); also seen as graft 7 in Fig. 5(a). Definitive position: bilateral mesoderm layer adjacent to the receding streak in a stage 12 embryo.

Grafts 5, 6, and 7 had the following movements in common: medial (to streak), ventral, and cephaloperipheral in the mesoderm layer.

Grafts Twelve Hours Before Stage 5

At 12 hours before stage 5, the gross appearance of the blastoderm is no longer like H-H stage 3+. The streak is narrower in comparison with the width of the blastoderm and has increased in length as well. The blastoderm will therefore be termed an early stage 4. The 41 grafts were well scattered throughout the epiblast and dorsal streak. The following observations may be made:

It is increasingly clear that the location of grafts placed in the preectoderm zones *A, B, C,* or *D* determines the location of the labeled cells in the ectoderm of the reincubated embryo. The details of this arrangement are: (1) The two grafts to cephalic zone *A* were distributed to extraembryonic ectoderm ventral and cephalic to the head. The five grafts to lateral and caudal zone *A*—locations shown in Fig. 7(a)—moved away from the streak, the cephalolateral movements being the most prominent; see Fig. 7(b). None of these grafts moved toward the streak. (2) The laterocephalic regions of zone *B* were distributed to ventrolateral head epithelium, and grafts to the caudal end of the zone were distributed to ectoderm of the trunk, often near the cephalic end of the streak. In this

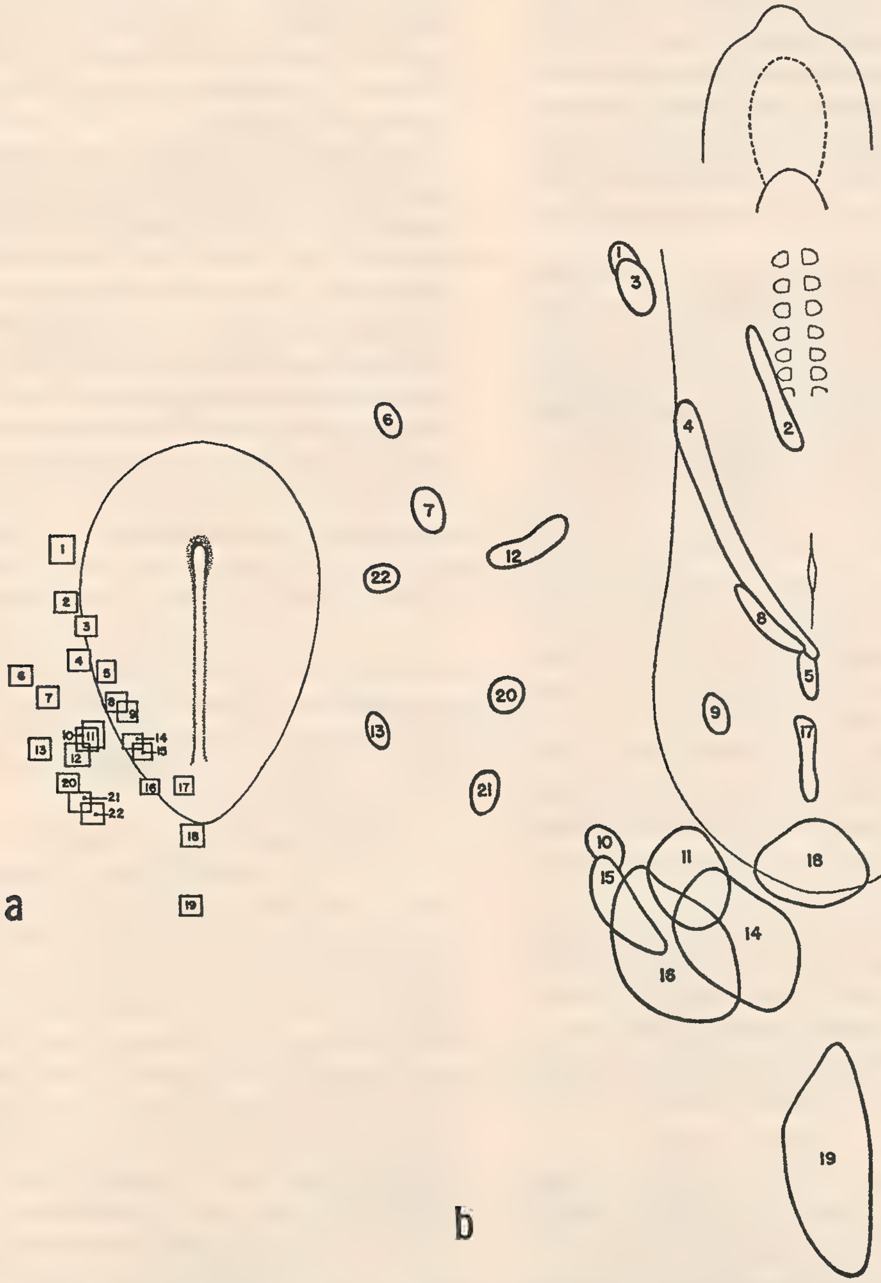

Fig. 7. (a) Location and numbering of 19 grafts to caudolateral zones *AB* placed in stage 4 recipient embryos, ventral view. Grafts 2, 4, 13, 14, and 16 were placed at 12 hours before stage 5; grafts 5, 9, 11, 15, 18, 19, 21, and 22 were placed at 9 hours before stage 5; and grafts 1, 3, 6, 7, 8, 10, 12, 17, and 20 were placed at 6 hours before stage 5. (b) Distribution of labeled cells in ectoderm or epiblast after reincubation to foregut stages.

area they could not be distinguished from extraembryonic ectoderm. Grafts placed medially in this zone, that is, closest to zone *C*, were distributed to the boundary between neural plate and epidermis. (3) A graft placed at the midline cephalic part of the preneural tube zone *C* is distributed to the cephalic neuropore; if the graft is placed in a slightly lateral and caudal position, it is folded into the midbrain; if placed near the premesoderm border, it appears in the spinal cord. (4) A similar arrangement exists in the ventral neural tube zone *D*, where grafts placed in the cephalic part contribute cells to the forebrain, and grafts placed in the caudal end (adjacent to prenotochord) contribute cells to the spinal cord. A graft placed away from the midline close to the boundary between zones *C* and *D* appears more dorsally in the neural tube, but still in the ventral half. Grafts placed in the more cephalic parts of the neural tube zones *C* and *D* (destined for forebrain and midbrain) elongate less with morphogenesis than do grafts placed close to the ectoderm-mesoderm boundary.

Since almost the entire preparaxial zone *G* is mapped and large areas of zone *F* as well, the limits and subdivisions of the premesoderm zones are better defined at this stage. The following observations may be made: (1) Grafts placed adjacent to the invaginating area are the first to enter the streak; those placed in areas adjoining or straddling the preectoderm zones are among the last to enter the streak. (2) Areas adjacent to notochord and endoderm are destined for medial paraxial mesoderm; those adjacent to nephrotome are destined for lateral paraxial mesoderm. (3) The boundary between preparaxial and prelateral plate mesoderm (prenephrotome) is in epiblast at a level about halfway down the streak.

Cells from grafts to the more cephalic areas of the preendoderm zone *E* are distributed to definitive locations of endoderm similar to those reported at previous stages but at more medial regions. The caudal end of the zone is not mapped at this stage.

The cephalic end of the streak was again the site of the prenotochord surrounded by the preventral neural tube zone. Since grafts have never been placed exclusively in the prenotochord region, the zone is probably quite small, diffusely scattered, or localized dorsoventrally within the thickened epiblast of the environs of Hensen's node.

> *Cephalic graft straddling zones D and H*—Fig. 1(g); graft site shown in Plate 5(a), (b); labeling time, 3½ hours; estimated labeling 27 hours later: neural tube, 60–80 per cent; notochord, <10 per cent. At the 10-somite stage, labeled cells from this graft were found scattered in the cephaloaxis of the embryo, beginning in ventral spinal cord at a level 49 sections into the head and extending caudally to the BW level. Labeled cells were distributed to notochord from a level 132 sections caudal to the AIP, caudally into the bulb. This distribution is illustrated in Plate 5(c) and in the radioautographs, Plate 5(d), (e). Labeled cells from this graft therefore moved ventrally (notochord) and cephalad (notochord and neural tube).

Grafts Nine Hours Before Stage 5

At 9 hours before stage 5, the blastoderm by gross observation differs from that at the preceding stages in its increase in size and streak length. The 51 grafts were scattered in all epiblast-dorsal streak zones, the greatest concentration being in preparaxial, preendoderm, and prenotochord zones. The following observations may be made:

The behavior of grafts to the preneural tube zones was similar to that described at previous stages—case reports below; Plates 6 and 7. As with previous stages, because so few grafts were placed in this region, the preectoderm-premesoderm boundary at the caudal ends of zones *B* and *C* was poorly defined. Six of the eight grafts—Fig. 7(a)—placed in caudolateral zone *A* moved cephalolaterally away from the streak. The two grafts migrating toward the streak were placed adjacent to the preinvaginating zones and were apparently pulled passively toward the streak as the preinvaginating zones receded toward the streak. Since they were near the streak when fixed, there is a possibility that they consisted partly of premesoderm.

The premesoderm zones were known to be actively migrating to the streak at these stages—case report below—but were approximately the same size and shape at this stage as at the previous stage. This suggests that cell division may, for a while at least, keep pace with loss into the streak.

The arrangement of the preendoderm zone *E* is similar to that of previous stages. Preendoderm from the graft to the most cephalic end of the zone moved to the yolk-sac endoderm cephalic to the AIP and to the midline ventral and dorsal gut—case report below. The graft placed in the central part of the zone moved to the lateral walls of the gut, and the strip of endoderm ventral to the somites. The graft to the caudal end of the zone was distributed to midline *area pellucida* from the somite region into the caudal *area pellucida.* This was the last stage at which a graft could be distributed exclusively to endoderm.

Labeled cells from the three most caudal of the six grafts to the prenotochord zone were distributed to the most cephalic limits of the definitive notochord, or within 30 sections of its origin—case report below; Table 3; Fig. 8. However, labeled cells were distrib-

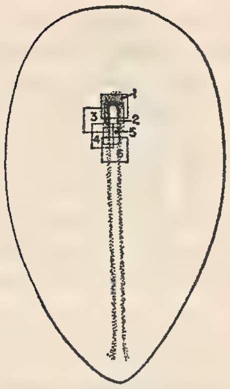

Fig. 8. Location and numbering of six grafts to prenotochord zone *H* in stage 4 recipient embryos 9 hours before stage 5, ventral view. Grafts are numbered by position: the most cephalic was graft 1; the most caudal, graft 6. All were approximately the same size except graft 5, which was somewhat smaller than the others. Grafts 1, 2, and 6 were placed in midline dorsal streak. Grafts 4 and 5 were on the right side near the center of the streak. Graft 3 was slightly lateral to the streak. Distribution of labeled cells in the notochord of the six recipient embryos is described in Table 3.

uted to the bulb and the caudal fourth of the notochord (cephalic end of the streak) in only the three cephalic grafts. All six grafts contributed cells to one or more other tissues (Table 3). This suggests that the prebulb cells are located in the cephalic end of the prenotochord zone whereas nonbulb cells are located in the caudal end of the zone, and that the bulb comes to lie caudal to notochord because it is the last to invaginate at the cephalic end of the streak.

Graft to zones A and B—Graft site shown in detail in Plate 6(a), (b); labeling time, 4¼ hours; estimated labeling 20½ hours later, 60–90 per cent. When fixed at the 6-somite stage, labeled cells from this graft were distributed to proamnion and ventral head ectoderm. The labeled area began at a level 10 sections cephalic to the top of the head at the *area pellucida* border and extended caudomedially as a narrow well-circumscribed strip into ventral ectoderm of the right side of the head to the cephalic neuropore, where one labeled cell was found in the dorsal neural tube. This distribution is illustrated in the retouched photograph of Plate 6(c), and in the radioautographs of Plate 6(d–f). Labeled cells from this graft therefore stretched in the cephalocaudal direction and were folded dorsally as the head formed.

Graft to zone D—Graft site shown in detail in Plate 7(a), (b); labeling time, 3 hours; estimated labeling 26 hours later, 40–60 per cent. At the 12-somite stage, labeled cells from this graft were distributed to ventral neural tube, beginning at the neuropore, where the width of the labeled area was almost one fourth the width of the neural tube, and extended

TABLE 3. DISTRIBUTION OF CELLS FROM SIX GRAFTS PLACED IN PRENOTOCHORD ZONE *H* AT STAGE 4, NINE HOURS BEFORE STAGE 5

Graft Number*	Stage of Host When Fixed (No. of Somites)	Level at Which Labeled Notochord Cells Begin	Level at Which Labeled Notochord Cells End	Tissues Labeled in Addition to Notochord
1	12	Origin	Caudal and cephalic bulb	Ventral neural tube, endoderm, paraxial mesoderm
2	5	Origin	Cephalic bulb	Endoderm, paraxial mesoderm
3	7	Near origin	Cephalic bulb	Endoderm, paraxial mesoderm
4	5	3 sections caudal to AIP	122 sections caudal to AIP (BW level 178 sections caudal to AIP)	Endoderm, paraxial mesoderm
5	4	7 sections caudal to AIP	74 sections caudal to AIP (BW level 115 sections caudal to AIP)	Endoderm, paraxial mesoderm
6	10	Origin	40 sections caudal to AIP (BW level 175 sections caudal to AIP)	Endoderm, mesoderm

* See Fig. 8 for numbering.

into spinal cord to end 30 sections above the BW level. One labeled cell appeared in the notochord at the 63rd, 73rd, and 80th sections caudal to the AIP. The distribution of labeled neural tube cells is seen in Plate 7(c), and in the radioautographs of Plate 7(d), (e).

Graft to cephalic end of zones E and H—Graft site also numbered as 1 in Plate 4(a); labeling time, 2½ hours; estimated labeling 27 hours later: notochord and mesoderm, <10 per cent; neural tube and endoderm, 50–65 per cent. At the 12-somite stage, labeled cells from this graft were distributed to (1) yolk-sac and gut endoderm, beginning 96 sections cephalic to the top of the head, in a median area about as wide as the head, extending caudally to the AIP, entering medioventral gut, extending to foregut, and appearing in midline dorsel gut for 16 sections; (2) mesoderm in paraxial head and endocardium; (3) notochord from its origin caudally into the bulb; and (4) ventral neural tube, beginning at the level of origin of the notochord and extending caudally into the streak in close association with the notochord. A radioautograph through the trunk of this embryo is illustrated in Plate 5(b). Cells from the graft therefore moved ventrally (endoderm, mesoderm, and notochord); and cephalically, fanning out slightly to paraxial areas. As foregut formed, the caudal end of the labeled endoderm, with its associated labeled mesoderm, was folded into the gut.

Graft to premesoderm zone F—Labeling time, 4¼ hours; estimated labeling 20½ hours later: right side, 20–40 per cent; left side, 10–30 per cent; location of graft illustrated in Plate 8(a), (b). At the 6-somite stage, labeled cells from this graft were distributed to two columns of lateral plate mesoderm, beginning on the right at a level 50 sections caudal to the AIP and, on the left, 65 sections caudal to the AIP. From here they extended caudally, ending close to the streak on the right 78 sections caudal to the BW level and on the left 77 sections caudal to the BW level. This difference is illustrated in the retouched photograph of Plate 8(c). Labeled cells are seen in the radioautographed sections of Plate 8(d–h). Movements of labeled cells from this graft were therefore medial to streak, ventral, and laterocephalic into mesoderm of right and left sides.

Graft to laterocaudal zone F—Labeling time, 3 hours; estimated labeling 17 hours later: epiblast and dorsal streak, 60–80 per cent; mesoderm and ventral streak, 20–50 per cent. At the 2-somite stage, labeled cells from this graft were distributed to right epiblast and dorsal streak, beginning at a level 105 sections caudal to the BW level. Four sections caudally, labeled mesoderm began on the right side near the streak, and labeled cells disappeared from epiblast. Ten sections later, mesoderm began on the left side. At the 120th section caudal to the BW level, labeled cells disappeared from the streak; that is, from left mesoderm at the 128th section caudal to the BW level, and from right mesoderm at the 132nd section caudal to the BW level. Labeled cells from this graft therefore moved (1) medially to the streak, (2) ventrally, and (3) caudolaterally into mesoderm.

Grafts Six Hours Before Stage 5

At six hours before stage 5, the difference between this and the preceding stage is largely a matter of increase in blastoderm size and streak length. In addition, the width of the streak has decreased relative to the width of the *area pellucida.* The blastoderm has assumed an elongated oval shape, with some tapering at the caudal end; see Plate 3(d). The 41 grafts, seen in Fig. 1(i), were well scattered; thus again all areas were represented. The following observations may be made:

The arrangement within the preectoderm zones was similar to that at preceding stages. However, the caudal ends of zones *B* and *C* were better visualized; they contributed cells to caudal neural tube and epidermis alongside the somites and extended to the streak at the BW level—case report below; Plate 10. Seven of the nine grafts placed in the caudolateral parts of zone *A*—Fig. 7(a)—moved peripherally away from the streak—Fig. 7(b). The most prominent single movement, however, was cephalolateral. The two grafts that moved toward the streak were situated at the medial border of zone *A* and so were drawn toward the streak by their association with the preinvagination zones.

The premesoderm zones were characterized by an overall decrease in width and an increase in length of the invaginating area of the streak—compare Fig. 1(h) with Fig. 1(i)—a growth that parallels the increase in streak length during this stage and suggests that the streak grows in length as a result of increase in the premesoderm invaginating area.

The arrangement of the area within the premesoderm zones was similar to that at previous stages. After 18 hours of reincubation, the most peripheral parts of the zone had moved to the streak and were seen in the process of invagination—case report below; Plate 9. The medial parts of the zone were distributed to somites and the proximal parts (at the streak), to mesoderm of the head. Two of the three grafts placed in the caudodorsal streak—zone *F*, Fig. 1(i)—moved to U-shaped areas of caudolateral mesoderm after invagination. The third graft, the most cephalic of the three, was distributed to two narrow elongated columns in recipient *area pellucida,* on each side of the node. It was thus similar to the other two except that it lacked the connection between the columns. The three grafts migrated in directions similar to those of the grafts placed in the same sites 15 hours before stage 5 (Fig. 5), but they were distributed to less peripheral mesoderm.

The four grafts to the preendoderm zone—case reports below; Fig. 9—contributed cells to increasingly limited areas of gut (lateral wall) and central blastoderm of the trunk and BW level. The arrangement within the preendoderm zone appeared to be similar to that at previous stages, with the migration of endoderm from the streak primarily to mediocephalic *area pellucida.* Quite possibly some of this movement is the result of regression of the streak, which exaggerates the cephalic movement at the expense of caudal expansion.

There were no grafts to the caudal part of the prenotochord zone at this stage. The only graft containing prenotochord was associated with paraxial mesoderm.

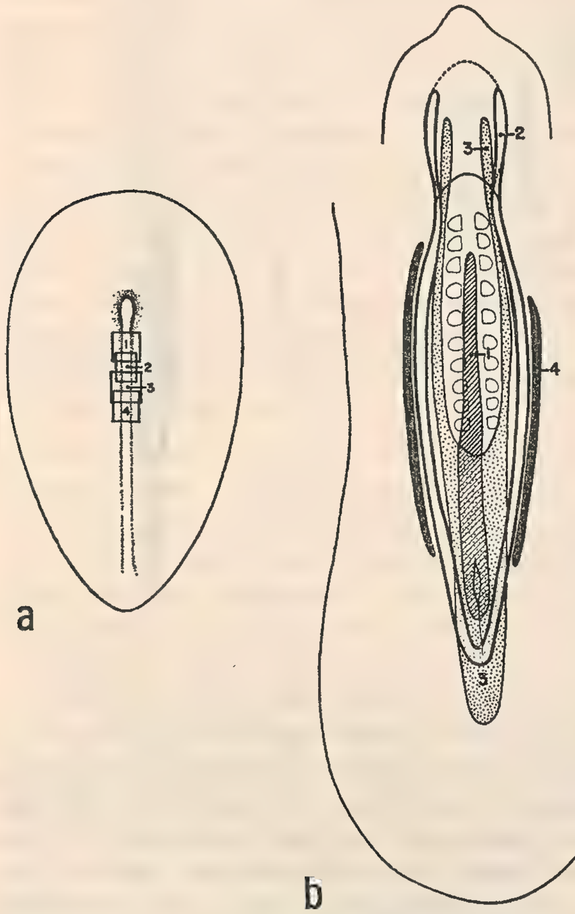

Fig. 9. (a) Location and numbering of four grafts to preendoderm zone *E* in stage 4 recipient embryos six hours before stage 5, ventral view. (b) Distribution of labeled cells from these grafts after reincubation to foregut stages. Numbers 1–4 refer to the four grafts described on pp. 89–90.

Graft to zones B and C—Graft site seen in Plate 10(a), (b); labeling time, 3½ hours; estimated labeling 18 hours later, 70–90 per cent. At the 5-somite stage, labeled cells from this graft were distributed to neuropore, beginning at the first section of the head, and from here they extended ventrally into epithelium of the ventral surface of the head and into dorsal neural tube from neuropore and into forebrain and midbrain to a level 24 sections caudal to the neuropore. This distribution is seen in the retouched photograph, Plate 10(c). Movements of the cells in this graft were therefore cephalocaudal lengthening, and folding into neural tube and epithelium of the head and trunk. Radioautographs of Plate 10 (d–f) illustrate these relations.

Graft to lateral zone F—Graft site in Plate 9(a), (b); labeling time, 3½ hours; estimated labeling 18 hours later: epiblast, 50–80 per cent; right mesoderm, 20–40 per cent; left mesoderm, <10 per cent. At the 4.5-somite stage, labeled cells from this graft were distributed to a well-circumscribed area of epiblast, beginning just lateral to the primitive streak at a level just caudal to the BW level. From here the cells extended caudally and medially to the streak. At a level 25 sections caudal to the BW level, a labeled cell was observed in the loosely packed mesoderm of the right side. Six sections later, two labeled cells were seen in the right mesoderm and one in the left. Labeled cells disappeared from epiblast at the 31st section caudal to the BW level. They disappeared from the streak 46 sections caudal to the BW level. As the labeled epiblast graft moved toward the streak, its medial half was drawn in a relatively caudal direction. As these medial cells neared the streak, they broke away, entered the ventral streak, and moved to either right or left mesoderm. The location of the cells in relation to the recipient embryo at the time of fixing is shown in Plate 9(c), and in the serial radioautographs of Plate 9(d–i). Because the embryo was fixed at stage 8, it is not known whether or not the labeled cells in epiblast would have invaginated.

Graft to cephalic end of zone E—Square 1 of Fig. 9(a); labeling time, 3¼ hours; estimated labeling 19 hours later: mesoderm, 20–50 per cent; endoderm, 10–20 per cent. At the 7-somite stage, labeled cells from this graft were distributed to bilateral paraxial mesoderm from head to somite levels; and to medial endoderm, beginning 34 sections caudal to the AIP and ending in the midline 30 sections caudal to the BW level; see Fig. 9(b). Movements of these cells were ventral and cephalic away from the streak.

Graft to cephalomedial zone E—Square 2 in Fig. 9(a); labeling time, 3¼ hours; estimated labeling 19 hours later: mesoderm, 10 per cent; endoderm, 60–90 per cent. At the 6-somite stage, labeled cells from this graft were distributed to bilateral paraxial mesoderm of the head, extending caudally to a level 20 sections below the AIP, and to two columns of endoderm, extending from lateral and dorsal foregut wall into yolk-sac endoderm caudal to the AIP. The two columns met in the midline 21 sections caudal to the BW level and disappeared 9 sections later; see Fig. 9(b). Movements of cells from this graft were therefore ventral, and cephalolateral away from the streak.

Graft to caudomedial zone E—Square 3 in Fig. 9(a); labeling time, 2½ hours; estimated labeling 24 hours later: endoderm, 40–50 per cent; right mesoderm, 10–30 per cent; left mesoderm, 5 per cent. At the 11-somite stage, labeled cells from this graft were distributed to the head mesoderm, beginning 40 sections caudal to the top of the head and ending at a level 10 sections cephalic to the AIP, and to two columns of yolk-sac endoderm. The first begins at a level 5 sections caudal to the AIP, the second 41 sections caudal to the AIP. These two labeled columns met 76 sections caudal to the AIP and then were distributed to the entire medial section of the embryo caudally to a level 52 sections caudal to the BW level; see Fig. 9(b). Movements of the cells from this graft were therefore ventral and cephalolateral away from the streak. Some endoderm cells moved very slightly in a caudal direction.

Graft to caudal zone E—Square 4 in Fig. 9(a); labeling time, 2½ hours; estimated labeling 27 hours later: mesoderm, 20–40 per cent; endoderm, 20–30 per cent. At the 14-somite stage, labeled cells from this graft were distributed to bilateral paraxial and lateral plate mesoderm, beginning 36 sections caudal to the top of the head and extending through proximal somatic and splanchnic mesoderm to end 148 sections caudal to the AIP; and to yolk-sac endoderm, beginning on right and left 20 sections caudal to the AIP and extending as two narrow columns caudally, ending just cephalic to the BW level. Movements of cells from this graft were therefore ventral, and cephalolateral away from the streak. Mesoderm moved farther cephalad than endoderm.

Grafts Three Hours Before Stage 5

At three hours before stage 5, the blastoderms were by gross examination identical with those of the definitive primitive-streak stage (H-H stage 4+). The streak is usually at least three fourths the length of the blastoderm. Occasionally the beginning of a head process was noted cephalic to the node. However, it should be emphasized that though the blastoderms looked like those of H-H stage 4+, the distinction was actually based on the time of reincubation required to reach stage 5. The 31 grafts represented all zones, even if not as completely as might be desired Fig. 1(j). The following observations may be made:

The arrangement of the cephalic ends of the preectoderm zones was like that at previous stages—case report for zone *C* below; the caudal ends adjacent to the preinvaginating areas had moved closer to the streak.

Three grafts to the premesoderm-preectoderm boundary are shown in Fig. 10(a) and case reports below. After reincubation to 15-, 13-, and 7-somite stages, these grafts had converged slightly, being dis-

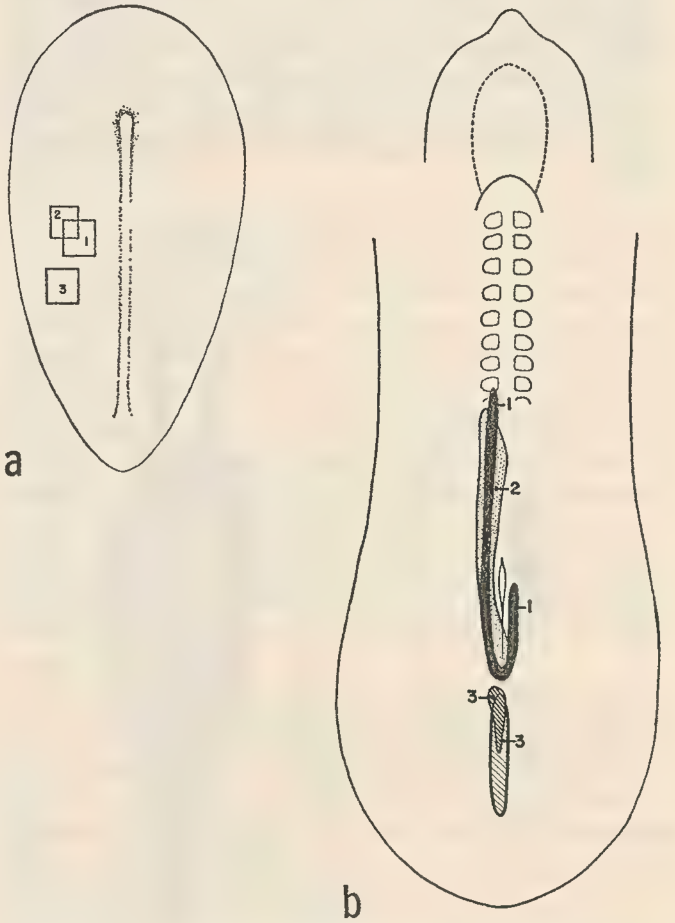

Fig. 10. (a) Location and numbering of three grafts to preectoderm zones (A and or B) and extending into premesoderm zone *F* of stage 4+ recipient embryos three hours before stage 5, shown in Fig. 1(j), ventral view. (b) Distribution of labeled cells from these grafts after reincubation to foregut stages. These three grafts are described on pp. 90–91. The cephalic portions of grafts 1 and 2 were located in the dorsal layer (epiblast or ectoderm), while the caudal areas were in both right and left mesoderm. The darker hatched extension of graft 3 was located in the dorsal (epiblast or ectoderm) layer. The lighter hatched portion appeared in right and left mesoderm of the *area pellucida.*

tributed to epiblast and mesoderm or streak. In grafts 1 and 2, the mesoderm moved cephalically after invagination—Fig. 10(b)—but in graft 3, the mesoderm moved caudally. This suggests that (1) the caudal end of the streak at the 7-somite stage is located halfway between the BW level and the caudal end of the *area pellucida;* (2) the caudal end of the streak is like the ventral lip of a blastopore in function (the site of lateral plate mesoderm invagination); (3) regression of the streak is the result of decrease in the length of the premesoderm invagination area; and (4) the remainder of the premesoderm zones converge at the tail bud.

One graft contributed cells to the preendoderm zone at this stage. Cells from this graft to the upper third of the streak were distributed to two narrow columns situated bilaterally over the caudal somite region, which met in the endoderm ventral to the receding streak, and to paraxial mesoderm.

The prenotochord zone at this stage was not well defined because only its cephalic border was located (adjoining the ventral neural tube zone).

Graft to caudal end of zone C—Graft site illustrated in Plate 11(a), (b); labeling time, 3¾ hours; estimated labeling 18½ hours later, 50–80 per cent. At the 9-somite stage, labeled cells were distributed to a well-circumscribed area of dorsal spinal cord, beginning at a level 48 sections caudal to the AIP and ending 204 sections caudal to the AIP (7 sections cephalic to the BW level) in a position slightly lateral to midline streak. The distribution of these cells is seen in Plate 11(c). Radioautographs of Plate 11(d–f) are representative sections through the neural tube. Movements of cells from this graft were therefore cephalocaudal elongation, and medial folding into neural tube.

Graft to zones B and F—Graft 1 in Fig. 10(a); labeling time, 3¼ hours; estimated labeling 25½ hours later: right side, 20–40 per cent; left side, 10 per cent. At the 15-somite stage, labeled cells from the graft were distributed to mesoderm, beginning on the right at the last somite (120 sections caudal to the AIP). From here the labeled area extended through paraxial mesoderm to the receding streak. At a level 246 sections caudal to the AIP, several labeled cells appeared in right epiblast (zone *B*) at the edge of the lateral streak. Movements of labeled cells from the graft were therefore medial to streak, ventral, and cephalolateral into mesoderm; see Fig. 9(b).

Graft to zones B and F—Graft 2 in Fig. 10(a); labeling time, 4 hours; estimated labeling 22 hours later: epiblast, 60–80 per cent; mesoderm, 20–40 per cent. At the 13-somite stage, labeled cells from this graft were distributed to a well-circumscribed area of ectoderm or epiblast dorsal to the somites, beginning at a level 65 sections caudal to the AIP. At a level 97 sections caudal to the AIP, the first mesoderm cells appeared on the right side in an area in which the lateral plate could not be distinguished from paraxial mesoderm. At a level 130 sections caudal to the AIP, labeled epiblast (zone *B*) was distributed to the streak in close association with labeled mesoderm on the right. Labeled cells were seen in both right and left streak for 31 sections, but did not appear in left mesoderm. Movements of cells from this graft were therefore medial; cephalocaudal elongation with the lateral side of the graft moving laterally and the medial side moving caudally into the streak; ventral; and after invagination, cephalic again in mesoderm on the right; see Fig. 10(b).

Graft to zones A, B, and F—Graft 3 in Fig. 10(a); labeling time, 3 hours; estimated labeling 17½ hours later: epiblast and streak, 50–70 per cent; mesoderm, 20–30 per cent. At the 7-somite stage, labeled cells from this graft were distributed to a well-circumscribed area of right epiblast adjacent to the streak, beginning 39 sections caudal to the BW level (zones *A* and *B*). Three sections later, cells had also appeared in the mesoderm of both sides. Although labeled cells appeared in dorsal streak for 25 sections, the distribution of mesoderm continued for 50 sections, ending 33 sections cephalic to the caudal end of the *area pellucida.* Movements of the cells from this graft were therefore medial, ventrolateral, and caudal.

Grafts at Stage 5

At 0–3 hours before stage 5, the blastoderms had a relatively short primitive streak, which varied between one fourth and one third the length of the *area pellucida.* They were therefore comparable to H-H stages 5− to 5. The 21 grafts placed at this stage were not as well scattered as at previous stages Fig. 1(k). Epiblast grafts to the cephalic areas of zones *A–D* are hard to place because of difficulties in dissecting epiblast from endoderm-mesoderm. The following observations may be made:

The preectoderm-premesoderm boundary is found closer to the streak than at the previous stage, but the caudal limits of the preectoderm zones are more clearly defined. In the one case where a graft straddled preectoderm and premesoderm areas, labeled cells were distributed to epiblast, streak, and premesoderm areas.

Only one graft was placed exclusively in a premesoderm zone. The boundaries of the premesoderm zones are therefore approximated in Fig. 1(k).

No grafts were placed in the region of Hensen's node nor at the cephalic end of the streak. The boundaries of the preendoderm and prenotochord zones are therefore also approximated.

ENDODERM–MESODERM GRAFTS

Grafts placed in the epiblast-dorsal streak, where graft locations and distributions after reincubation varied markedly, were invaluable in the study of epiblast and invagination movements and in the study of ectoderm. However, for the study of endoderm-mesoderm, the disadvantage of such grafts was that the endoderm-mesoderm movements observed may have taken place in epiblast, in the streak, or in the endoderm-mesoderm layer after invagination. The second group of grafts, to be described, were designed for study of the endoderm-mesoderm movements after invagination.

The endoderm-mesoderm grafts were placed in the stage 5 embryo at a time when staging of both donor and recipient embryos was better controlled (see Methods). Both donor and recipient embryos were assured of being homologous, and all areas could be studied simultaneously by individually grafting every fragment from a grid cut from the right side of the blastoderm—Fig. 11(a)—and fixing an embryo from each square of the grid at each stage between 6 and 12.

With the use of the endoderm-mesoderm grafts, the formation of such mesoderm organs as the heart and the *area vasculosa* (including the formation of the amniocardiac vesicles and the complicated folding of the splanchnic mesoderm layer) may be studied in detail and the formation of the foregut described. This information is recorded in a series of maps (Figs. 11, 13, and 14) and in Plate 10. Dividing results into two sections—mesoderm movements and endoderm movements—is necessary because the two layers migrate separately.

Movements of the Grafts

Mesoderm squares

Mesoderm appeared in all squares of stage 5 embryos except 1 and 2 (Fig. 11). Squares 3 and 4 contained only small amounts of mesoderm, presumably at their caudal ends. Occasionally no mesoderm was present in square 3. Mesoderm was present in square *A* only once (Fig. 11). The movements of the mesoderm squares between stages 5 and 6 are seen by comparing Fig. 11(a), stage 5, with Fig. 11(b). The corners of the previously square grafts are rounded because the donor square is rounded off slightly, and the corners of the recipient bed are also rounded off slightly. They are oval because of the cephalocaudal elongation of the *area pellucida*. Study of radioautographic sections shows that dorsal cells (mesoderm) of the graft have migrated cephalolaterally at a faster rate than the ventral cells (endoderm). This separation of dorsal and ventral cells is even more apparent at stage 7, seen by comparing Figs. 11(c) and 13(c). The separation in square 7 is illustrated in Plate 12(a) and in the radioautographed sections of Plate 12(b–d).

At stage 8, the dorsal or mesoderm portion of the squares in the laterocaudal positions (*B–G*, squares 17–18) have moved farther into *area opaca*, as have the lateral parts of squares 11, 13, and 15; see Fig. 11(d). The position of the labeled mesoderm cells at stage 9 suggests that the laterocaudal grafts are rotating from the *area pellucida* into the *area opaca;* see Fig. 11(e). The overlapping of the grafts seen in this drawing is the result of variations in size and shape among the recipient blastoderms and minor variations in graft placement. It should be emphasized that this overlapping does not occur in the embryos, but only in the composite map which represents the combined distribution of the separately grafted squares.

By stage 10, the mesoderm squares have elongated even farther; see Fig. 11(f). The medial side of square 7, for example, has contributed cells to paraxial mesoderm of the head and trunk and to nephrotome. Its lateral side has separated into splanchnic and somatic layers; see Plate 12(e). The somatic layer has moved cephalolaterally into the *area vasculosa,* while the splanchnic layer, being attached to endoderm, is pulled in a relatively caudal and medial direction into the space ventral to the gut. Here it folds into a dorsal fold next to the gut, and into a ventral fold next to the yolk-sac endoderm, seen in Plate 12(e), right side. The most proximal portion of the splanchnic fold participates in the formation of dorsal mesentery, beginning at the nephrotome; dorsal mesoderm (dorsal fold of the splanchnic layer); endothelium and endocardium—Plate 12(f); dorsal myocardium—Plate 12(f); and ventral myocardium (ventral fold of the splanchnic layer). From here the splanchnic layer extends cephalolaterally as ventral mesoderm and meets the splanchnic mesoderm of square *C*. Square *C* in turn extends into the *area vasculosa* to join somatic mesoderm at the lateral limit of the amniocardiac vesicles.

By stages 11 and 12, cells from squares 4 and 6 have moved cephalically into the midline regions of the head, where they are distributed to dorsal and ventral head mesoderm; Fig. 11(g) and (h) does not show this because of lack of space. Beginning at the level of the foregut, cells from square 6 are distributed only to the mesoderm dorsal to the gut, including notochord from its origin to the AIP. Cells from square 8 contribute to head mesoderm near the neural tube and

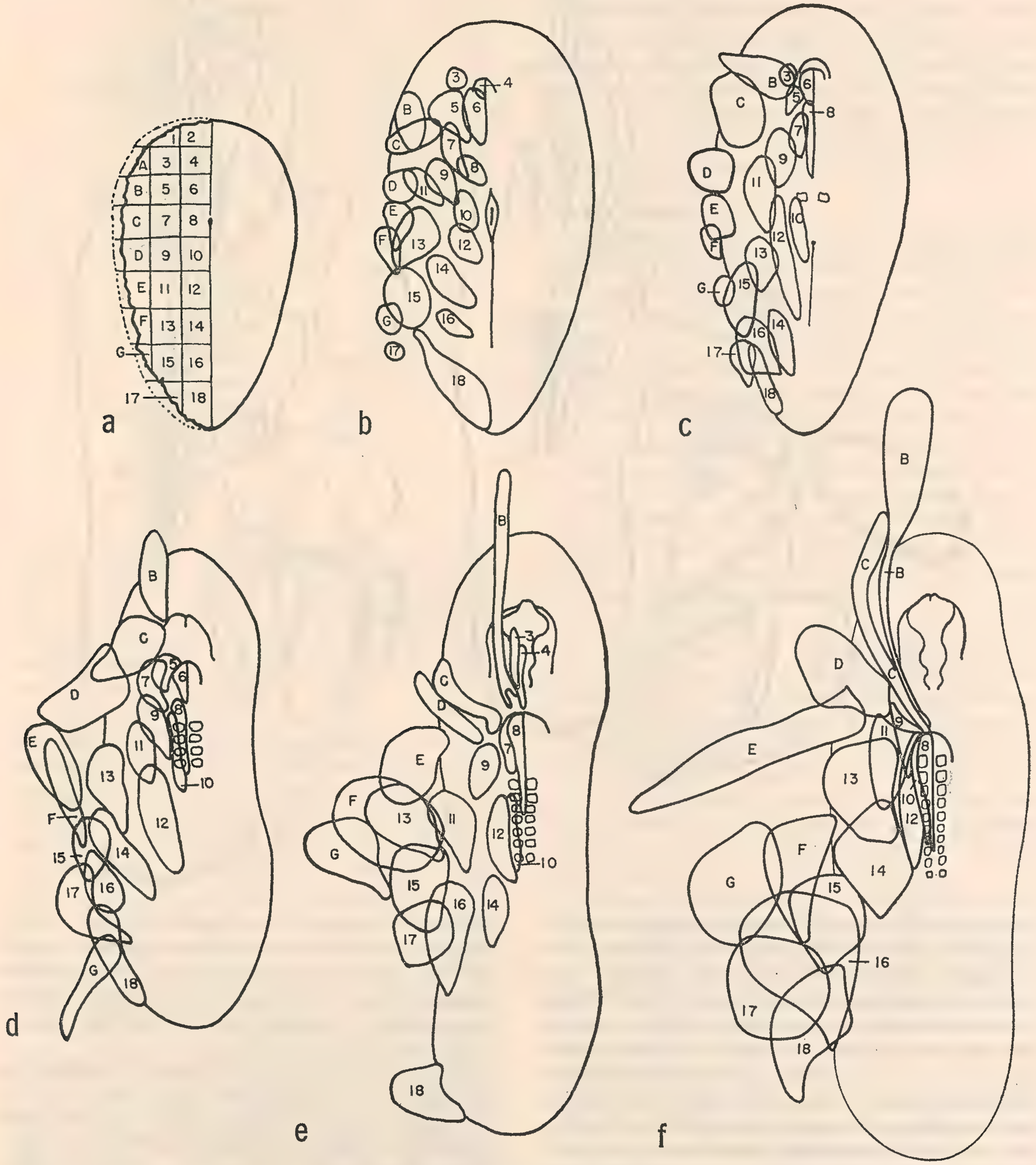

Fig. 11. Movement of the mesoderm portion of labeled endoderm-mesoderm grafts placed at stage 5. (a) Donor divided into 25 squares, ventral view. (b) By stage 6, both blastoderm and individual squares begin to elongate. (c) By stage 7, squares have moved peripherally from the streak. (d) At stage 8, there is continued movement into *area vasculosa.* (e) Stage 9. (f) Stage 10. (g) (opposite page) Stage 11. (h) Stage 12. Note wide swing into ala of right *area vasculosa.* Overlapping in grafts in *area vasculosa* is due to anatomical variations of recipient embryos. Once invaginated, mesoderm does not cross midline. Head mesoderm is not shown.

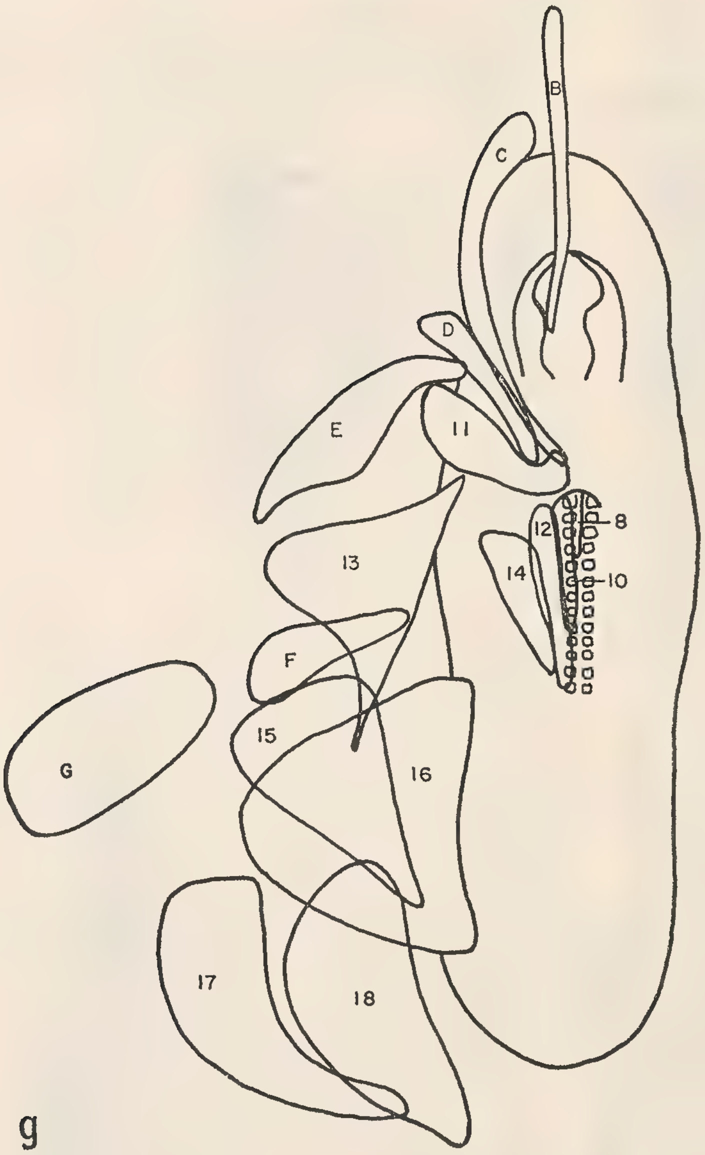

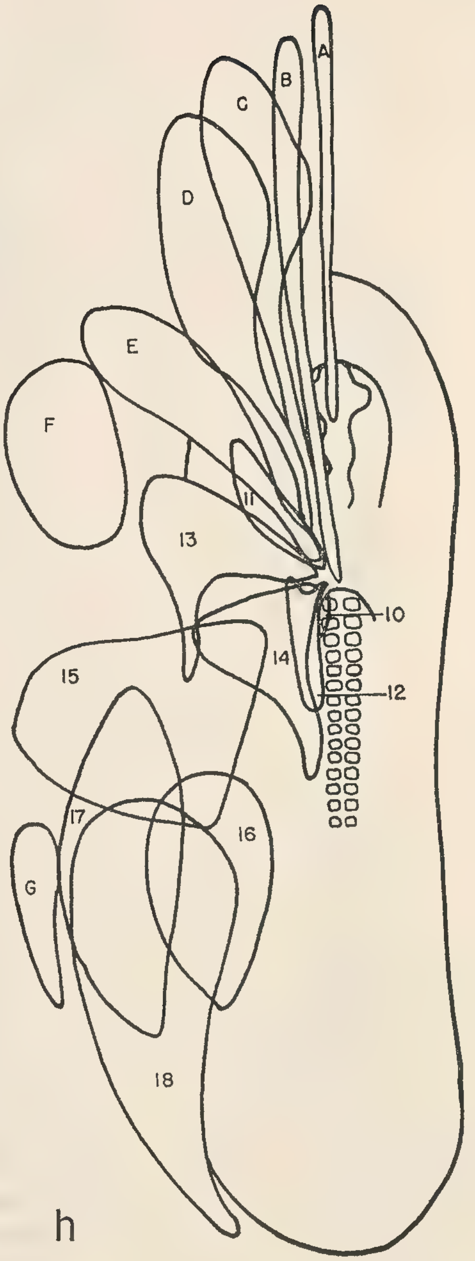

extend caudally through the somite region, where they are distributed to medial portions of the somites or to mesoderm adjacent to the notochord. Square 8 contributes to notochord from the level of the AIP into the somite region. The last labeled cells from square 8 are notochord cells at the level of the last somite. Squares 6 and 8 contribute to endothelium in their respective regions. In the head, labeled endothelial cells contribute to the aorta and cardinal system and in the trunk, to subendodermal endothelium. The endothelium appears to bridge a gap between the more cephalically migrating dorsal mesoderm and the more slowly migrating endoderm.

The medial sides of squares 7 and 9 contribute to nephrotome and paraxial mesoderm of the head and trunk. The lateral sides, along with the caudal half of square 5, square 11, and parts of squares 12, 13, and 14, contribute to myocardium. Squares 3 and 4 and the cephalic end of squares 5 and *B* contribute to endocardium and ventral mesentery, forming a continuous endothelial connection between heart and the ala of the *area vasculosa.*

Though the cephalic part of square *B* contributes to endocardium, its ventromedial edge, along with the ventromedial edges of squares *C* and *D,* are folded into myocardium. Mesoderm from square *A* and the lateral halves of squares *B–F,* 11, and 13 have moved cephalolaterally into the *area vasculosa* to contribute to the ala. The movement into the ala is a rotation cephalolaterally from its axis at the heart. At stage 5, the wing edge is horizontal and consists of the mesoderm of squares *A* and *B.* As the head fold forms, the medial side of

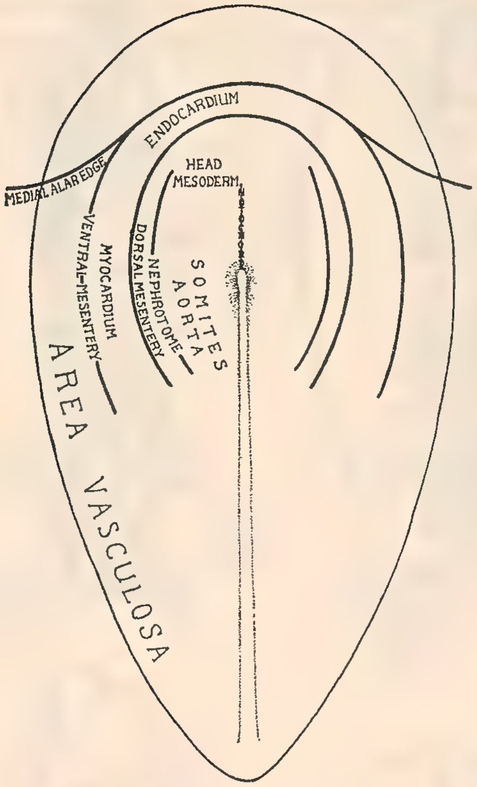

Fig. 12. Mesoderm map of the stage 5 embryo, ventral view. The labels on the left side refer to the distribution of mesoderm from that area after reincubation to stage 12. The map is based upon radioautographic reconstructions of the 23 endoderm-mesoderm grafts from the grid—Fig. 11(a)—which contributed to the mesoderm layer of the recipient embryos at stage 12; see Fig. 11(h).

square *B,* which contributes to myocardium, remains relatively stationary. During the next 24 hours, the lateral side, with square *A,* rotates 90° into the region cephalad to the head, where it appears in the midline. The lateral sides of squares *C–E,* 11, and 13 are also spread out over the *area vasculosa.* And just as the feathers at the tip of a wing are more widely spaced than the quills at the base, so the mesoderm at the lateral side of each graft is thinner than the medial side and covers a larger area.

The overlapping of grafts in the *area vasculosa* is even more extensive at stage 12 than at stage 9. This again appears to be the result of variations in expansion of the *area vasculosa,* since nearly all graft overlapping is seen in the lateral or nonaxis parts of a graft. Because the variations are not as noticeable in the medial sides, the heart can be mapped in detail (Rosenquist and DeHaan, 1966).

Square *G* and squares 15–18 have also moved peripherally into the *area vasculosa,* but do not participate in the formation of the ala. Square 14 lies in the *area pellucida* but, like square *B,* appears to be migrating cephalolaterally into the *area vasculosa,* with a portion destined for myocardium.

At stage 12, mesoderm from square 10 and a sizable portion of square 12 appears in somites and other paraxial structures; see Fig. 11(h). This finding agrees with the observations on the epiblast-dorsal streak grafts, which demonstrated that the paraxial entrance to the streak extends through the upper 33–40 per cent of the streak, adjacent to squares 10 and 12.

Endoderm squares

The movements of the 25 endoderm squares may be observed by comparing the drawings in Fig. 13(a–h), since each drawing shows the distribution of the 25 grafts fixed at each stage between 6 and 12. At stage 6—Fig. 13(b)—the labeled cells are distributed to oval areas. This appears to be the result of healing of the incompletely reexpanded square graft in a recipient bed, where the originally square corners also had become rounded off, and to the generalized cephalocaudal elongation during the interval between stages 5 and 6.

By stage 7—Fig. 13(c)—parts of squares 4 and 6 have folded into the gut. Squares *A,* 1–3, and 5 are clustered around the AIP. The rest of the grafts have elongated in a cephalocaudal direction and moved peripherally away from the streak.

At stage 8, the medial half of square 5 has folded into the gut along with additional parts of squares 4 and 6; see Fig. 14(a). The overlapping of some grafts appears to be the result of variations of blastoderm size and shape, and errors in graft placement, as the overlapping varies from stage to stage and does not involve dilution of the label.

The ovals continue to elongate between stages 8 and 9, and peripheral movements are most prominent cephalic to the node. Continued folding into the gut has occurred; see Figs. 13(e) and 14(b).

By stage 10, all of squares 4–6 and parts of squares 7 and 8 appear in the gut (Fig. 18). The distribution of the endoderm of square 7 in the yolk sac and gut is seen in Plate 12(e). Fig. 14(c) shows a corner of square 3 in the gut; it was on the verge of entering at stage 9 and was definitely included at stage 11. A radioautograph showing the labeled cells in the ventral gut wall is seen in Plate 12(g).

By stage 11, the blastoderm has lengthened; see Fig. 11(g). The endoderm grafts have also increased in size, mostly in the cephalocaudal direction. The midline portions of squares 12, 14, and 16 have moved caudally into an area of streak that appears to be no longer a grossly active site of invagination. In these regions, the endoderm cells are evenly scattered throughout the thin endoderm layer, as there are no labeled cells in the depths of the streak. Square 9 is

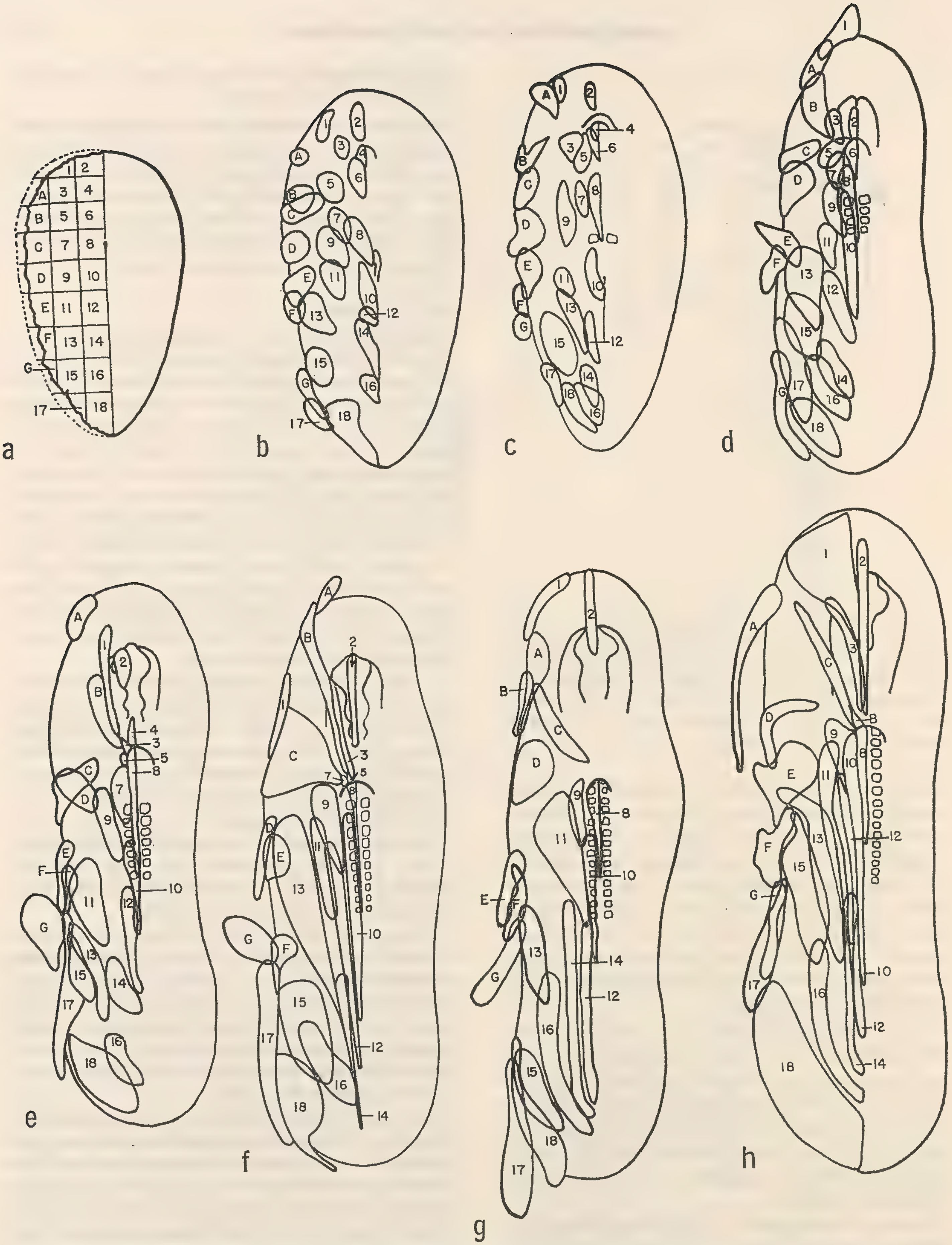

Fig. 13. Endoderm movements between stages 5 and 12 reconstructed from labeled endoderm-mesoderm grafts placed at stage 5. (a) Donor divided into the 25 endoderm squares, ventral view. (b) Position of grafts at stage 6 after 4–5 hours of reincubation. (c) Stage 7. (d) Stage 8. (e) Stage 9. (f) Stage 10. (g) Stage 11. (h) Stage 12. Gut endoderm is not included. The endoderm moves peripherally away from the streak but the cephalic movements are the more prominent. During this interval, at least, *area pellucida* endoderm does not contribute cells to *area opaca.*

seen confined to the yolk-sac endoderm in Fig. 13(g). However, as it was on the verge of invagination at stage 10 and is nicely included at stage 12, it is probably normally included also at stage 11, seen in Fig.

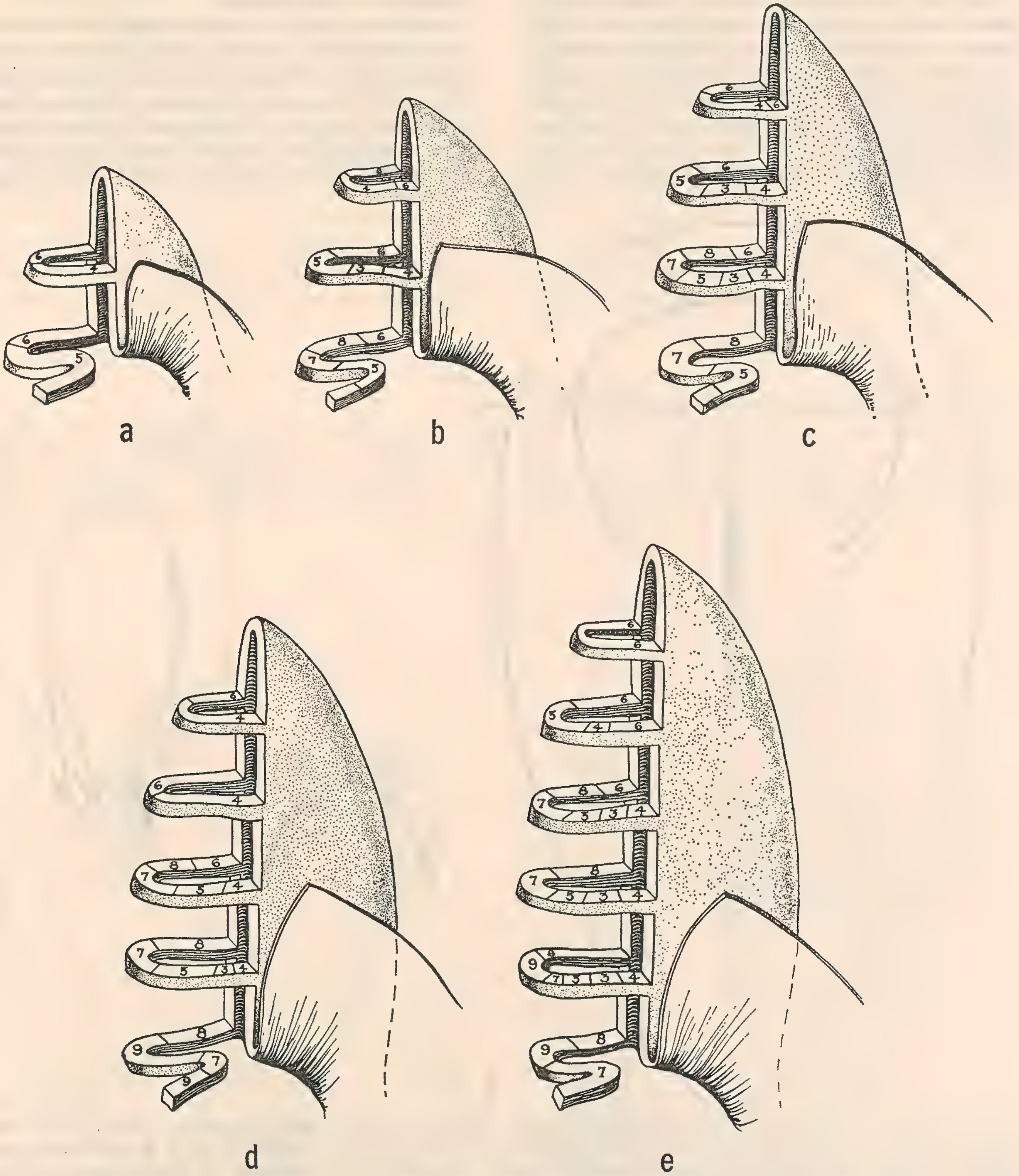

Fig. 14. Cutaway drawing of development of the foregut from the endoderm at stage 5. Endoderm-mesoderm grafts placed in recipient embryos at stage 5 are numbered as in Fig. 13. (a) Stage 8 foregut, ventral view; yolk-sac endoderm, ventral mesoderm, and sections of right gut removed. Squares 4, 5, and 6 contribute to foregut. (b) Stage 9. (c) Stage 10. (d) Stage 11. (e) Stage 12. All or part of squares 3–9 appear in foregut, the result of progressive invagination at the AIP.

14(d). Like square 3 (stage 10 above), this graft reflects the results of incomplete expansion of the corners of a square graft as it heals in its recipient bed.

At stage 12, there were no major changes in either gut or yolk-sac surface; see Figs. 13(h) and 14(e). However, the following observations may be made:

Endoderm from square 1 migrates to an unusually wide area of yolk-sac surface, being distributed to some regions usually covered by squares 2 and 3. This means that the graft expanded more rapidly over the recipient bed than did the host endoderm. The edges of recipient bed had probably retracted after the homologous square was excised and discarded, illustrating the adaptability of both the recipient surface and the graft to various grafting situations.

Squares *A* and *E–G* extend slightly into the *area opaca;* but squares *B* and *C,* which did not include yolky *area opaca* with the graft, were pulled medially to the AIP, where a small portion of square *B* had moved into the gut. This appears to have resulted from more rapid and complete healing of the medial side of the graft so that the grafted square *B* was

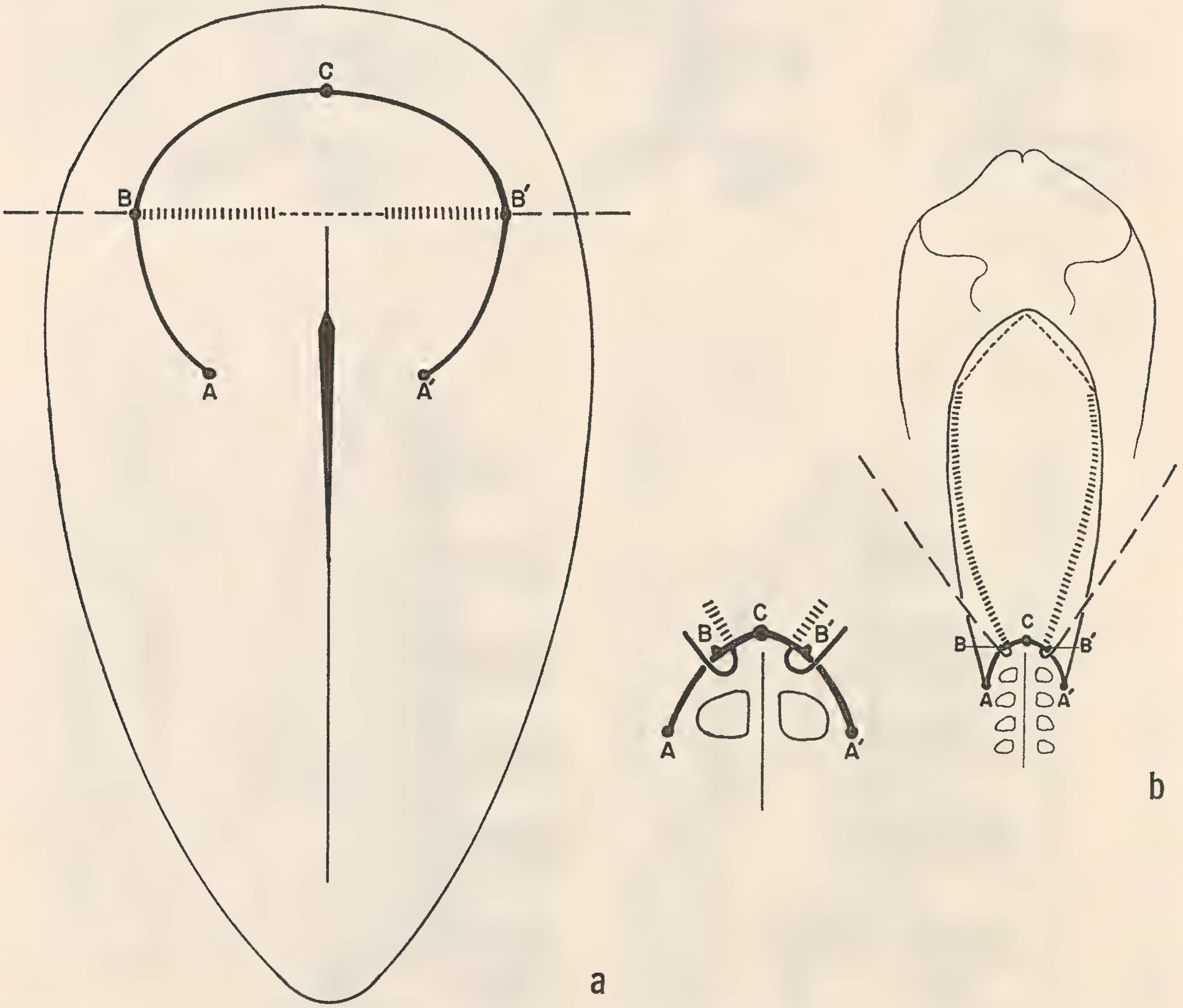

Fig. 15. Endoderm movements associated with gut formation (drawn to scale). (a) Head-process-stage embryo, ventral view. Endoderm enclosed within the curved line *ABCB′A′* is included in gut at stage 12. Horizontal line *B–B′* corresponds to the horizontal carbon mark placed on endoderm by Bellairs's (1953*b*) experiment 2. (b) By stage 12, Bellairs's mark *B–B′* was observed to extend from right yolk-sac endoderm into right ventral gut, right dorsal gut, tip of foregut, left dorsal gut, ventral gut, and yolk-sac endoderm. Bellairs based her concept of gut formation on the observation that after reincubation to foregut stages, points *B* and *B′* met at ventral gut. The present study demonstrates that though *B* and *B′* approach each other at the AIP, they never meet; they are always separated by the endoderm along the curved line *BCB′*, which has been compressed into the thickened ventral gut wall between *B* and *B′*.

drawn farther medially than usual. Rechecking the photograph made after grafting shows the donor fragment as slightly more contracted than usual and slightly more medially placed.

The lateral *area pellucida–area opaca* boundary appears to move cephalically with respect to both the embryonic axis and the *area opaca.* This movement is illustrated in squares 1, *A, B, E–G,* and 17 at stage 11; *D* and *F* at stage 10; and *C* and *E* at stage 9.

The ventral gut wall at a level just cephalic to the AIP consists of cells from grafts 3–5 and 7, and parts of graft 9; see Fig. 14(e). Endoderm from square 8 and parts of square 9 are distributed to the dorsal gut surface. This suggests that the greater thickness of ventral over dorsal gut wall is due to compression and not to increased mitotic rate. The area of endoderm pushed together at the AIP is illustrated in Fig. 15(a). In this drawing of the stage 5 embryo, *A* and *A′* are located at a point between squares 7 and 9, *B* and *B′* between squares 7 and 5, and *C* in the midline at the cephalic edge of square 4, so the curved line *ABCB′A′* crosses through squares 9, 7, 5, 3, and 4. By stage 12, the endoderm enclosed within this curved line has moved into the foregut, and cells along line *ABCB′A′* are gathered into the narrow space between *A* and *A′*; see Fig. 15(b). Endoderm from the rest of square 9 and from square 8, not participating in this compression, constitutes the dorsal gut wall. For convenience, line *ABCB′A′* will henceforth be called the AIP line.

DISCUSSION

The results of this study are in agreement with many aspects of the work, often subjected to criticism, of previous investigators. However, the results also contradict other aspects, some of which refer to organization of the various layers of the blastoderm at primitive-streak and head-process stages, others to movements of cells during these stages. These agreements and disagreements are discussed in the next sections.

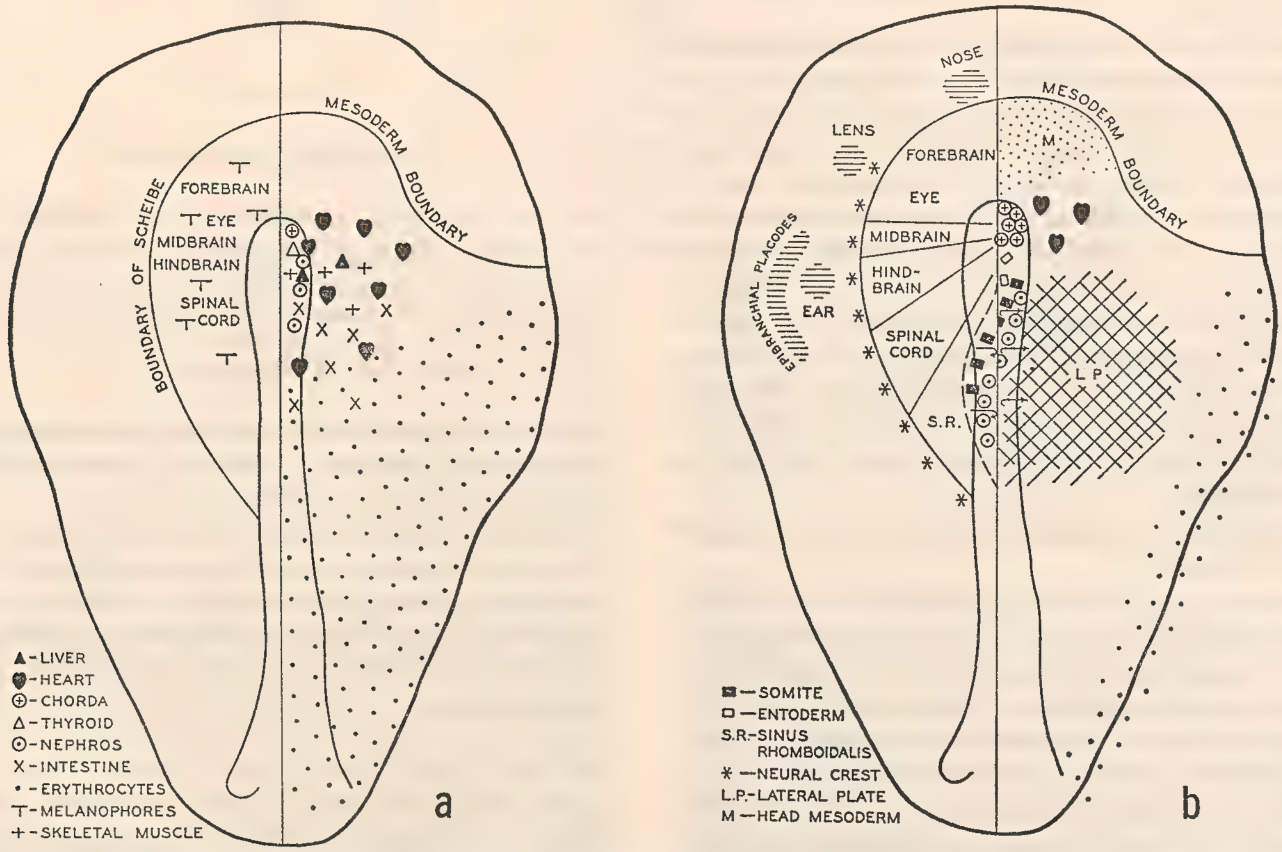

Fig. 16. (a) Distribution of potencies in the definitive primitive-streak-stage blastoderm tested under various experimental conditions. Rudnick's (1944) Fig. 9. (b) Prospective area map of the definitive primitive-streak blastoderm. Rudnick's (1944) Fig. 10.

ORGANIZATION OF BLASTODERM

Epiblast at stage 3+ to 4

Among the investigators who have described the organization of the primitive-streak-stage epiblast are Rudnick (1944) and Spratt (1952). In constructing her first map—Fig. 16(a)—Rudnick drew upon the results of investigators who had grown blastoderm fragments on the chorioallantoic membrane (CAM) or in other environment. In her second map—Fig. 16(b)—she interpreted the vital dye staining experiments of Wetzel (1929) and Pasteels (1937). Spratt's map—Fig. 16(c)—was the result of carbon marking of the epiblast. Though the present experiments resulted in separate maps, only one—Fig. 1(j)—describes epiblast organization at the definitive primitive-streak stage. This map may be compared with those of Rudnick and Spratt as follows:

Both Rudnick and Spratt present the neural plate as divided into pie-shaped wedges clustered around the cephalic end of the streak. In both cases, the most cephalic wedges are destined for the forebrain, the most caudal wedges for the spinal cord. Rudnick illustrates the wedges converging into Hensen's node; Spratt shows them cephalic to the node. The present experiments are in agreement with Spratt (Plates 5, 6, 7, 10, and 11).

Both Rudnick and Spratt show epidermal structures in the area surrounding the neural tube ectoderm. That nonneural-tube ectoderm is located in this area is in agreement with the present study, which, however, subdivides the region into (1) an epidermis zone *B* (which would correspond to the region designated by Rudnick as nose, lens, ear, and epibranchial placodes, and by Spratt as skin); and (2) an extraembryonic zone *A* which includes the proamnion. This subdivision adds considerably to our knowledge of this region. However, since some of Spratt's embryos were incubated to the 20-somite stage, his study may define the caudal limits of the area more precisely than does the present study.

All three maps localize prenotochord in the cephalic end of the streak.

Rudnick's map shows preendoderm at the cephalic end of the streak, an interpretation of her own studies (1935) and those of Hunt (1937*a, b*). Both investigators cultured epiblast and endoderm-mesoderm separately on CAM and discovered that the gut differentiated from the dorsal graft. Though Hunt believed the cephalic end of the streak contained preendoderm cells, Rudnick was more cautious, concluding that either preendoderm or endodermal inductive tissue was present in the dorsal streak at this stage. Spratt's map shows no preendoderm areas. The present study, with its tracing of cells from epiblast and dorsal streak into the endoderm on numerous occasions, confirms the concepts introduced by Rudnick and Hunt.

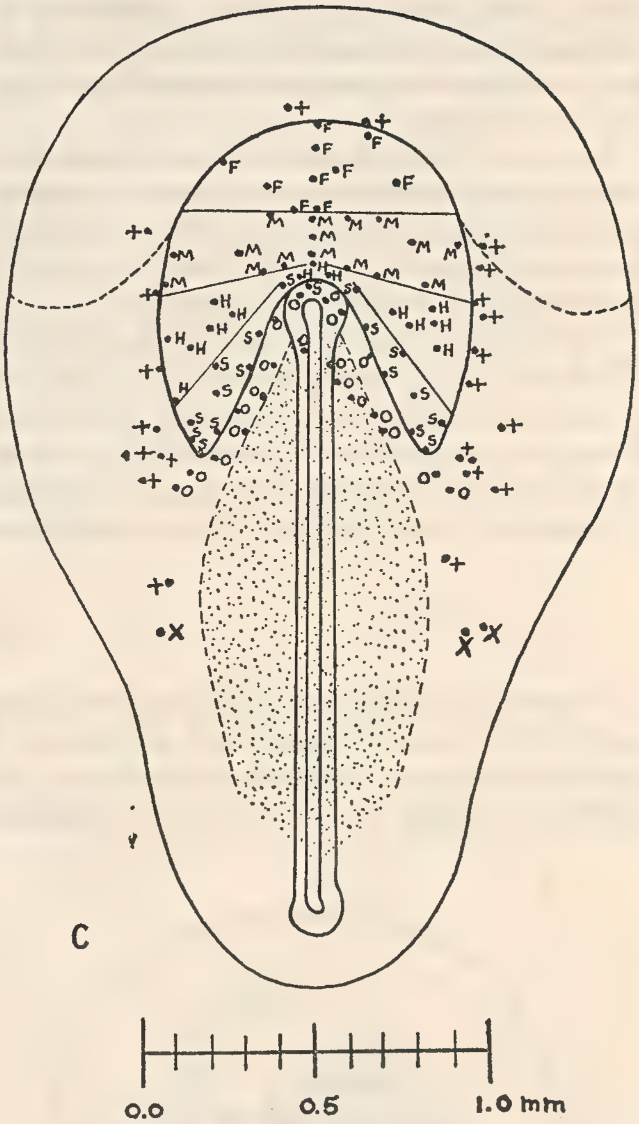

Fig. 16(c). Summary of pellucid area of the definitive primitive-streak blastoderm: fate of carbon marks. Spratt's (1952) Fig. 3. F: forebrain, M: midbrain, H: hindbrain, S: spinal cord, O: tail-bud epiblast, +: head and trunk skin, ×: trunk skin at the 20th somite level.

Rudnick's presomite nephros zone and Spratt's preinvoluted mesoderm zone are in the same areas as the combined preinvagination zones *E, F,* and *G.* Rudnick's nephros approximates the boundary between preparaxial and lateral plate mesoderm. She does not locate the latter.

Epiblast at stage 5

Spratt (carbon marking, 1952) and Rawles (CAM grafts, 1936) have both described the organization of the epiblast at head-process stages in map form. Their interpretations may be compared with the present study as follows:

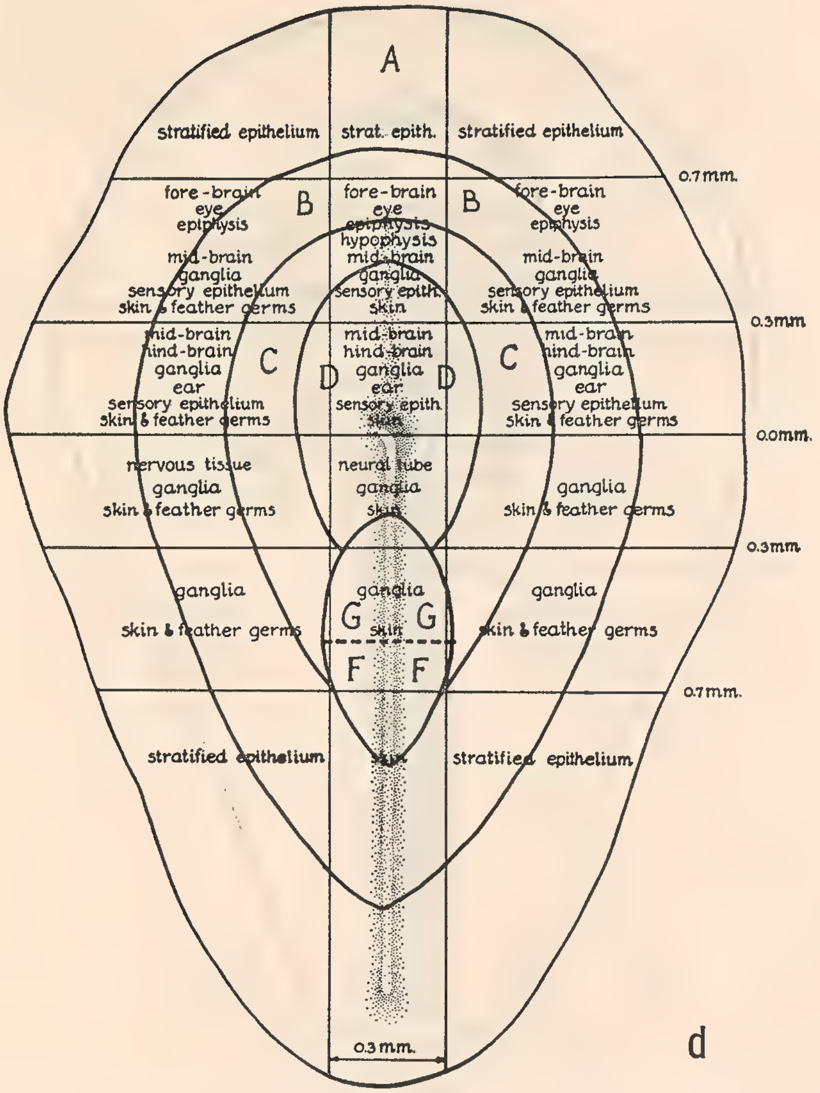

Fig. 16(d). Map showing the localization of developmental potencies of ectoderm structures in grafted pieces of the head-process blastoderm. Rawles's (1936) Fig. 7. Epiblast-dorsal streak zones *A–H* superimposed.

The preneural tube zones of this study are superimposed on Rawles's ectoderm potency map in Fig. 16(d). The letters *A–H* in the map and in the subsequent discussion refer to the eight epiblast dorsal streak zones previously described. Rawles described epithelial structures that are in the peripheral zones *A* and *B,* and her neural tube corresponds to zones *C* and *D.* In the preinvagination zones *F* and *G,* however, she discovered ganglia, presumably ectodermal derivatives. This finding is compatible with the present study if it may be assumed that Rawles's central streak fragment was in some cases slightly wider than that of the present study (extending into zones *B* or *C*), or if it may be assumed that the ganglia differentiated from fragments cut from later head-process-stage embryos in which the prospective medullary plate had moved closer to the streak.

Spratt is more precise about the neural tube zones than Rawles; see Fig. 16(e). With the use of carbon marks, he has located spinal cord in the epiblast adjacent to Hensen's node and midbrain-forebrain in more cephalic regions. Because the area he called "tail bud epiblast" was closer to the streak at stage 5 than at stage 4, he concluded that the preinvoluted mesoderm zone had become smaller. The present study is in agreement with this interpretation; see Fig. 1(k).

Mesoderm at primitive-streak stages

Previous studies of the mesoderm at primitive-streak stages describe the organization only in the area surrounding the node of the definitive primitive-streak embryo. In this region, Rudnick (1932, CAM grafts) found heart and mesonephros, and Spratt (1955, 1957, direct carbon marking) found somites and notochord. However, neither investigator attempted to determine the peripheral limits of the mesoderm at this stage.

The present study is in agreement with both Rudnick's and Spratt's interpretations for stage 4+ but

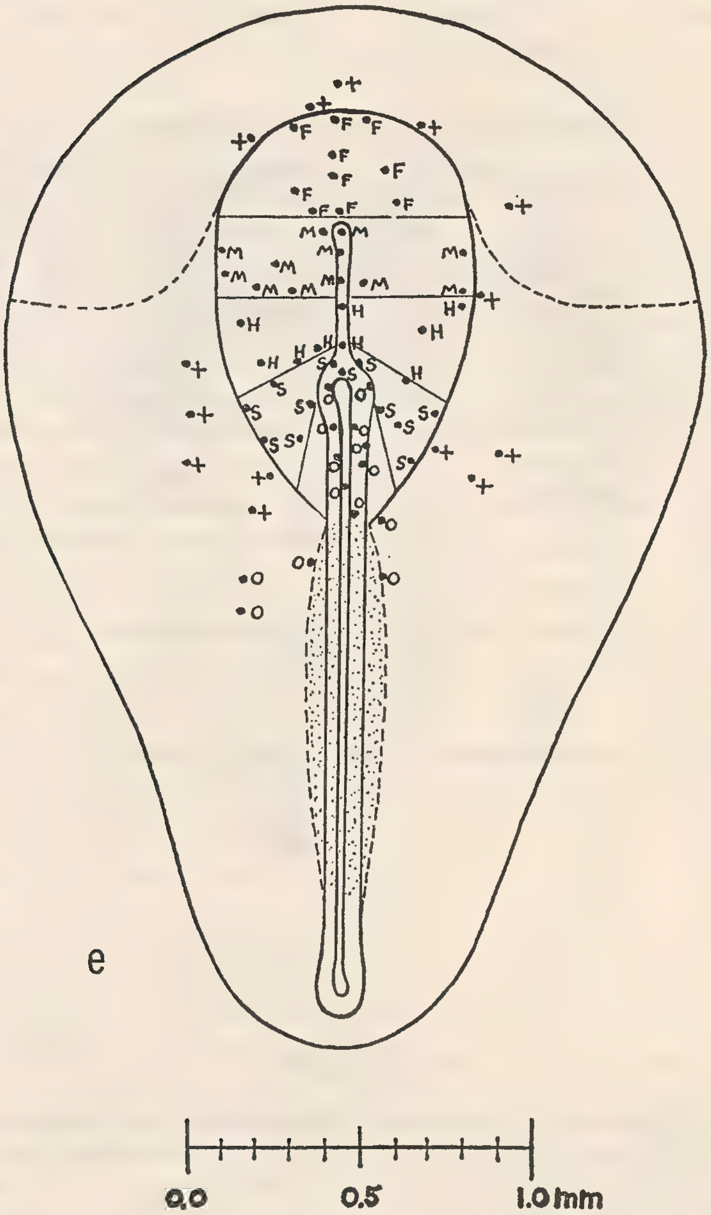

Fig. 16(e). Summary map of the pellucid area of the medium head-process blastoderm: fate of carbon marks. Spratt's (1952) Fig. 4. For code see Fig. 16(c).

maintains that the middle layer of the stage 3+ blastoderm may be primarily preextraembryonic endoderm because, at stage 3+ (1) the majority of embryonic preendoderm lies in the cephalic dorsal streak or epiblast zone *E* (Figs. 2 and 3, Plate 4, and case reports); (2) pre-*area vasculosa* mesoderm lies in caudal dorsal streak or adjacent epiblast (Figs. 2 and 5); and (3) almost the entire preembryonic mesoderm lies in epiblast preinvagination zones (Figs. 2 and 3, and case reports).

Mesoderm at head-process stages

Our knowledge of the organization of mesoderm at head-process stages has been based primarily on the indirect studies of Rawles (1936, CAM grafts). Rawles's map of mesoderm potencies—Fig. 16(f)—locates such highly differentiated mesoderm structures as muscle, mesonephros, cartilage, bone, adrenal, gonad, and spleen close to the streak, and, in more peripheral areas, heart. The present study is in general agreement with these potency areas—compare Fig. 16(f) with Fig. 12; it also allows location of an erythrocyte-vascular zone in caudolateral *area pellucida,* a localization not possible with CAM grafts because of the similarity of this tissue to the vascular tissue of the host CAM.

Endoderm at primitive-streak stages

Previous experimental work relating to the organization of the endoderm has consisted of attempts to (1) define the limits of the pregut area with marking experiments (Bellairs, 1953*b*), and (2) locate the endoderm po-

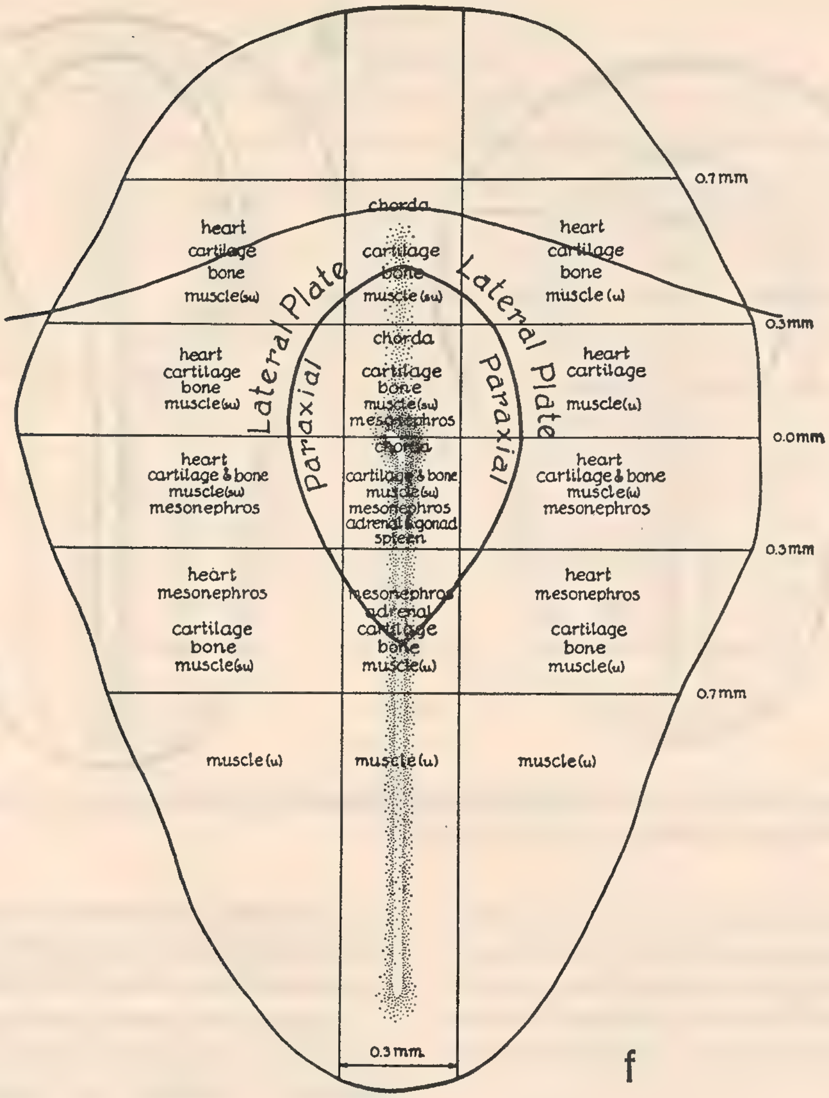

Fig. 16(f). Map showing the localization of developmental potencies of mesodermal structures in grafted pieces of the head-process blastoderm. Rawles's (1936) Fig. 8. Boundary between lateral plate and paraxial mesoderm (this study) superimposed.

tencies in various regions by the use of CAM grafts (Rudnick and Rawles, 1937; Rudnick, 1938).

Bellairs applied carbon marks to primitive-streak stages and reincubated the embryos to foregut stages (24–36 additional hours). By recording which marks were incorporated into gut, she defined the pregut area as an elongated oval surrounding Hensen's node—left side, Fig. 16(g). Bellairs's study has the following weaknesses: substaging of primitive-streak-stage embryos was not precise; the stage of fixation varied; and, though the map does not reflect it, carbon marks in a few embryos were atypical. Bellairs believed that in some instances the embryos were fixed before the marks had had time to be included in the foregut.

Rudnick and Rawles attempted to culture endodermal structures from blastoderm fragments in CAM. In this environment, the gut differentiated from 14 per cent of blastoderm fragments, which included a part of the node or its environs. These authors believed the results may have been poor because the cuts at the node interrupted the normal induction of endoderm by mesoderm.

Rudnick also attempted to grow endoderm structures from blastoderm fragments cultured in plasma clots. In this environment, full-thickness (three-layered) fragments never formed endoderm structures, though they occasionally produced epithelial layers or closed vesicles. Hypoblast grafts would not differentiate at all.

The present study, by not systematically mapping the endoderm-mesoderm layer at primitive-streak stages with the use of a grid as was done for stage 5, does not provide the details that would localize the pregut in the endoderm prior to stage 5. However, indirect information about the arrangement of cells in the epiblast is provided by study of the epiblast-dorsal streak grafts, which show that (1) all pregut endoderm, and much nongut endoderm as well, are still in

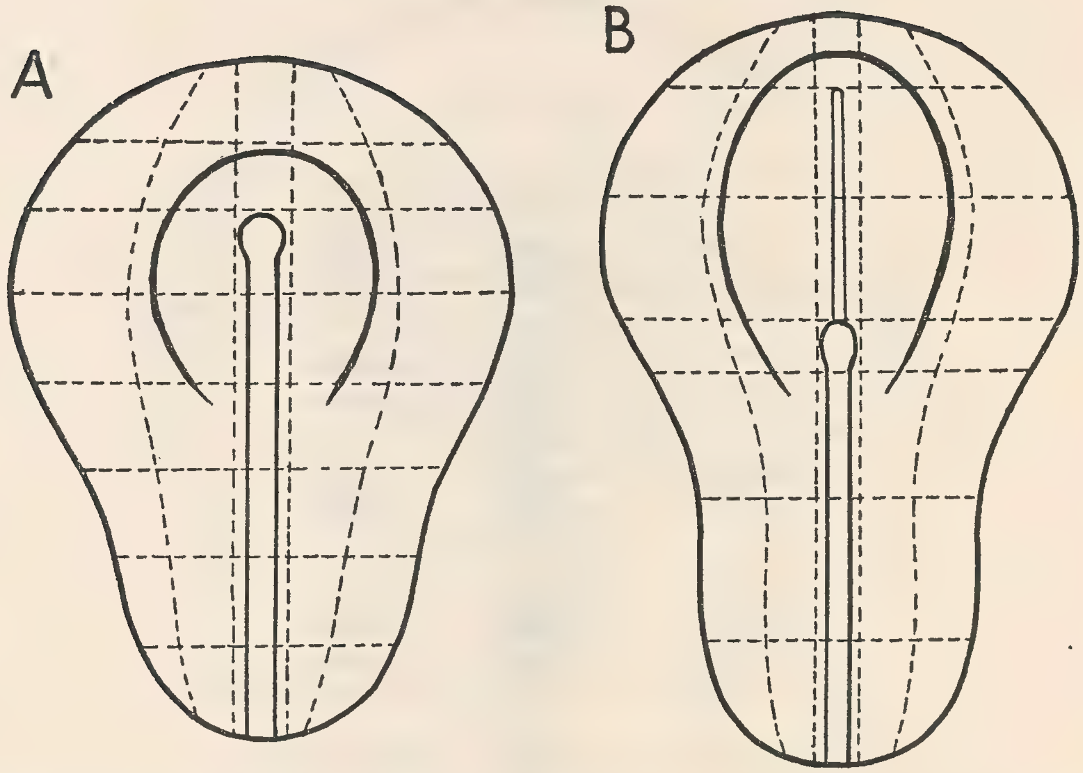

Fig. 16(*g*). The presumptive foregut area (inside curved line) indicated by carbon marking experiments: (*A*) the long-streak stage: (*B*) the head-process stage. Bellairs's (1953*b*) Fig. 5.

epiblast dorsal streak at stage 3+ (15 hours before stage 5); (2) some pregut endoderm is still in epiblast-dorsal streak at stage 4, six hours before stage 5 (Fig. 9). This implies that the endoderm at stage 3+ must be primarily nongut (peripheral *area pellucida*) endoderm.

Endoderm at stage 5

Previous investigations relating to endoderm organization at stage 5 have been attempts to define the limits of the pregut area with marking experiments (Bellairs, 1953*a*) and to locate the endoderm potencies in various regions by the use of CAM grafts (Rawles, 1936).

Bellairs marked the endoderm of long head-process-stage embryos with carbon particles. From the position of the marks at foregut stages, she constructed the map of foregut areas seen on the right in Fig. 16(g). Comparison of this figure with the presumptive foregut at stage 4 shows considerable enlargement. The cephalic margin at head-process stages is in cephalic *area pellucida;* the lateral margin extends about halfway to the *area pellucida* margin. The lengthening of this zone appears to be due to enlargement of the area cephalic to the node and to regression of the streak.

Rawles's map of endoderm potencies at head-process stages—Fig. 16(h)—shows that the following endoderm structures differentiated from CAM grafts: epithelial tubes, thyroid, liver, respiratory tract, anterior gut, stomach, and intestine. The gut and intestinal areas lie in the regions surrounding Hensen's node, which agrees with the work of Bellairs.

Though the present study outlines the pregut areas at earlier head-process stages than those studied by Rawles or Bellairs, the comparison shows excellent agreement between the three. In both the present study and Bellairs's, the *area pellucida* endoderm is divided into a nearly oval central gut zone, and a zone of yolk-sac endoderm. However, in the present study a distinction is made between endoderm destined for dorsal gut and that destined for ventrolateral gut (Fig. 18).

MOVEMENTS OF CELLS

Epiblast-ectoderm cells

Migration of primitive-streak-stage epiblast toward the streak, described in the vital dye marking experiments of Wetzel (1929), Pasteels (1937)—Fig. 16(i)—and Malan (1953), and the carbon marking experiments of Spratt (1946), was interpreted as preinvagination movements. Spratt and Haas (1965, carbon and carmine marking, vital dye staining), interpreted the migration as the physical result of rapid axial elongation of the streak, with convergence of epiblast cells into the grooves or folds beside the streak. These authors denied that the epiblast cells moved into the streak.

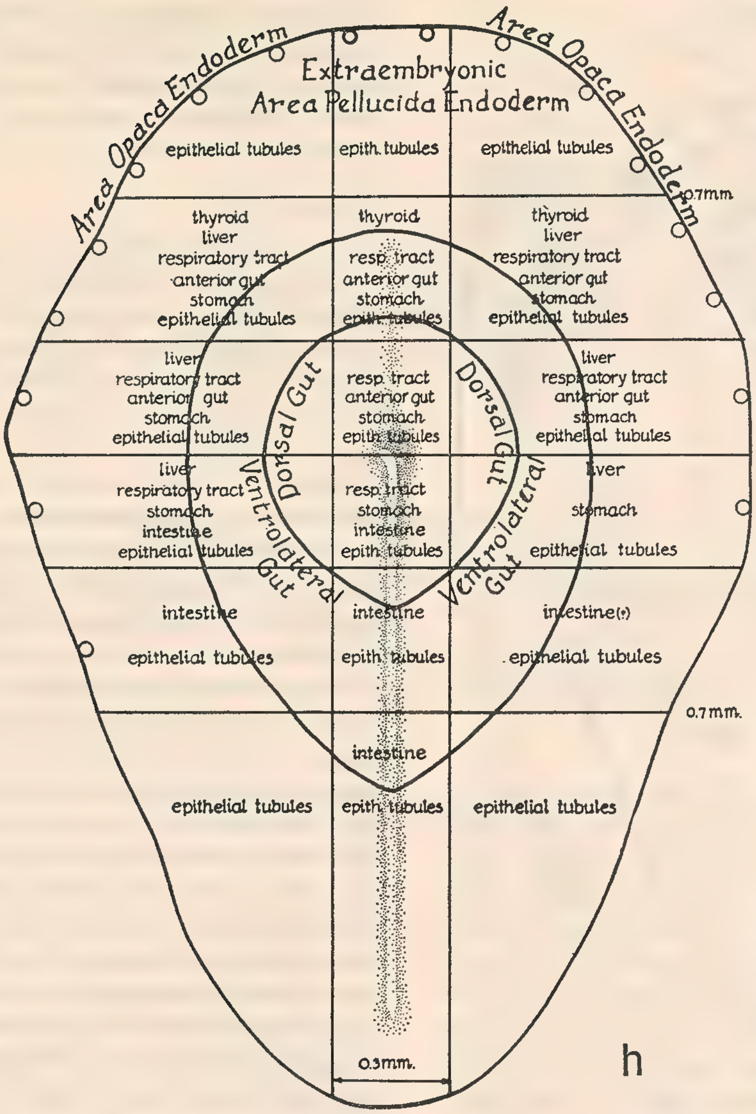

Fig. 16(h). Map showing the localization of developmental potencies of endodermal structures in grafted pieces of the head-process blastoderm. Rawles's (1936) Fig. 8. Extraembryonic, ventrolateral gut, and dorsal gut zones superimposed.

A laterocephalic movement of midline epiblast cephalic to the streak to cephalic *area pellucida* was described in the vital dye experiments of Wetzel (1929), Pasteels (1937)—Fig. 16(i)—and Malan (1953). Spratt's carbon marking experiments (1947, 1952) describe similar movements in epiblast at the definitive primitive-streak stages; but Spratt interprets them as the result of regression of the node rather than cephalic migration of cells away from the streak.

The present study agrees in finding both types of movements as described above, but not with Spratt and Haas's interpretation (see discussion of streak, p. 106), and interprets the movements to cephalic *area pellucida* as part of a generalized peripheral migration of epiblast away from the streak as spokes extend from the hub of a wheel. The direction of elongation (cephalocaudal or lateromedial) of a graft placed in peripheral epiblast depends upon its original location and the time elapsing between placement and fixation. This movement, since it takes place in peripheral regions, contradicts neither the concept of invagination at the streak nor the concept of a caudally moving streak.

Mesoderm cells

These studies have contributed to our present concepts of mesoderm movements:

1. With the use of vital dye staining, Pasteels (1937) described a cephalolateral migration of recently invaginated mesoderm, and Spratt and Haas (1965) recorded a cephalic movement of cells from the middle layer of the streak into notochord and somites.

2. By direct marking with carbon inserted into mesoderm through incisions in epiblast or endoderm, Spratt (1952) noted a cephalic movement of mesoderm lateral to the node. After reincubation, the carbon particles were distributed to somites. Le Douarin (1964), by similar methods but at slightly later stages, described a cephalic migration of prehepatic mesoderm.

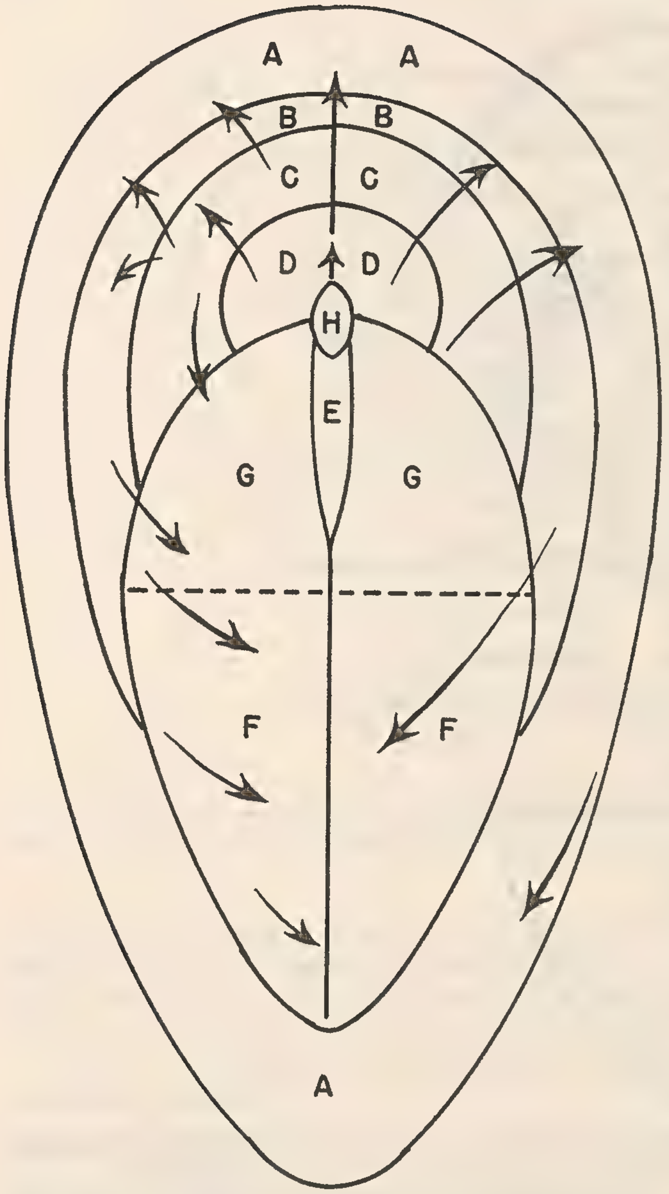

Fig. 16(i). Epiblast movements of primitive-streak-stage embryos: Vital dye staining experiments compared with those here reported, ventral view. *Left side:* arrows show direction of epiblast movements as interpreted by Wetzel (1929); *right side:* those of Pasteels (1937). Superimposed on this are the eight epiblast zones of Fig. 1(a–h). The cephalic movements represent elongation of preectoderm zones; the arrows toward streak represent movements of preendoderm-mesoderm toward the streak.

3. By using time-lapse cinematography, DeHaan (1963*b*) observed a crescent-shaped area of cells in cephalolateral *area pellucida* that moved cephalomedially into the heart.

4. In vitro migration of premyocardial mesoderm to the cephalic end of an underlying endoderm bed was described by DeHaan (1964).

The present study does not conflict with any of these findings. However, it demonstrates that (a) the movements described by Pasteels were probably those of preendoderm in addition to premesoderm; (b) the movements observed by Le Douarin and DeHaan were for splanchnic mesoderm only; and (c) mesoderm migration is not confined to cephalolateral or cephalomedial directions, but moves peripherally from the streak in all directions.

Endoderm cells

A laterocephalic migration of endoderm at primitive-streak stages was described by Pasteels (1937) and Malan (1953), using vital dye stains, and by Bellairs (1953*a*) and Spratt and Haas (1960), using carbon marks. Spratt and Haas (1960) and Bellairs (1953*b*) also described a laterocaudal movement away from the streak. Spratt and Haas (1965), using vital dye stains, described a lateral migration of endoderm from the streak into the extraembryonic endoderm underlying *area vasculosa.* The present study confirms both laterocephalic and laterocaudal movement. It also demonstrates that, at least between stages 5 and 12, endoderm cells do not move from *area pellucida* into *area opaca.*

In the course of marking the endoderm with carbon, Bellairs noted that some of the carbon marks moved to foregut with reincubation. In one experiment, the center of a horizontal carbon mark—represented as line *B–B′* in Fig. 15(a)—placed on a head-process-stage blastoderm, moved to dorsal and ventral foregut. Since points *B* and *B′* met in ventral gut—Fig. 15(b)—Bellairs assumed that all endoderm cells between them had moved obliquely backward to the midline and fused. She concluded that the cephalic end of the gut is formed as a pocket between this obliquely backward movement of lateral endoderm and a forward movement of endoderm adherent to the cephalically moving head process.

From the present study three observations may be made. (1) Points *B* and *B′*—(Fig. 15(a)—do not actually meet in ventral gut but are separated by all the cells along the AIP line. This is accomplished by a stretching and elongation of the intervening tissue. (2) Gut formation may be the result of progressive folding or invagination of pregut endoderm at the AIP. At stage 7, for example, only parts of squares 4–6 appear in the gut (innermost arched line of the left side of Fig. 18). By stage 8, part of square 5 and by stage 9 all or parts of squares 3–6 are enclosed. The outermost arched line represents the AIP line at stage 12. (3) On the other hand, after stage 9, the AIP lip may stabilize in squares 3 and 4 so that the invagination movements continue only in squares 5, 7, 9, and 11 (right side of Fig. 18). Both possibilities seem equally plausible and possible. The writer does not favor one over the other at this time.

Function and Organization of the Streak

Numerous investigators have been occupied with studies that attempt to define the function and organi-

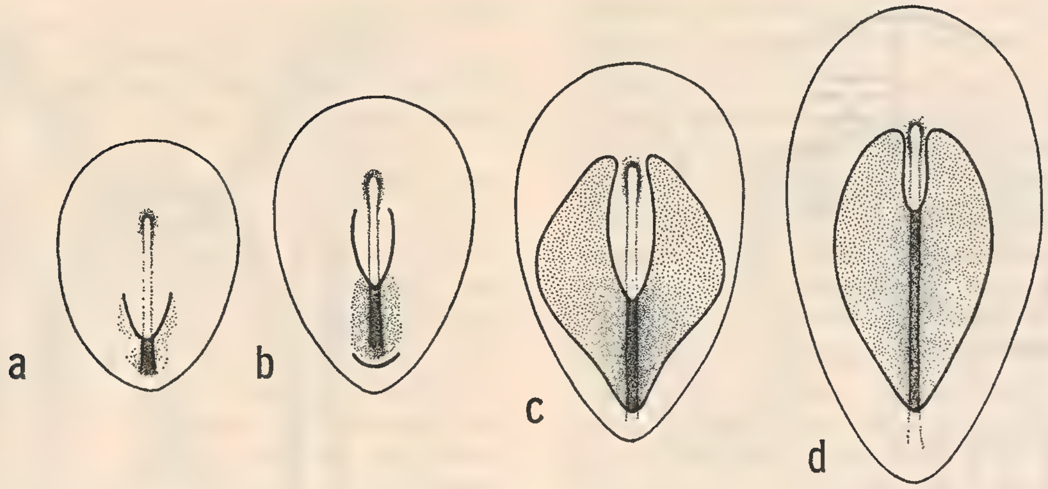

Fig. 17. Changes in the premesoderm area of epiblast-dorsal streak between stages 3+ and 4+, ventral view. (a) 18 hours prior to stage 5. Peripheral limits of premesoderm zone unmapped. Invagination area (heavy stippling) occupies one fourth to one third the length of the streak. (b) 15 hours before stage 5. Invagination area of the streak slightly longer than in (a). (c) 12 hours before stage 5. Premesoderm zone is heart-shaped, with deep indentation (light stippling: peripheral premesoderm). Premesoderm invagination zone has lengthened to include almost half the length of the streak. (d) 3 hours before stage 5 (definitive primitive-streak stage). Premesoderm zone is heart-shaped. The invagination area occupies three fourths the length of the streak. This study suggests that growth of the streak between stages 3+ and 4+ is due to increase in length of the mesoderm invagination area.

zation of the streak. Its possible role as a blastopore was suspected long before Graper (1929), Wetzel (1929), Pasteels (1937), Spratt (1947), and Malan (1953) described the epiblast-to-streak movements, and before Pasteels (1937), Malan (1953), and Hunt (1937*a*) described the streak-to-interior movements that seem to confirm this theory. Hunt cut the blastoderms where the dorsal streak had been stained and observed cell movements in the cut edge through an apposed glass surface. Though Hunt's experiments showed 3 of the 80 labeled cells observed to enter endoderm, there was always the possibility that the cut had so disturbed the organization of the chick that anomalous movements resulted.

Spratt and Haas (1965) have recently described experiments that they have interpreted as supporting the concept that the streak is a blastema. These investigators stained the layers of the streak with carmine particles and vital dye. By use of the dye they marked the center of one side of the streak at stages 2–5 and observed marked cells in ectoderm, mesoderm, and endoderm 10–24 hours later.

However, to prove that the streak was a blastema, Spratt and Haas needed to demonstrate that (1) neither epiblast, middle, nor ventral layer cells moved into the streak, and (2) cells moved from the streak into ectoderm, mesoderm, and endoderm. Their experiments fail to do this. In fact, the authors imply that some cells may have joined the streak, by their statement that "None of our experiments show any *pronounced* morphogenetic (i.e., gastrulation type) movements in the uppermost layer of unincubated blastoderms" (italics author's); and their statements about streak cells joining ectoderm are equally vague: cells were found at 10–24 hours of reincubation in "ectodermal derivatives of the embryo's body" (type and location of derivative and stage at which found are not mentioned). They did demonstrate that streak cells moved to axial mesoderm (notochord and somites) but only prior to stages 2–4. There was no evidence that streak cells contributed to *area vasculosa*. Their experiments indicated movement to endoderm, but only before stage 4 and only to extraembryonic areas underlying the *area vasculosa*.

On the other hand, the experiments here reported show that there is movement of epiblast toward the streak, invagination at the streak, and subsequent migration to both homolateral and heterolateral mesoderm, movements that are not compatible with the concept that the streak is a blastema but are compatible with the traditional view that the streak is a type of blastopore. These three conditions are described in the following paragraphs.

Movement of epiblast to streak was seen on numerous occasions (Plates 4, 8, and 9). In fact, this study suggests that growth of the streak between stages 3+ and 5 results from increasing movements of the epiblast to the streak with a resulting increase in length of the premesoderm invagination center (Fig. 17). These movements to the streak are known to continue until at least the 15-somite stage (Fig. 10).

Invagination at the streak was seen on numerous occasions (Plate 9). Its results were demonstrated in every unilaterally placed graft to premesoderm or pre-

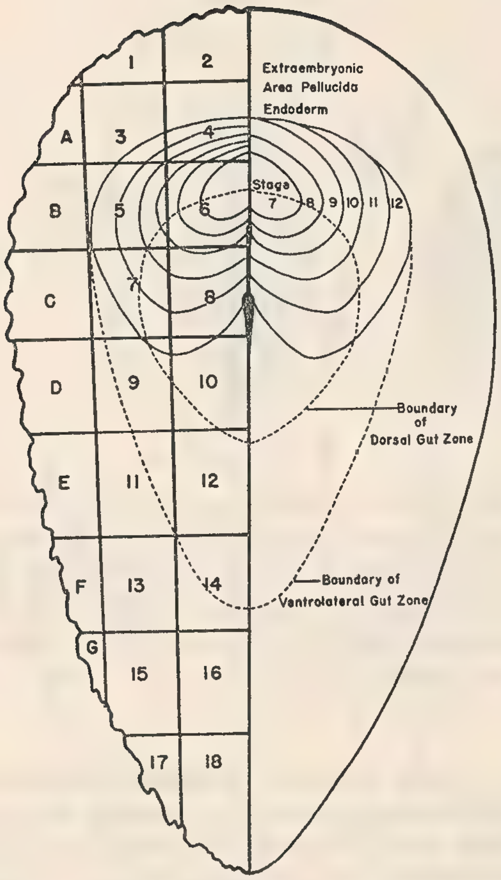
1
2
Extraembryonic Area Pellucida Endoderm
A
3
4
B
5
6
Stage 7
8
9
10
11
12
C
7
8
D
9
10
Boundary of Dorsal Gut Zone
E
11
12
F
13
14
Boundary of Ventrolateral Gut Zone
G
15
16
17
18

Fig. 18. Formation of the gut from the head-process-stage endoderm, ventral view. *Left side:* Superimposed on the 25 squares (see text p. 74 and Fig. 13) are six arches (solid lines). The innermost arch encloses the area of the stage 5 endoderm present in the gut at stage 7. The outermost arch encloses the endoderm present in the gut at stage 12. A progressive invagination of concentric rings of endoderm appears to have taken place. *Right side:* Alternative explanation: at about stage 9, the AIP becomes fixed in squares 3 and 4 so that folding ceases cephalically but continues laterally. The interrupted lines subdivide the stage 5 pregut endoderm into two zones: an outer ventrolateral and an inner dorsal gut zone. The AIP lines are comparable to the sections of the gut shown in Fig. 14(a–e).

endoderm zones; invagination at the primitive groove at the cephalic end of the streak is suggested by a study of the prenotochord zone at nine hours before stage 5 (Fig. 8 and Table 3), but invagination at the caudal end of the streak is suggested on several other occasions, including embryo 3 of Fig. 10(a), also described in Results at 3 hours before stage 5.

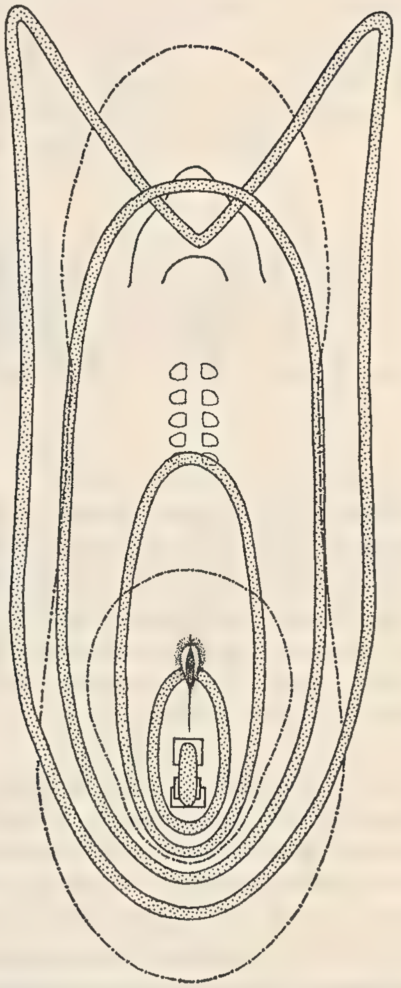

Fig. 19. Mesoderm movements between stages 3+ and 8–9, ventral view, a diagrammatic combination of Fig. 5(a), 15 hours before stage 5, and 5(b), stages 8–9 blastoderm. The cephalic end of the streak is identical for both embryos. Graft sites in the stage 3+ embryo are identical with grafts 1–4 in Fig. 5(a). The inner oval stippled zone at the streak represents the premesoderm invagination zone at stage 3+. After invagination, cells from this area spread out between endoderm and ectoderm as larger and larger ovals. The largest oval represents the distribution at stages 8–9. The midline cephalic arch has folded caudoventrally into endocardium and ventral mesentery. The wider spaces between loops cephalic to the node compared with the narrow spaces caudal to the streak may be the result of regression of the streak.

Migration of endoderm and mesoderm from the streak was observed on numerous occasions both in the epiblast-dorsal streak and the endoderm-mesoderm grafts (Plate 4, grafts 1 and 2; and Plate 12).

SUMMARY

The morphogenesis of the primitive-streak stage and the head-process stage of the chick embryo was studied by grafting tritiated thymidine labeled tissue squares to homologous sites in similarly staged recipient embryos (Plates 1, 2, and 3). Systematic reconstruction of radioautographed sections of these embryos after reincubation up to and including H-H stage 12 demonstrated that cells from the grafts participated normally in the morphogenetic movements of the host embryos. The reconstructions and operating diagrams have made

possible reliable maps of movements between stages 3+ and 12 (Figs. 1, 11, 12, 13, 15, and 18).

The following areas have been located in epiblast between stages 3+ and 5: preectoderm, preendoderm, premesoderm, and prenotochord—Fig. 1(a–c).

Preectoderm is located in peripheral epiblast, enclosing the epiblast zones that will be invaginated; see Fig. 1(d–k). Preectoderm near premesoderm is pulled toward the streak; that located peripherally and in areas surrounding Hensen's node moves peripherally. Preectoderm is folded into neural tube, epithelium covering head and trunk, and extraembryonic ectoderm, including proamnion. Movements are essentially as found by previous workers, who had used vital stains.

The most surprising discovery in the primitive-streak-stage embryo was a preendoderm zone (Fig. 1, zone *E*) in central epiblast. As cells from this zone enter the streak, they mix with cells from the opposite side when these descend ventrally and migrate into the endoderm layer (Plate 4). This study suggests that at stage 3+ nearly all the invaginated cells of the embryo will come to lie in the endoderm.

The premesoderm areas (Fig. 1, zones *F* and *G*) are located in epiblast caudolateral to the preendoderm area. Although at stage 3+ premesoderm has contact with the streak at only its caudal end, at stage 4 increasingly larger areas of premesoderm have access to the streak, where the premesoderm cells mix with cells from the opposite epiblast, descend ventrally, and migrate into the mesoderm of both right and left sides (Plate 9). Since grafts to the streak do not remain in the streak, nor do those entering it from lateral epiblast, the streak is not a blastema, but a modified blastopore. The most caudomedial parts of the premesoderm zone are the first to invaginate (Figs. 5, 19). The most peripheral parts are the last to invaginate (Fig. 10). The cephalic ends of the zone contain preparaxial mesoderm; the caudal ends, prelateral plate mesoderm. The boundary between the two ends is the nephrotome.

The prenotochord zone is located at Hensen's node. This study suggests that cells from this zone invaginate at the cephalic end of the streak (Fig. 8).

Mesoderm moves between endoderm and ectoderm, contributing cells to the endocardium, the head and paraxial mesoderm cephalically, the *area vasculosa* and heart laterally, and the *area vasculosa* caudally (Fig. 5). The amniocardiac vesicles are formed when the lateral plate separates into somatic and splanchnic layers. The dorsal or somatic layer continues to migrate into the *area opaca,* while the splanchnic layer is pulled in a relatively caudomedial direction, where it contributes to the mesocardia and heart (Plate 12). The alae of the *area vasculosa* result from mediocephalic rotation of the *area vasculosa* cephalic to the head.

After invagination, the endoderm moves peripherally, independently of the mesoderm. At H-H stage 6, the endoderm halfway between Hensen's node and the cephalic end of the *area pellucida* begins to fold, initiating foregut formation. The surrounding endoderm is stretched and elongated in preparation for progressive invagination. By stage 12, an oval area of endoderm has been enclosed in the gut. The margins of the oval are compressed into the AIP, where they form the thickened ventral wall of the foregut (Figs. 14, 15).

Besides confirming in unequivocal fashion the invaginating movements that had been ascertained with vital dye staining and carbon marking methods by previous investigators, this method has permitted the movements of large areas of epiblast to be traced into the streak, where they descend ventrally and are distributed bilaterally in the endoderm and mesoderm.

ACKNOWLEDGMENTS

The author wishes to acknowledge the technical assistance of William R. Duncan, Leo A. Kormann, Ellen Legum, and Isabelle Williams. Thanks go to James Ebert, Robert DeHaan, and Mary Rawles for their interest in this work, and special appreciation to Dorothea Rudnick for her comments and criticisms during the preparation of the manuscript. The author is a National Institutes of Health Postdoctoral Fellow (National Heart Institute Fellowship No. 2-F2-HE-20, 074-02).

LITERATURE CITED

Abercrombie, M., and G. Causey. 1950. Identification of transplanted tissues in chick embryos by marking with phosphorus-32. *Nature, 166,* 229–230.

Balinsky, B. I., and H. Walther. 1961. The migration of presumptive mesoblast from the primitive streak of the chick as studied with the electron microscope. *Acta Embryol. Morphol. Exptl., 4,* 261–283.

Bellairs, R. 1953*a*. Studies on the development of the foregut in the chick blastoderm. 1. The presumptive foregut area. *J. Embryol. Exptl. Morphol., 1,* 115–124.

Bellairs, R. 1953*b*. Studies on the development of the foregut in the chick blastoderm. 2. The morphogenetic movements. *J. Embryol. Exptl. Morphol., 1,* 369–385.

Butler, E. 1935. The developmental capacity of regions of the unincubated chick blastoderm as tested in chorioallantoic grafts. *J. Exptl. Zool., 70,* 357–389.

Clarke, L. F. 1936. Regional differences in eye-forming capacity of the early chick blastoderm as studied in chorioallantoic grafts. *Physiol. Zool., 9,* 102–128.

DeHaan, R. L. 1963*a.* Regional organization of pre-pacemaker cells in the cardiac primordia of the early chick embryo. *J. Embryol. Exptl. Morphol., 11,* 65–75.

DeHaan, R. L. 1963*b.* Migration patterns of the precardiac mesoderm in the early chick embryo. *Exptl. Cell Res., 29,* 544–560.

DeHaan, R. L. 1964. Cell interactions and oriented movements during development. *J. Exptl. Zool., 157,* 127–138.

Elias, S., and S. Sandor. 1965. A biostatistical study of the early morphogenesis of the chick embryo and its appendages. *Rev. Roumaine Embriol. Cytol., 2,* 115–159.

Fraser, R. C. 1954. Studies on the hypoblast of the young chick embryo. *J. Exptl. Zool., 126,* 349–400.

Graper, L. 1929. Die Primitiventwicklung des Hühnchens nach stereokinematographischen Untersuchungen, kontrolliert durch vitale Farbmarkierung und Verglichen mit der Entwicklung anderer Wirbeltiere. *Arch. Entwicklungsmech. Organ. (Berlin), 116,* 382–429.

Hamburger, V., and H. L. Hamilton. 1951. A series of normal stages in the development of the chick embryo. *J. Morphol., 88,* 49–92.

Hunt, T. E. 1932. Potencies of transverse levels of the chick blastoderm in the definitive streak stage. *Anat. Record, 55,* 41–69.

Hunt, T. E. 1937*a.* The development of gut and its derivatives from the mesectoderm and mesentoderm of early chick blastoderms. *Anat. Record, 68,* 349–363.

Hunt, T. E. 1937*b.* The origin of entodermal cells from the primitive streak of the chick embryo. *Anat. Record, 68,* 449–460.

Le Douarin, N. 1964. Étude expérimentale de l'organogenèse du tube digestif et du foie chez l'embryon de poulet. *Bull. Biol. France Belg., 98,* 544–676.

Malan, M. E. 1953. The elongation of the primitive streak and the localization of the presumptive chordamesoderm on the early chick blastoderm studied by means of colored marks with nile blue sulphate. *Arch. Biol., 64,* 149–188.

Messier, B., and C. P. LeBlond. 1957. Preparation of coated radioautographs by dipping sections in fluid emulsion. *Proc. Soc. Exptl. Biol. Med., 96,* 7–10.

New, D. A. T. 1955. A new technique for the culture of the chick embryo in vitro. *J. Embryol. Exptl. Morphol., 3,* 326–331.

Pasteels, J. 1937. Études sur la gastrulation des vertèbres meroblastiques. III. Oiseaux. *Arch. Biol. (Paris), 48,* 381–488.

Rawles, M. E. 1936. A study in the localization of organ-forming areas of the chick blastoderm of the head process stage. *J. Exptl. Zool., 72,* 271–315.

Rawles, M. E. 1943. The heart-forming areas of the early chick blastoderm. *Physiol. Zool., 16,* 22–42.

Rawles, M. E. 1952. Transplantation of normal embryonic tissues. *Ann. N. Y. Acad. Sci., 55,* 302–312.

Rosenquist, G. C., and R. L. DeHaan. 1966. Migration of precardiac cells in the chick embryo: a radioautographic study. *Carnegie Inst. Wash., Publ.* 625, *Contrib. Embryol.,* this volume, 111–121.

Rudnick, D. 1932. Thyroid forming potencies of the early chick blastoderm. *J. Exptl. Zool., 62,* 287–317.

Rudnick, D. 1935. Regional restriction of potencies in the chick during embryogenesis. *J. Exptl. Zool., 71,* 83–99.

Rudnick, D. 1938. Differentiation in culture of pieces of the early chick blastoderm. *Anat. Record, 70,* 351–368.

Rudnick, D. 1944. Early history and mechanics of the chick blastoderm. *Quart. Rev. Biol., 19,* 187–212.

Rudnick, D. 1948. Prospective areas and differentiation potencies in the chick blastoderm. *Ann. N. Y. Acad. Sci., 49,* 761–772.

Rudnick, D. 1955. Teleosts and birds. In *Analysis of Development.* B. H. Willier, P. A. Weiss, and V. Hamburger, eds., W. B. Saunders Co., Philadelphia, pp. 297–314.

Rudnick, D., and M. E. Rawles. 1937. Differentiation of the gut in chorioallantoic grafts from chick blastoderms. *Physiol. Zool., 10,* 381–395.

Sirlin, J. L. 1956. Tracing morphogenetic movements by means of labeled cells. *Arch. Entwicklungsmech. Organ. (Berlin), 148,* 489–493.

Spratt, N. T., Jr. 1946. Formation of the primitive streak in the explanted chick blastoderm marked with carbon particles. *J. Exptl. Zool., 103,* 259–304.

Spratt, N. T., Jr. 1947. Regression and shortening of the primitive streak in the experimental chick blastoderm. *J. Exptl. Zool., 104,* 69–100.

Spratt, N. T., Jr. 1952. Localization of the prospective neural plate in the early chick blastoderm. *J. Exptl. Zool., 120,* 109–130.

Spratt, N. T., Jr. 1955. Analysis of the organizer center in the early chick embryo. I. Localization of prospective notochord and somite cells. *J. Exptl. Zool., 128,* 121–164.

Spratt, N. T., Jr. 1957. Analysis of the organizer center in the early chick embryo. II. Studies of the mechanics of notochord elongation and somite formation. *J. Exptl. Zool., 134,* 577–612.

Spratt, N. T., Jr., and H. Haas. 1960. Morphogenetic movements in the lower surface of the unincubated and early chick blastoderm. *J. Exptl. Zool., 144,* 139–157.

Spratt, N. T., Jr., and H. Haas. 1965. Germ layer formation and the role of the primitive streak in the explanted chick. I. Basic architecture and morphogenetic tissue movements. *J. Exptl. Zool., 158,* 9–37.

Vakaet, L. 1962. Some new data concerning the formation of the definitive endoblast in the chick embryo. *J. Embryol. Exptl. Morphol., 10,* 38–57.

Waddington, C. H. 1932. Experiments on the development of chick and duck embryos cultivated in vitro. *Phil. Trans. Roy. Soc. London, Ser. B., 221,* 179–230.

Weston, J. 1963. A radioautographic analysis of the migration and localization of trunk neural crest cells in the chick. *Develop. Biol., 6,* 279–310.

Wetzel, R. 1929. Untersuchungen am Hühnchen. Die Entwicklung des Keims wahrend der erste beidern Bruttage. *Arch. Entwicklungsmech. Organ. (Berlin), 119,* 188–321.

PLATES

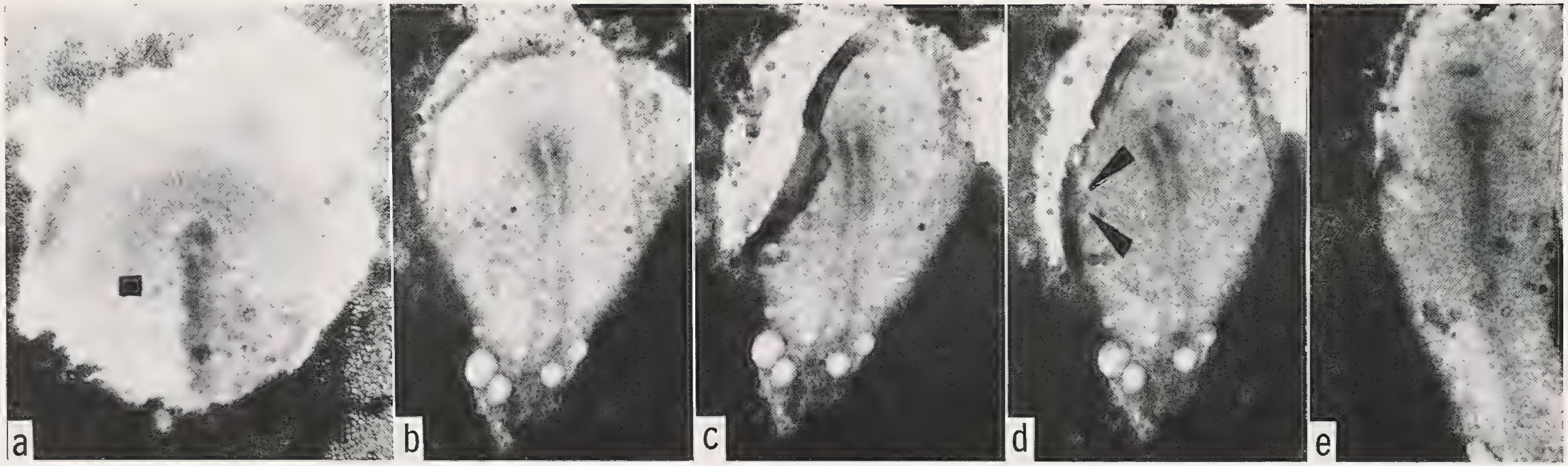

Photographs by Richard D. Grill

PLATE 1

Epiblast-dorsal streak grafting technique. (a) Donor embryo, ventral surface. Endoderm-mesoderm of *area pellucida* and adjacent *area opaca* has been removed; the site of tissue to be removed for grafting is shown in black. (b) Ventral surface of the recipient blastoderm before (c) endoderm-mesoderm flap is folded toward the streak in preparation for grafting. (d) After the homologous donor square of epiblast is inserted, the endoderm-mesoderm flap is replaced. Graft is still visible (arrows) dorsal to reexpanding endoderm-mesoderm flap. (e) At four hours of reincubation, graft site is no longer visible.

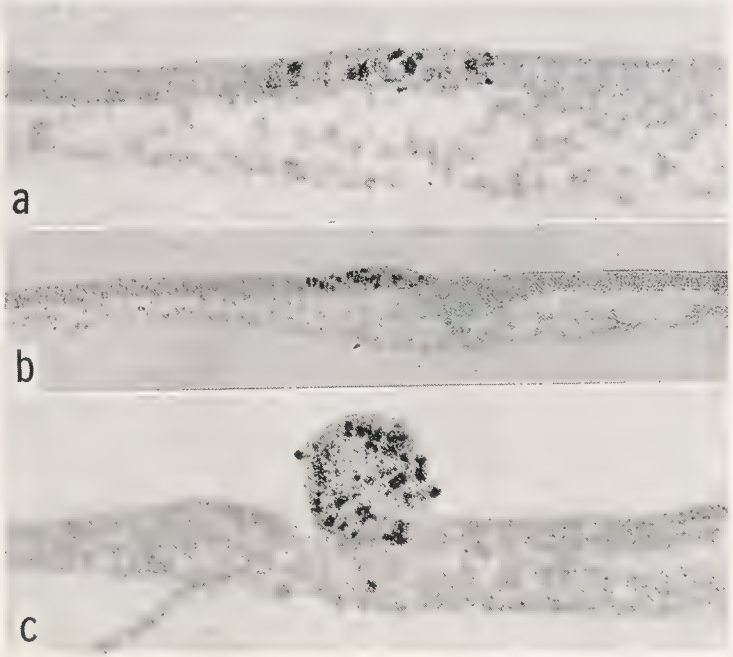

PLATE 2

Healing of epiblast grafts, ventral views. Graft to zone *F*—labeling time, 3 hours; estimated labeling $3\frac{3}{4}$ hours later, 60–80%. (a) Radioautographed section, ×200, of caudal end of the graft. Healing was complete; no irregularities were noted. (b) Radioautographed section, ×100, of a more cephalic end of the graft; slight irregularity in epiblast but all edges well healed. (c) Radioautographed section, ×200, of a second graft to zone *F*—labeling time, 3 hours; estimated labeling $3\frac{3}{4}$ hours later, 60–80%. The irregularity seen was an exaggeration of the improper healing noted in (b); here, a part of the graft extended dorsally from the epiblast; the graft, however, has migrated to the streak at the normal rate, carrying the unhealed portion with it, an abnormality that might not be observed in the gross preparation. (These embryos are not described in the case reports in text.)

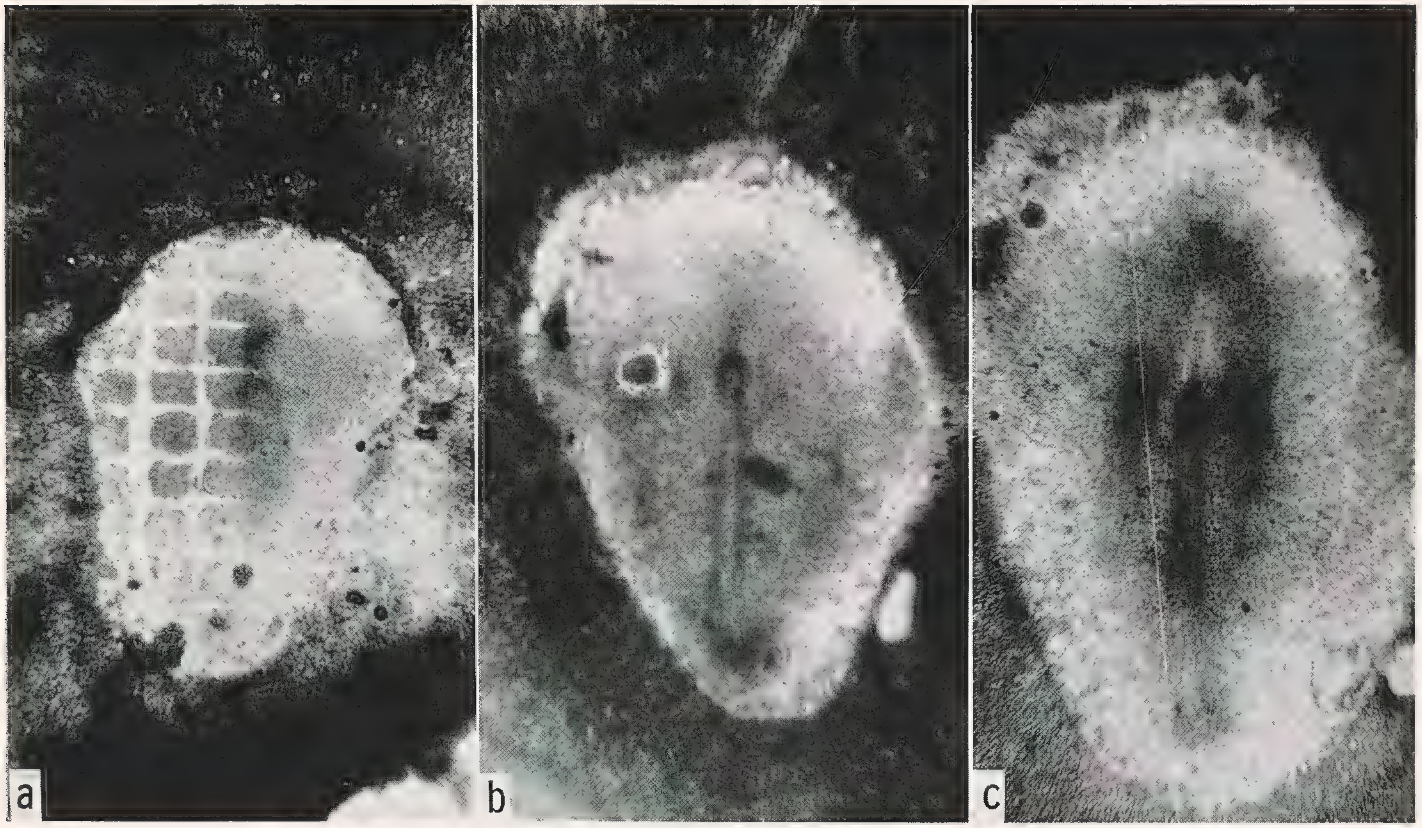

PLATE 3

Endoderm-mesoderm grafting technique, ventral views. (a) Donor embryo (stage 5) in which endoderm-mesoderm of right half is divided into 25 squares. (b) Recipient embryo also at stage 5. Square 7, seen in Figs. 11(a), 13(a), has been removed from the donor and placed in the homologous site in the recipient. (c) Same embryo two hours later (stage 6−). The edges of the graft have reexpanded to meet the endoderm-mesoderm of the recipient; graft site is no longer visible.

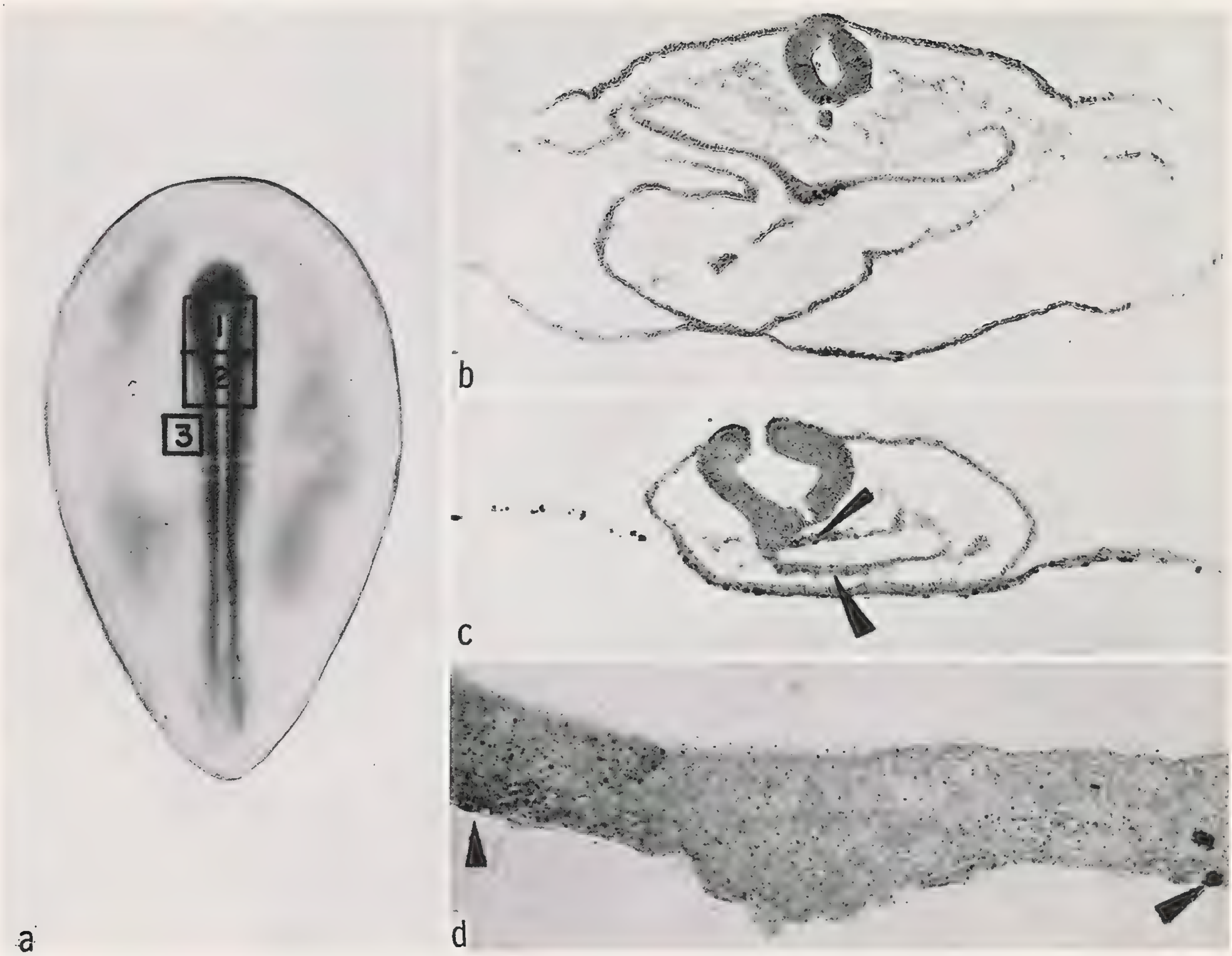

PLATE 4

(a) Three grafts to preendoderm zone *E,* ventral view. Graft 1, placed at the cephalic tip of the streak nine hours before stage 5, contributed labeled cells to midline ventral gut, and yolk sac and ventral neural tube as illustrated in the radioautographed section (b), ×100—labeling time, 2½ hours; estimated labeling 27 hours later, at the 12-somite stage, 30% (described on p. 88). Graft 2, placed in the midline streak, just caudal to the node at 16 hours before stage 5, contributed cells to ventral neural tube, notochord and paraxial mesoderm, and yolk-sac and gut endoderm. The labeled cells in yolk-sac and dorsoventral gut endoderm (arrows) are illustrated in the radioautographed section (c), ×100—labeling time, 2½ hours; estimated labeling 27 hours later, at the 5-somite stage: neural tube and endoderm, 60%; notochord and mesoderm, 10% (described on p. 83). Graft 3, placed in right epiblast adjacent to the streak 15 hours before stage 5, contributed cells to endoderm on both right and left sides of the streak, as illustrated in the radioautographed section (d), ×400—labeling time, 3 hours; estimated labeling 18½ hours later, at stage 6—: right endoderm and mesoderm, 20–30%; left endoderm and mesoderm, 5–10% (described on p. 83).

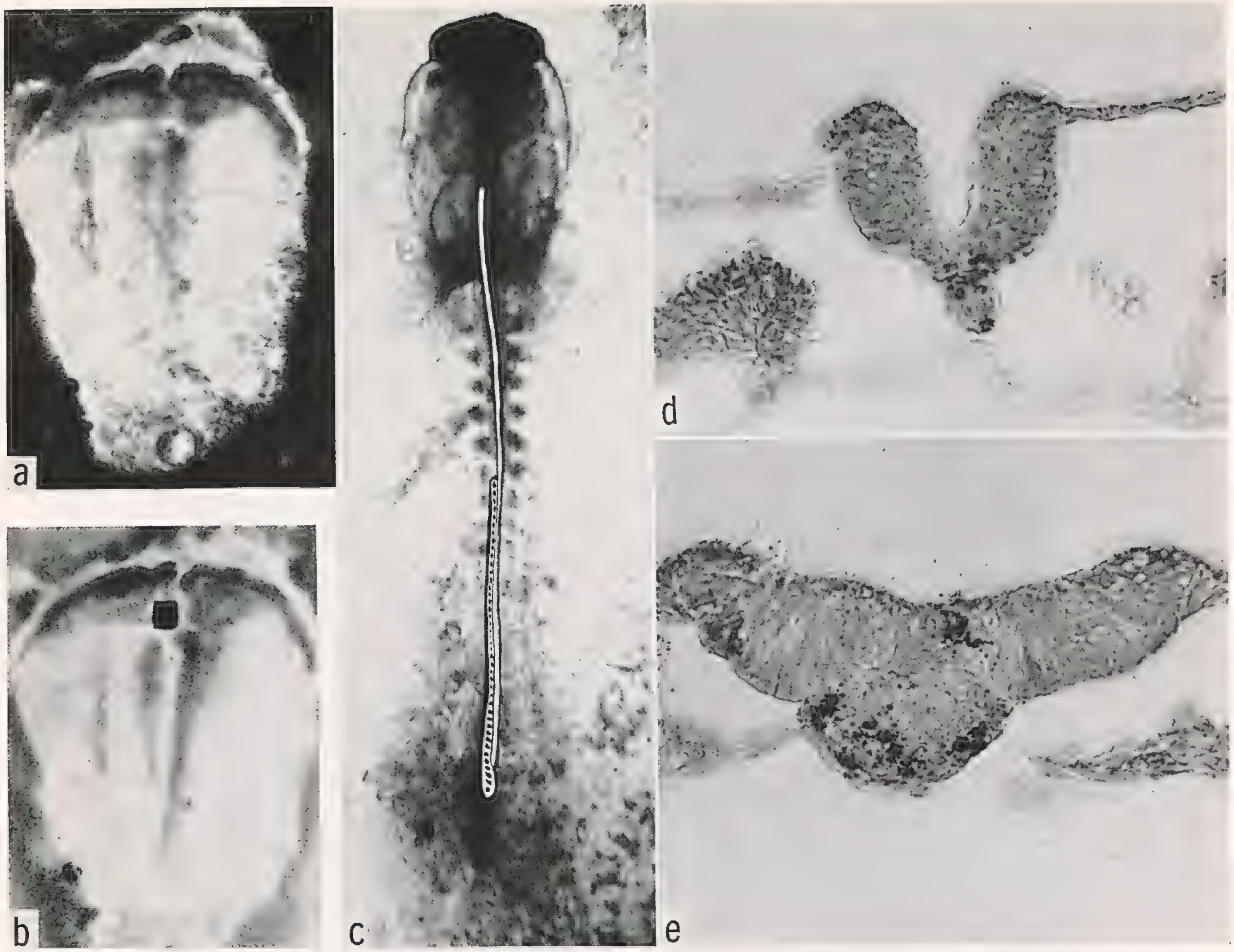

PLATE 5

Epiblast graft to prenotochord and preventral neural tube zones, ventral views. (Embryo described on p. 86.) (a) and (b) Donor square is visible behind reexpanding endoderm-mesoderm flap. (c) At time of fixing 27 hours later. The distribution of labeled notochord cells is indicated in diagonal pattern extending from somite region into bulb; labeled ventral neural tube cells in white outline.

Radioautographed sections, ×500, (d) 0.8 mm and (e) 1.8 mm caudal to the AIP, to show labeled notochord and ventral neural tube cells.

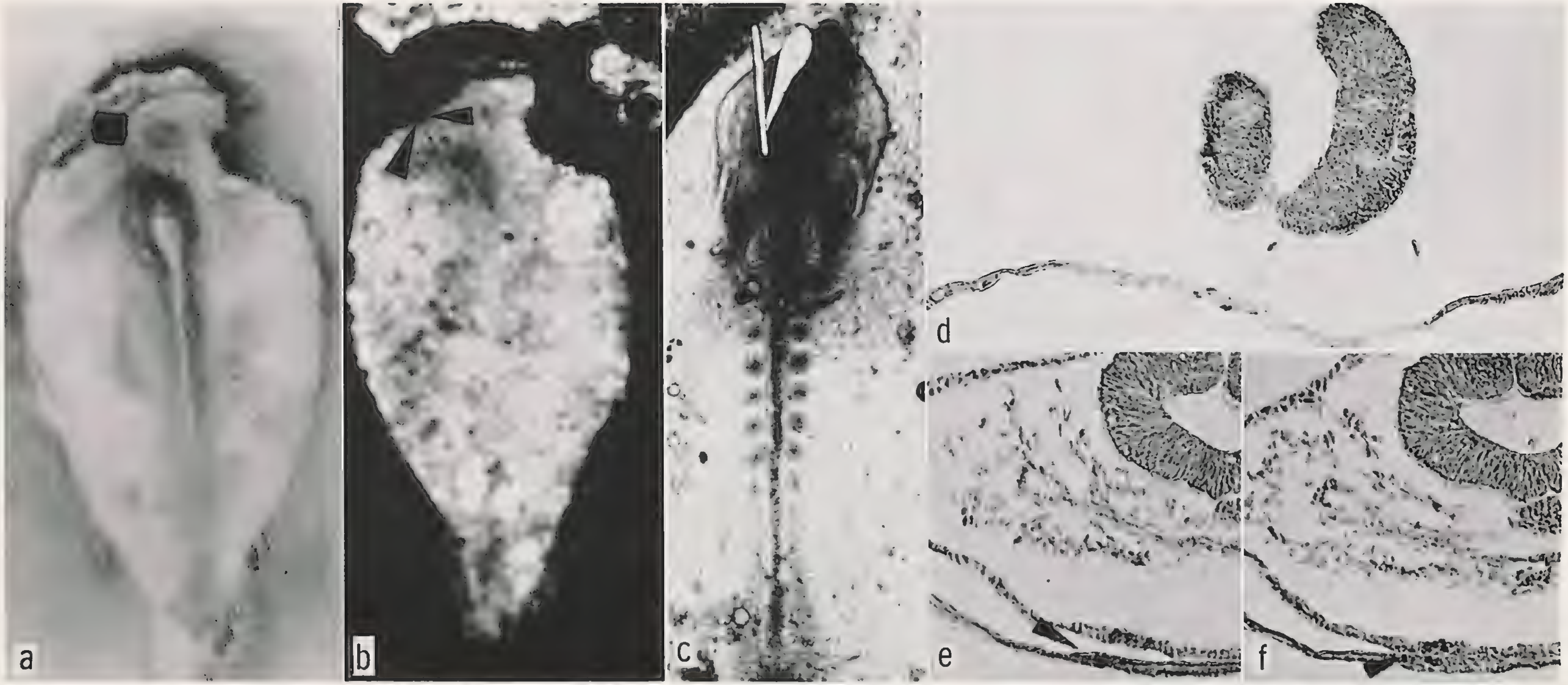

PLATE 6

Epiblast graft straddling preextraembryonic and preepidermal ectoderm zones, ventral views. (Embryo described on p. 87.) (a) and (b) Grafted embryo before reincubation. The donor square dorsal to reexpanding endoderm-mesoderm flap is indicated by arrows. (c) Before fixing 20 hours later, labeled cells distributed to regions outlined in white.

Radioautographed sections, ×200: (d) At anterior neuropore. (e) Section near head fold. Labeled epithelial cells are distributed to the ventral side of the head and also in the dorsal layer of the yolk sac. (f) Section through head fold. Cells in extraembryonic ectoderm areas are marked with arrows.

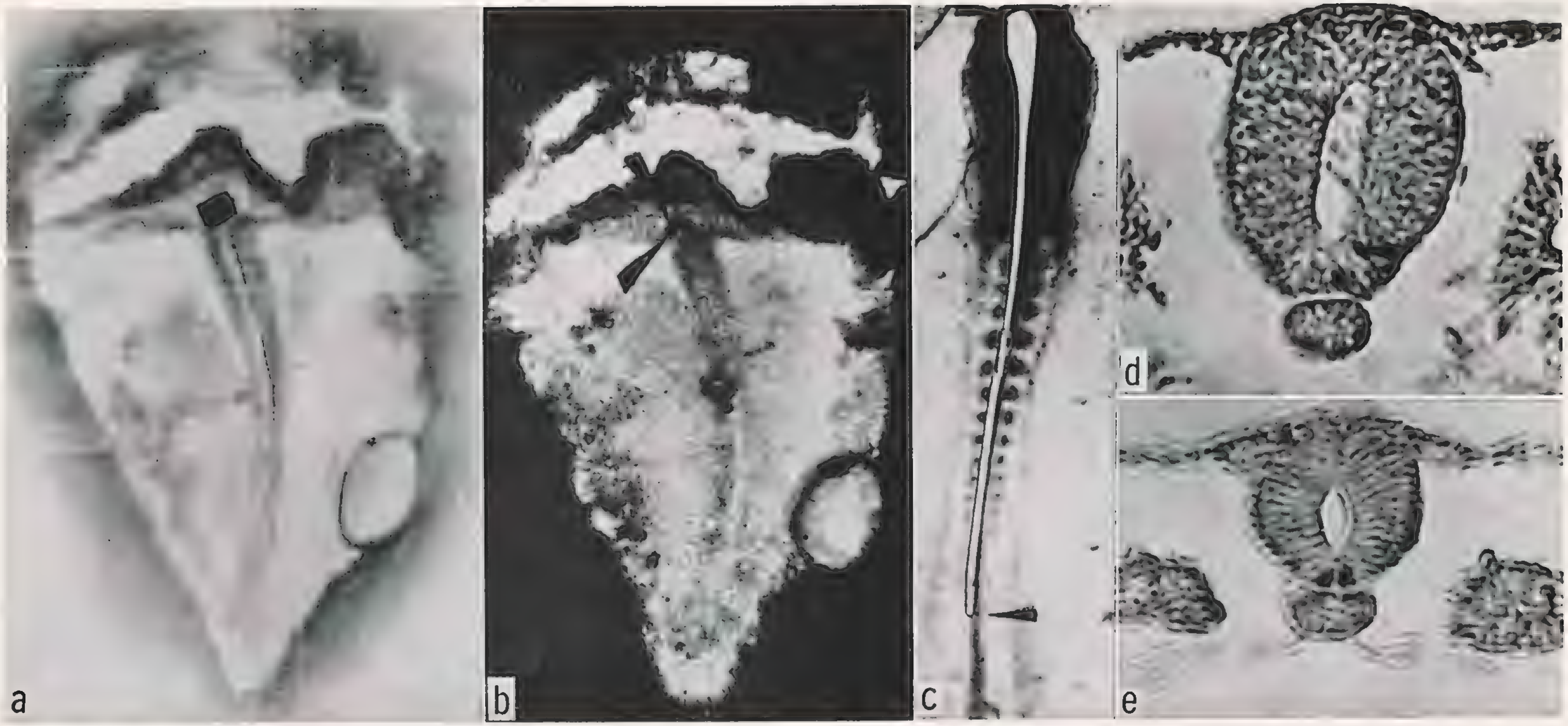

PLATE 7

Epiblast graft to preventral neural tube zone, ventral view. (Embryo described on p. 87.) (a) and (b) Grafted embryo before reincubation. The labeled donor square dorsal to reexpanding endoderm-mesoderm is indicated by arrows. (c) Before fixing 26 hours later (retouched photograph). Clear area shows general distribution of labeled cells in ventral neural tube.

Radioautographed sections, ×300, (d) at level of AIP, and (e) at level of last somite.

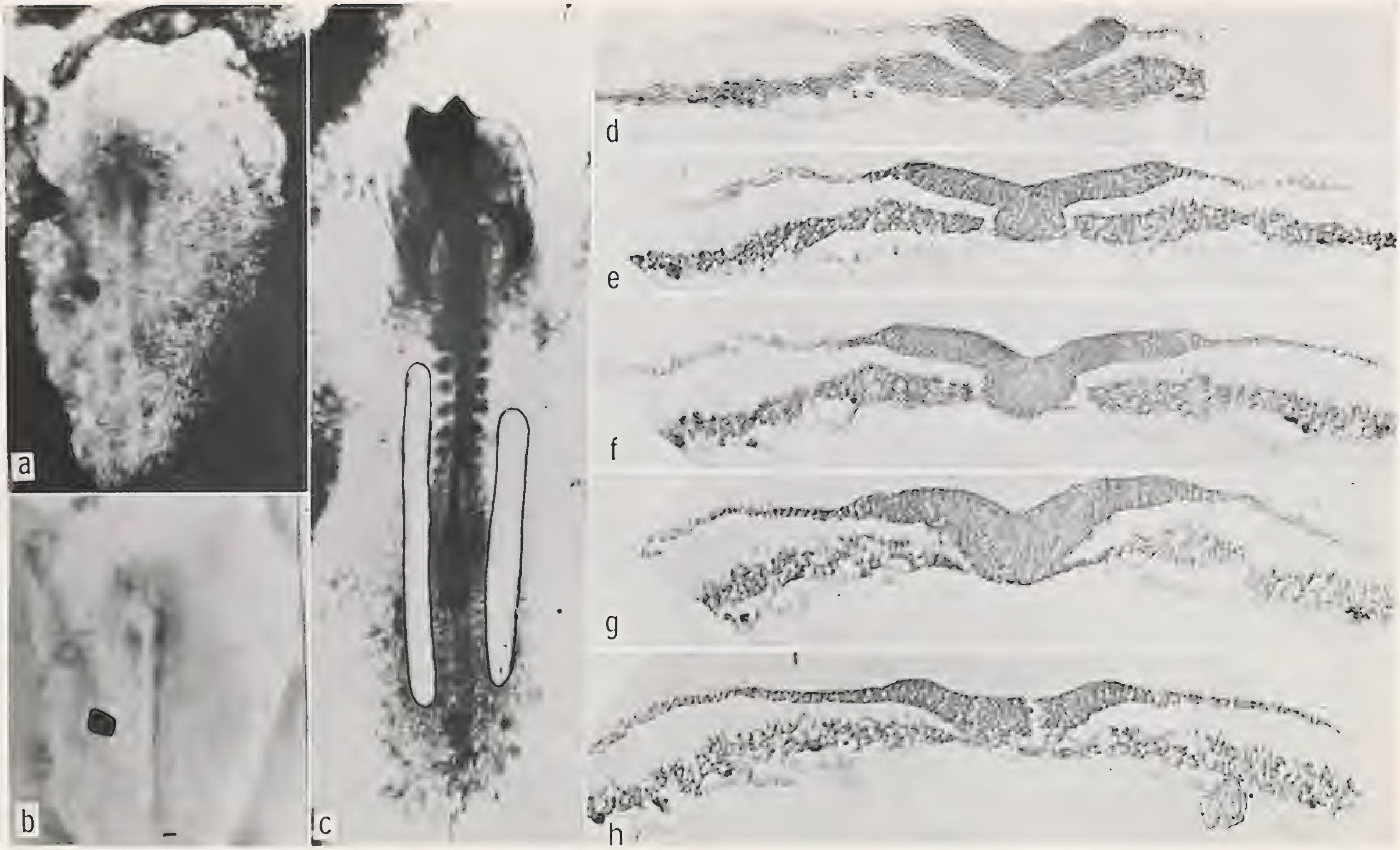

PLATE 8

Graft to prelateral plate mesoderm zone of epiblast, ventral view. (Embryo described on p. 88.) (a) and (b) Embryo after placement of graft, which is just visible behind reexpanding endoderm-mesoderm flap. (c) At time of fixing 20 hours later. The bilateral distribution of this mesoderm in lateral plate regions is shown by the white outline over photograph, which also indicates the levels of radioautographed sections (d–h), ×200.

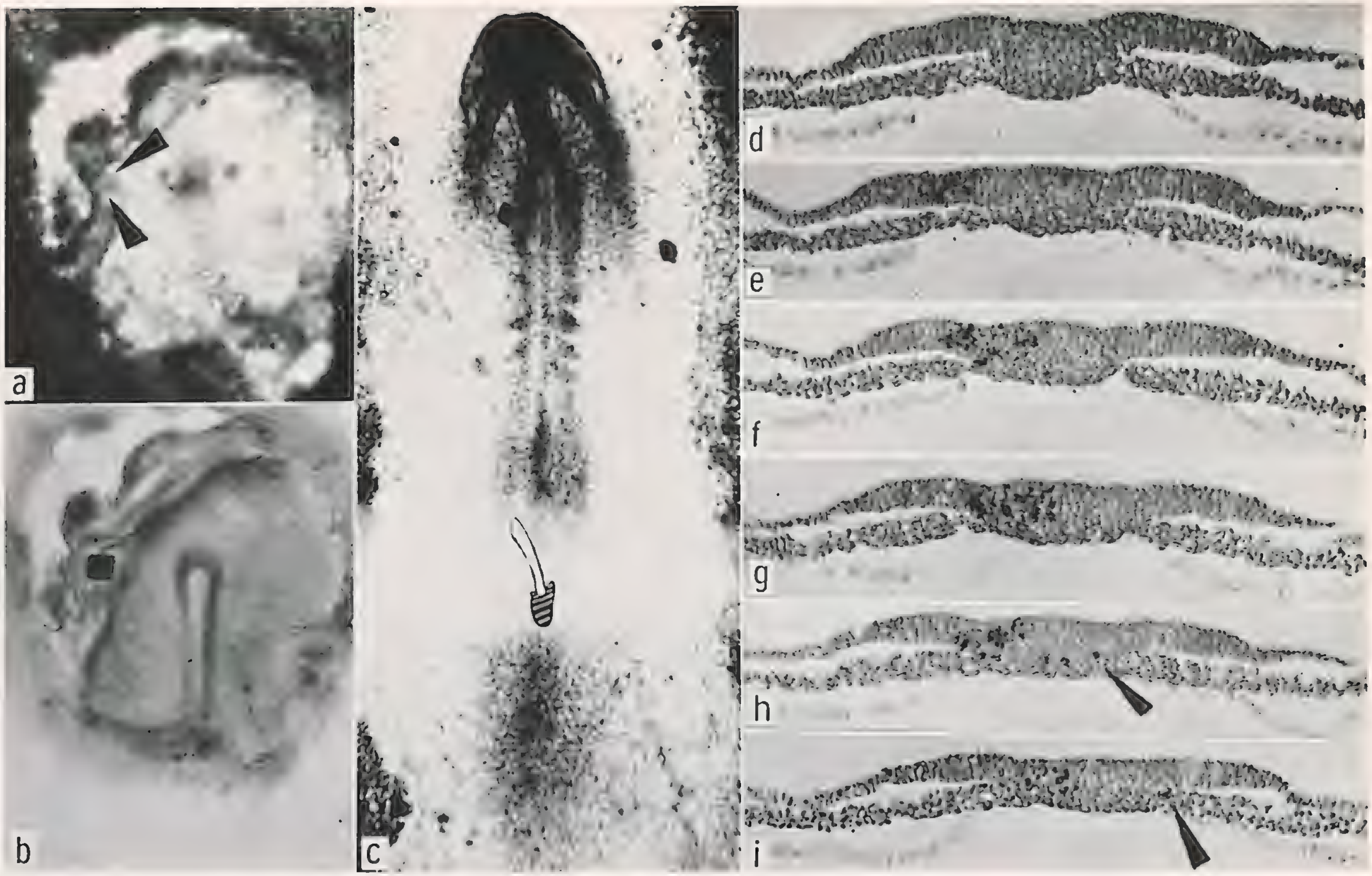

PLATE 9

Graft to premesoderm and presumably preectoderm zones of epiblast seen also straddling zones *B* and *F*, Fig. 1(a). (Embryo described on p. 89.) (a) and (b) Recipient embryo after graft is placed on right side. Graft site just visible dorsal to reexpanding endoderm-mesoderm flap. (c) Photograph 18 hours later, before fixing. Labeled square has elongated to extend from epiblast (presumably preectoderm area) to streak (white outline) and into right and left mesoderm layers (diagonal black and white).

Radioautographed sections (d–e) illustrate the progressive appearance of labeled cells closer to streak, where they descend to ventral areas (f) and (g) to appear in mesoderm of right and left side (h), (i). Arrows indicate labeled cells in left mesoderm.

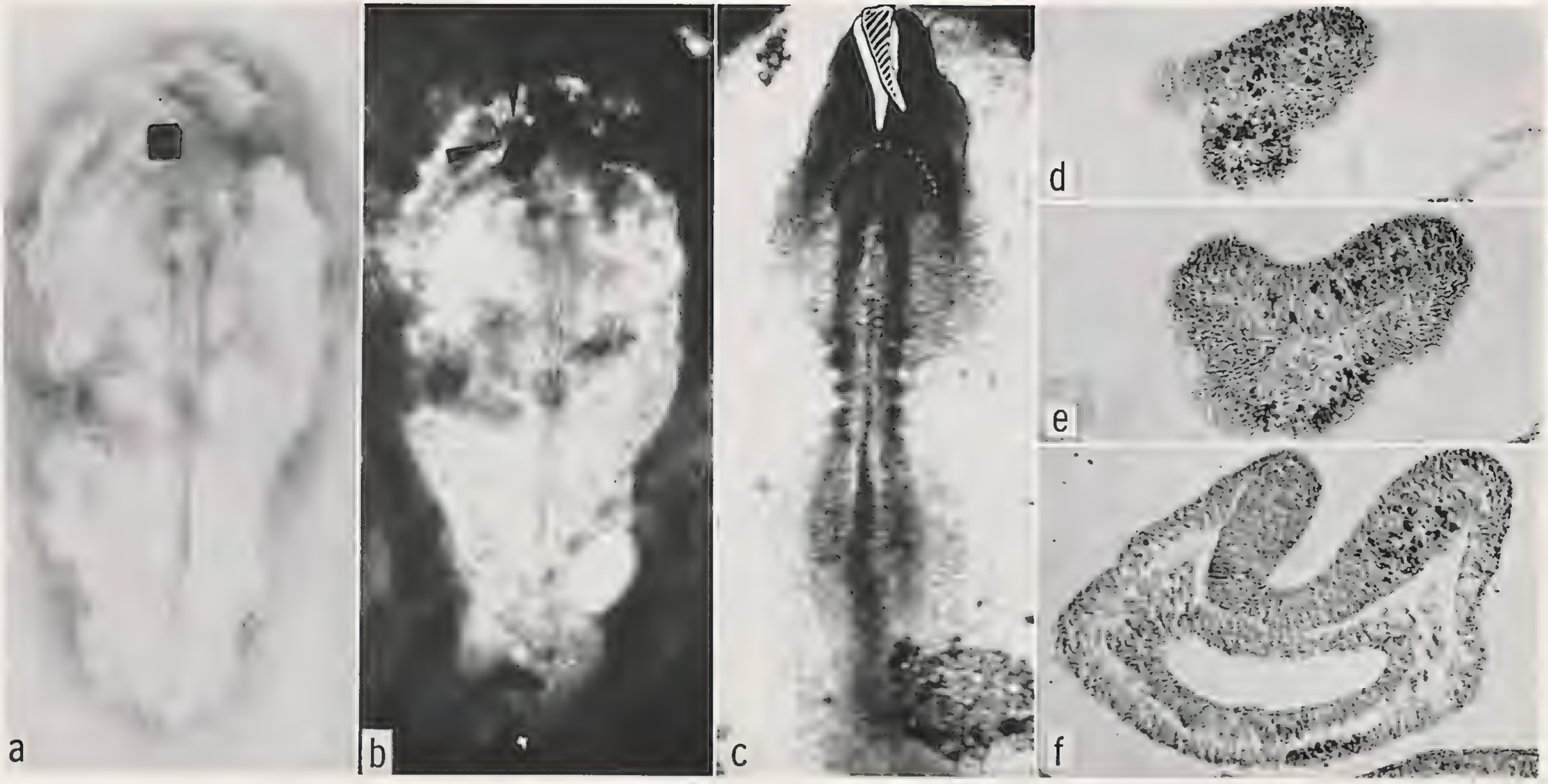

PLATE 10

Epiblast graft straddling preepidermal and predorsal neural tube ectoderm zones, ventral view. (Embryo described on p. 89.) (a) and (b) Grafted embryo before reincubation. The donor square dorsal to reexpanding endoderm-mesoderm flap is indicated by arrows. (c) Before fixing 18 hours later (retouched photograph). Distribution of labeled cells in epidermal epithelium (diagonal pattern), neural tube cells (white).

Radioautographed sections, ×200, (d) and (e) through tip of head and (f) more caudal level showing labeled cells in neural tube and ventral epidermis.

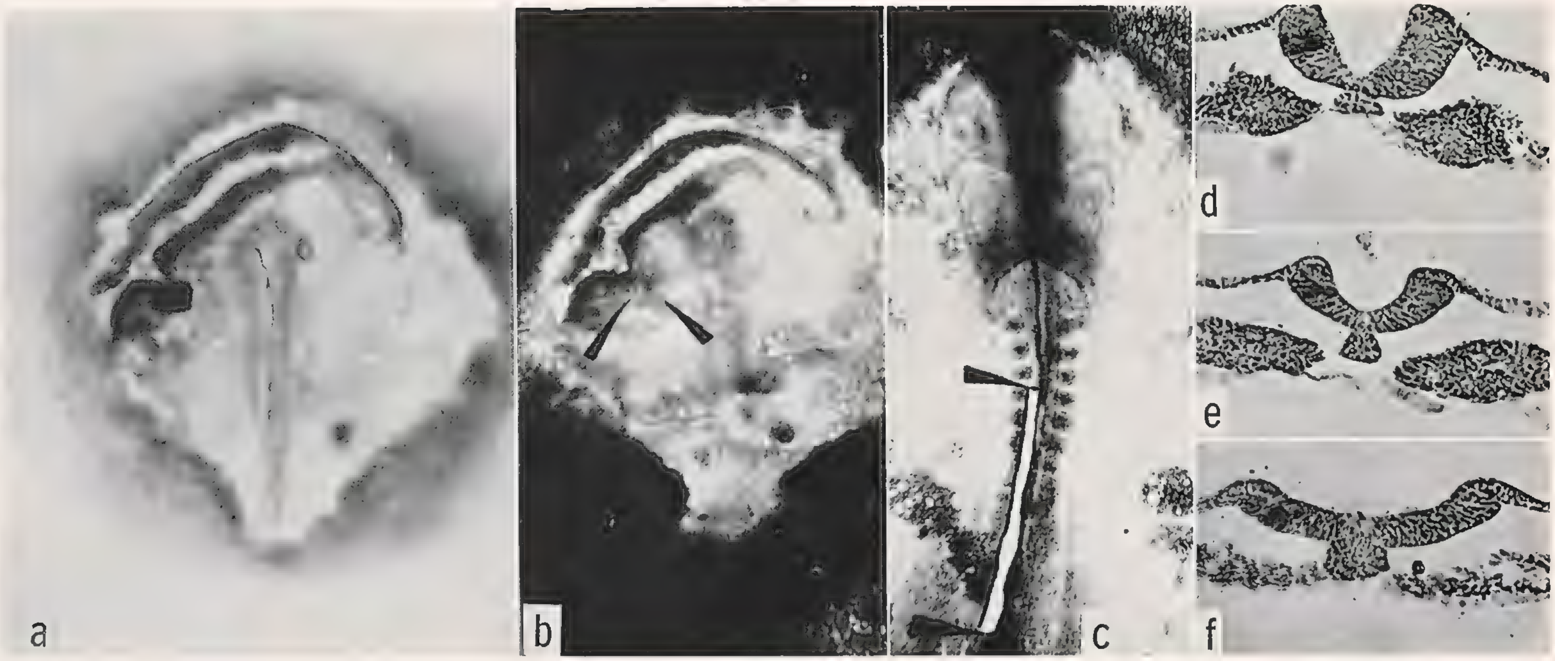

PLATE 11

Epiblast graft to predorsal neural tube zone, ventral view. (Embryo described on p. 91.) (a) and (b) Embryo before reincubation. The labeled donor square dorsal to reexpanding endoderm-mesoderm is indicated by arrows. (c) Before fixing 18 hours later (retouched photograph). Labeled cells in dorsal neural tube outlined in white between black arrows. Radioautographed sections, ×200, (d) at level of 3rd somite, (e) at 7th somite, and (f) nearing BW level, to show labeled cells unilaterally in dorsal neural tube.

PLATE 12

Independent migration of endoderm-mesoderm layers, ventral views. (a) Positions of endoderm-mesoderm layers of a square 7 grafted embryo reincubated to stage 7; see Figs. 11(c), 13(c)—labeling time, 3 hours; estimated labeling $7\frac{1}{2}$ hours later: endoderm, 80–90%.

Radioautographed sections at levels 1, 2, and 3 show (b) labeled mesoderm, (c) labeled mesoderm and endoderm, and (d) labeled endoderm alone. (e) Ventral side of the stage 10 embryo after about 19 hours of reincubation. The yolk-sac endoderm, endocardium, and endothelium have been removed. Square 7 has separated into a dorsal (somatic) and ventral (splanchnic) layer. Consequently, labeled mesoderm cells are distributed to the ala of the *area vasculosa,* somatic fold, nephrotome and paraxial mesoderm, dorsal mesocardium, and dorsal and ventral myocardial folds. The endoderm square is distributed to the ventrolateral wall of the right gut. (For clarity, shown in left gut.) (f) Radioautographed section, ×200, to show labeled cells in endocardium and myocardium. (g) Radioautographed section, ×200, to show endoderm distribution in ventral gut wall—labeling time, 10 hours; estimated labeling 17 hours later: endoderm and mesoderm, 90–100%.

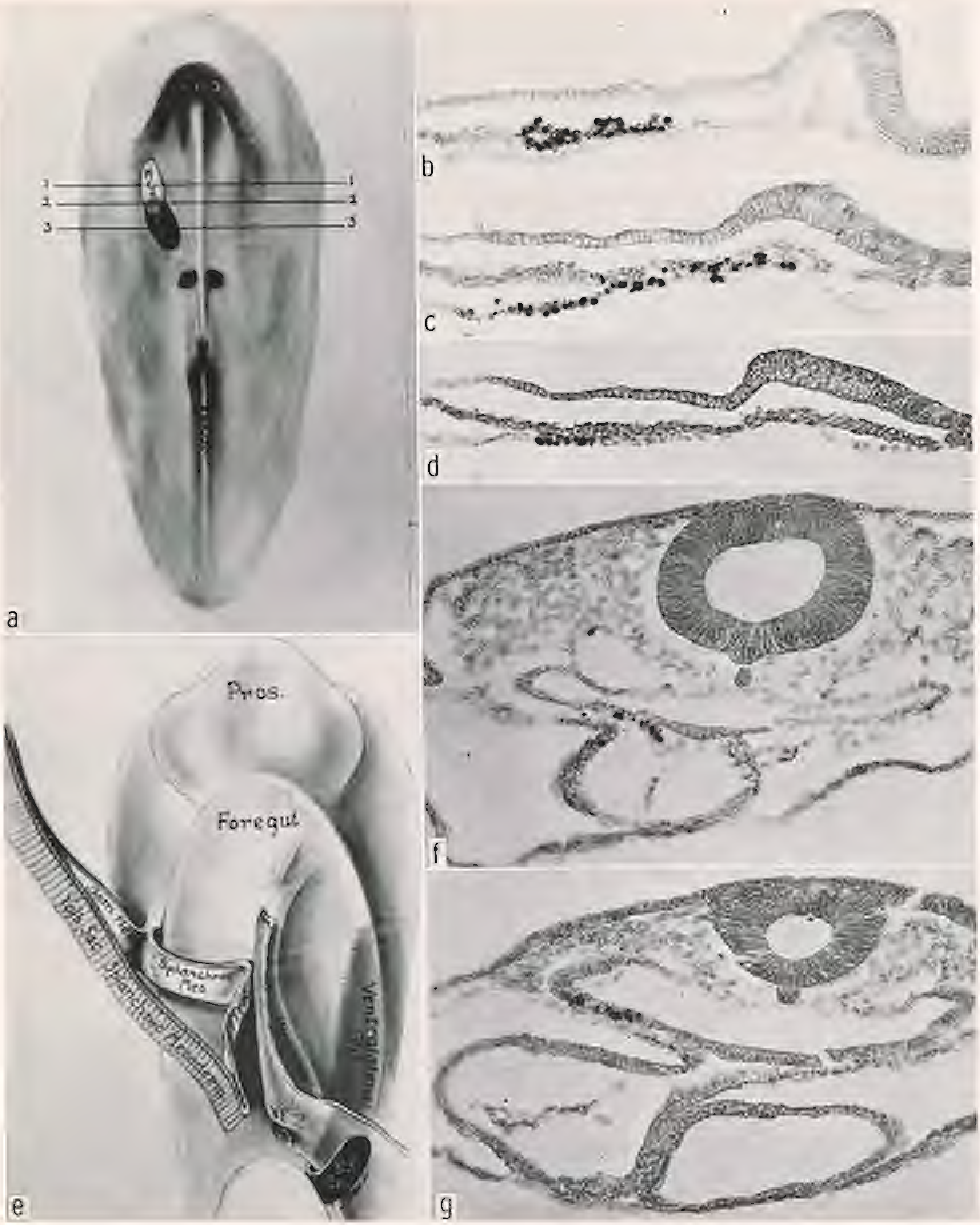
1
2
3
1
2
3
a
b
c
d
Pros.
Foregut
Splanchn. Mes
Yolk Sac Splanchnic Mesoderm
f
e
g

CONTRIBUTIONS TO EMBRYOLOGY, NO. 263

MIGRATION OF PRECARDIAC CELLS IN THE CHICK EMBRYO: A RADIOAUTOGRAPHIC STUDY

GLENN C. ROSENQUIST AND ROBERT L. DEHAAN
Carnegie Institution of Washington, Department of Embryology, Baltimore, Maryland

(With 2 plates and 3 figures)

CONTENTS

PAGE

METHODS 114
RESULTS 114
DISCUSSION 118
SUMMARY 120
ACKNOWLEDGMENTS 120
LITERATURE CITED 121

MIGRATION OF PRECARDIAC CELLS IN THE CHICK EMBRYO: A RADIOAUTOGRAPHIC STUDY

In the chick embryo, there is neither gross nor histologic indication of a heart-forming region (HFR) until the lateral plate mesoderm thickens at about the stage of three somites. It has therefore been of interest to embryologists since the turn of the century to locate the prospective heart cells in the early embryo and trace their movements as they take up definitive positions to form the heart in the ventral midline. (For reviews, see Copenhaver, 1955; DeHaan, 1965*a*.)

Studies by Graper (1907), who used microsurgical intervention, and by Pasteels (1936) and others, who used vital dyes, indicated that tissues with cardiogenic potential were present in the early blastoderm laterally, on both sides of the embryonic axis. By explanting fragments of the blastoderm, other workers have been able to localize these tissues somewhat more precisely. From a diffuse distribution throughout the prestreak embryo (Olivo, 1928; Butler, 1935), cells with heart-forming capacity in the primitive-streak-stage embryo have been found to be restricted mainly to the caudal half of the blastoderm near the cephalic end of the streak (Hunt, 1932; Rawles, 1936; Rudnick, 1938; Spratt, 1942).

In the head-process-stage embryo, Rawles (1943) determined which fragments of the blastoderm were capable of forming histologically identifiable heart muscle when transplanted to eight- to nine-day-old host embryos as chorioallantoic grafts. Her results indicated that heart-forming material was localized in a bilateral pair of oval zones on either side of the embryonic axis, which were not connected in the midline (Fig. 1). The subsequent cephalomesial migration of this mesoderm as it forms the cardiogenic crescent of the early head-fold embryo and its continued movement into the primitive tubular heart have been traced by DeHaan (1963*a, b*) with the use of time-lapse microcinematography.

These observations have yielded a coherent general picture of how the early heart is formed. However, the methods used have not been ideally suited for constructing fate maps. They do not allow precise definition of the boundaries of formative regions, nor is there any assurance that cells capable of forming a given tissue in an explant are the ones that would form the tissue in the intact embryo. This point (see Discussion) has been treated by Rudnick (1948) and by Rosenquist (1966).

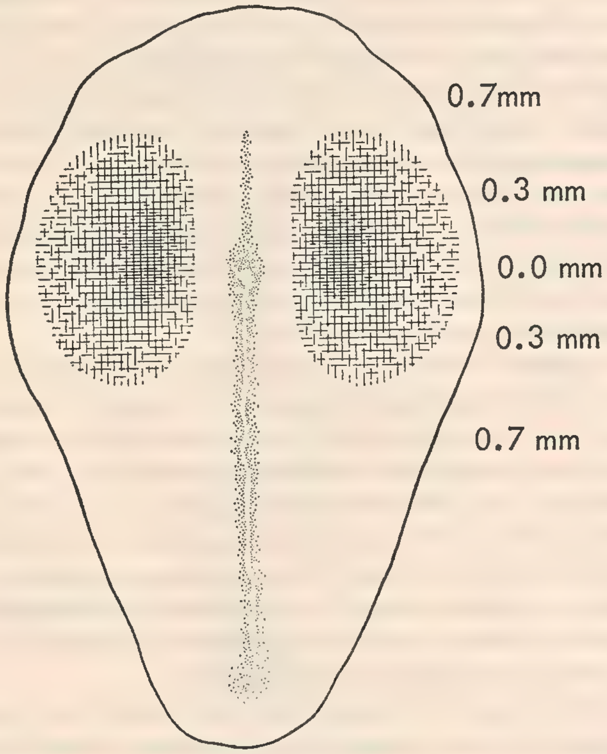

Fig. 1. Heart-forming regions according to Rawles (1943).

The technique of replacing small fragments of blastoderm with implants of homologous tissue labeled with tritiated thymidine overcomes most of the objections mentioned. The implanted tissue heals in rapidly and participates in the normal development of the recipient. The label is carried by individual cells. If proper precautions are taken it does not diffuse, nor is it diluted over a 48-hour period. Moreover, with this technique additional information can be obtained about the degree of intermixing of cells from different regions of the embryo.

A series of such implants has been made in an attempt to map systematically the entire epiblast of the primitive-streak embryo and the hypoblast (endoderm-mesoderm) of the head-process embryo (Rosenquist, 1966). The present paper is a detailed study of those embryos of the series in which labeled cells were found in the heart of the host embryo after incubation to the stage of 16 somites.

METHODS

Rectangular fragments of blastoderm from stages 3+ to 5 donor embryos (staged according to Hamburger and Hamilton, 1951), previously incubated with tritiated thymidine, were implanted into the matching site of unlabeled host embryos of the same age. Embryos carrying grafts were reincubated to the desired stage, and fixed, sectioned, and studied by radioautography, as described by Rosenquist (1966). The 102 embryos included for study in the present paper were those in which labeled cells were found in some part of the heart at stage 12; or, if the embryo was fixed before stage 12, in regions known to be destined for heart at stage 12.

Eighteen of these embryos carried grafts implanted into the host epiblast at stage 3+ or stage 4. Eighty-four had received endoderm-mesoderm grafts at stage 5, in the grid pattern described by Rosenquist (1966); see Fig. 3(a). The embryos of stages 3+ and 4 have been further subdivided into five groups on the basis of the number of hours after operation required to reach a definitive stage 5, as described by Rosenquist (1966). Table 1 shows the time at which each graft was implanted and the stage of fixation.

TABLE 1. Summary of Implantation and Fixation of Precardiac Tissue Grafts

Stage at Implantation	No. of Hours	Stage at Fixation							
		6	7	8	9	10	11	12	Totals
3	15–17	0	0	1	1	0	1	0	3
4	12–14	0	0	0	0	2	0	3	5
4	9–11	1	0	1	1	0	0	1	4
4	6–8	0	0	1	1	1	1	0	4
4	3–5	1	0	0	1	0	0	0	2
5*	0	12	12	12	12	12	12	12	84
									102

* Endoderm-mesoderm grafts.

The degree of mixing between labeled and unlabeled cells was estimated on sections prepared for radioautography. For this series, donor embryos were incubated with tritiated thymidine for 2.7, 4.5, and 10.0 hours before reaching stage 5. Host embryos carrying implants from the donors were reincubated for periods of from 0.5 to 26.0 hours, then fixed and sectioned. The proportion of labeled vs. unlabeled cells was determined in regions carrying label by counting the labeled and unlabeled cells in each section; see Table 2. In embryos fixed only a few hours after implantation of the grafts, the label was still localized in the compact block of precardiac graft cells. In these embryos, every tenth section through the graft region was counted. In embryos fixed at stages 10 and 12, labeled cells were found in narrow elongated areas of myocardium. In these embryos every section through the labeled region was counted. Unlabeled cells were counted only if they were located between two or more labeled cells.

TABLE 2. Percentage of Labeled Cells in Labeled Tissues

Embryo	Incubation With Tritiated Thymidine, hours	Stage at Implantation	Stage at Fixation	Reincubation After Implantation, hours	Number of Sections Counted*	Cells Within Labeled Region		Label, per cent
						Labeled	Unlabeled	
4827-10	2.7	5	5	0.5	6	225	237	48.5
41124-2	2.7	5	12	26.0	26	144†	147†	49.5
41215-3	4.5	5	6	4.5	4	148	58	71.8
41215-13	4.5	5	6	4.5	7	166	98	61.0
41110-5	10.0	5	10	14.0	18	283†	7	97.6

* In embryos fixed at stages 5 and 6, every tenth section through labeled region was counted. In embryos fixed at stages 10 and 12, all sections through labeled region were counted.

† Myocardium.

RESULTS

Prospective heart cells could be localized as early as stage 3+ (15–17 hours before stage 5) in implants made into the prelateral plate region of the epiblast, about midway down the length of the streak and extending from the midline laterally about halfway to the edge of the pellucid area. The initial positions of these grafts are shown as shaded rectangles in Fig. 2(a). Implants into adjacent regions, shown as nonshaded rectangles, yielded labeled cells in a variety of mesodermal and endodermal structures in the later

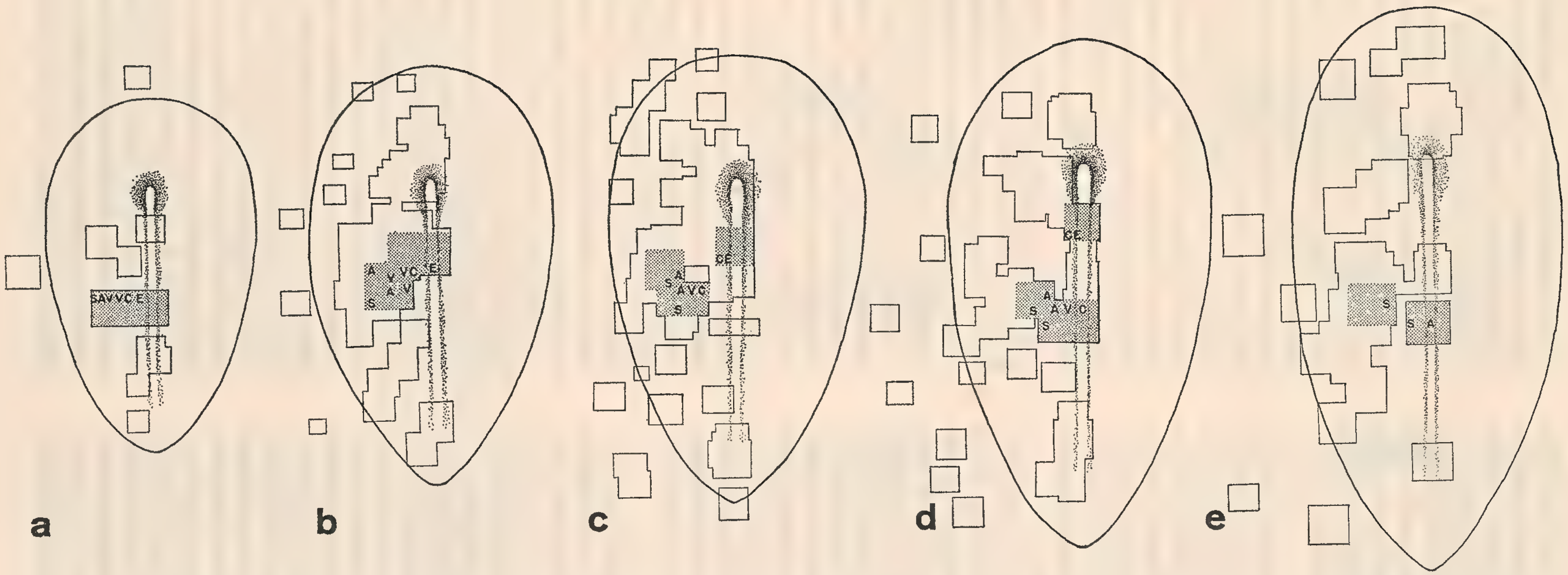

Fig. 2. Heart-forming area of the epiblast, to show sequence of invagination of precardiac material in a localized area of the streak. (a) Fifteen hours before stage 5. Total grafted area, light outline. Cells from shaded areas later appeared in right and left precardiac mesoderm, by first moving to the streak where mixing and invagination took place. (b) Twelve hours before stage 12. Conal and endocardial cells seen in dorsal streak, but bulk of myocardium still in lateral epiblast. (c) Nine hours before stage 5. Premyocardial material now seen in streak. (d) Six hours before stage 5. Preheart material closer to streak. (e) Three hours before stage 5. Last cells to invaginate are sinoatrial cells. At stage 5, no preheart cells were seen in streak. Presumptive localization of cells within a single graft is arbitrary and based upon the observation that more lateral grafts carry caudal preheart areas; the caudal areas are the last to reach the streak. A = atrium; C = conus; E = endocardium; S = sinus; V = ventricle.

Executed by Judith Baer

embryo (Rosenquist, 1966) but not in the heart. The positions of epiblast grafts containing preheart cells at each succeeding stage up to the head-process embryo are shown in Fig. 2(b–e). From an initial region in the lateral epiblast, these cells move medially toward the streak. Preconus cells reach the dorsal streak 12–14 hours before stage 5. They are followed through the streak within a few hours by prospective ventricular tissue, and then, in sequence, by preatrium and presinus.

An embryo carrying a precardiac epiblast graft is shown in Plate 1(a). The site of the graft is midway between the streak and the lateral edge of the *area pellucida.* Four hours later, as seen in Plate 1(b), the implanted tissue has moved medially; labeled cells are shown entering the streak in a radioautograph of a cross section. It is clear that while the labeled implant remains in the epiblast it retains its compact organization, exhibiting little dispersion of cells.

As labeled cells move into the streak, the graft begins to lose its coherent structure. Graft tissue mixes with unlabeled cells from regions on the opposite side. Labeled cells descend to the ventral streak and are then scattered in the mesoderm moving away from the streak. Labeled cells scattered in the myocardium, endocardium, and body mesenchyme of the embryo at stage 12 are shown in Plate 1(c), which is a radioautograph of a cross section of the same embryo illustrated in Plate 1(a), after 38 hours of reincubation. Although epiblast implants were all made unilaterally, they consistently contributed labeled cells to both right and left sides of the heart, approximately in bilaterally symmetrical positions.

The last prospective sinus cells apparently reach the streak about three hours before stage 5, as shown in Fig. 2(e), and immediately descend to mesoderm. All presinus mesoderm has migrated from the streak by stage 5, as shown by study of the endoderm-mesoderm grafts made into embryos at that stage (see below).

The movements of the preendocardial cells are largely independent of those of the prospective myocardium. Some prospective conus endocardial cells begin to move into the streak before the premyocardium, indicating that they are mixed with, or at the border of, the preendoderm region of the stage 3+ epiblast; see Rosenquist (1966), his Fig. 1(d). At 15–17 hours before stage 5, a few preendocardial cells are found already in the dorsal streak, about halfway down its length. Over the next 10 hours, additional conal endothelial cells appear in progressively more cephalic regions of the streak, and by stage 5 these cells are located cephalic to the head process, scattered in with the prechordal mesenchyme.

After invagination, preheart cells move either directly cephalically, or cephalolaterally with the lateral plate mesoderm. The great bulk of the cells move cephalolaterally, forming the broad lateral wings of a horseshoe-shaped heart-forming crescent. In Fig. 3(a), the right half of this crescent is superimposed on the grid pattern of grafts of endoderm-mesoderm implanted in the stage 5 embryo. The heavily shaded region always contributes cells to the heart, although there are more preheart cells in the lateral wings of the crescent than in the cephalomedial bridge. The lightly stippled zones along the peripheral and medial edges of the crescent indicate regions that sometimes contain prospective heart cells. This zone of uncertainty is apparently the result of differences in size of the embryos at the time of operation and slight differences in the location of the cuts from one embryo to the next, as well as the natural variation in extent of heart-forming material in different embryos.

By making graphic reconstructions of each of the grafted, sectioned embryos after reincubation to stages 6–12, it has been possible to determine the location in the cardiogenic crescent and definitive heart taken by labeled cells implanted in each of the grid locations at stage 5. The position and extent of the cardiogenic mesoderm as it forms the heart between stages 6 and 12 are shown in Fig. 3 (b–h). Plate 2 illustrates such reconstructions of embryos at stages 10 and 12, to show the location of grafted fragments in the tubular heart.

Between stages 7 and 8, the lateral plate mesoderm divides into dorsal (somatic) and ventral (splanchnic) layers, with formation of the amniocardiac vesicles. The thickened precardiac mesodermal plate separates from the splanchnic layer, in close association with the endoderm. Between these two, the delicate endothelial layer of endocardium appears. The endodermal folding that forms the anterior intestinal portal (AIP) and early foregut is normally initiated in a shallow arc that crosses the midline between squares 4 and 6, seen in Fig. 3(a), (b). As the foregut lengthens, the lateral wings of the cardiogenic crescent swing ventromedially, fusing in the midline to form the epimyocardial gutters and ventral mesocardium. As this occurs, mesoderm previously closest to the midline remains dorsal, while that in more lateral regions of the pellucid area extends to the ventral body wall. Thus, the mesoderm in squares 6, 8, 10, and 12 remains close to the embryonic axis; that in squares 5, 7, 9, and 11 folds ventrally around the foregut to form the dorsalmost portions of the conoventricular region. Mesoderm in squares *B* and *C,* being more lateral, contributes mainly to the ventral aspects of the heart and ventral mesocardium. As shown in Plate 2, however, this situation is complicated by the oblique direction of the folding movements of the AIP, which causes the pre-

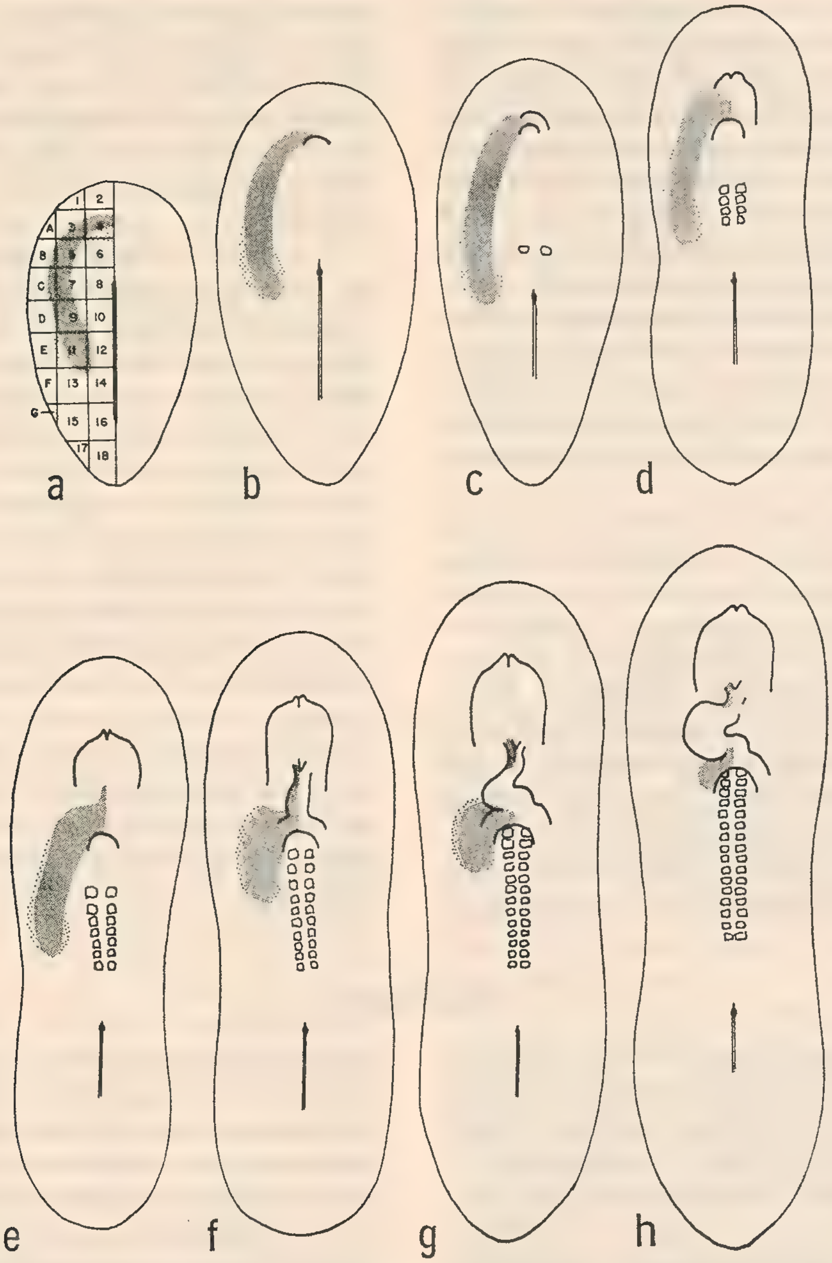

Fig. 3. Embryos at stages 5–12, ventral view, to show the limits of preheart mesoderm. Densely hatched half-crescent represents mesoderm that consistently forms heart. Lighter hatched areas represent mesoderm that contributes to the heart in some embryos but not in others. In (a) the grid of endoderm-mesoderm implants is shown. Grid squares are lettered according to Rosenquist (1966). By stage 12 (h) most of precardiac mesoderm has formed definitive heart tissue of right half of the conus (shaded), ventricular loop (hidden on dorsal aspect), and sinoatrial tissue (shaded). The stages represented in (b–g) illustrate the position of the heart-forming cells in the intermediate stages 6–11.

cardiac mesoderm to be stretched in a caudoventral direction. Thus, squares 5, 7, and 9 all contribute to the dorsal aspect of the heart at their cephalic ends, but swing lateroventrally in more caudal parts of the organ.

At stage 10 or 11, the splanchnic folds begin to fuse dorsal to the primitive heart tube under the floor of the foregut, separating the heart from dorsal mesocardium. Prospective heart tissue continues to move cephalomedially, adding to the caudal end of the heart, as the AIP moves relatively caudally with elongation of the foregut. At stage 10, seen in Plate 2(a), mesoderm from square 9 forms the caudalmost end of the differentiated myocardium. Mesoderm from square 11 lies caudal to the AIP, in the splanchnic mesoderm dorsal to the omphalomesenteric veins. By stage 12, seen in Plate 2(b), square 11 is well incorporated into the atrioventricular wall, whereas prospective sinoatrial material is formed mainly by portions of squares 12, 13, and 14. Moreover, cells located in the ventricle at stage 10 (square 7) are found for the most part in the conoventricular region by stage 12.

When the positions of squares implanted at stage 5, seen in Fig. 3(a), are compared with the sites that those fragments come to occupy in the formed heart (Plate 2), it is apparent that the epimyocardial layer of the splanchnic mesoderm, once formed, moves and folds as a cohesive sheet. The implanted fragments of endoderm-mesoderm that were rectangular at stage 5 become folded, elongated, and otherwise distorted in shape as they contribute to the myocardial wall. However, the outline of the labeled tissue remains discernible. Labeled cells are not widely scattered in the myocardium, in contrast to the result obtained with epiblast grafts, which become mixed with unlabeled cells as they descend through the streak before forming mesoderm (Plate 1).

To confirm this impression that little or no mixing occurs between labeled and unlabeled cells, those within the labeled region of host embryos were counted to determine whether the percentage of labeled cells diminishes with time of development after implantation. The results are summarized in Table 2. If the donor was incubated with 1 μc of tritiated thymidine for 2.7 hours before implantation, approximately 50 per cent of its cells became labeled, as seen on embryo 4827-10, fixed only 30 minutes after implantation. However, even after 26 hours of reincubation, during which embryo 41124-2 developed to the stage of 16 somites, the same percentage of cells exhibited label. When the donor tissue was incubated for 4.5 hours with the label, 60–70 per cent of its cells became labeled. After 10 hours of incubation with label, 97.6 per cent of the graft cells carried radioactive nuclei, even after the embryo had developed to the stage of 10 somites.

From Plate 2 it is apparent that the contributions of the left and the right lateral wings of the cardiogenic crescent to the formed heart change with development. At stage 10, seen in Plate 2(a), material from the right HFR forms the entire right half of the myocardial tube of the heart, but makes no contribution to the left half of the heart. In other words, labeled cells placed on the right side of the stage 5 recipient do not cross the ventral midline of the heart. By stage 12, however, what was originally the ventral midline has separated from the ventral mesocardium and moved around to the right dorsal aspect of the heart, seen in Plate 2(b). This distortion, which may be the result of differential growth of the organ, results in a much greater part of the ventral myocardial wall being formed from left precardiac mesoderm than from right, in a manner analogous to that reported by Wilens (1955) for the amphibian heart and by Van Mierop *et al.* (1963) for the human.

DISCUSSION

The sequence of events leading to heart formation that emerges from the present study differs in certain important respects from the widely accepted version based upon previous investigations of cardiogenesis.

In the prestreak embryo, early workers found heart-forming capacity widespread throughout the blastoderm. Olivo (1928) obtained pulsating heart muscle in cultures of peripheral fragments of unincubated blastoderms, but not in similar cultures of the central area. From embryos of the same stage, Butler (1935) found heart muscle, grown as chorioallantoic membrane grafts, developing in both cephalic and caudal halves of the blastoderm. As the primitive streak forms, cells with heart-forming capacity are apparently localized mainly in the caudal half of the blastoderm, near the streak (Rudnick, 1938) and extending no farther than 0.2 mm cephalic to Hensen's node (Rawles, 1936; Hunt, 1932; Spratt, 1942).

The present study clarifies the details of this localization, showing that prospective heart cells in the stage 3+ embryo (15–17 hours before stage 5) are already restricted to limited regions of the lateral epiblast on each side of the forming streak. They are localized more caudally in the embryo than was previously thought (Rudnick, 1955), nearer to the midstreak level than to the node. It is clear, moreover, that these cells converge upon the streak, descend through it, and then migrate out to bilaterally symmetrical positions in the lateral plate mesoderm. This observation confirms the early experiments of Rudnick (1938) and Spratt (1947); it does not support Spratt's more recent contention that the primitive streak is a blastema-like growth center rather than a line of invagination (Spratt and Haas, 1965), (for details, see Rosenquist, 1966).

In the head-process embryo, Rawles's (1943) grafts to chorioallantoic membrane demonstrated that there were broad separate bilateral HFRs that did not meet in the midline. More recent evidence indicates that mesoderm resembling cardiac tissue in certain biochemical properties is similarly distributed in broad separate bilateral zones. For example, embryonic heart tissue is known to be rich in glycogen. Chiquoine (1957) localized cells of the splanchnic mesoderm that stained heavily with Periodic-acid Schiff reagent in two areas that were lateral to the streak of the mouse embryo corresponding to Rawles's HFRs. The preheart cells are also susceptible to poisoning by oxidative inhibitors such as sodium fluoride (Spratt, 1950) and antimycin A (Reporter and Ebert, 1965). When sodium fluoride was applied to the stage 5 chick embryo, Duffey and Ebert (1957) produced localized areas of cell necrosis and edema, again corresponding to Rawles's HFRs. Furthermore, at stage 5, Ebert (1953, 1955) found that immunologically reactive groups of cardiac myosin and actin were restricted mainly to the same bilateral HFRs.

In contrast, the present study indicates that the cells actually forming the heart are localized in bilateral regions that are longer and narrower than those indicated by Rawles. Moreover, they are connected across the midline by a bridge of prospective endocardial cells and myocardial cells of the conus, as seen in Fig. 3(a), (b). The bridge is composed of material that descended through the streak early in stage 4 and migrated as mesoderm in a direct cephalic route past Hensen's node, preceding the first notochord cells (Fig. 2).

It is not difficult to reconcile these different interpretations of the preheart localization in the stage 5 embryo.

1. Rawles examined grafts in cross section after eight to nine days' growth on the chorioallantoic membrane. She scored them as positive if she found histologically recognizable masses of myocardial tissue, negative if she did not. It would not have been possible for her to recognize isolated myocardial cells, nor could isolated endocardial tissue be distinguished from other endothelial sheets or tubes. She reported such endothelial structures as being abundant in grafts obtained from both medial and lateral fragments of the pellucid area cephalic to the node (Rawles, 1936).

2. The biochemical evidence cited above as supporting Rawles's map of the HFR may be equally subject to other interpretations. Sodium fluoride produces striking bilateral oval areas of edema and necrosis, matching the HFR. Such inhibitors, however, also have pronounced deleterious effects on other mesoderm widespread throughout the embryo, including midline regions (Duffey and Ebert, 1957; McKenzie and Ebert, 1960; Reporter and Ebert, 1965). Similarly, although immunologically reactive groups of cardiac myosin are largely localized in the lateral areas of the stage 5 embryo, Ebert (1953) consistently found traces of such activity in the median section of the embryo. He therefore concluded (p. 340), that at this stage his data were "not in complete agreement with the finding by Rawles that the median area does not produce heart when grafted to the chorioallantoic membrane."

3. Explantation of grafts and their subsequent "self-differentiation" provide information about organ-forming potencies; implantation of labeled cells, which participate in the normal development of the embryo, indicates the prospective fate of those cells. It is widely accepted that organ-forming potency is more widespread than prospective fate. It should, therefore, be expected that the areas containing cells with heart-forming capacity, shown as explants, do not coincide exactly with the regions containing the prospective heart cells—a point well recognized by Rawles. In discussing her mapping experiments, she states that "Each organ-forming area indicated on the maps presumably represents a field that is capable of producing the organ in question but only a small portion of which actually forms the organ during normal development" (Rawles, 1936, pp. 310–311). We may therefore conclude that the "cardiogenic crescent," described many years ago in early somite embryos (Mollier, 1906), is present much earlier—as soon as lateral plate and prechordal material have migrated through the streak.

One of the most striking results of the present study is that in the formation of the heart from stages 5 to 12, the epimyocardial layer of the splanchnic mesoderm moves and folds as a cohesive sheet (Plate 2). Moreover, this sheet is continuous medially with the dorsal mesocardium and nephrogenic mesoderm and laterally with the ventral mesocardium and prospective yolk-sac mesoderm. In an earlier study, based upon observations of embryos developing in vitro with the aid of time-lapse cinematography, it was reported that the heart-forming mesoderm is composed of clusters of cells, which migrate as independent entities upon the endoderm (DeHaan, 1963*b*). The direction of their movements as the lateral HFR became organized between stages 5 and 6 was described as random. From stages 6 to 10, however, they were reported to migrate in parallel routes cephalomedially in the cardiogenic crescent.

This view of an early random movement of the precardiac mesoderm now requires reevaluation. In the present study, labeled premyocardial cells implanted at stage 5 are never found to have mixed with adjacent unlabeled material. Even with a fragment such as square 7, seen in Fig. 2(a), which includes only the medial half of the right crescent, the boundary between labeled and unlabeled myocardium does not fray at the edges, but is sharply demarcated. Moreover, the percentage of labeled cells within the labeled tissue is dependent only on the length of incubation of the donor tissue with the label, not on the period of reincubation after implantation of the tissue into the host (Table 2). Thus, the labeled cells do not become diluted while the heart forms, as would be expected if mixing of labeled and unlabeled cells occurred.

Prospective endocardium, on the other hand, behaves quite differently from the epimyocardium. It does not appear to retain its integrity as a cohesive sheet. Labeled cells within the endocardium of the stage 12 heart do not generally coincide in position as a bloc with the labeled myocardium. Instead, they may be scattered throughout the length of the organ, from the conus to the sinoatrial region. Thus, as prospective endocardial cells separate from the splanchnic mesoderm between stages 5 and 8, they apparently follow routes into the heart independent of the epimyocardial sheet. The cells at the cephalic tip of the midline prechordal mesenchyme are those which most often appear to be scattered as endocardial cells to the caudal portions of the heart, as they are drawn ventrally and then caudally on the midpoint of the AIP.

However, in another respect, the results reported here corroborate and extend the earlier cinematographic studies. DeHaan (1963*b*) pointed out that the myocardial mesoderm is not carried passively into the midline by the folding endoderm but moves cephalically over that layer. The point is illustrated in the companion paper to this (Rosenquist, 1966, Plate 12), showing clearly that the labeled precardiac mesoderm of fragment 7 moves in a cephalic and slightly medial direction relative to the labeled endoderm in the few hours between stage 5 (stage of implantation) and stage 7 (stage of fixation). Since we now know that this mesoderm moves mainly as a cohesive sheet and that these movements can take place on the endoderm in vitro (DeHaan, 1964), it seems reasonable to hope for an understanding of the mechanisms and control of such movements from continued studies.

It was also reported (DeHaan, 1963*a*) that the cardiogenic crescent was organized in a cephalocaudal sequence as early as stage 6, into prospective conal, ventricular, atrial, and sinoatrial regions. Evidence was provided that prepacemaker cells were localized within each of these regions with intrinsic pulsation rates appropriate to the cardiac subdivision; that is, the most cephalic preconus tissues developed slow spontaneous rhythms in isolation, and progressively more caudal tissues showed more rapid rates, with pacemakers from the presinus regions being the most rapid (DeHaan, 1963*c*, 1965*b*). The cephalocaudal organization of the crescent from conus to sinus has been confirmed recently, with carbon marks placed in the mesoderm *in ovo*, by N. Le Douarin (1964). The distribution of pacemaker cells has been corroborated by G. Le Douarin *et al.* (1965). From the results given here, it is apparent that this cephalocaudal pattern in the cardiogenic crescent is in fact presaged by the organization of the prospective heart cells while still in the epiblast of the early streak embryo. Preconus cells appear to be localized closer to the streak and descend through it first, to be followed by preventricle, preatrium, and presinus, in that order.

SUMMARY

Small squares of blastoderm were removed from embryos in culture and replaced with matching squares taken from donor embryos incubated in tritiated thymidine. Epiblast grafts were put into embryos at stages 3+–4, and grafts of endoderm-mesoderm were put into embryos at stage 5. Recipient embryos were reincubated to stages 6–12, then fixed and prepared for radioautographic examination. The present report is a study of 102 embryos in which labeled cells were found in the heart-forming mesoderm or heart tissue at stage 12.

Prospective heart cells are localized in the epiblast of the 3+ embryo in separate lateral regions about midway down the length of the forming streak. These cells converge upon the streak, mix with their neighbors from the opposite side, and descend to a more ventral position. They emerge from the streak and migrate cephalically and laterally as prechordal and lateral plate mesoderm.

At stage 5, prospective heart cells have all joined the mesoderm and are located in a horseshoe-shaped zone, continuous across the midline in the prechordal plate region. The lateral wings of this arc correspond approximately to Rawles's bilateral HFRs. From stages 5 to 12 the precardiac mesoderm as part of the splanchnic folds, moves cephalomesially, independently of the endoderm. The epimyocardium moves and folds as a cohesive sheet. Endocardial cells, which retain a closer association with both gut and yolk-sac endoderm, are scattered throughout the heart in small groups. The cephalocaudal organization of the stage 5 crescent into preconal, preventricular, preatrial, and presinus regions is presaged by the organization of the prospective heart cells in the stages 3–4 epiblast, and is maintained throughout stages 6–12 as the tubular heart is formed.

ACKNOWLEDGMENTS

The authors wish to acknowledge the technical assistance of Leo A. Kormann, Ellen Legum, William R. Duncan, and Isabelle Williams. The careful, critical reading of the manuscript by Dr. James D. Ebert and Dr. Dorothea Rudnick is greatly appreciated. Glenn C. Rosenquist is a National Institutes of Health Postdoctoral Fellow (National Heart Institute Fellowship No. 2-F2-HE-20, 074-02).

LITERATURE CITED

Butler, E. 1935. The developmental capacity of regions of the unincubated chick blastoderm as tested in chorioallantoic grafts. *J. Exptl. Zool., 70,* 357–389.

Chiquoine, A. D. 1957. The distribution of polysaccharides during gastrulation and embryogenesis in the mouse embryo. *Anat. Record, 129,* 459–515.

Copenhaver, W. M. 1955. Heart, blood vessels, blood and entodermal derivatives. In *Analysis of Development,* B. H. Willier, P. A. Weiss, and V. Hamburger, eds., W. B. Saunders Co., Philadelphia, pp. 440–461.

DeHaan, R. L. 1963*a.* Organization of the cardiogenic plate in the early chick embryo. *Acta Embryol. Morphol. Exptl., 6,* 26–38.

DeHaan, R. L. 1963*b.* Migration patterns of the precardiac mesoderm in the early chick embryo. *Exptl. Cell Res., 29,* 544–560.

DeHaan, R. L. 1963*c.* Regional organization of prepacemaker cells in the cardiac primordia of the early chick embryo. *J. Embryol. Exptl. Morphol., 11,* 65–76.

DeHaan, R. L. 1964. Cell interactions and oriented movements during development. *J. Exptl. Zool., 157,* 127–138.

DeHaan, R. L. 1965*a.* Morphogenesis of the vertebrate heart. In *Organogenesis,* R. L. DeHaan and H. Ursprung, eds., Holt, Rinehart and Winston, New York, pp. 377–419.

DeHaan, R. L. 1965*b.* Development of pacemaker tissue in the embryonic heart. *Ann. N. Y. Acad. Sci., 127,* 7–18.

Duffey, L. M., and J. D. Ebert. 1957. Metabolic characteristics of the heart-forming areas of the early chick embryo. *J. Embryol. Exptl. Morphol., 5,* 324–339.

Ebert, J. D. 1953. Analysis of the synthesis and distribution of the contractile protein, myosin, in the development of the heart. *Proc. Natl. Acad. Sci. U. S., 39,* 333–344.

Ebert, J. D. 1955. Some aspects of protein biosynthesis in development. In *Aspects of Synthesis and Order in Growth,* D. Rudnick, ed., Princeton University Press, Princeton, N. J., pp. 69–112.

Graper, L. 1907. Untersuchungen über die Herzbildung der Vögel. *Arch. Entwicklungsmech. Organ. (Berlin), 24,* 375–410.

Hamburger, V., and H. L. Hamilton. 1951. A series of normal stages in the development of the chick embryo. *J. Morphol., 88,* 49–92.

Hunt, T. E. 1932. Potencies of transverse levels of the chick blastoderm in the definitive streak stage. *Anat. Record, 55,* 41–70.

Le Douarin, N. 1964. Étude expérimentale de l'organogenèse du tube digestif et du foie chez l'embryon de poulet. *Bull. Biol. France Belg., 98,* 591–676.

Le Douarin, G., G. Obrecht, and E. Coraboeuf. 1965. Activité électrique transmembranaire de vésicules pulsatiles différenciées en culture organotypique par des fragments de l'aire précardiaque de l'embryon de poulet. *Compt. Rend. Acad. Sci. (Paris), 260,* 287–290.

McKenzie, J., and J. D. Ebert. 1960. The inhibitory action of antimycin A in the early chick embryo. *J. Embryol. Exptl. Morphol., 8,* 314–320.

Mollier, S. 1906. Die erste Anlage des Herzens bei den Wirbeltieren. In *Handbuch der Vergleichenden und experimentellen Entwicklungslehre der Wirbeltiere,* O. Hertwig, ed., Fischer, Jena, Germany, Vol. I, 1019–1051.

Olivo, O. M. 1928. Précoce détermination de l'ébauche du coeur dans l'embryon de poulet et sa différenciation histologique et physiologique *in vitro. Compt. Rend. Assoc. Anat. (Prague), 23,* 357–374.

Pasteels, J. 1936. Analyse des mouvements morphogénétiques de gastrulation chez les oiseaux. *Bull. Acad. Roy. Belg., 22,* 737–752.

Rawles, M. E. 1936. A study in the localization of organ-forming areas in the chick blastoderm of the head-process stage. *J. Exptl. Zool., 72,* 271–315.

Rawles, M. E. 1943. The heart-forming areas of the early chick blastoderm. *Physiol. Zool., 16,* 22–42.

Reporter, M. C., and J. D. Ebert. 1965. A mitochondrial factor that prevents the effects of antimycin A on myogenesis. *Develop. Biol., 12,* 154–184.

Rosenquist, G. C. 1966. A radioautographic study of labeled grafts in the chick blastoderm. Development from primitive-streak stages to stage 12. *Carnegie Inst. Wash. Publ.* 625, *Contributions to Embryology,* this volume, pp. 71–110.

Rudnick, D. 1938. Differentiation in culture of pieces of early chick blastoderm. II. Short primitive streak stages. *J. Exptl. Zool., 79,* 399–425.

Rudnick, D. 1948. Prospective areas and differentiation potencies in the chick blastoderm. *Ann. N. Y. Acad. Sci., 49,* 761–772.

Rudnick, D. 1955. Teleosts and birds. In *Analysis of Development,* B. H. Willier, P. A. Weiss, and V. Hamburger, eds., Philadelphia, W. B. Saunders Co., pp. 297–314.

Spratt, N. T. 1942. Location of organ-specific regions and their relationship to the development of the primitive streak in the early chick blastoderm. *J. Exptl. Zool., 89,* 69–101.

Spratt, N. T. 1947. Regression and shortening of the primitive streak in the explanted chick blastoderm. *J. Exptl. Zool., 104,* 69–100.

Spratt, N. T. 1950. Nutritional requirements of the early chick embryo. III. The metabolic basis of morphogenesis and differentiation as revealed by the use of inhibitors. *Biol. Bull., 99,* 120–135.

Spratt, N. T., and H. Haas. 1965. Germ layer formation and the role of the primitive streak in the chick. I. Basic architecture and morphogenetic tissue movements. *J. Exptl. Zool., 158,* 9–38.

Van Mierop, L. H. S., R. D. Alley, H. W. Kausel, and A. Stranahan. 1963. Pathogenesis of transposition complexes. I. Embryology of the ventricles and great arteries. *Am. J. Cardiol., 12,* 216–225.

Wilens, S. 1955. The migration of heart mesoderm and associated areas in Amblystoma punctatum. *J. Exptl. Zool., 129,* 579–606.

PLATES

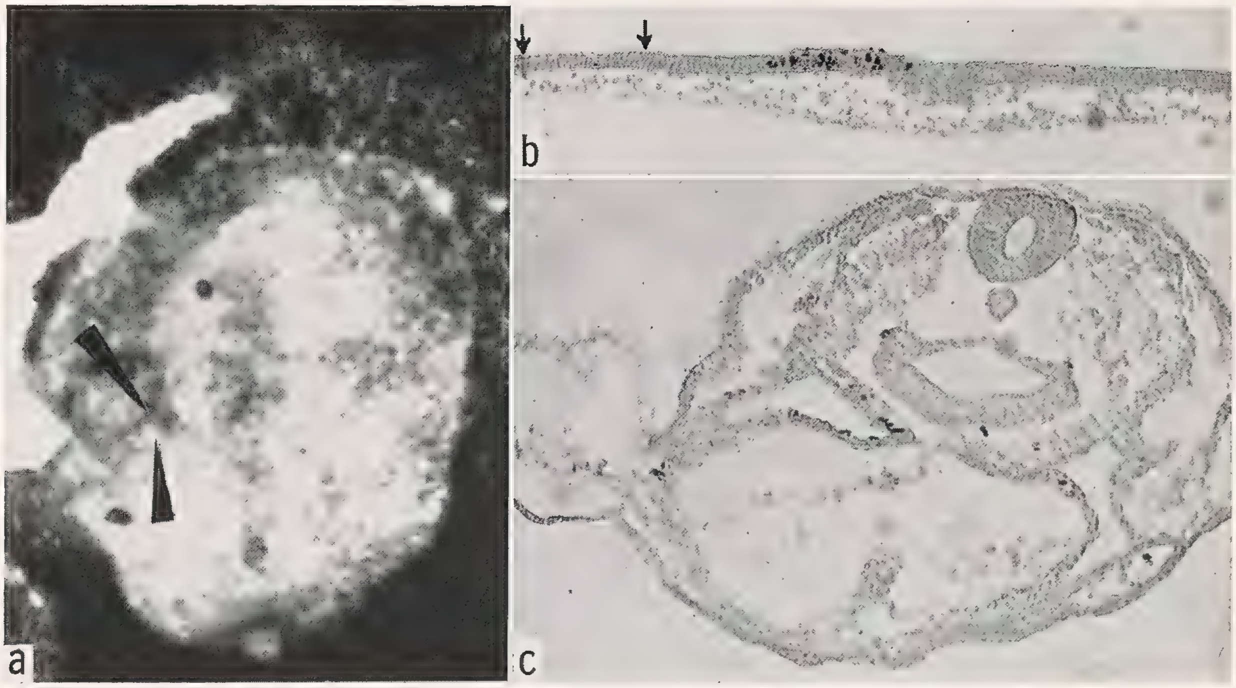

PLATE 1, (a–c)

To show migration of labeled precardiac cells into the primitive streak and their later position in definitive heart tissue.

(a) Embryo 5526-37. Ventral view, early stage 4 (14 hours before stage 5) carrying epiblast grafts (arrows). Photographed live after operation; × 20.

(b) Cross section through an embryo (5525-7) similar to that shown in (a) fixed 4 hours after implantation of labeled graft. Original site of the graft is shown between arrows. During time between implantation and fixation, labeled cells have moved toward the streak and are just entering it; × 100.

(c) Cross section through the same embryo shown in (a) fixed at stage 12. Note labeled cells scattered in the myocardium and endocardium as well as in other mesoderm; × 200.

Photographs by Richard D. Grill

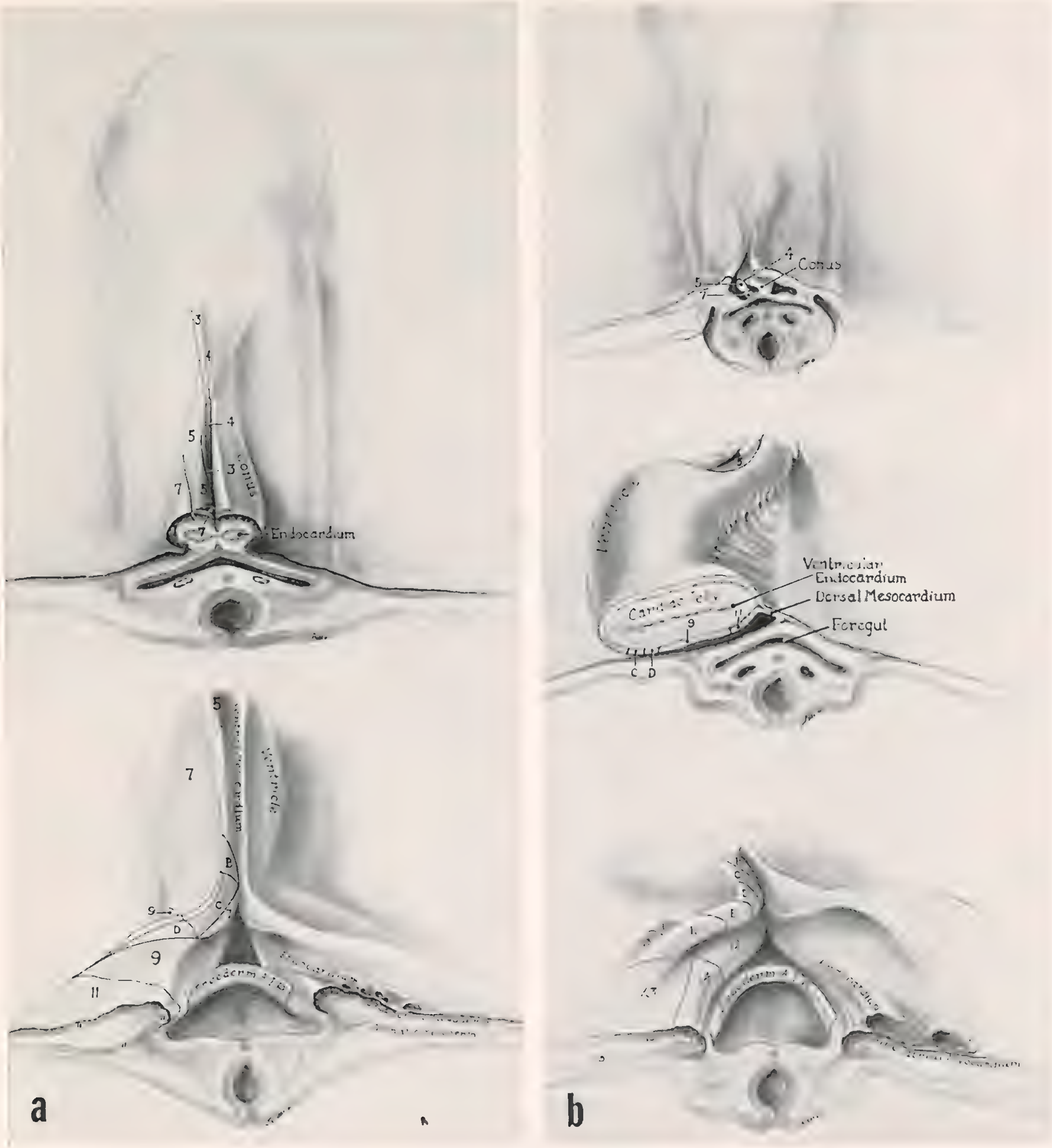

PLATE 2, (a) and (b)

Embryos reconstructed from radioautographed cross sections. Yolk-sac endoderm and attached splanchnic mesoderm have been removed. Distribution of cells on the basis of grid pattern of implants made at stage 5 is shown; *cf.* Fig. 3(a). (a) Embryo with 10 somites. (b) Embryo with 16 somites. Because of torsion of the heart after separation from the ventral mesocardium, implants to the embryo's right heart-forming region now lie mainly in the dorsal aspect of the ventricular loop.

Executed by Judith Baer

CONTRIBUTIONS TO EMBRYOLOGY, CARNEGIE INSTITUTION OF WASHINGTON

INDEX OF AUTHORS
VOLUMES I–XXXVIII
1915–1966

INDEX OF AUTHORS

VOLUMES I–XXXVIII

1915–1966

Adams, E. *See* White, R. F.

Adams, Eleanor C. *See* Hertig, A. T.

Allen, Edgar 1927. The menstrual cycle of the monkey, *Macacus rheus:* observations on normal animals, the effects of removal of the ovaries and the effects of injections of ovarian and placental extracts into the spayed animals. xix, 1–44.

Allen, Edgar, J. P. Pratt, Q. U. Newell, L. J. Bland. 1930. Human tubal ova; related early corpora lutea and uterine tubes. xxii, 45–75.

Andersen, Dorothy H. 1926. Lymphatics and blood-vessels of the ovary of the sow. xviii, 107–123.

Andersen, Dorothy H. 1927; Lymphatics of the Fallopian tube of the sow. xix, 135–147.

Ardran, G. M. *See also* Reynolds, S. R. M.

Arey, Leslie B. 1938. The history of the first somite in human embryos. xxvii, 233–269.

Atwell, Wayne J. 1930. A human embyro with seventeen pairs of somites. xxi, 1–24.

Baker, J. Tyler. *See also* Reynolds, S. R. M.

Bardeen, C. R. 1920. The height-weight index of build in relation to linear and volumetric proportions and surface-area of the body during post-natal development. ix, 483–554.

Barry, Lee Willis. 1920. The effects of inanition in the pregnant albino rat, with special reference to the changes in the relative weights of the various parts, systems, and organs of the offspring. xi, 91–136.

Bartelmez, George W. 1933. Histological studies on the menstruating mucous membrane of the human uterus. xxiv, 141–186.

Bartelmez, George W. 1957. The form and the functions of the uterine blood vessels in the rhesus monkey xxxvi, 153–181.

Bartelmez, George W. 1962. The proliferation of neural crest from forebrain levels in the rat. xxxvii, 1–12.

Bartelmez, George W., and A. S. Dekaban. 1962. The early development of the human brain. xxxvii, 13–32.

Bartelmez, George W., and Herbert M. Evans. 1926. Development of the human embryo during the period of somite formation including embryos with 2 to 16 pairs of somites. xvii, 1–67.

Bartelmez, George W., with the collaboration of Mary P. Blount. 1954. The formation of neural crest from the primary optic vesicle in man. xxxv, 55–71.

Bartelmez, George W., with the collaboration of George W. Corner and Carl G. Hartman. 1951. Cyclic changes in the endometrium of the rhesus monkey *(Macaca mulatta)*. xxxiv, 99–144.

Bartelmez, George W. *See also* Corner, G. W.

Bast, T. H. 1930. Ossification of the otic capsule in human fetuses. xxi, 53–82.

Baxter, James S. 1935. Development of the female genital tract in the American opossum. xxv, 15–35.

Bean, Robert Bennett, 1920. Notes on the postnatal growth of the heart, kidneys, liver, and spleen in man. ix, 263–284.

Bensley, C. M. 1951. Cyclic fluctuations in the rate of epithelial mitosis in the endometrium of the rhesus monkey. xxxiv, 87–98.

Berger, Charles A. 1938. Multiplication and reduction of somatic chromosome groups as a regular developmental process in the mosquito, *Culex pipiens*. xxvii, 209–232.

Bland, L. J. *See* Allen, E.

Blount, Mary P. *See* Bartelmez, G. W.

Böving, Bent G. 1962. Anatomical analysis of rabbit trophoblast invasion. xxxvii, 33–55.

Boyd, James Dixon. 1937. The development of the human carotid body. xxvi, 1–31.

Boyden, Edward A. 1940. A volumetric analysis of young human embryos of the 10- and 12-somite stage. xxviii, 157–191.

Boynton, E. P. *See* Hines, M.

Bremer, John L. 1935. Postnatal development of alveoli in the mammalian lung in relation to the problem of the alveolar phagocyte. xxv, 83–110.

Brewer, John I. 1938. A human embryo in the bilaminar blastodisc stage (the Edwards-Jones-Brewer ovum). xxvii, 85–93.

Brewer, John I. *See also* Jones, H. O.

Buell, Charles Elbert, Jr. 1922. Origin of the pulmonary vessels in the chick. xiv, 11–26.

Burns, Robert K. 1942. The origin and differentiation of the epithelium of the urinogenital sinus in the opossum, with a study of the modifications induced by estrogens. xxx, 63–83.

Burns, Robert K., Jr. 1945. The differentiation of the phallus in the opossum and its reactions of sex hormones. xxxi, 147–162.

Burns, Robert K., Jr. 1945. The effects of male hormone on the differentiation of the urino-genital sinus in young opossums. xxxi, 163–175.

Cash, James R. 1921. On the development of the lymphatics in the stomach of the embryo pig. xiii, 1–15.

Chacko, Anna W., and S. R. M. Reynolds. 1954. Architecture of distended and nondistended human umbilical cord tissues, with special reference to the arteries and veins. xxxv, 135–150.

Clark, Eliot L. *See* Clark, E. R.

Clark, Eliot R. 1915. An anomaly of the thoracic duct with a bearing on the embryology of the lymphatic system. ii, 45–54.

Clark, Eliot R., and Eleanor Linton Clark. 1920. On the orgin and early development of the lymphatic system of the chick. ix, 447–482.

Coffman, C. M. *See* DeLanney, L. E.

Congdon, E. D. 1922. Transformation of the aortic-arch system during the development of the human embryo. xiv, 47–110.

Corner, George W. 1915. The corpus luteum of pregnancy, as it is in swine. ii, 69–94.

Corner, George W. 1920. On the widespread occurrence of reticular fibrils produced by capillary endothelium. ix, 85–93.

Corner, George W. 1920. A case of true lateral hermaphroditism in a pig with functional ovary. xi, 137–142.

Corner, George W. 1921. Abnormalities of the mammalian embryo occurring before implantation. xiii, 61–66.

Corner, George W. 1921. Cyclic changes in the ovaries and uterus of the sow, and their relation to the mechanism of implantation. xiii, 117–146.

Corner, George W. 1923. Ovulation and menstruation in *Macacus rhesus*. xv, 73–101.

Corner, George W. 1929. A well-preserved human embryo of 10 somites. xx, 81–101.

Corner, George W. 1942. The fate of the corpora lutea and the nature of the corpora aberrantia in the rhesus monkey. xxx, 85–96.

Corner, George W. 1948. Alkaline phosphatase in the ovarian follicle and in the corpus luteum. xxxii, 1–8.

Corner, George W., and George W. Bartelmez. 1954. Early abnormal embryos of the rhesus monkey. xxxv, 1–9.

Corner, George W., with the collaboration of Carl G. Hartman and George W. Bartelmez. 1945. Development, organization, and breakdown of the corpus luteum in the rhesus monkey. xxxi, 117–146.

Corner, George W. *See also* Bartelmez, G. W.; Hartman, C. G.; Heuser, C. H.; Streeter, G. L.

Cowdry, E. V. 1916. The structure of chromophile cells of the nervous system. iv, 27–43.

Cowdry, E. V. 1918. The mitochondrial constituents of protoplasm. viii, 39–160.

Crowder, Roy E. 1957. The development of the adrenal gland in man, with special reference to origin and ultimate location of cell types and evidence in favor of the "cell migration" theory. xxxvi, 193–210.

Cuajunco, Fidel. 1927. Embryology of the neuromuscular spindle. xix, 45–72.

Cuajunco, Fidel. 1940. Development of the neuromuscular spindle in human fetuses. xxviii, 95–128.

Cuajunco, Fidel. 1942. Development of the human motor end plate. xxx, 127–152.

Cummins, H. 1929. The topographic history of the volar pads (walking pads; *Tastballen*) in the human embryo. xx, 103–126.

Cunningham, R. S. 1916. On the development of the lymphatics of the lungs in the embryo pig. iv, 45–68.

Cunningham, R. S., F. R. Sabin, and C. A. Doan. 1925. The development of leucocytes, lymphocytes, and monocytes from a specific stem-cell in adult tissues. xvi, 227–276.

Cunningham, R. S. *See also* Doan, C. A.; Sabin, F. R.

Danchakoff, Vera. 1920. Myeloid metaplasia of the embryonic mesenchyme in relation to cell potentialities and differential factors. xi, 1–32.

Danchakoff, Vera. 1926. Lens ectoderm and optic vesicles in allantois grafts. xviii, 63–78.

Danchakoff, Vera, and V. E. Danchakoff. 1930. The age factor in grafts. xxi, 125–140.

Danchakoff, V. E. *See* Danchakoff, Vera.

Davenport, Charles B. 1938. Bodily growth of babies during the first postnatal year. xxvii, 271–305.

Davis, C. L. 1923. Description of a human embryo having twenty paired somites. xv, 1–51.

Davis, C. L. 1927. Development of the human heart from its first appearance to the stage found in embryos of twenty paired somites. xix, 245–284.

De Allende, Inés L. C., Ephraim Shorr, and Carl G. Hartman. 1945. A comparative study of the vaginal smear cycle of the rhesus monkey and the human. xxxi, 1–26.

DeHaan, Robert L. *See* Rosenquist, Glenn C.

Dekaban, A. S. *See* Bartelmez, G. W.

DeLanney, L. E. and J. D. Ebert, in collaboration with C. M. Coffman and A. M. Mun. 1962. On the chick spleen: origin; patterns of normal development and their experimental modification. xxxvii, 57–85.

Vries, Pieter A. de, and John B. de C. M. Saunders. 1962. Development of the ventricles and spiral outflow tract in the human heart. xxxvii, 87–114.

Doan, Charles A. 1922. The circulation of the bone-marrow. xiv, 27–46.

Doan, Charles A., R. S. Cunningham, and F. R. Sabin. 1925. Experimental studies on the origin and maturation of avian and mammalian red blood-cells. xvi, 163–226.

Doan, Charles A. *See also* Cunningham, R. S.; Sabin, F. R.

Duesberg, J. 1915. Recherches cytologiques sur la fécondation des Ascidiens et sur leur développment. iii, 33–70.

Duesberg, J. 1920. Cytoplasmic structures in the seminal epithelium of the opossum. ix, 47–84.

Ebert, J. D. *See* DeLanney, L. E.

Emerson, Bettina M. *See* Hines, M. xxxiv, 1–18.

Essick, Charles R. 1915. Transitory cavities in the corpus striatum of the human embryo. ii, 95–108.

Essick, Charles R. 1920. Formation of macrophages by the cells lining the subarachnoid cavity in response to the stimulus of particulate matter. ix, 377–388.

Evans, Herbert McLean, and Katharine J. Scott. 1921. On the differential reaction to vital dyes exhibited by the two great groups of connective-tissue cells. x, 1–55.

Evans, Herbert McLean. *See also* Bartelmez, G. W.

Faulconer, Robert J. 1951. Observations on the origin of the Müllerian groove in human embryos. xxxiv, 159–164.

Finley, Ellen B. 1922. The development of the subcutaneous vascular plexus in the head of the human embryo. xiv, 155–162.

Fitz-Gerald, Patrick A. M. F. 1940. Defective development of the cerebral cortex involving symmetrical bilateral areas. xxviii, 193–217.

Flexner, Louis B. 1929. The development of the meninges Amphibia: a study of normal and experimental animals. xx, 31–49.

Flexner, Louis B. and I. Gersh. 1937. The correlation of oxygen consumption, function and structure in the developing metanephros of the pig. xxvi, 121–127.

Forbes, Thomas R. 1940. Studies on the reproductive system of the alligator. IV. Observations on the development of the gonad, the adrenal cortex, and the Müllerian duct. xxviii, 129–155.

Forbes, Thomas R. 1942. On the fate of the medullary cords of the human ovary xxx, 9–15.

Gardner, Ernest. *See also* O'Rahilly, R.

George, W. C. 1942. A presomite human embryo with chorda canal and prochordal plate. xxx, 1–7.
Gersh, I. 1937. The correlation of structure and function in the developing mesonephros and metanephros. xxvi, 33–58.
Gersh, I., and Arthur Grollman. 1941. The vascular pattern of the adrenal gland of the mouse and rat and its physiological response to changes in glandular activity. xxix, 111–125.
Gersh, I. *See also* Flexner, L. B.
Gilbert, Christine, and Chester H. Heuser. 1954. Studies in the development of the baboon *(Papio ursinus)*: a description of two presomite and two late somite stage embryos. xxxv, 11–54.
Gilbert, Perry W. 1957. The origin and development of the human extrinsic ocular muscles. xxxvi, 59–78.
Gillman, Joseph. 1948. The development of the gonads in man, with a consideration of the role of fetal endocrines and the histogenesis of ovarian tumors. xxxii, 81–131.
Gray, D. J. *See* O'Rahilly, R.
Gregory, P. W. 1930. The early embryology of the rabbit. xxi, 141–168.
Grodzinski, Z. 1930. Area vitellina of chick blastoderm in tissue cultures. xxii, 155–171.
Grollman, A. *See* Gersh, I.

Hamilton, Clara Eddy. 1949. Observations on the cervical mucosa of the rhesus monkey. xxxiii, 81–101.
Harris, John W. S., and Elizabeth Ramsey. 1966. The morphology of human uteroplacental vasculature. xxxviii, 43–58.
Harris, John W. S. *See also* Ramsey, Elizabeth M.
Hartman, Carl G. 1927. Observations on the ovary of the opossum *(Didelphis virginiana)*. I. Accessory ovaries of Beigel, and other outgrowths from the ovarian surface. II. Some cases of defective corpora lutea correlated with pathological uteri and death of embryos. III. On the possible occurrence of an adrenal rest in an opossum ovary, xix, 285–300.
Hartman, Carl G. 1932. Studies in the reproduction of the monkey *Macacus (Pithecus) rhesus*, with special reference to menstruation and pregnancy. xxiii, 1–161.
Hartman, Carl G. 1942. Further attempts to cause ovulation by means of gonadotropes in the adult rhesus monkey. xxx, 111–126.
Hartman, Carl G., and G. W. Corner. 1941. The first maturation division of the macaque ovum. xxix, 1–6.
Hartman, Carl G. *See also* Bartlemez, G. W.; Corner, G. W.; De Allende, I. L. C.; Lewis, W. H.
Heard, Osborne O., (described by) 1957. Methods used by C. H. Heuser in preparing and sectioning early embryos. xxxvi, 1–18.
Hertig, Arthur T. 1935. Angiogenesis in the early human chorion and in the primary placenta of the macaque monkey. xxv, 37–81.
Hertig, Arthur T., and John Rock. 1941. Two human ova of the pre-villous stage, having an ovulation age of about eleven and twelve days respectively. xxix, 127–156.
Hertig, Arthur T., and John Rock. 1945. Two human ova of the pre-villous stage, having a developmental age of about seven and nine days respectively. xxxi, 65–84.
Hertig, Arthur T., and John Rock. 1949. Two human ova of the pre-villous stage, having a developmental age of about eight and nine days respectively. xxxiii, 169–186.
Hertig, Arthur T., John Rock, Eleanor C. Adams, and William J. Mulligan. 1954. On the preimplantation stages of the human ovum: A description of four normal and four abnormal specimens ranging from the second to the fifth day of development. xxxv, 199–220.
Hertig, Arthur T. *See also* Heuser, C. H.; White, R. F.
Heuser, Chester H., John Rock, and Arthur T. Hertig. derivatives in the pig. xv, 121–139.
Heuser, Chester H. 1927. A study of the implantation of the ovum of the pig from the stage of the bilaminar blastocyst to the completion of the fetal membranes. xix, 229–243.
Heuser, Chester H. 1930. A human embryo with 14 pairs of somites. xxii, 135–153.
Heuser, Chester H. 1932. A presomite human embryo with a definite chorda canal. xxiii, 251–267.
Heuser, Chester H., and George W. Corner. 1957. Developmental horizons in human embryos. Description of age group X, 4 to 12 somites. xxxvi, 29–39.
Heuser, Chester H., John Rock, and Arthur T. Hertig. 1945. Two human embryos showing early stages of the definitive yolk sac. xxxi, 85–99.
Heuser, Chester H., and George L. Streeter. 1929. Early stages in the development of pig embryos, from the period of initial cleavage to the time of the appearance of limb-buds. xx, 1–29.
Heuser, Chester H. and George L. Streeter. 1941. Development of the macaque embryo. xxix, 15–55.
Heuser, Chester H., and George B. Wislocki 1935. Early development of the sloth *(Bradypus griseus)* and its similarity to that of man. xxv, 1–13.
Heuser, Chester H. *See also* Gilbert, C.; Streeter, G. L.
Hines, Marion. 1942. The development and regression of reflexes, postures, and progression in the young macaque. xxx, 153–209.
Hines, Marion, and E. P. Boynton. 1940. The maturation of "excitability" in the precentral gyrus of the young monkey *(Macaca mulatta)*. xxviii, 309–451.
Hines, Marion, and Bettina M. Emerson. 1951. Development of the spinal cord in the fetal and infant macaque. I. Growth, as increase in size. xxxiv, 1–18.
Hunter, Richard H. 1930. Observations on the development of the human female genital tract. xxii, 91–107.

Ingalls, N. William. 1918. A human embryo before the appearance of the myotomes. vii, 111–134.
Ingalls, N. William. 1920. A human embryo at the beginning of segmentation, with special reference to the vascular system. xi, 61–90.

Jenkins, George B. 1920. A study of the superior olive. ix, 157–172.
Jenkins, George B. 1921. Relative weight and volume of the component parts of the brain of the human embryo at different stages of development. xiii, 41–60.
Johnson, Franklin Paradise. 1917. A human embryo of twenty-four pairs of somites. vi, 125–168.
Jones, H. O. and John I. Brewer. 1941. A human embryo in the primitive-streak stage (Jones-Brewer ovum I). xxix, 157–165.
Jones, H. O. *See also* Brewer, J. I.

Key, J. A. *See* Wislocki, G. B.
King, Jessie L. 1926. Menstrual records and vaginal smears in a selected group of normal women. xviii, 79–94.

Koff, Arthur K. 1933. Development of the vagina in the human fetus. xxiv, 59–90.
Krafka, Joseph Jr. 1941. The Torpin ovum, a presomite human embryo. xxix, 167–193.
Kunitomo, Kanae. 1918. The development and reduction of the tail, and of the caudal end of the spinal cord. viii, 161–198.

Langworthy, Orthello R. 1926. Relation of onset of decerebrate rigidity to the time of myelinization of tracts in the brainstem and spinal cord of young animals. xvii, 125–140.
Langworthy, Orthello, R. 1927. Correlated physiological and morphological studies of the development of electrically responsive areas in the cerebral cortex of the opossum. xix, 149–175.
Langworthy, O. R. 1927. Histological development of cerebral motor areas in young kittens correlated with their physiological reaction to electrical stimulation. xix, 177–207.
Langworthy, Orthello R. 1929. A correlated study of the development of reflex activity in fetal and young kittens and the myelinization of tracts in the nervous system. xx, 127–171.
Langworthy, Orthello R. 1930. Medullated tracts in the brain stem of a seventh-month human fetus. xxi, 37–52.
Langworthy, Orthello R. 1933. Development of behavior patterns and myelinization of the nervous system in the human fetus and infant. xxiv, 1–57.
Langworthy, Orthello R. *See also* Weed, L. H.
LaVelle, Faith Wilson. 1951. A study of hormonal factors in the early sex development of the golden hamster. xxxiv, 19–53.
Lee, Ferdinand C. 1923. On the lymph-vessels of the liver. xv, 63–72.
Lewis, Margaret Reed. 1917. Development of connective-tissue fibers in tissue cultures of chick embryos. vi, 45–60.
Lewis, Margaret Reed, 1920. Muscular contraction in tissue cultures. ix, 191–212.
Lewis, Margaret R., and Warren, H. Lewis. 1926. Transformation of mononuclear blood-cells into macrophages, epithelioid cells, and giant cells in hanging-drop blood-cultures from lower vertebrates. xviii, 95–120.
Lewis, Warren H. 1920. The cartilaginous skull of a human embryo twenty-one millimeters in length. ix, 299–324.
Lewis, Warren H. 1926. Cultivation of embryonic heart-muscle. xviii, 1–21.
Lewis, Warren H. 1929. The effect of various solutions and salts on the pulsation rate of isolated hearts from young chick embryos. xx, 173–192.
Lewis, Warren H. 1929. Macrophages and other cells of the deep fascia of the thigh of the rat. xx, 193–212.
Lewis, Warren H. 1935. Rat malignant cells in roller tube cultures and some results. xxv, 161–172.
Lewis, Warren H., and Carl G. Hartman. 1933. Early cleavage stages of the egg of the monkey *(Macacus rhesus)*. xxiv, 187–201.
Lewis, Warren H. and Carl G. Hartman. 1941. Tubal ova of the rhesus monkey. xxix, 7–14.
Lewis, Warren H. and Elsie Starr Wright. 1935. On the early development of the mouse egg. xxv, 113–143.
Lewis, Warren H. *See also* Lewis, M. R.
Limson, Marciano. 1932. Observations on the bones of the skull in white and negro fetuses and infants. xxiii, 205–222.
Lineback, Paul E. 1920. Studies on the longitudinal muscle of the human colon, with special reference to the development of the taeniae. xi, 33–44.
Long, J. Herman. 1940. Growth in vitro of ovarian germinal epithelium. xxviii, 89–93.
Lynn, W. Gardner. 1942. The embryology of *Eleutherodactylus nubicola,* an anuran which has no tadpole stage. xxx, 27–62.

Macklin, Charles Clifford. 1916. Binucleate cells in tissue cultures. iv, 69–106.
Macklin, Charles Clifford. 1920. The development and function of macrophages in the repair of experimental bone-wounds in rats vitally stained with trypan-blue. ix, 1–46.
Macklin, Charles Clifford. 1921. The skull of a human fetus of 43 millimeters greatest length. x, 57–103.
Mall, Franklin Paine. 1915. On the fate of the human embryo in tubal pregnancy. i, 104 pp.
Mall, Franklin Paine. 1916. The human magma réticulé in normal and in pathological development. iv, 5–26.
Mall, Franklin Paine. 1917. Cyclopia in the human embryo. vi, 5–33.
Mall, Franklin Paine, and A. W. Meyer. 1921. Studies on abortuses: a survey of pathologic ova in the Carnegie Embryological Collection. xii, 364 pp.
Marchetti, Andrew A. 1945. A pre-villous human ovum accidentally recovered from a curettage specimen. xxxi, 107–115.
Markee, J. Eldridge. 1940. Menstruation in intraocular endometrial transplants in the rhesus monkey. xxviii, 219–308.
Martínez-Esteve, Pedro. 1942. Observations on the histology of the opossum ovary. xxx, 17–26.
Maximow, Alexander. 1925. Tissue-cultures of young mammalian embryos. xvi, 47–113.
McKenzie, John. 1962. The development of the sternomastoid and trapezius mucles. xxxvii, 121–129.
Menke, John F. 1935. Photodynamic action on normal and malignant cells in vitro. xxv, 145–160.
Meyer, Arthur William. 1915. Fields, graphs, and other data on fetal growth. ii, 55–68.
Meyer, Arthur William. 1920. Hydatiform degeneration in tubal and uterine pregnancy. ix, 325–364.
Meyer, Arthur William. *See also* Mall, F. P.
Miller, William Snow. 1920. A morphological study of the tracheal and bronchial cartilages. ix, 285–298.
Moffett, Benjamin C., Jr. 1957. The prenatal development of the human temporomandibular joint. xxxvi, 19–28.
Mossman, Harland W. 1937. Comparative morphogenesis of the fetal membranes and accessory uterine structures. xxvi, 129–246.
Mulligan, William J. *See* Hertig, A. T.
Mun, A. M. *See* DeLanney, L. E.
Muratori, Giulio. 1937. Embryonal germ-cells of the chick in hanging-drop cultures. xxvi, 56–69.
Myers, Burton D. 1920. A study of the development of certain features of the cerebellum. ix, 365–375.

Narbaitz, Roberto. 1962. The primordial germ cells in the male human embryo. xxxvii, 115–119.
Newell, Q. U. *See* Allen, E.

Norris, Edgar H. 1937. The parathyroid glands and the lateral thyroid in man: their morphogenesis, histogenesis, topographic anatomy and prenatal growth. xxvi, 247–294.

Norris, Edgar H. 1938. The morphogenesis and histogenesis of the thymus gland in man: in which the origin of the Hassall's corpuscles of the human thymus is discovered. xxvii, 191–207.

O'Rahilly, Ronan. 1966. Early development of the eye in staged human embryos. xxxviii, 1–42.

O'Rahilly, Ronan, D. J. Gray, and Ernest Gardner. 1957. Chondrification in the hands and feet of staged human embryos. xxxvi, 183–192.

Padget, Dorcas Hager. 1948. The development of the cranial arteries in the human embryo. xxii, 205–261.

Padget, Dorcas H. 1957. The development of the cranial venous system in man, from the viewpoint of comparative anatomy. xxxvi, 79–140.

Payne, Fernandus. 1925. General description of a 7-somite human embryo. xvi, 115–124.

Pratt, J. P. *See* Allen, E.

Prichard, M. M. L. *See* Reynolds, S. R. M.

Ramsey, Elizabeth Mapelsden. 1937. The Lockyer embryo: an early human embryo *in situ.* xxvi, 99–119.

Ramsey, Elizabeth Mapelsden, 1938. The Yale embryo. xxvii, 67–84.

Ramsey, Elizabeth Mapelsden. 1949. The vascular pattern of the endometrium of the pregnant rhesus monkey *(Macaca mulatta).* xxxiii, 113–147.

Ramsey, Elizabeth Mapelsden. 1954. Venous drainage of the placenta of the rhesus monkey *(Macaca mulatta).* xxxv, 151–173.

Ramsey, Elizabeth Mapelsden and John W. S. Harris. 1966. Comparison of uteroplacental vasculature and circulation in the rhesus monkey and man. xxxviii, 59–70.

Ramsey, Elizabeth Mapelsden. *See also* Harris, John W. S.

Reichert, F. L. 1921. On the fate of the primary lymph-sacs in the abdominal region of the pig, and the development of lymph-channels in the abdominal and pelvic regions. xiii, 17–39.

Reitzer, Robert. 1920. The sino-ventricular bundle: a functional interpretation of morphological findings. ix, 143–156.

Reynolds, S. R. M. 1949. Adaptation of uterine blood vessels and accommodation of the products of conception. xxxiii, 1–19.

Reynolds, S. R. M., G. M. Ardan, and M. M. L. Prichard. 1954. Observations on regional circulation times in the lamb under fetal and neonatal conditions. xxxv, 73–92.

Reynolds, S. R. M., and J. Tyler Baker. 1951. Effect of parity in women on the pattern of uterine enlargement during the latter half of gestation. xxxiv, 75–86.

Reynolds, S. R. M *See also* Chacko, A. W.

Rienhoff, W. F., Jr. 1930. Gross and microscopic structure of thyroid gland in man. xxi, 97–123.

Rock, John. *See* Hertig, A. T.; Hertig, A. T. *et al.;* Heuser, C. H.; White, R.F.

Ropes, Marian W. 1930. Phagocytic activity and morphological variations of the ciliated epithelial cells of the trachea and bronchi in rabbits. xxii, 77–90.

Rosenquist, Glenn C. 1966. A radioautographic study of labeled grafts in the chick blastoderm: development from primitive-streak stages to stage 12. xxxvii, 71–110.

Rosenquist, Glenn C., and Robert L. DeHaan. 1966. Migration of precardiac cells in the chick embryo: a radioautographic study. xxxviii, 111–121.

Rossman, I. 1942. On the lipin and pigment in the corpus luteum of the rhesus monkey. xxx, 97–109.

Sabin, Florence. R. 1915. On the fate of the posterior cardinal veins and their relation to the development of the vena cava and azygos in the embryo pig. iii, 5–32.

Sabin, Florence R. 1917. Origin and development of the primitive vessels of the chick and of the pig. vi, 61–124.

Sabin, Florence R. 1920. Studies on the origin of blood-vessels and of red blood-corpuscles as seen in the living blastoderm of chicks during the second day of incubation. ix, 213–262.

Sabin, Florence R. 1922. Direct growth of veins by sprouting. xiv, 1–10.

Sabin, Florence R., C. A. Doan and R. S. Cunningham. 1925. Discrimination of two types of phagocytic cells in the connective tissues by the supravital technique. xvi, 125–162.

Sabin, Florence R. *See also* Cunningham, R. S.; Doan, C. A.

Saglik, Saïm. 1938. Ovaries of gorilla, chimpanzee, orang-utan and gibbon. xxvii, 179–189.

Saunders, John B. de C. M. *See* de Vries, P. A.

Schopper, Werner. 1935. The Walker rat carcinoma no. 72 in tissue culture. xxv, 173–181.

Schultz, Adolph H. 1920. The development of the external nose in whites and negroes. ix, 173–190.

Schultz, Adolph H. 1929. The technique of measuring the outer body of human fetuses and of primates in general. xx, 213–257.

Schultz, Adolph H. 1937. Fetal growth and development of the rhesus monkey. xxvi, 71–97.

Schultz, Adolph H. 1940. Growth and development of the chimpanzee. xxviii, 1–63.

Schultz, Adolph H. 1941. Growth and development of the orang-utan. xxix, 57–110.

Schultz, Adolph H. 1949. The palatine ridges of primates. xxxiii, 43–66.

Scipiades, Elemér, Jr. 1938. Young human ovum detected in uterine scraping. xxvii, 95–105.

Scott, K. J. *See* Evans, H. M.

Sensenig, E. Carl. 1949. The early development of the human vertebral column. xxxiii, 21–41.

Sensenig, E. Carl. 1951. The early development of the meninges of the spinal cord in human embryos. xxxiv, 145–157.

Sensenig, E. Carl. 1957. The development of the occipital and cervical segments and their associated structures in human embryos. xxxvi, 141–151.

Settle, George W. 1954. Localization of the erythrocyte-forming areas in the early chick blastoderm cultivated in vitro, xxxv, 221–237.

Shields, Randolph T. 1923. On the development of tendon sheaths. xv, 53–61.

Shikinami, Jujiro. 1926. Detailed form of the Wolffian body in human embryos of the first eight weeks. xviii, 49–61.

Shipley, P. G., and G. B. Wislocki. 1915. The histology of the poison-glands of *Bufo agua* and its bearing upon the formation of epinephrin within the glands. iii, 71–90.

Shorr, Ephraim, *See* De Allende, I. L. C.

Smith, E. Ide. 1957. The early development of the trachea and esophagus in relation to atresia of the esophagus and tracheoesophageal fistula. xxxvi, 41–57.

Spaulding, Milo Herrick. 1921. The development of the external genitalia in the human embryo. xiii, 67–88.

Speert, Harold. 1948. The normal and experimental development of the mammary gland of the rhesus monkey, with some pathological correlations. xxxii, 9–65.

Squier, Raymond R. 1932. The living egg and early stages of its development in the guinea-pig. xxiii, 223–250.

Straus, W. L., Jr. 1927. Growth of the human foot and its evolutionary significance. xix, 93–134.

Streeter, George L. 1918. The histogenesis and growth of the otic capsule and its contained periotic tissue-spaces in the human embryo. vii, 5–54.

Streeter, George L. 1918. The development alterations in the vascular system of the brain of the human embryo. viii, 5–38.

Streeter, George L. 1920. A human embryo (Mateer) of the presomite period. ix, 389–424.

Streeter, George L. 1920. Weight, sitting height, head size, foot length, and menstrual age of the human embryo. xi, 143–170.

Streeter, George L. 1922. Development of the auricle in the human embryo. xiv, 111–138.

Streeter, George L. 1926. The "Miller" ovum—the youngest normal human embryo thus far known. xviii, 31–48.

Streeter, George L. 1927. Development of the mesoblast and notochord in pig embryos. xix, 73–92.

Streeter, George L. 1930. Focal deficiencies in fetal tissues and their relation to intra-uterine amputation. xxii, 1–44.

Streeter, George L. 1942. Developmental horizons in human embryos. Description of age group xi, 13 to 20 somites, and age group xii, 21 to 29 somites. xxx, 211–245.

Streeter, George L. 1945. Development horizons in human embryos. Description of age group XIII, embryos about 4 or 5 millimeters long, and age group XIV, period of indentation of the lens vesicle. xxxi, 27–63.

Streeter, George L. 1945. Developmental horizons in human embryos. Descriptions of age groups XV, XVI, XVII, and XVIII, being the third issue of a survey of the Carnegie Collection, xxxii, 133–203.

Streeter, George L. 1949. Development horizons in human embryos (fourth issue). A review of the histogenesis of cartilage and bone. xxxiii, 149–169.

Streeter, George L. *Prepared for publication by* Chester H. Heuser and George W. Corner. 1951. Developmental horizons in human embryos. Description of age groups XIX, XX, XXI, XXII, and XXIII, being the fifth issue of a survey of the Carnegie Collection. xxxiv, 165–196.

Streeter, G. L. *See also* Heuser, C. H.; Wislocki, G. B.

Sturgis, Somers H. 1949. Rate and significance of atresia of the ovarian follicle of the rhesus monkey. xxxiii, 67–80.

Sugiyama, S. 1926. Origin of thrombocytes and of the different types of blood cells as seen in the living chick blastoderm. xviii, 121–147.

Thurlow, Madge DeG. 1917. Quantitative studies on mitochondria in nerve-cells. vi, 35–44.

Torrey, Theodore W. 1954. The early development of the human nephros. xxxv, 175–197.

Traut, Herbert F. 1923. The structural unit of the human kidney. xv, 103–120.

Van der Stricht, O. 1918. The genesis and structure of the membrana tectoria and the crista spiralis of the cochlea. vii, 55–86.

Van der Stricht, O. 1920. The arrangement and structure of sustentacular cells and hair-cells in the developing organ of Corti. ix, 109–142.

Van der Westhuysen, O. P. *See* Wislocki, G. B.

Van Wagenen, G. *See* Wells, L. J.

Walmsley, Robert. 1938. Some observations on the vascular system of a female fetal finback. xxvii, 107–178.

Watt, James Crawford. 1915. Description of two young twin human embryos with 17–19 paired somites. ii, 5–44.

Weed, Lewis H. 1917. The development of the cerebro-spinal spaces in pig and in man. v, 116 pp.

Weed, Lewis H. 1920. The experimental production of an internal hydrocephalus. ix, 425–446.

Weed, Lewis H., and Orthello R. Langworthy. 1926. Physiological study of cortical motor areas in young kittens and in adult cats. xvii, 89–106.

Weller, G. Louis, Jr. 1933. Development of the thyroid, parathyroid and thymus glands in man. xxiv, 93–139.

Wells, L. J., and G. van Wagenen. 1954. Androgen-induced female pseudohermaphroditism in the monkey *(Macaca mulatta)*: Anatomy of the reproductive organs. xxxv, 93–106.

Wells, L. J. 1954. Development of the human diaphragm and pleural sacs. xxxv, 107–134.

Wen, I. Chuan. 1930. Ontogeny and phylogeny of the nasal cartilages in primates. xxii, 109–134.

West, Cecil M. 1925. The development of the gums and their relationship to the deciduous teeth in the human fetus. xvi, 23–45.

West, Cecil M. 1930. Description of a human embryo of eight somites. xxi, 25–35.

Wharton, Lawrence R., Jr. 1949. Double ureters and associated renal anomalies in early human embryos. xxxiii, 103–112.

Wheeler, Theodora. 1918. Study of a human spina bifida monster with encephaloceles and other abnormalities. vii, 87–110.

Wheeler, Theodora. 1920. Variability in the spinal column as regards defective neural arches (rudimentary spina bifida). ix, 95–107.

Wilson, Karl M. 1926. Origin and development of the rete ovarii and the rete testis in the human embryo. xvii, 69–88.

White, R. F., A. T. Hertig, J. Rock, and E. Adams. 1951. Histological and histochemical observations on the corpus luteum of human pregnancy, with special reference to corpora lutea associated with early normal and abnormal ova. xxxiv, 55–74.

Wilson, Karl M. 1926. Correlation of external genitalia and sex-glands in the human embryo. xviii, 23–30.

Wilson, Karl M. 1945. A normal human ovum of sixteen days development (the Rochester ovum) xxxi, 101–106.

Wislocki, George B. 1920. Experimental studies on fetal absorption. I. The vitally stained fetus. II. Behavior of the fetal membranes and placenta of the cat toward colloidal dyes injected into maternal blood-stream. xi, 45–60.

Wislocki, George B. 1921. Further experimental studies on fetal absorption. III. The behavior of the fetal membranes and placenta of the guinea-pig toward trypan blue injected into the maternal blood-stream. IV. Behavior of the placenta and fetal membranes of the rabbit toward trypan blue injected into the maternal blood-stream. xiii, 89–101.

Wislocki, George B. 1925. On the placentation of the sloth *(Bradypus griseus)*. xvi, 5–21.

Wislocki, George B. 1927. On the placentation of the tridactyl sloth *(Bradypus griseus)* with a description of some characters of the fetus.

Wislocki, George B. 1929. On the placentation of primates, with a consideration of the phylogeny of the placenta. xx, 51–80.

Wislocki, George B. 1930. On an unusual placental form in the Hyracoidea: its bearing on the theory of the phylogeny of the placenta. xxi, 83–95.

Wislocki, George B. 1930. On a series of placental stages of a platyrrhine monkey *(Ateles geoffroyi)* with some remarks upon age, sex and breeding period in platyrrhines. xxii, 173–192.

Wislocki, George B. 1932. On the female reproductive tract of the gorilla, with a comparison of that of other primates. xxiii, 163–204.

Wislocki, George B., and J. A. Key. 1921. The distribution of mitochondria in the placenta. xiii, 103–115.

Wislocki, George B., and George L. Streeter. 1938. On the placentation of the macaque *(Macaca mulatta)*, from the time of implantation until the formation of the definitive placenta. xxvii, 1–66.

Wislocki, George B. and O. P. van der Westhuysen. 1940. The placentation of *Procavia capensis*, with a discussion of the placental affinites of the Hyracoidea. xxviii, 65–88.

Wislocki, George B. *See also* Heuser, C. H.; Shipley, P. G.

Witschi, Emil. 1948. Migration of the germ cells of human embryos from the yolk sac to the primitive gonadal folds. xxxii, 67–80.

Woollard, H. H. 1922. The development of the principal arterial stems in the forelimb of the pig. xiv, 139–154.

Wright, E. S. *See* Lewis, W. H.